



HAL
open science

New insights into the roles of cytoplasmic F-actin self-organization using two model systems: *Xenopus* egg extracts and mouse oocytes

Alexandra Colin

► To cite this version:

Alexandra Colin. New insights into the roles of cytoplasmic F-actin self-organization using two model systems: *Xenopus* egg extracts and mouse oocytes. *Biological Physics* [physics.bio-ph]. Université Paris sciences et lettres, 2017. English. NNT : 2017PSLEE034 . tel-01804191

HAL Id: tel-01804191

<https://theses.hal.science/tel-01804191>

Submitted on 31 May 2018

HAL is a multi-disciplinary open access archive for the deposit and dissemination of scientific research documents, whether they are published or not. The documents may come from teaching and research institutions in France or abroad, or from public or private research centers.

L'archive ouverte pluridisciplinaire **HAL**, est destinée au dépôt et à la diffusion de documents scientifiques de niveau recherche, publiés ou non, émanant des établissements d'enseignement et de recherche français ou étrangers, des laboratoires publics ou privés.

THÈSE DE DOCTORAT

de l'Université de recherche Paris Sciences et Lettres
PSL Research University

Préparée à l'École Normale Supérieure

Étude du rôle de l'auto-organisation de l'actine cytoplasmique
au sein de deux systèmes modèles : extraits cellulaires de
Xénope et ovocytes de souris

New insights into the roles of cytoplasmic F-actin self-
organization using two model systems: Xenopus egg extracts
and mouse oocytes

Ecole doctorale n°388

Chimie physique et chimie analytique de Paris Centre

Spécialité Biophysique

Soutenue par **Alexandra COLIN**
le **15 septembre 2017**

Dirigée par **Zoher GUEROUI**

COMPOSITION DU JURY :

Mme. HELFER Emmanuèle
CINaM, Rapporteur

M. THERY Manuel
CEA, Rapporteur

M. NEDELEC François
EMBL Heidelberg, Examinateur

Mme. VERLHAC Marie-Hélène
CIRB, Collège de France, Examinatrice
Présidente du jury

M. GUEROUI Zoher
ENS Ulm, Directeur de thèse



Department of
CHEMISTRY



Rien n'est aussi dangereux que la certitude d'avoir raison.
Rien ne cause autant de destruction que l'obsession
d'une vérité considérée comme absolue.
François Jacob, *Le jeu des possibles*

Remerciements

Arrivée au terme de ces trois années de thèse, je dois avouer avoir énormément appris, aussi bien au niveau scientifique qu'au niveau humain ; c'est la raison pour laquelle je souhaite remercier un certain nombre de personnes.

Tout d'abord, je voudrais remercier mon jury : Emanuèle Helfer et Manuel Théry, mes rapporteurs, pour avoir accepté de lire mon manuscrit pendant l'été, ainsi que François Nédélec et Marie-Hélène Verlhac pour avoir accepté de faire partie du jury.

Zoher, merci pour ton encadrement pendant ma thèse. Merci pour ces projets stimulants et pour ton enthousiasme scientifique. Merci aussi de m'avoir donné l'opportunité d'aller présenter mon travail dans des écoles d'été et dans des congrès. Les rencontres que j'ai pu y faire ont été très constructives et ces expériences ont vraiment été très formatrices.

Merci à Ludovic Jullien pour son accueil dans le laboratoire et pour ses conseils scientifiques toujours avisés. Au niveau du département, merci à tous les gens "non-scientifiques" (Marie, Stéphanie, Anne, *etc.*) pour leur présence au quotidien.

Côté collaboration, je souhaite remercier Marie-Hélène, d'abord pour avoir injecté tous ces ovocytes pour moi, et pour ces giga de données passés à travers une centaine de WeTransfer ! Merci aussi pour ton optimisme dans les manips. Marie-Emilie, merci pour les discussions scientifiques et pour les moments qu'on a pu passer en congrès à Heidelberg ou à Roscoff. Merci à Maria et à Raphaël pour les discussions scientifiques et à tous les membres de l'équipe du Collège de France pour leur aide lors des manips que j'ai pu effectuer là-bas.

Côté labo maintenant ! Marie-Aude, j'ai adoré râler avec toi ; merci pour ton investissement sans bornes dans le laboratoire. Isabelle, merci d'avoir été là pour les problèmes aussi bien professionnels que personnels. Thomas, merci pour les discussions tardives et tes conseils toujours précieux. Merci à tous les autres membres du pôle de chimie-biophysique, ça a été un vrai plaisir de travailler avec vous pendant ces trois années au laboratoire. Merci aux thésards/post-docs pour nos petites sorties bars à vin/karaoké/Chapi-Chapo ainsi que les pizzas du vendredi midi.

Et enfin merci à LA Gueroui's team : Jérémie, merci pour ton accueil quand j'étais en stage et pour m'avoir tout appris sur le clonage ! Rémi, merci pour nos discussions sur l'égalité entre les Hommes et les bactéries ainsi que pour tes manipettes. Louise, merci d'être restée dans le 5ème et de nous rendre visite régulièrement ; sans rancune pour ce cahier de labo si bien tenu ! Marina, merci pour tes "Tu veux voir un truc trop cool ?!" et tes films de granules où le suspense de savoir si elles vont fusionner est insouten-

able ! Merci aussi pour nos discussions autour de notre passion commune pour Virginie Despentès ou autres sujets variés ! Wei-An, merci pour tes conseils en séries ; un jour il faudra vraiment que tu nous donnes ton secret pour le laser-tag. Shunichi, merci de nous avoir fait découvrir la gastronomie japonaise et bonne continuation dans la découverte de l'œnologie française ! Eliane, merci de m'avoir fait partager tes voyages et bonne continuation pour la suite. Alberto, merci pour ta compagnie aux heures tardives au labo et bonne continuation aux Pays-Bas. Mary, merci pour ton entrain devant les bactéries magnétiques, je te souhaite le meilleur pour ta thèse qui commence. Malgré sa chaleur, la mezzanine exigüe va sûrement beaucoup me manquer, alors comptez sur moi pour repasser par là (de préférence un mercredi ou un vendredi, libanaisdumarché oblige) !

C'est un peu compliqué à lister mais merci à tous les gens du département de chimie que j'ai pu croiser au cours de ma thèse et avec qui j'ai eu des conversations passionnantes à propos de sujets scientifiques (ou non scientifiques d'ailleurs !). Sans oublier Sam et Baptiste pour les P-B et Caro pour nos déjeuners/café. Merci aussi à tous les gens que j'ai pu croiser dans mes enseignements à Jussieu. I would also like to address a special thank to Ted for the manuscript reading, it was a true help!

Je remercie enfin mes ami-e-s avec qui j'ai pu partager les déconvenues et les moments agréables d'une thèse. Merci pour votre écoute, votre joie de vivre et pour tous ces débats qu'on peut avoir sur tout et n'importe quoi. Spéciale dédicace aux chimistes du Teddy's, aux ienchs de la Croix Valmer/Meribel, aux copains de prepa et à tous les autres qui se reconnaîtront.

Un grand merci aussi à mes parents pour m'avoir toujours donné les moyens de faire ce qui me plaisait et pour m'avoir soutenue moralement pendant toute la durée de ces études (9 ans quand même, ne vous inquiétez pas c'est vraiment fini maintenant !). Merci à ma famille et à celle de Jérém pour avoir été là pendant toute la durée de cette thèse.

Et pour finir, merci à toi Jérém de me supporter tous les jours (dans tous les sens du terme). Nos aventures ne font que commencer et je suis persuadée que le meilleur reste à venir.

Contents

| | |
|--|-----------|
| Preface | 5 |
| 1 Cytoskeleton Polymer Assembly. Comparison of F-actin and Microtubule Properties | 7 |
| 1.1 Spontaneous polymerization of polar polymers | 8 |
| 1.1.1 Actin filaments nucleate spontaneously with the help of nucleators | 8 |
| 1.1.2 Microtubules are dynamic polar polymers | 10 |
| 1.2 Mechanical properties | 11 |
| 1.3 Filament polymerization generates forces | 12 |
| 1.4 Various roles of molecular motors associated with filaments | 14 |
| 1.4.1 Motors associated with microtubules | 14 |
| 1.4.2 Motors associated with actin | 15 |
| 1.4.3 Link between F-actin and microtubules <i>via</i> molecular motors . . . | 16 |
| 1.5 Structure generation by cytoskeletal filaments | 18 |
| 1.5.1 F-actin | 18 |
| 1.5.2 Microtubules | 19 |
| 2 Choice of a Model System: Different Approaches to Answer a Biological Question | 23 |
| 2.1 Top-down and bottom-up approaches | 24 |
| 2.1.1 Top-down approaches | 24 |
| 2.1.2 Bottom-up approaches | 25 |
| 2.2 Confinement of biomimetic systems: putting back the boundary in the equation | 27 |
| 2.2.1 Methods of confinement | 27 |
| 2.2.2 Confinement of purely <i>in vitro</i> systems | 29 |
| 2.2.3 Confinement of egg extracts | 32 |
| 2.3 Model systems used in our studies | 35 |
| 2.3.1 <i>Xenopus</i> egg extracts | 35 |
| 2.3.2 Actin-intact egg extracts | 36 |
| 2.3.3 The mouse oocyte | 37 |
| 3 Methods | 39 |
| 3.1 <i>Xenopus</i> egg extracts protocols | 40 |
| 3.1.1 <i>Xenopus</i> egg extracts preparation | 40 |
| 3.1.2 Cycling of cell extracts | 41 |
| 3.1.3 Encapsulation of egg extracts | 41 |
| 3.1.4 Typical experiment in <i>Xenopus</i> egg extracts | 42 |

| | | |
|----------|---|------------|
| 3.2 | Mouse oocytes protocols | 43 |
| 3.2.1 | Extraction of oocytes | 43 |
| 3.2.2 | Injection of oocytes | 43 |
| 3.3 | Visualization with microscopy | 44 |
| 3.4 | Visualization and perturbation of the cytoskeleton | 45 |
| 3.4.1 | Nucleation of F-actin and microtubules in egg extracts | 45 |
| 3.4.2 | Visualization of cytoskeleton in egg extracts and mouse oocytes | 47 |
| 3.4.3 | Perturbation of actin and microtubule cytoskeletons | 48 |
| 3.5 | Particle tracking | 49 |
| 3.5.1 | Introduction to Mean Square Displacement (MSD) | 49 |
| 3.5.2 | Particle tracking to decipher F-actin properties | 50 |
| 3.5.3 | Tools for particle tracking in mouse oocytes | 51 |
| 3.5.4 | Icy tracking | 54 |
| 4 | Triggering Signaling Pathways Using F-actin Self-organization | 59 |
| 4.1 | Introduction | 60 |
| 4.1.1 | How to build heterogeneity in a cell? | 60 |
| 4.1.2 | Regulation of signaling pathways by F-actin in natural occurring systems | 62 |
| 4.1.3 | Ultrasensitive signaling pathways | 64 |
| 4.2 | Article 1: Triggering signaling pathways using F-actin self-organization | 65 |
| 4.2.1 | Presentation of the article | 65 |
| 4.2.2 | Manuscript | 65 |
| 4.3 | Conclusion | 92 |
| 5 | Probing the Physical Constraints Induced by Cytoplasmic F-actin on Microtubule Dynamics of Asters and Spindle-like Organizations | 93 |
| 5.1 | Introduction | 94 |
| 5.1.1 | Context | 94 |
| 5.1.2 | Outlook on studies about actin-microtubule interactions | 94 |
| 5.2 | Article 2: Probing the physical constraints induced by cytoplasmic F-actin on microtubule dynamics of asters and spindle-like organizations | 98 |
| 5.2.1 | Presentation of the article | 98 |
| 5.2.2 | Manuscript | 98 |
| 5.3 | Discussion | 126 |
| 5.3.1 | Perspectives of the work | 126 |
| 5.3.2 | Regulation of F-actin through the cell cycle | 127 |
| 5.3.3 | F-actin misregulation in pathological cases | 127 |
| 5.3.4 | Conclusion | 128 |
| 6 | Spatiotemporal Characterization of the Active Diffusion Driving Nucleus Centering in Mouse Oocytes | 129 |
| 6.1 | Introduction | 130 |
| 6.1.1 | Context | 130 |
| 6.1.2 | How a cell can find its geometric center? Nucleus and spindle positioning in various organisms | 130 |
| 6.1.3 | Spindle migration mechanism in mouse oocytes | 134 |
| 6.2 | Article 3: Spatiotemporal characterization of the active diffusion driving nucleus centering in mouse oocytes | 135 |

| | | |
|---|--|------------|
| 6.2.1 | Presentation of the article | 135 |
| 6.2.2 | Manuscript | 135 |
| 6.3 | Discussion | 163 |
| 6.3.1 | Oil droplets as biomimetic objects and force sensors | 163 |
| 6.3.2 | Homeostasis of actin networks | 163 |
| 6.3.3 | Conclusion | 164 |
| Conclusion | | 165 |
| A Magnetophoresis in Biological Systems | | 167 |
| A.1 | Introduction | 168 |
| A.2 | Description of the objects used for magnetophoresis | 168 |
| A.2.1 | Magnetic nanoparticles | 168 |
| A.2.2 | Ferritin clusters | 169 |
| A.2.3 | Magnetic manipulation | 170 |
| A.3 | Nanoparticles manipulation in mouse oocytes | 172 |
| A.4 | Magnetophoresis of ferritin clusters in water and egg extracts | 173 |
| A.4.1 | Magnetophoresis in water droplets | 173 |
| A.4.2 | Magnetophoresis of an aster in egg extracts | 175 |
| B Protocol for RanQ69L and Utrophin-Ran purification | | 207 |
| Bibliography | | 209 |

Preface

It is fascinating when looking in nature to think of how a complex organism can be formed. Multicellular organisms usually organize from a single cell, that in most cases is completely symmetric (Figure 1).

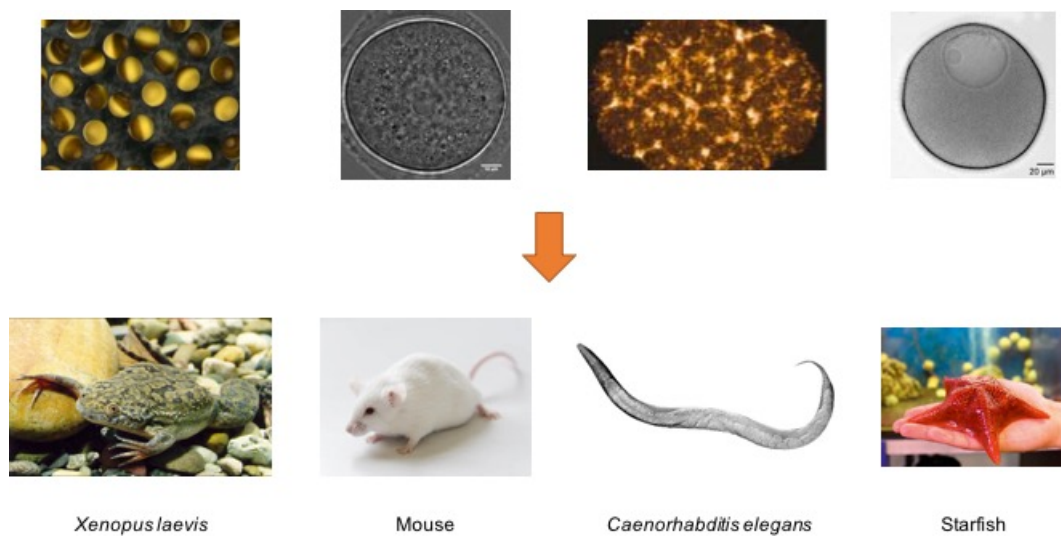


Figure 1: Organization of complex organisms from single egg cells.

With this complexity of biological systems, it is essential to find broad principles that defines the organization of a cell. In our case we are mainly interested in the cytoskeleton self-organization that plays a key role in maintaining the cell heterogeneity.

Self-organization has been widely studied in chemistry and physic for a long time (Benard rolls for example) [1]. Interestingly, self-organization can be seen at many different scales of living systems: from the collective motion of a bacterial colony to the organization of an ecosystem through the formation of regular patterns in the fur of animals. Eric Karsenti defines the goal of the science of self-organization as "the identification of the principles and mechanisms by which an ensemble of agents in interaction evolves toward a particular dynamical temporal or spatial pattern" [1]. For example, order can emerge from collective physical interactions, reaction-diffusion processes or from the nonlinear kinetic properties of chemical reactions. Cytoskeleton polymers (actin, microtubule, intermediate filaments) have been shown to be predominant in the self-organization of the cell.

In this PhD work, we developed new experimental and analytical tools to study the role of cytoplasmic F-actin self-organization in two model systems: *Xenopus* egg extracts and mouse oocytes.

Organization of the manuscript This manuscript is divided in six chapters.

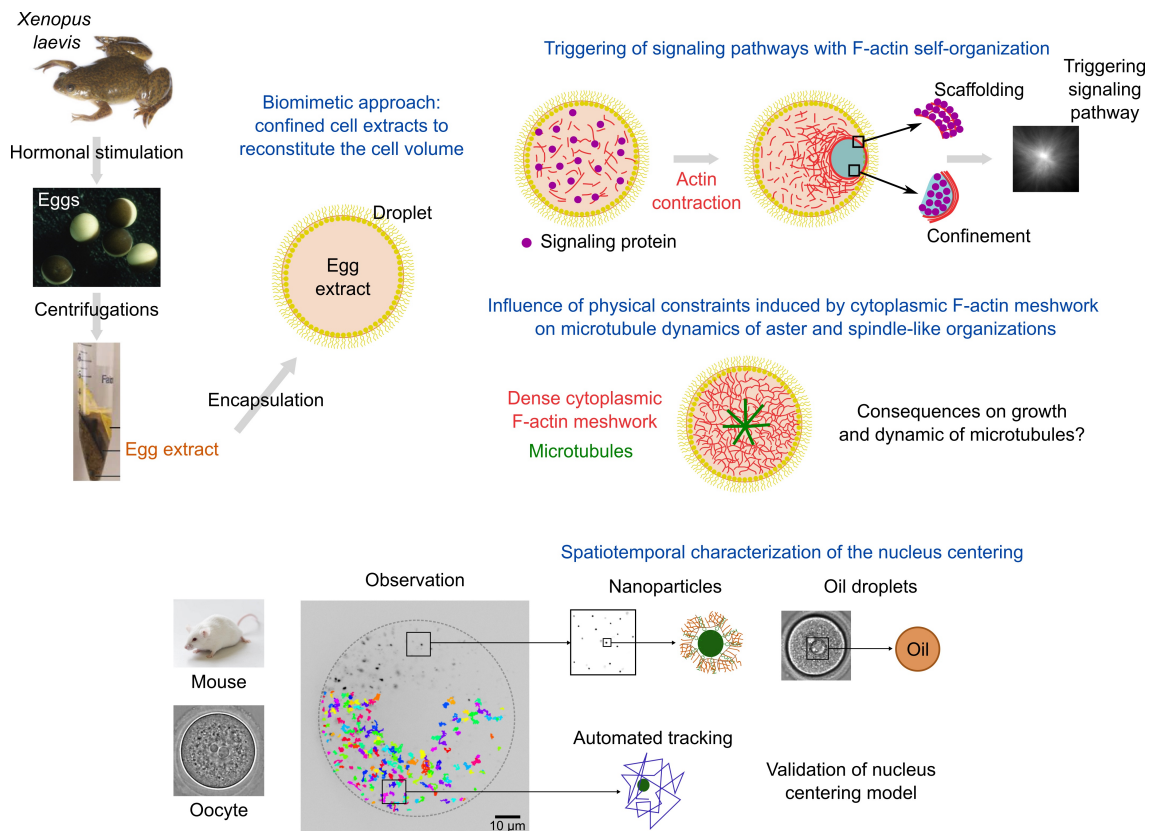
In the first chapter, actin and microtubules are introduced as well as their properties and biological roles. The second chapter presents the two model systems (*Xenopus* egg extracts and mouse oocytes) that we used in our studies and a presentation of the approaches we chose (top-down *vs* bottom-up approaches). The third chapter introduces the methods used during this PhD.

The fourth chapter is the presentation of an proof-of-concept experiment where we demonstrated that F-actin can be used to trigger signaling pathways. Those results were published in *Scientific Reports* in 2016.

The fifth chapter presents a project in which we have shown how cytoplasmic F-actin can constraint microtubule growth and dynamics in aster and spindle-like organizations in *Xenopus* egg extracts. Those results are currently in revisions in *Current Biology*.

The sixth chapter describes a new analytical method in mouse oocytes that we used to confirm the mechanism of nucleus centering during Prophase I. Thanks to this approach, we gained a better understanding of the centering process. Those results are presented in a manuscript in preparation for submission.

After a general discussion and conclusion, an appendix presents some data about manipulation of magnetic objects in living systems. A part of those results are currently in revisions in *Scientific Reports*.



Chapter 1

Cytoskeleton Polymer Assembly. Comparison of F-actin and Microtubule Properties

The cytoskeleton of eukaryotic cells contains three types of filaments: actin, microtubules and intermediate filaments. These filaments act at different levels of the cell (mobility, structure, resistance to pressure *etc.*); they are responsible for the shape and mechanics of the cell, which are often related to its function. They have been widely studied in an individual manner (independently of each other). In recent years, studies started to show the importance of the interaction between these filament families in fundamental biological properties. In this chapter, we will present the properties (biochemical, physics *etc.*) of actin and microtubules.

Contents

| | |
|---|-----------|
| 1.1 Spontaneous polymerization of polar polymers | 8 |
| 1.1.1 Actin filaments nucleate spontaneously with the help of nucleators | 8 |
| 1.1.2 Microtubules are dynamic polar polymers | 10 |
| 1.2 Mechanical properties | 11 |
| 1.3 Filament polymerization generates forces | 12 |
| 1.4 Various roles of molecular motors associated with filaments | 14 |
| 1.4.1 Motors associated with microtubules | 14 |
| 1.4.2 Motors associated with actin | 15 |
| 1.4.3 Link between F-actin and microtubules <i>via</i> molecular motors . | 16 |
| 1.5 Structure generation by cytoskeletal filaments | 18 |
| 1.5.1 F-actin | 18 |
| 1.5.2 Microtubules | 19 |

1.1 Spontaneous polymerization of polar polymers

1.1.1 Actin filaments nucleate spontaneously with the help of nucleators

Actin filaments (also called F-actin) are nucleated from monomers of G-actin, a globular protein of 42 kDa. The actin monomers spontaneously assemble to produce elongated and stable filaments with a diameter of about 7 nm. The resulting filaments are right-handed double-stranded helix of actin monomers [2]. Actin filaments are polar because one end of the filament ("barbed" or "plus" end) will grow faster than the other end ("pointed" or "minus" end) (Figure 1.1). This difference in velocity of polymerization is due to the assymetry of the actin monomer. The filament assembly is regulated by binding ATP on the actin monomer.

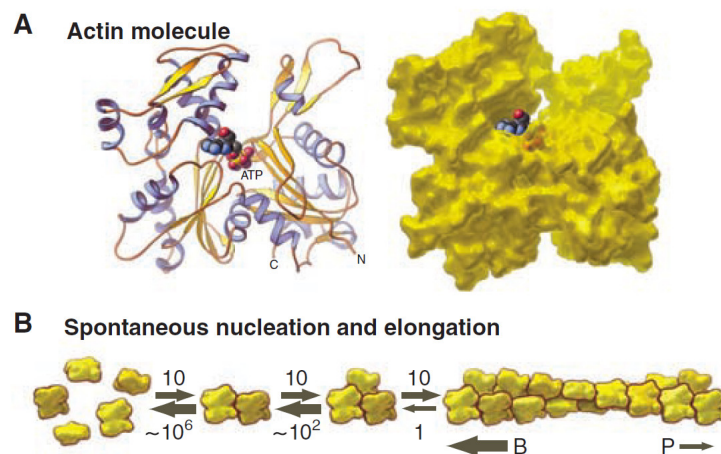


Figure 1.1: F-actin polymerization from monomers. The monomers spontaneously self-assemble to form a filament. **B** stands for barbed-end and **P** stands for pointed-end of the filament. *Extracted from [3].*

A lot of accessory proteins exist to change the topology of the filaments. For example, the nucleators can give rise to branched networks, parallel networks or anti-parallel networks. The motor proteins associated with actin (myosin is the most well known) can transport material through the network (myosin V) or create contractility (myosin II). In this section, we will describe some actin nucleators; motors will be described later in this chapter. Two nucleators will be described: the formins and the Arp2/3 complex.

Formins

Actin monomers can spontaneously assemble to elongate a filament but the polymerization rate is very slow because the formation of the filament is thermodynamically defavorable. Formin is a straight-actin-filament nucleator that nucleates actin filaments from monomers and then promotes their elongation by staying attached to the barbed end. FH1 and FH2 are two domains of formin which are widely present throughout living organisms. The FH2 domain dimerizes in a donut structure in which the two FH2 interact within each other. Usually the FH2 domain is sufficient to catalyse the nucleation. Thanks to *in vitro* reconstitutions of F-actin nucleation from formins, it was shown that

FH2 is processive and stays at the barbed end of the filament during the whole elongation process [4] (Figure 1.2). Formins also have a role of protection: by staying attached to the barbed end of the filament, they prevent the capping proteins from binding to the barbed end and therefore prevent severing of filaments [5]. It was also shown that formins can generate forces [6].

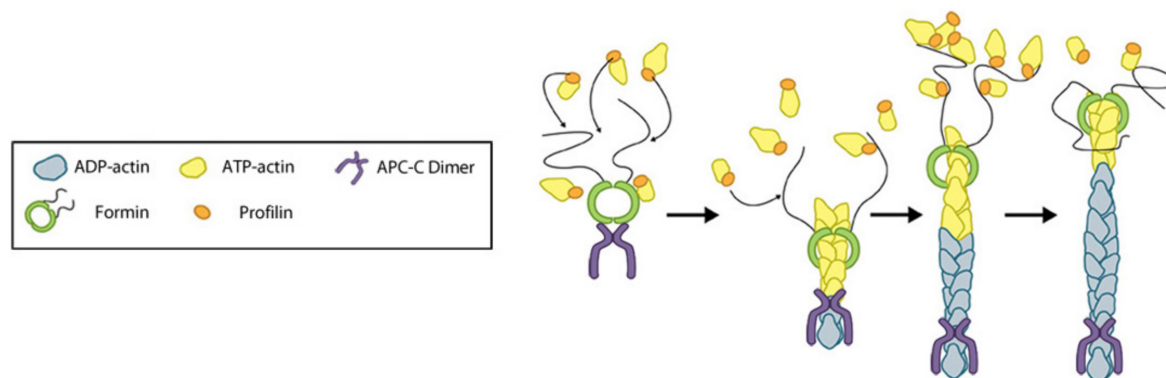


Figure 1.2: Mechanism of actin nucleation by formins. *From mechanobio.info website.*

Arp2/3 complex

The Arp2/3 complex allows the formation of branched networks. It was determined to be the main actor for the assembly of actin network at the leading edge of motile cells. The complex (formed of seven subunits) initiates the filament as a branch on pre-existing filaments. This branching is created with an angle of 70° ([7], Figure 1.3a). The WASP (Wiscott-Aldrich Syndrom Protein)/scar proteins activate the Arp2/3 complex via the VCA domain. The WASP proteins are regulated by the small G proteins (Rho, Rac, Cdc42). The combination of G proteins, WASP complex and Arp2/3 complex allows to spatiotemporally control the topology and the dynamics of F-actin (Figure 1.3b).

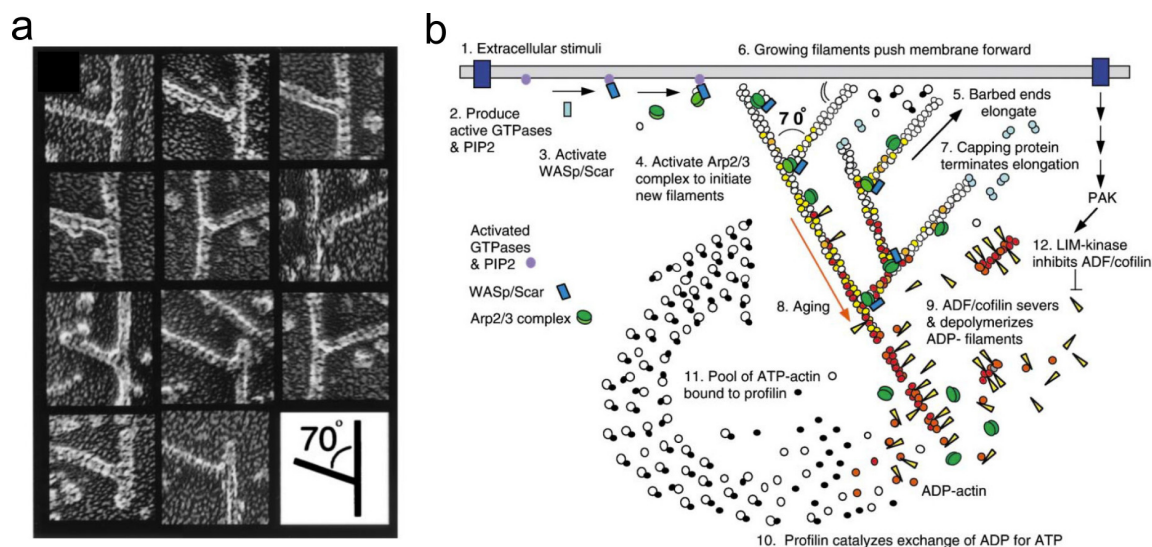


Figure 1.3: **a.** Electron micrographs of Arp2/3 complex on actin filaments. *Extracted from [7].* **b.** Coordination between G proteins, WASP and Arp2/3 for spatiotemporal control of actin nucleation and topology. *Extracted from [8].*

1.1.2 Microtubules are dynamic polar polymers

Microtubules are nucleated from the assembly of dimers of tubulin. A hetero-dimer of tubulin is a globular protein composed of one α -tubulin and one β -tubulin. Dimers of tubulin assemble to make a protofilament and the association of 13 protofilaments in a tube of 24 nm in diameter forms the microtubule (Figure 1.4a). Like actin filaments, microtubules are polar polymers: indeed the orientation of the dimers leads to a polymer with one extremity (+) that will polymerize faster than the other extremity (-). Microtubules are longer than actin filaments; this leads to different mechanical properties (described later). The formation of microtubules is not thermodynamically favorable; like nucleators for actin, accessory proteins for microtubules exist to promote the polymerization.

In addition, microtubules alternate between periods of rapid growth and disassembly, a process called dynamic instability. This stochastic non-equilibrium behaviour depends on the binding of GTP on β -tubulin (that points toward the fast-growing end of the filament) during the polymerization of the microtubule. Dynamic instability was first described by Mitchison and Kirschner [9]. They showed that this alternation between growth and shrinkage phases was a general property of microtubules and proposed that growing microtubules present a GTP cap whereas shrinking microtubules do not. This phenomenon is illustrated in Figure 1.4b. Polymerization dynamics of microtubules are critical for their biological functions.

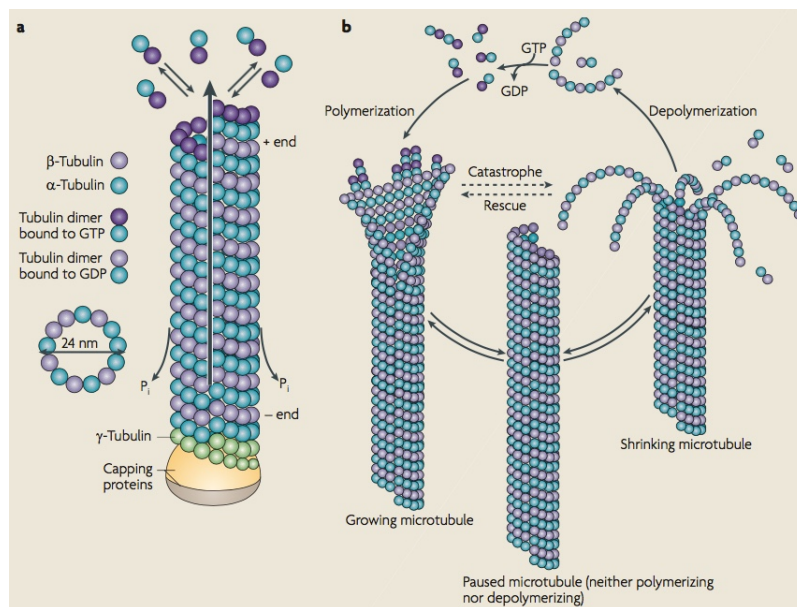


Figure 1.4: (a) Microtubule nucleation from dimers of tubulin added at the plus-end of the microtubule. (b) Microtubule polymerization is a dynamic process, alternating phases of growth and shrinkage. *Extracted from [10].*

In our case, we are mainly interested in the organization of microtubules into radial arrays, called asters. Astral microtubule arrays can be generated by local nucleation from MTOCs (MicroTubule Organizing Centers) [11] or by microtubule-motor self-organization [12] (described in Chapter 2). In MTOCs, the minus-ends of microtubules are anchored at the level of the MTOC and the plus-ends explore the cell space. In eukaryotic cells, the principal MTOC is the centrosome. It is composed of two centrioles and the pericentriolar material (Figure 1.5a). The two centrioles are oriented perpendicularly to each other.

In the pericentriolar material, γ -tubulin and other proteins can be found. γ -tubulin is a primer player in microtubule organization acting as a template for the correct assembly of microtubules. It is found in the γ -TuRC (γ -tubulin ring complex), which has a characteristic ring shape that is seen through electron microscopy (Figure 1.5b). The γ -TuRC stabilizes microtubules by capping the minus end and therefore preventing the depolymerization. γ -tubulin is found to localize in the centrosomes as well as in the non-centrosomal MTOCs; it is acting as a nucleator and provides stable binding sites for tubulin dimers (Figure 1.5). It was also found to be localized at the spindle during cell division, and therefore required for proper spindle formation.

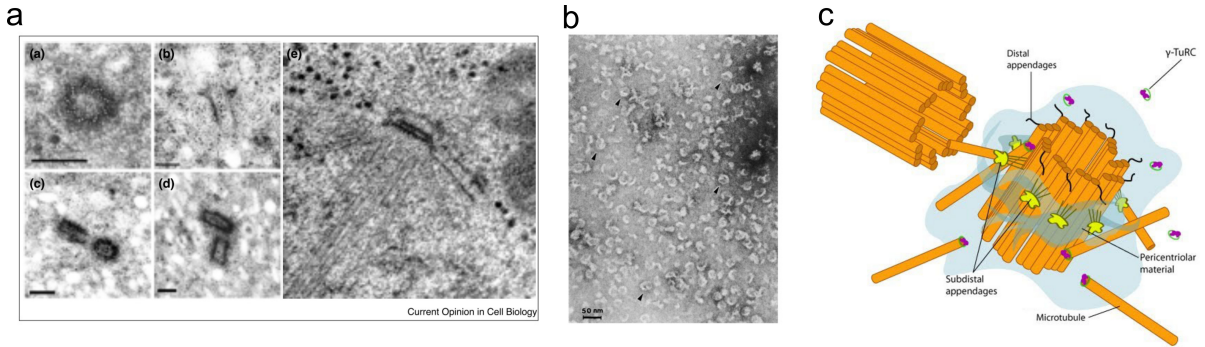


Figure 1.5: (a) Electronic Microscopy of centrosomes from mammalian cells. *Extracted from [13]*. (b) Electronic Microscopy of γ -TuRC. *Extracted from [14]*. (c) Scheme of centrosome organization. *Extracted from mechanobio website*.

In conclusion, both actin and microtubule filaments are polar. This property will be important for the topology of filament networks and for the transport along them. Both filaments have a helical symmetry which gives them straight properties. We will now show how the structure of these filaments has an impact on their mechanical properties.

1.2 Mechanical properties

The mechanical properties of the cytoskeleton fibers can be described by the **persistence length** (hereafter called L_p). The persistence length is the length on which a polymer is straight/rigid; it is related to the resistance of the filament to thermal fluctuations. At lengths greater than L_p , the filament will start to bend. From a geometrical point of view, it can be described as the length above which the angular correlation is lost (Equation 1.1 and Figure 1.6).

$$\langle \cos [\theta(s) - \theta(0)] \rangle = \exp \left(-\frac{s}{2L_p} \right) \quad (1.1)$$

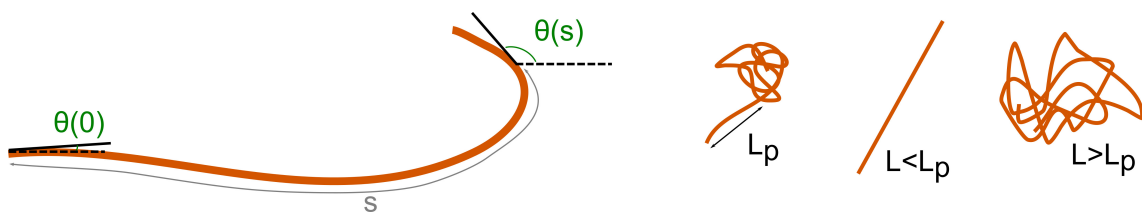


Figure 1.6: Definition of the persistence length.

L_p can be related to the flexural rigidity with the principle of Equipartition of Energy (Equation 1.2, E is the Young modulus and I the second moment of inertia of the cross-section).

$$L_p = \frac{EI}{k_B T} \quad (1.2)$$

The values of L_p for the cytoskeletal polymers used here are given in Table 1.2. Microtubules have a very long L_p (5 mm) compared to the cell length; they are rigid at the scale of the cell. To the contrary, actin filaments have a small L_p compared to the cell length; they are semi-flexible in a cell. We will see in the next chapters that these differences in L_p can be related to the role of each polymer in the cell.

| Polymer | L_p | Method | Reference |
|--------------|------------------|-------------------------------------|--------------------------------|
| Actin | 15 μm | Fluorescence Microscopy | Ott <i>et al.</i> 1993 [15] |
| Microtubules | 5 mm | Observation of thermal fluctuations | Gittes <i>et al.</i> 1993 [16] |

Table 1.1: Evaluation of persistence length for cytoskeletal polymers.

1.3 Filament polymerization generates forces

For both actin and microtubule filaments, polymerization takes place at the (+) end of the polymer by addition of a new monomer or dimer. When polymerization is located next to a wall (obstacle), it was shown that the polymerization can generate a force that will move the obstacle or the filament; this phenomenon is called the **Brownian Ratchet**.

The notion of Brownian Ratchet was first developed in physics by M. Smoluchowski (1912) and then by R. Feynman (1962). It was a thought experiment, stipulating that it was possible to extract useful work from random (thermal) fluctuations in presence of a thermal gradient. For the cytoskeleton polymers (and more precisely actin), it was first formalized by Peskin *et al.* in 1993 [17]. In this paper, they formulated a mechanistic theory to explain the force generated by a polymerization process of rigid filaments. They conclude that if the obstacle diffuses with a diffusion coefficient D , it will move, due to thermal motions. These oscillations of the obstacle will provide sufficient space ($x > 2\delta$) to incorporate a new monomer of actin (Figure 1.7). Then the polymerization of the filament is unblocked and the axial force generated by the polymerization is of an order of magnitude of 8 pN for a single actin fiber.

The polymerization velocity of a filament is dependent on the force applied at the growing extremity of the polymer (Figure 1.7). The relationship between the velocity and the force is given in Equation 1.3. $v(f)$ is the polymerization velocity (dependent on the force f); α and β are k_{on} and k_{off} respectively; $\omega = \frac{f\delta}{k_B T}$ is the dimensionless work done against the load in adding one monomer (the notations are the same as in Figure 1.7).

$$v(f) = \delta \left(\alpha \exp^{-\omega} - \beta \right) \quad (1.3)$$

Researchers set-up experiments to study the brownian ratchet for microtubules growing against barriers. Most of the time, the barrier is not fluctuating; it is the position of the assembling filament itself that is moving [18]. This does not change the ratchet behavior, as long as the fluctuations in the gap size are sufficiently fast and the applied load is not

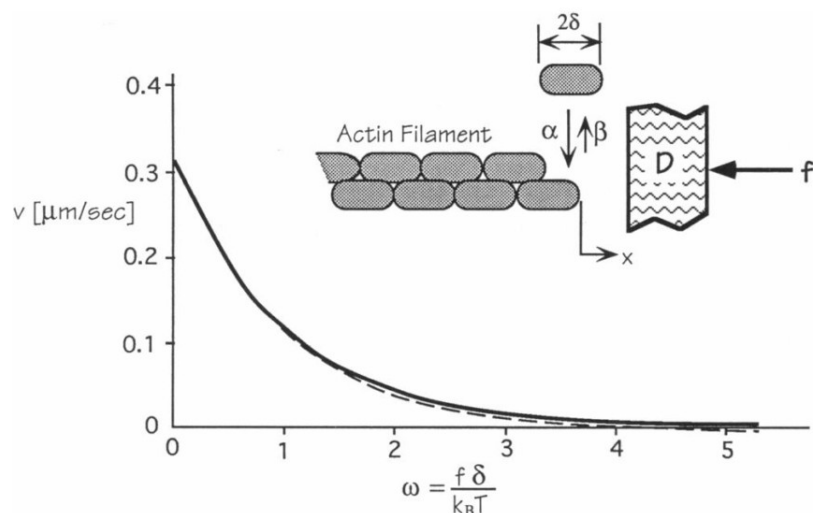


Figure 1.7: Brownian Ratchet model. *Extracted from [17].*

itself dependent on the gap size. Dogterom and Yurke [18] designed an assay to study how an opposing force reduces the growth velocity of microtubules. They showed that growth velocity of microtubules decreases with increasing force (Figure 1.8). Mogilner and Osner [19] have provided quantitative explanation of the experimental results of Dogterom and Yurke [18]. They considered microtubules as 13 crosslinked protofilaments growing independently from each other. This parameter led to a model that fit the experimental data.

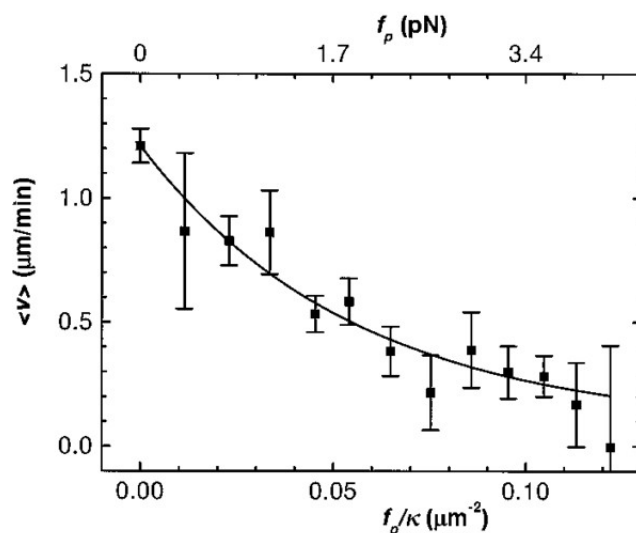


Figure 1.8: Microtubule growth velocity decreases as a function of force (*Extracted from [18].*)

Further into the mechanism of Brownian Ratchet, Janson *et al.* [20] performed experiments of microtubules growing against a barrier, and compared them, in experiments where the tubulin concentration was varied. Their results showed that when they changed the concentration of tubulin, they observed the same effect on the growth velocity as when they applied a force. Their results suggest that the force is just playing on the k_{on} (that

is dependent on the local concentration of tubulin dimers). This is a strong indication that force promotes catastrophes only by limiting the rate of tubulin addition at the (+) end of the microtubule.

Shrinking microtubules can also generate forces of several pN [21]. Pushing and pulling forces can be generated during either polymerization or depolymerization.

1.4 Various roles of molecular motors associated with filaments

Molecular motors convert energy obtained from ATP hydrolysis into mechanical work (chemo-mechanical transduction). Briefly, upon ATP binding, the head of the motor will undergo a conformational change that will allow the motor to move along its track. The best known role of motors is the cargo transport along cytoskeletal fibers inside the cell. Mechanical signal transduction can also be mediated by molecular motors, in hair cells of the inner ear for example [22]. Most molecular motors have a directional movement (movement toward the plus or minus end of polarized actin or microtubule). Two behaviors of motors can be distinguished: a motor can move along a track for a long distance without detaching; this behavior is called processivity. A non-processive motor is a motor that will detach from the track usually after one catalytic cycle. Non-processive motors often work in group.

Structural data from electron microscopy and dynamic data from single-molecule techniques have made significant contributions to the understanding of the behavior of molecular motors. For example, Atomic Force Microscopy (AFM), single-molecule fluorescence microscopy and optical tweezers have been widely used to evaluate key parameters of molecular motors (force generated by a single motor or step size for example). Single-molecule experiments confirmed that motors undergo conformational change while attached to the filaments [23].

1.4.1 Motors associated with microtubules

Microtubule motors are crucial for the assembly of microtubule arrays in interphase or during metaphase with the spindle assembly. Most studied microtubule motors are dyneins and kinesins. Kinesins move toward the (+) end of microtubules whereas dyneins move toward the (-) end of microtubules. An illustration of these motors is given in Figure 1.9. Kinesins and dyneins are known to mediate rapid and directed intracellular transport of material. This overcomes the limits of diffusion which becomes a highly inefficient mechanism to transport materials over long distances, in a crowded environment such as the cell.

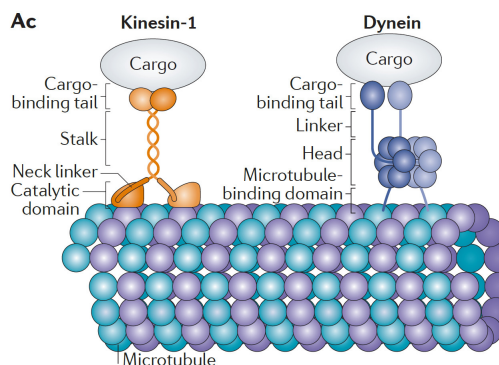


Figure 1.9: Scheme of kinesin and dynein on a microtubule. *Extracted from [23].*

Dynein

Microtubule motors are essential for bringing microtubule ends together, to focus them into poles. Verde *et al.* [24] showed that taxol aster assembly occurs through a reorganization of microtubules sliding along each other, under the action of cytoplasmic dynein (model given in Figure 1.10). This *in vitro* result was interesting to put in perspective with the data showing that dynein is strongly enriched at the spindle poles. Some motor-associated proteins, such as NuMA also play an important role in pole focusing.

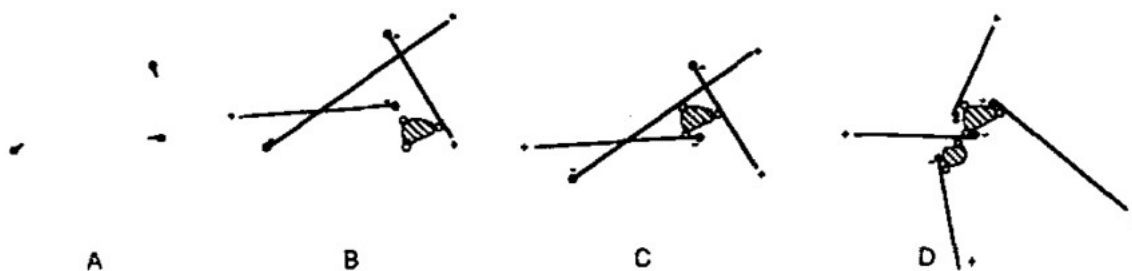


Figure 1.10: Model for taxol aster assembly in metaphase egg extracts. *Extracted from [24].*

Kinesin-5

In most organisms, kinesin-5 was found to interconnect microtubules in the central space of the spindle where it drives spindle flux. It was shown to be able to slide antiparallel microtubules. This motor walks slower than the microtubule grows. It is an important parameter for preventing the separation of the half-spindles, which would result in spindle collapse.

1.4.2 Motors associated with actin

Best known actin-based motors are myosins. Two types of movement can be exerted by myosins: they can generate forces between actin filaments that will produce contraction (essential during cell migration and cell division), and they can associate with cargos and move them along actin filaments over short distances [3]. Two myosins that play an important role in our systems, myosin II and myosin V, are described below:

Myosin II

Myosin II is involved in the force generation in cellular morphological changes. In physiological conditions, myosin II molecules assemble into multimeric assemblies that are able to generate gliding of actin filaments past one another (Figure 1.11a). The coexistence of actin and myosin filaments leads to contraction of the network (Figure 1.11b). It was shown that the addition of a cross-linker to myosin II and actin filaments is necessary to generate sufficient forces of contraction at physiological ATP concentrations [25].

Myosin V

Myosin V is a processive motor: it moves along its track for many successive chemo-mechanical cycles by alternating keeping one head bound to the track while moving forward the other head (Figure 1.11c,d). This motor step is about 36 nm (corresponding to the distance between two binding sites on the actin filament); it can perform hundreds of steps before detaching [26]. In mouse oocytes, myosin V covers actin vesicles and allows them to actively move in the cell [27].

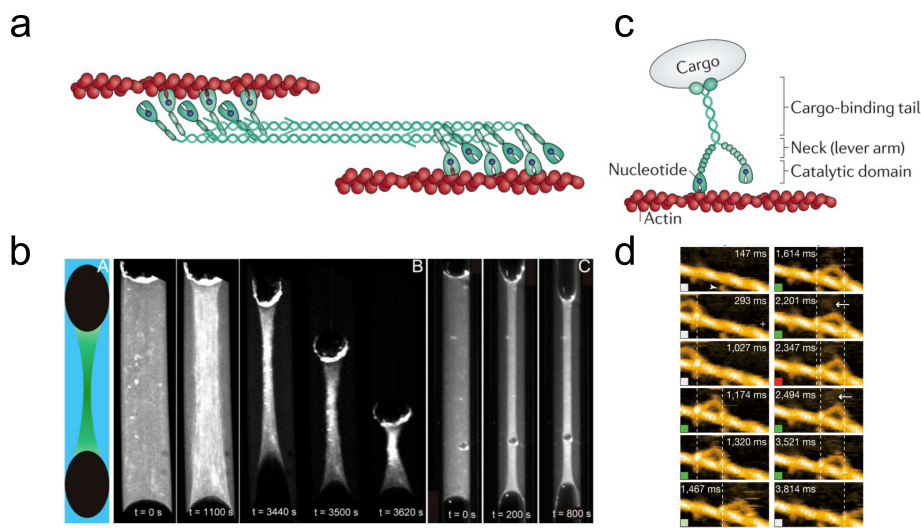


Figure 1.11: (a) Scheme of myosin II organization in supramolecular assembly. (b) Contraction of actomyosin networks in *Xenopus* egg extracts. (c) Scheme of myosin V organization. (d) AFM images showing processive movement of myosin V on an actin filament. Adapted from [23, 25, 28].

1.4.3 Link between F-actin and microtubules *via* molecular motors

In linking actin and microtubules cytoskeleton with motor proteins, two options can be considered: existence of unconventional motors that will link both actin and microtubule cytoskeleton, and existence of a cooperation between the known motors that associate with actin or microtubules. Both options are present in nature. Some example follow:

Cooperation between known molecular motors

Huang *et al.* [29] showed that myosin V can interact with a microtubule-based transport motor (KhcU, mouse ubiquitous kinesin heavy chain). The authors showed that the two molecular motors can bind to each other and form a complex *in vitro* and *in vivo*. Their results prove that the transport of vesicles can be coordinated through the direct interaction of motor molecules from different transport networks. This study introduces the concept of "hetero-motor" complexes; in this model, the activity of the complex is regulated so that only one motor in the complex is dominant at any given time. The advantage of such a complex is that a vesicle can be bound to only one complex and be transported on both actin and microtubule tracks. A vesicle with multiple motors will be able to change its filament track easily just by switching motor activity. Such a combination gives the opportunity to the vesicle to be transported by microtubules in an actin-poor region and vice versa.

In *Xenopus*, melanophores (pigment organelles) can be transported by microtubule or actin motors. Some studies [30, 31] suggest that the granule transport occurs through a coordinated microtubule- and actin-based transport. Kinesin, dynein and myosin V cooperate in the dispersion of pigment granules, while during aggregation, myosin V is switched off. Therefore, both actin and microtubule networks are required for proper melanosome distribution in melanophores.

Myosin X: an unconventional motor that links actin and microtubules

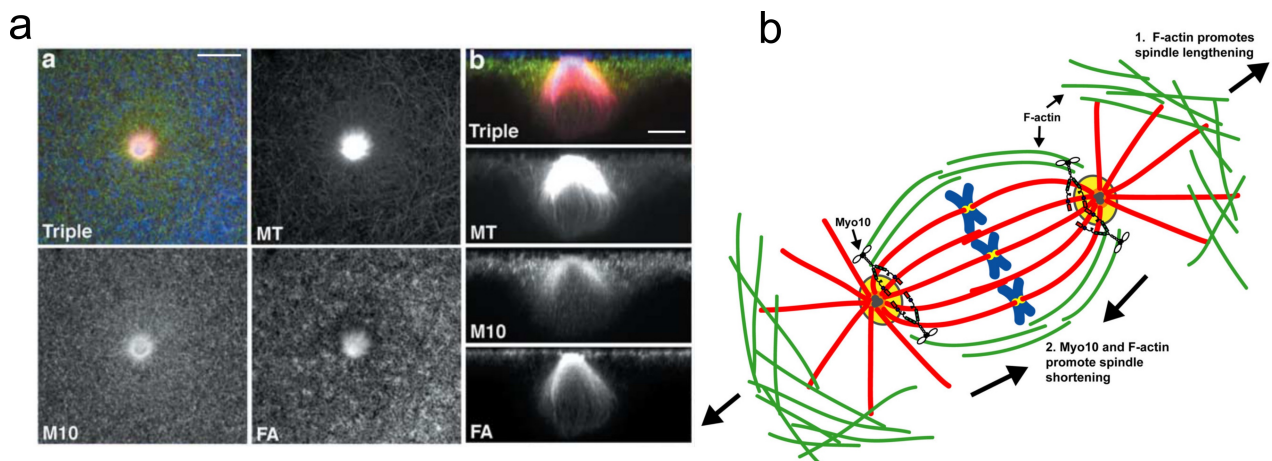


Figure 1.12: (a) Co-localization of myosin X with pole of meiotic spindle and actin cortex. *Extracted from [32]*. (b) Model for spindle length regulation by F-actin and myosin X. *Extracted from [33]*.

Myosin X was first described by Weber *et al.* [32] and was shown to be a potential microtubule-F-actin linker *in vitro* and *in vivo*. Myosin X localizes in the region where the spindle contacts with the F-actin cortex (Figure 1.12a) and was shown to be required for the correct positioning of the nucleus in *Xenopus* oocytes. In addition, disruption of myosin X severely impaired meiotic spindle assembly, showing that myosin X is essential for proper F-actin-meiotic spindle association. Later Woolner *et al.* [33] showed that myosin X is essential for proper spindle anchoring, normal spindle length, spindle pole

integrity and progression through metaphase. In addition, their study also detailed the role of F-actin in the assembly of mitotic spindle (this aspect is covered in **Chapter 5**). Indeed, they showed the existence of dynamic actin cables within the mitotic spindle and that F-actin and myosin X play both overlapping and distinct roles during mitosis (Figure 1.12b). More recently, Kwon *et al.* [34] showed that myosin X is required, in addition to dynein, to orient and position centrosomes and mitotic spindles in eukaryotic cells.

Other molecular motors linking actin and microtubules will be introduced in **Chapter 5** (more specifically regarding spindle formation and robustness).

1.5 Structure generation by cytoskeletal filaments

By establishing long-range order in the cytoplasm, the cytoskeleton controls the physical properties of a cell. Different architectures of networks will determine the mechanical stiffness, the dynamics of their assembly, their polarity, and the type of molecular motors with which they associate. The cytoskeletal network also has a central role in transmitting compressive and tensile stresses and in sensing the mechanical micro-environment.

1.5.1 F-actin

The actin cytoskeleton has a wide variety of architectures that are associated with specific functional structures. Different network architectures forming different structures found in cells are illustrated in Figure 1.13.

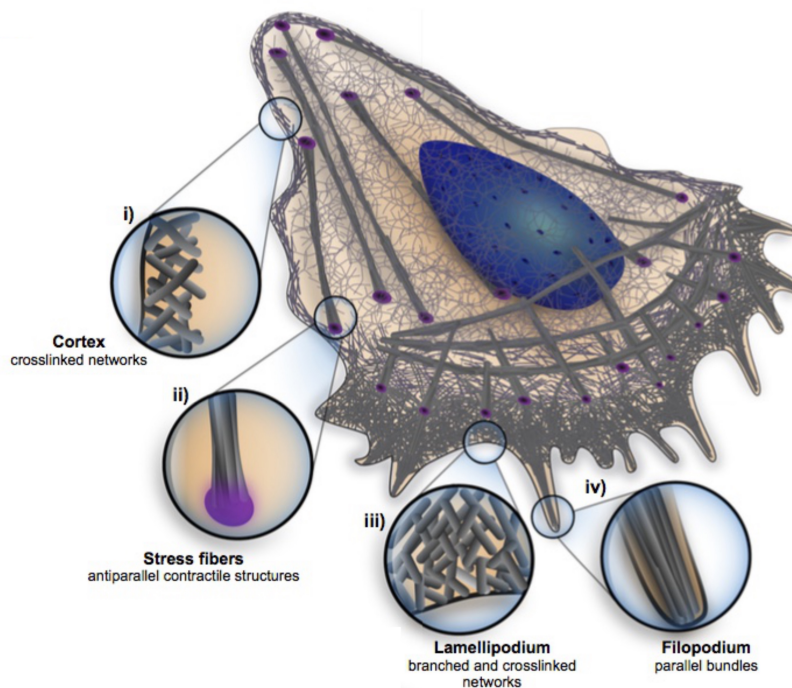


Figure 1.13: Examples of actin architectures found in cells. *Extracted from [2].*

Just beneath the plasma membrane, a thin actin layer called **cortical network** can be found. Because of its ability to carry tension loads in multiple directions, this type of

network is predominant for the maintenance of cell shape. Its contractile behavior is due to the presence of myosin II in the network.

The **stress fibers** are formed from anti-parallel bundled actin filaments, stabilized with cross-linkers. They connect the cell cytoskeleton to the extracellular matrix via focal adhesion sites. The antiparallel filaments can also be found in muscle cells or in the contractile ring acting during cytokinesis.

The branched networks are mainly observed at the leading edge of motile cells, in a structure called **lamellipodium**, that forms a quasi-two-dimensional network. The main mode of assembly of the lamellipodium is *via* the Arp2/3 complex.

The **filopodia**, composed of parallel bundles of filaments, are found at the front of the cell and are important for directional response of the cell when sensing its environment. In parallel bundles, all the barbed ends are oriented in the same direction and the filaments are maintained in close contact with cross-linking proteins (α -actinin or fascin, for example).

Another type of actin network has been widely described recently: the **cytoplasmic actin** (also called bulk actin) network. This kind of meshwork is predominant in large cells like oocytes. The cytoplasmic actin has been shown to be essential for the long-range transport in large cells. For example, in starfish oocytes, this cytoplasmic F-actin meshwork was shown to be essential to gather the chromosomes and therefore ensuring proper spindle formation (Figure 1.14, [35, 36, 37]). Here the actin acts as a net: the chromosomes are trapped in the contractile structure and passively gathered and transported. In mouse oocytes, the cytoplasmic actin meshwork was shown to be the driving force of spindle migration during meiosis. This phenomenon will be described later in the manuscript (Chapters 2 and 6).

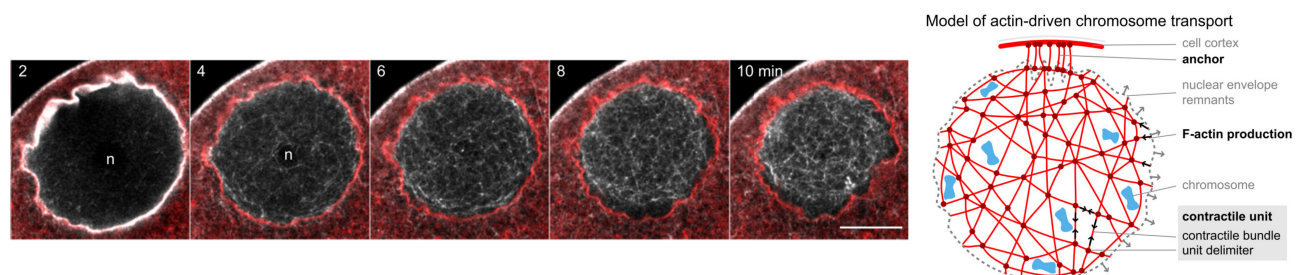


Figure 1.14: Chromosome gathering in starfish oocytes is mediated by cytoplasmic actin. Left: visualization of the contractile actin network. Actin (grey) is labelled with GFP-utrophin. Endomembranes are shown in red. Right: model for chromosome congression. Adapted from [36].

1.5.2 Microtubules

Microtubule patterns observed *in vivo* can be categorized in four classes: asters, antiparallel overlaps, bundles and contractile networks (Figure 1.15). These patterns, alone or combined give rise to a wide variety of microtubule architectures in cells.

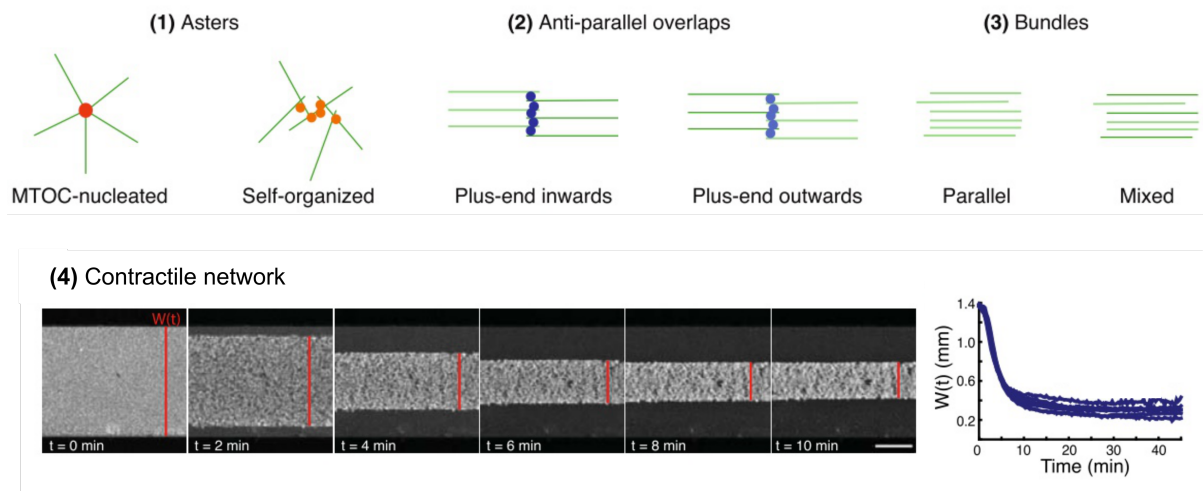


Figure 1.15: Microtubules patterns observed *in vivo*. Adapted from [38, 39].

Asters are involved in spindle formation. MTOC-nucleated or self-organized asters are found in spindles from various organisms. Anti-parallel overlaps are also found in the spindle. Sliding of those microtubules permits a correct segregation of the chromosomes. In addition, dynamic instability allows the microtubules to search the cellular space quickly.

Radial arrays of microtubules function as highways for intracellular traffic. The transport of proteins and organelles in the cell takes place on long parallel bundles of microtubules.

Bundles of microtubules are also important for the maintenance of cell shape and cell polarization.

Contractile networks of microtubules have recently been described quantitatively [39]. Microtubules nucleated in egg extracts and confined in millimeter-wide channels slowly contract in a dynein-dependent manner.

In conclusion, F-actin and microtubules share similar characteristics of assembly. Indeed, both filaments assemble from monomers in polar polymers. These assemblies do not have the same mechanical properties: microtubules are stiffer than actin filaments. The motors associated with the filaments are specific for each family, even if the motors share the same biochemical characteristics. The cytoskeleton filaments can be considered as dynamic supramolecular assemblies. These polymers are very dynamic because of their intrinsic properties (as discussed earlier in this chapter). These dynamic properties are very important in the structures generated, because they allow the polymer to rapidly adapt to an environmental change. For example, the dynamic instability of microtubules plays a preponderant role in the spindle and especially during anaphase, where the step of chromosome separation is very fast. The metaphase spindle is a dynamic structure, out of equilibrium; this can be observed with speckle microscopy (Figure 1.16a, [40]). The same dynamic behavior of actin is very important at the front of migrating cells. Using FRAP (Fluorescence Recovery After Photobleaching) on the actin labelling at the front of a cell, researchers were able to see the fast turnover of actin (Figure 1.16b, [41]).

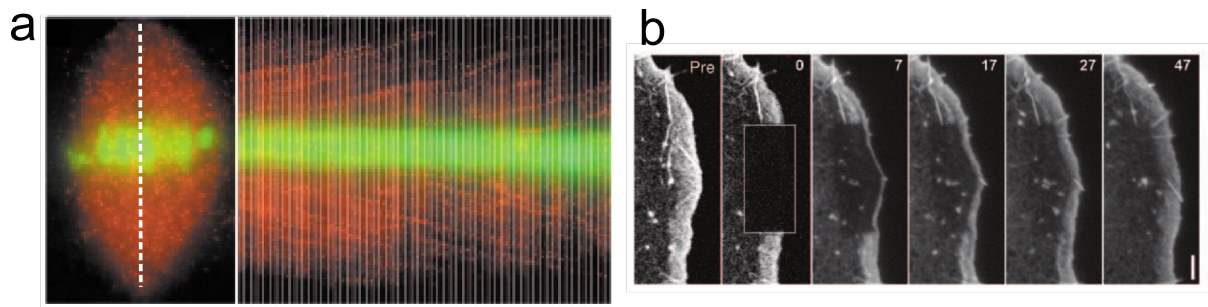


Figure 1.16: Structures assembled from actin and microtubule are dynamic. (a) Visualization of a spindle with fluorescent speckles. Tubulin is in red and the chromosomes in green. On the left the whole structure is represented. On the right, a kymograph taken on the white line is shown. (b) FRAP experiment on fluorescent actin at the front edge of a cell. Adapted from [42, 41].

The filaments discussed here assemble in structures that are very important for the biological function of the cell (Figure 1.17).

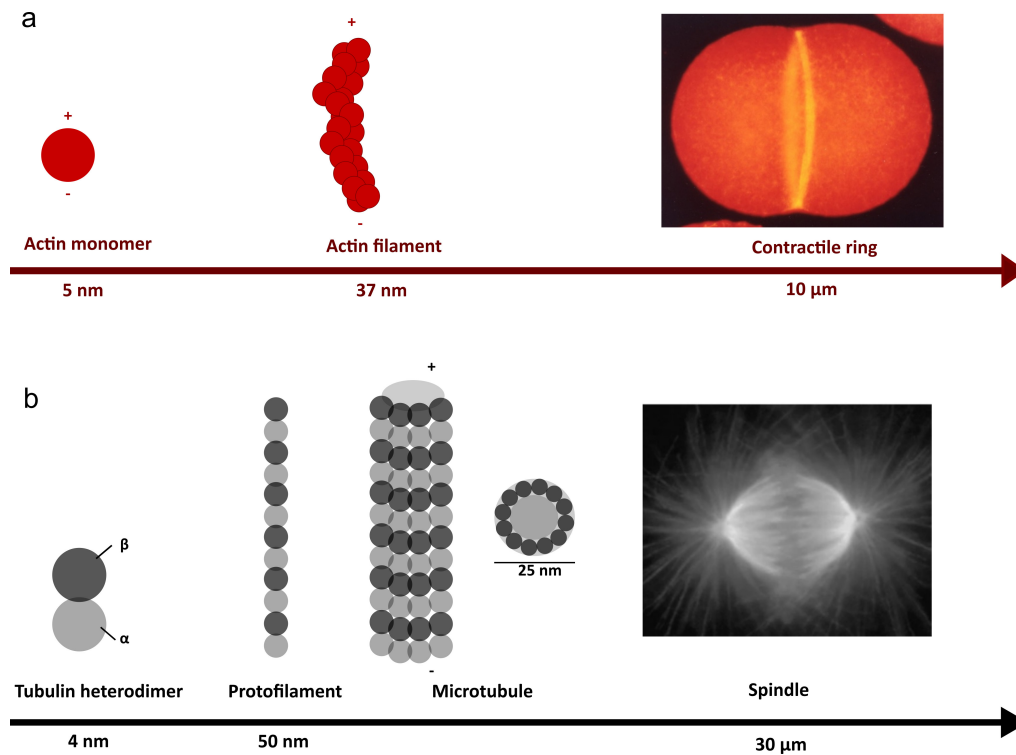


Figure 1.17: Length scales comparison of F-actin and microtubules polymerization and structure generation.

Chapter 2

Choice of a Model System: Different Approaches to Answer a Biological Question

There can be multiple ways to address a biological question. In this chapter, we will describe different ways researchers chose to answer important scientific questions. First, we will present the top-down and bottom-up approaches, and then we will present the confinement of biomimetic systems which has enabled researchers a closer view of biological systems. In the last part of this chapter, we will present the model systems we have been working on during this PhD work: *Xenopus* egg extracts and mouse oocytes.

Contents

| | | |
|------------|---|-----------|
| 2.1 | Top-down and bottom-up approaches | 24 |
| 2.1.1 | Top-down approaches | 24 |
| 2.1.2 | Bottom-up approaches | 25 |
| 2.2 | Confinement of biomimetic systems: putting back the boundary in the equation | 27 |
| 2.2.1 | Methods of confinement | 27 |
| 2.2.2 | Confinement of purely <i>in vitro</i> systems | 29 |
| 2.2.3 | Confinement of egg extracts | 32 |
| 2.3 | Model systems used in our studies | 35 |
| 2.3.1 | <i>Xenopus</i> egg extracts | 35 |
| 2.3.2 | Actin-intact egg extracts | 36 |
| 2.3.3 | The mouse oocyte | 37 |

2.1 Top-down and bottom-up approaches

2.1.1 Top-down approaches

Historically, biology has been a science of observation: the biologist saw something in the nature and tried to understand it, by observation. This would be the first step of what we can call "top-down" approach: watch a biological event in its entirety and try to understand it. The observation can be done by microscopy. High precision information about the structure can be obtained with electron microscopy. Fluorescence microscopy has made great advances in the last 30 years, and the development of fluorescent proteins opened new doors in the visualization of biological systems [43]. Using these new techniques, biologists are able to perturb a system. This is a very important aspect of the top-down approach: perturbing the system and watching its response to the perturbation, may provide very precise information regarding biological phenomena.

Classical methods to perturb a biological system are the following: drugs (chemical perturbation); mutants and siRNA (genetic perturbations); patterning (physical perturbation); optogenetics and magnetogenetics (spatiotemporal perturbations). Two examples where top-down approaches have helped to understand the role of F-actin during cell division follow:

Mutants to study the role cytoplasmic F-actin in spindle positioning

Leader *et al.* [44] generated and characterized a formin2-deficient mouse. Using data from this mouse, they demonstrated that formin-2 was required for the progression of the oocyte in meiosis and that it was a key player for asymmetrical positioning of the spindle (Figure 2.1a). They showed that in formin2-deficient mice, the polar body extrusion did not occur in 97 % of the cases. Later, Dumont *et al.* [45] used videomicroscopy to show that formin-2 controls the spindle migration to the cortex during the first meiotic division and is required for proper cytokinesis (Figure 2.1b).

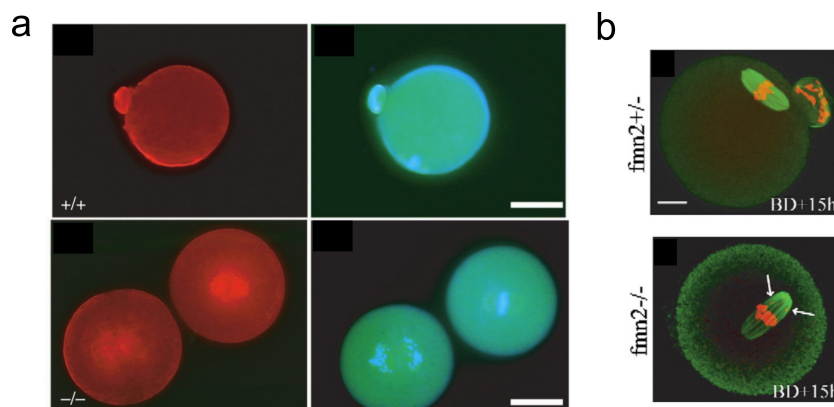


Figure 2.1: Phenotype observed in oocytes from control (top) or formin-2 deficient (bottom) mice. (a) Oocytes fixed for actin (red), tubulin (green) and chromosomes (blue). (b) Immunofluorescence of oocytes stained for microtubules (green) and chromosomes (ref). Adapted from [44, 45].

Micro-patterning to study the role of extracellular matrix in spindle positioning

Théry *et al.* [46] addressed the question of spindle orientation in mammalian cultured cells by using micro-patterning. With the combination of drugs and micro-patterning approaches, they showed that the determination of spindle orientation in cultured cells is largely dependent on the spatial distribution of the extracellular matrix and that membrane-associated filamentous actin was necessary to guide spindle orientation (Figure 2.2). Another advantage of patterning is that statistical analysis is possible because the shape of the cell is defined (in opposition with the diversity of forms that a cell can take in nature). Therefore, by aligning the cells, a "median cell" can be defined (to study the distribution of the spot of entry of a pathogen in a cell, for example). Another similar approach was described by Minc *et al.* [47] and consists of placing sea urchin oocytes in microfabricated chambers to study the influence of the geometry on their division. Since oocytes are bigger objects than cultured cells, a 3D confinement is necessary to study the impact of geometry on their division.

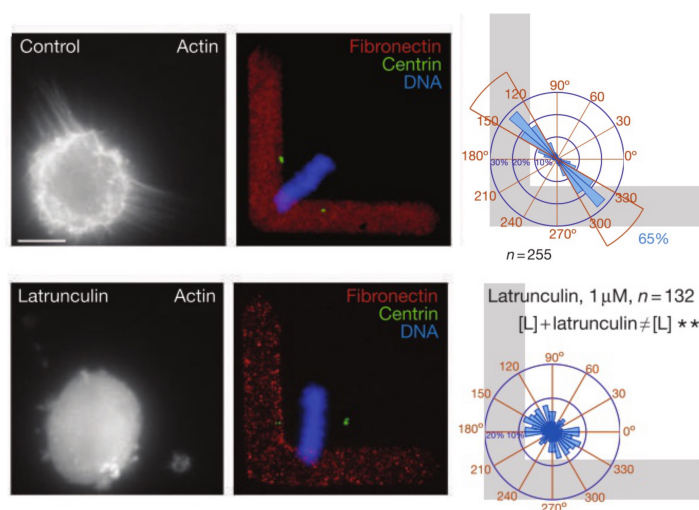


Figure 2.2: Patterning of adherent cells to show the influence of extracellular matrix and actin on spindle positioning. *Adapted from [46].*

2.1.2 Bottom-up approaches

Another way to analyze a biological system is the bottom-up approach. This can be seen as the opposite of the top-down approach. In biomimetic approach, a system is reconstituted from purified components. The bottom-up approach permits to mimic a biological system and then to identify the key molecular actors necessary and sufficient for the system. A precise tuning of the concentration of molecular actors is possible. In addition, these reconstituted systems often offer the opportunity to make quantitative measurement of important biological or physical parameters. Bottom-up approaches, also called *in vitro* reconstitutions, allow the systematic understanding of basic principles governing the organization of cytoskeleton architectures and provide a direct way to test the predictions of theoretical models. In the following sections, we will describe two examples where the bottom-up approaches helped to identify key molecular actors of biological processes where cytoskeleton is predominant.

Listeria propulsion reconstitution

Listeria and *Shigella* are bacteria that are known to bypass the actin signalling system of a cell to propulse themselves. Loisel *et al.* [48] used pure components of the actin cytoskeleton to reconstitute sustained movement of bacteria *in vitro*. By using a reconstituted motility medium they found that cofilin, an actin depolymerizing factor, is required in addition of the Arp2/3 complex for motility. Actin depolymerizing factors can increase up to 125 fold the filament turnover and increase the steady-state amount of ATP-G-actin, two properties that are essential for actin-based propulsion of those bacteria. After that, Cameron *et al.* [49] used ActA (identified to be important for actin-based motility) and coated it on beads. The simple fact of coating ActA on beads induces a movement whose rate is similar to the one of *Listeria* (Figure 2.3a). The phenomenon that they observed was a spontaneous symmetry breaking that could be explained by the fact that when actin filaments grew at the bead surface, material would accumulate. The stress will then increase in the network up to a critical value that will induce its rupture. This rupture creates an asymmetry in the pressure applied on the bead and as a consequence, the bead is displaced. In this system, the polymerization of F-actin is sufficient to generate and power large scale motion in viscous media. It was also possible to obtain the quantitative parameters of actin polymerization from the observation of an oil droplet (with actin polymerization promoters on its surface) deformation [50]. This was a demonstration that the mechanism of force generation is due to the elastic stresses exerted by the actin comet gel. Other reconstitution of actin polymerization around fluid vesicles gave a better understanding of the elementary steps of filament branching [51]. Reconstitution of giant unilamellar vesicles (GUVs) actin-based propulsion in controlled biochemical conditions allowed to show that concentration of Arp2/3 complex controls the transition between two types of propulsion.

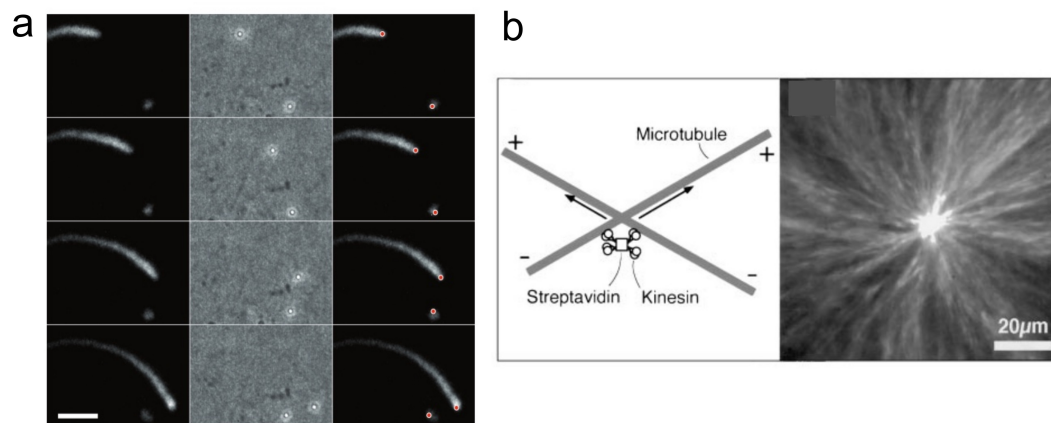


Figure 2.3: Two examples of bottom-up approaches. (a) ActA-coated beads moving in *Xenopus* egg extracts. (b) Self-organization of asters from stabilized microtubules, tetrameric kinesin and ATP. Adapted from [49, 12].

Self-organization of microtubules and motors

Nédélec *et al.* [12] used an extremely simplified system to reconstitute the formation of microtubule-based structures. By putting together tubulin, tetrameric kinesin and ATP, they managed to nucleate asters (Figure 2.3b). By changing the initial concentration

of the components, drastic changes of morphology could be seen: low concentration of kinesin induces vortices whereas higher kinesin concentration induces asters; very high kinesin concentrations induced microtubule bundles. Changing the ratio between the components and adding a second motor also allowed them to see a wide variety of structures [52]. Thus, three elements are sufficient to produce a large but limited variety of structures (asters, vortices or networks of poles connected by aligned microtubules). All the patterns were also observed with numerical simulations based on Langevin dynamics [53]. Therefore, cytoskeleton polymers reconstituted with binding proteins can spatially organize on the micrometer scale in the absence of physical confinement, with the polymer itself serving as scaffold for self-assembly. The kinetic parameters describing the properties and interactions of the components are sufficient to predict the structures produced by the ensemble.

2.2 Confinement of biomimetic systems: putting back the boundary in the equation

For experiments in bulk solution, the reaction space is of infinite size; on the contrary, in cells, the dimension of the reaction space is of the order of the persistence length of the cytoskeletal polymers. Because of the confinement of a biomimetic system within a membrane or a close compartment, the dimension of the reaction space is reduced to the order of magnitude of the persistence length. The boundary condition is added to guide the organization of the system. Confinement also imposes a limited amount of components, similar to what is found in biology, especially for isolated cells. Therefore, the morphology or the kinetics of a system can be determined by the fact that there is a limited amount of components in the confining volume. In the following sections, we will present examples of confined *in vitro* systems in 2D or in 3D; and will present recent studies regarding the confinement of *Xenopus* egg extracts in 2D or in 3D.

2.2.1 Methods of confinement

2D confinement: supported lipid bilayers

The plasma membrane plays a key role in many biological processes (cell division, cell migration *etc.*). The supported lipid bilayers are a powerful system that can be used to mimic the plasma membrane. They consist of a glass coverslip functionalized with various lipids that are separated from the substrate by a thin layer of water to allow lateral mobility of lipids. They are very stable and can be easily imaged with TIRF microscopy.

3D confinement

Chambers: Microfabricated chambers have been used for a long time to create 3D confinement of molecules. They are constructed using lithography by patterning a glass coverslip with layers of silicon, for example. The walls of the chamber can be coated with specific proteins [54].

Vesicles and droplets: 3D confinement can also be done in spherical compartments. Two main ways of generating those spherical compartments exist: formation of water-in-

oil emulsions, generating droplets; or encapsulation of water in a lipid bilayer, generating vesicles (Figure 2.4).

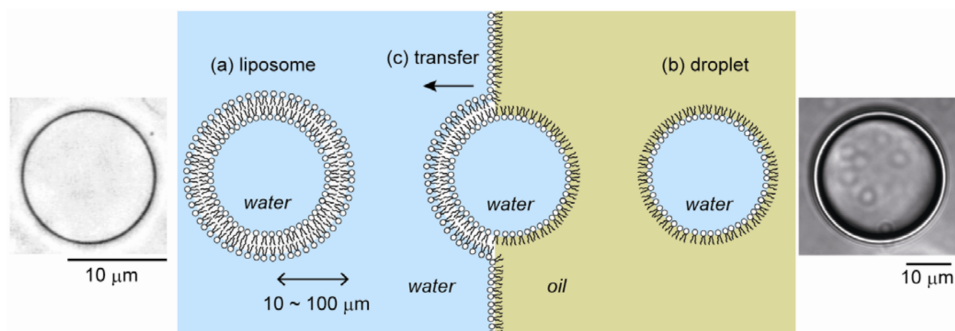


Figure 2.4: Principle of liposomes and droplets formation. *Extracted from [55].*

Droplets are generated *via* a water-in-oil emulsion. Phospholipids are usually dissolved in the oil to stabilize the interface of the emulsion. They act as a surfactant, reducing the surface tension between the oil and water phases, and so the droplet coalescence [56].

Vesicles (also called liposomes) are based on a lipid bilayer made of phospholipids. For the vesicles, the outside medium is the same as the inside medium of the vesicle. If vesicles are closer to an "artificial cell" because of their bilayer interface, they are more complicated to prepare than droplets. Pautot *et al.* [57] developed a method for systematically engineering vesicles with asymmetric bilayers. Table 2.1 recapitulates the properties of droplets and vesicles as well as their mode of formation.

| | Droplets | Vesicles (liposomes) |
|---------------------------------|--|--|
| Modes of formation | Shearing, sonication, microfluidics | Electroformation, sonication, freeze-drying, centrifugation |
| Size control? | Yes (<i>via</i> microfluidics) | Possible with microfluidics |
| Compatible with microfluidics? | Yes. Possibility of reagent mixing, droplet splitting, sampling, fusion, dilution, mixing, sorting | Yes but heavy procedure |
| Permeable? | No | Yes. Large polar molecules require the formation of pores through the membrane. |
| Shape | Spherical and rigid envelope | Deformable membrane. Cholesterol insertion increases the bending modulus, making the vesicles stiffer. |
| Encapsulation of biomolecules ? | Easy without denaturation | Dilution of biomolecules during the preparation of liposomes during the electro-formation. |

Table 2.1: Comparison of formation and properties of vesicles and droplets.

2.2.2 Confinement of purely *in vitro* systems

2D confinement

Reconstitution of the MinD system. A striking example for the 2D confinement of a purely *in vitro* system is the reconstitution of Min waves on a supported lipid bilayer that mimics the cell membrane [58]. In bacteria, the proteins MinC, MinD and MinE oscillate between the poles of the bacteria and find the cell center to position the division septum. These proteins are crucial for accurate cell division and were found to spontaneously form planar surface waves on a flat membrane *in vitro* (Figure 2.5a). With an *in vitro* system, a component can be easily removed. The *in vitro* system is also very convenient to play on the concentration of the proteins. Therefore, the authors showed that without MinE, MinD was homogeneously distributed on the membrane. On that basis, the authors explained how the presence of MinE in the system leads to surface waves. In this example, we see that a complex biological behavior can emerge from a limited number of components (here two proteins), a membrane and ATP. By patterning the membranes (and therefore being able to study the influence of geometric boundary on the wave pattern), Schweizer *et al.* [59] studied the influence of spatial confinement on the self-organization of the Min system. They found that the Min waves travel along the longest axis of the pattern (Figure 2.5a).

Patterning of actin nucleators. Reymann *et al.* [60] showed for the first time that it was possible to control the actin polymerization in space and time with micropatterning. By absorbing pWA on patterns generated with UV light, they showed that geometric barriers can influence the shape and dynamics of actin networks (Figure 2.5b). The nucleation geometry is important for the network architecture. This is reminiscent of observations made in cells where the cell boundary can dictate local reorganization of actin networks.

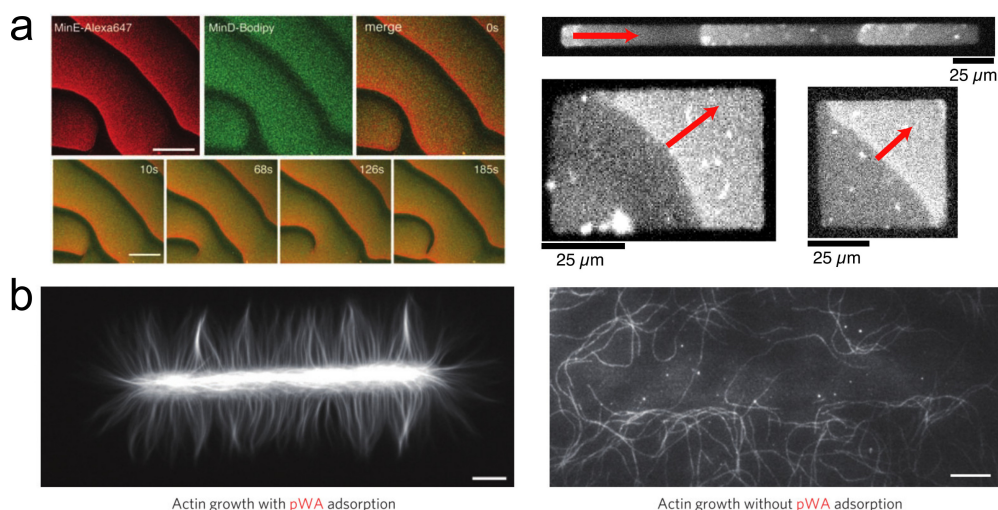


Figure 2.5: Examples of 2D confinement of *in vitro* systems. (a) Reconstitution of the Min waves on a supported lipid bilayer. Right: the arrows indicate the propagation direction of the wave. (b) Spatial organization of pWA influences the organization of actin network. Adapted from [58, 59, 60].

3D confinement

This type of confinement consists in encapsulating a biomimetic system in a 3D structure that can be, for example, a chamber or a droplet. The 3D confinement is an important parameter to take in account because in nature, most reactions are compartmentalized in cells or organelles; confinement in droplets can be used to recreate artificial compartments that mimic the volume of the cellular environment. The development of microfluidic technologies in the last 15 years has led to the development of cutting-edge technologies on droplets (generation of huge number of droplets, tunable/controllable-size). Microfluidic systems enable droplets to be generated and manipulated in a controlled and sophisticated manner. For example, in an automated microfluidic device, droplets can be generated at a rate of up to 10000 per second to form highly monodisperse emulsions. Thanks to microfluidics, it is possible to freely determine and regulate the content of the compartment as well as the number of compartments. Confinement of proteins or cell extracts is discussed below. Though, confinement of DNA and RNA is also possible and is a very powerful tool for genomics (cell-free translation for example) [61, 62].

Actin reconstitution. 3D reconstitution of actin has been a popular area of investigation. The actin cortex or the actin constriction ring, two structures that are very important for cell division have been studied.

Actin cortex reconstitution. The development of techniques to generate liposomes led to breakthroughs in the reconstitution of actin cortices. Pontani *et al.* [63] managed to mimic the actin cortex by activating actin polymerization specifically at the inner liposome membrane. The goal was to build a controlled system for studying cell mechanics. The authors chose to localize the N-WASP subdomain WWA (VVCA) from the WASP family proteins at the liposome membrane. With the creation of pores in the liposomes, the system can be perturbed in real time; therefore, just changing the salt concentration of the medium allowed them to trigger actin polymerization to the membrane (Figure 2.6a).

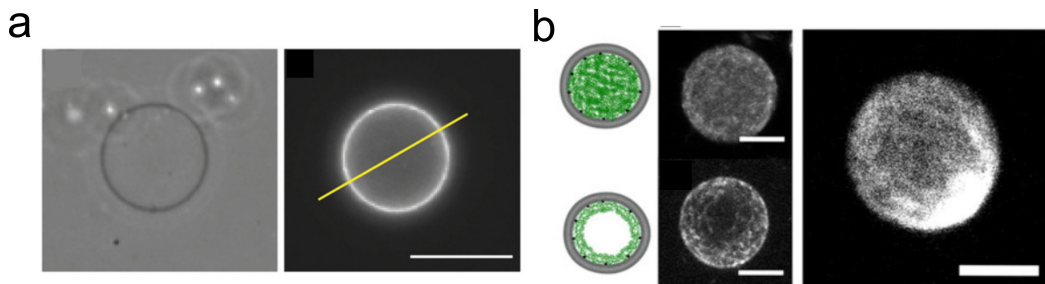


Figure 2.6: Reconstitution of actin cortices in liposomes. (a) Observation of actin nucleation at the membrane of a liposome. (b) Left: actin labelling in liposomes in absence of myosin. On the top, low attachment of the network. On the bottom, high attachment of the network to the membrane. Right: actin network in high attachment condition, in presence of myosin. *Adapted from [63, 64].*

In this study, the use of inverted emulsion technique permits to preserve protein integrity. Carvalho *et al.* [64] used the same system to reproduce active contractility (with

actomyosin cortical networks anchored to a liposome membrane) and to dissect the interplay between motor pulling forces, cortex-membrane anchoring and network connectivity. They showed that membrane anchoring and connectivity of the network are important parameters for the regulation of actin cortex remodeling and membrane-shape changes for cell polarization (Figure 2.6b).

Contractile ring reconstitution. Reconstitution of crosslinked actin networks in vesicles was done by Limozin and Sackmann [65] who studied the interaction between actin filaments and an artificial membrane. They encapsulated actin networks made of long actin filaments cross-linked by proteins (α -actinin and filamin) in giant liposomes. Phospholipid-cholesterol mixtures were used to mimic giant vesicles in size ranging from 5 to 30 μm . They reconstituted ring-like structures *in vitro*.

Reconstitution of contractile ring in droplets was performed by Miyazaki *et al.* [66] who showed that a ring-like arrangement can arise from the spontaneous assembly of actin filaments within spherical droplets (with a diameter smaller to the persistence length of actin filaments). Without spatial regulatory signals, the ring always assembles at the equator of the droplets (Figure 2.7). The authors hypothesized that this result is a minimization of the elastic energy of actin filaments at the equator. By playing on myosin concentration, they also managed to trigger the ring contraction, showing that myosin can regulate actin ring assembly and contraction. With this *in vitro* reconstitution, the authors proposed a confinement-induced self-assembly mechanism for the actin ring assembly, which provided indication of a direct contribution of the cell rounding to contractile ring assembly.

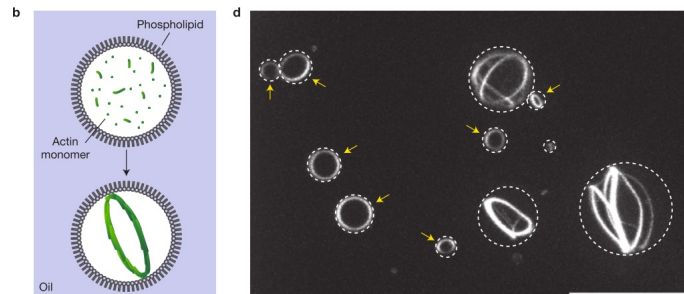


Figure 2.7: Reconstitution of actin ring self-assembly in droplet. *Extracted from [66].*

Microtubules reconstitution

Influence of confinement on microtubule shape. Elbaum *et al.* [67] studied microtubules in vesicles. They observed a very interesting phenotype in which when the membrane tension was changed, the microtubule shape was also changed. With low membrane tension, the microtubule protrudes without piercing the membrane, and above a critical membrane tension, the microtubule buckles and the vesicle reforms into a spherical shape (Figure 2.8a). These experiments represent a reconstitution of phenotypes observed in natural systems. In addition, a quantitative measurement of microtubule bending rigidity can be done. With the same system, Fygenson *et al.* [68] measured various parameters of the system (microtubule persistence length, stretching modulus of the vesicle membrane *etc.*). They studied the interaction between microtubules and the

confining membrane, and showed that forces generated by microtubule polymerization are sufficient to deform the membrane in different ways.

Influence of confinement on aster positioning. Holy *et al.* [69] studied how the positioning of an aster depends on its confinement. In **Chapter 6** different tricks of biological systems to find the geometric center of a cell are discussed. In this paper, they showed that the positioning of microtubules asters depends on the size and dynamic instability of the microtubules. Therefore, action of motors is not necessary for the positioning of aster; polymerization of microtubules itself is sufficient to center the MTOC (Figure 2.8b). Later Laan *et al.* [21] performed *in vitro* experiments in microfabricated chambers. Their results showed that cortical, dynein-mediated pulling forces generated at shrinking microtubule ends led to the efficient centering of microtubule asters in confining geometries.

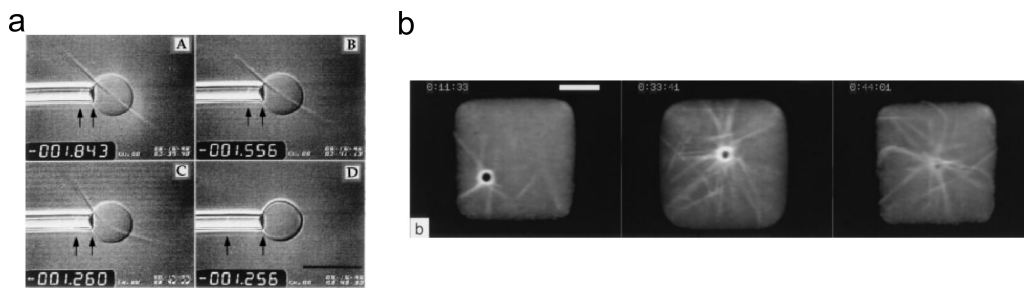


Figure 2.8: Microtubule reconstitutions. (a) Microtubules in vesicles change their shape as function of the membrane tension applied. (b) Aster positioning in microfabricated chambers. *Extracted from [67, 69].*

2.2.3 Confinement of egg extracts

Used in bulk, egg extracts reconstitute the biochemical environment of a cell but the information on the cell volume is lost. Indeed, just considering the volume parameter, the volume of a test tube is on the order of magnitude of microliters, whereas the typical volume of a cell is on the order of magnitude of picoliters. Therefore, there are obviously some phenomena that are missed when using egg extracts in bulk. For the past few years, researchers have started to use confined egg extracts. The basic idea is that by confining the egg extract, it is possible to mimic the natural configuration of a cell. The volume and the influence of a boundary are restored, as well as a limited amount of components in the compartment. Different confinements are possible; we will briefly introduce 2D and 3D confinement in droplets that we used in our studies.

2D confinement of egg extracts

For 2D confinement, two studies using *Xenopus* egg extracts stood up in the last few years. Both studies used supported lipid bilayers to reconstitute processes that normally localize at the plasma membrane.

Reconstitution of filopodia. Lee *et al.* [70] showed that by incubating supported lipid bilayers with high-speed actin-intact egg extracts, they were able to reconstitute

the physiological aspects of filopodia formation. With the reconstitution of what they call "filopodia-like structures" and by identifying molecular partners and kinetics of self-assembly of filopodia-like structures, they proposed a new mechanism for filopodia formation. This mechanism is based on an initiation by the Arp2/3 complex followed by an elongation with the recruitment of VASP and formins.

Reconstitution of cytokinesis. Nguyen *et al.* [71] set-up a cell-free system to reconstitute cytokinesis. A scheme of the set-up is shown in Figure 2.9. As in the previous example, they used supported lipid bilayers incubated with actin-intact cell extracts; in this case they localized RhoA activity at the level of the bilayer and were able to obtain a reconstituted actin cortex. They were able to confirm that Aurora kinase B is required for cleavage furrow induction, but were also able to decipher new mechanistic aspects of processes that are difficult to visualize in living cells (for example transport of the Chromosomal Passenger Complex along microtubules through a mechanism that requires two different kinesins).

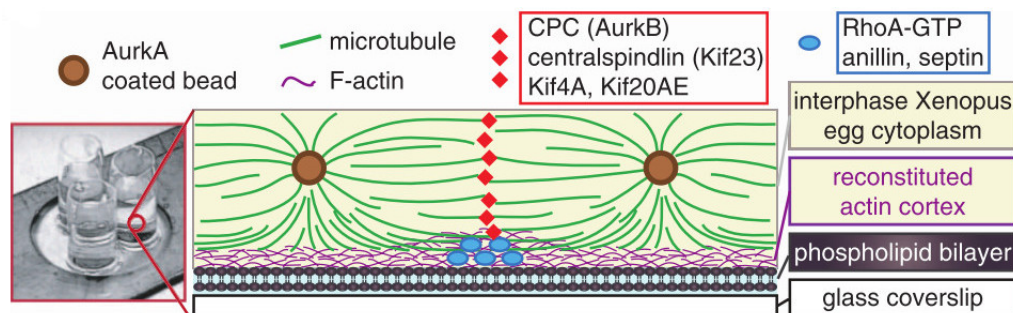


Figure 2.9: 2D cell-free system to study actin-microtubules interactions during cytokinesis. *Extracted from [71].*

Note that those two studies were also references studies for the fact that they are examining the relationship between actin and signaling pathways in reconstituted systems.

3D confinement of egg extracts

In this section, we limit the discussion to the confinement of egg extracts in droplets. Confinement in tubes [72] or in channels [73, 39] will not be addressed.

Confinement of microtubules and spindles structures

Confinement of stabilized microtubules. Pinot *et al.* [74] studied the organization of microtubules inside droplets of various sizes. They showed that the size of the droplet determines the shape of microtubule organization (Figure 2.10a). These results are supporting the hypothesis of a correlation between cell shape and intracellular cytoskeletal structures. A simple geometric confinement of microtubules with a rigid boundary can induce symmetry breaking resulting in asymmetric asters. This is an example of self-polarization, in absence of external cues.

Confinement of egg extracts with functionalized magnetic nanoparticles. Hoffmann *et al.* [75] and Bonnemay *et al.* [76] showed that combination of encapsulated egg extracts with magnetic control is possible, and that it is possible to trigger microtubule nucleation by aggregating nanoparticles coupled with signaling proteins. This is a proof of concept of magnetic control of spatiotemporal localization of biological processes in reconstituted systems. Bonnemay *et al.* pushed this magnetic control by engineering a gradient of magnetic nanoparticles coupled with signaling proteins; this provides a new bottom-up approach to examine symmetry breaking in cells and to spatiotemporally control signaling pathways in biological systems. Interestingly, in this case, the aster was positioned at the point where the gradient of Ran was weaker (Figure 2.10b).

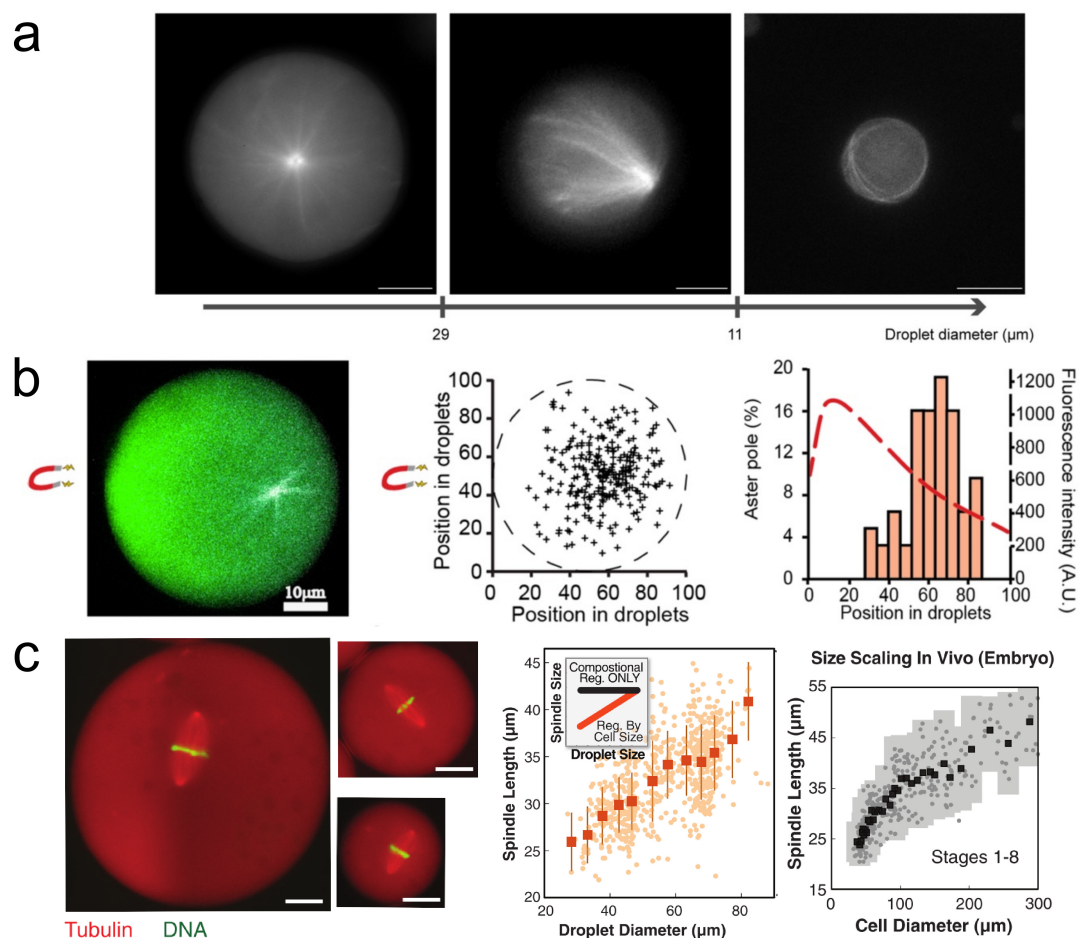


Figure 2.10: (a) Confinement of stabilized microtubules determines their shape. (b) Gradient of nanoparticles coupled with a microtubule nucleation factor induces microtubule nucleation and asymmetric positioning of the aster. (c) Spindle size depends on volume of confinement. Adapted from [74, 76, 77].

Confinement of bipolar spindles. In the same issue of the journal *Science*, Good *et al.* and Hazel *et al.* [77, 78] published studies about encapsulated *Xenopus* egg extracts to study the impact of the volume on the size of the spindle. This question is very important, especially during development when the size of the cell is changing dramatically in a small amount of time. They showed that there was a dependence between the size of the spindle and the confining volume. They based those results on

the fact that small droplets have a limited amount of components, which have an impact on the spindle size. They were able to relate this *in vitro* scaling to the one observed *in vivo* ([79], Figure 2.10c).

Confinement of actin-intact egg extracts

Spontaneous symmetry breaking. Pinot *et al.* [80] showed that the confinement of actin-intact cell extracts in droplets induces a spontaneous symmetry breaking. Just after the encapsulation of the extract, a centripetal flow of F-actin is generated and self-organizes into a contractile ring-like structure (Figure 2.11a). This interesting phenotype will be utilized in **Chapter 4**.

Actin cortex reconstitution. Abu Shah and Keren [81] encapsulated diluted *Xenopus* egg extracts and with the localization of specific nucleation factors at the surface of the droplet, they reconstituted an actin cortex (Figure 2.11b). More interestingly, they observed that this cortex underwent spontaneous symmetry breaking, reminiscent of polarization observed in early embryos.

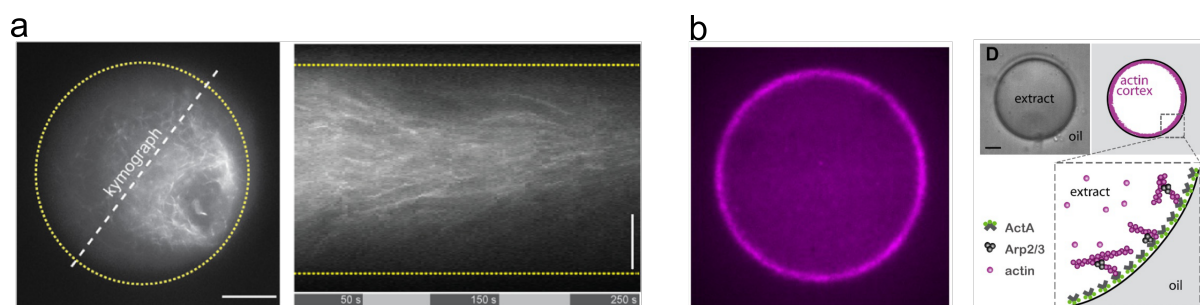


Figure 2.11: (a) Spontaneous symmetry breaking occurring when encapsulating an actin-intact egg extract in droplets. *Extracted from [80]*. (b) Reconstitution of an actin cortex with actin-intact egg extracts encapsulated in droplets. *Extracted from [81]*.

Using bottom-up approaches, proteins that are essential for a biological process can be identified. These studies are an essential step to understand mechanisms of signaling pathways regulation.

2.3 Model systems used in our studies

During my PhD, we decided to use two model systems to address the role of cytoplasmic F-actin in cell division. The first one, *Xenopus* egg extracts, is a hybrid between top-down and bottom-up approaches. The second one, mouse oocyte, is a top-down approach.

2.3.1 *Xenopus* egg extracts

We used *Xenopus laevis* as a model system to study issues related to cytoskeleton and cell division. *Xenopus laevis* is an aquatic amphibian measuring between 5 and 15 cm. By hormonal stimulation, it is possible to make it lay eggs. After several steps of centrifugation the cytoplasm from these eggs, also called egg extract, can be harvested (Figure 2.12 and next chapter for more details). This *in vitro* reconstituted system has been

widely used for studies on fundamental aspects of cell and molecular biology. In a test tube, all the components of a cell are available without the constraints of a membrane. Egg extracts have been used in a wide variety of research field: for example, they have been key to study DNA replication and repair, or chromosome condensation. They have also been key to understand phenomena related to cell division, and, in particular, the metaphase spindle.

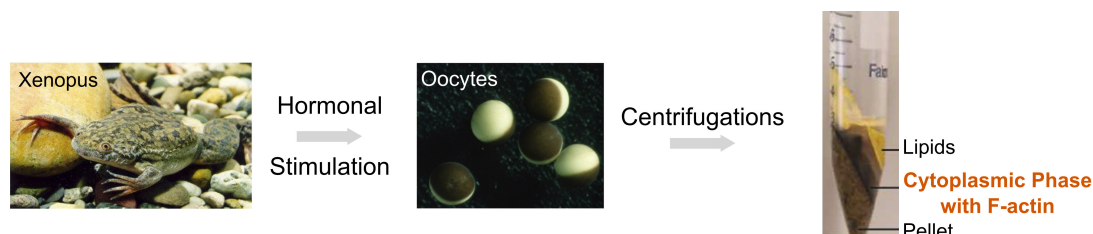


Figure 2.12: Preparation of *Xenopus* egg extracts.

For example, Heald *et al.* reconstituted a mitotic spindle around beads coated with DNA (acting as artificial chromosomes) [82]. This study was the first to show that centrosomes and kinetochores are dispensable for spindle formation. In addition, it was a proof that bipolarity is an intrinsic property of mitotic spindles because microtubules and motor proteins assemble in bipolar spindles around DNA in the absence of external polarity cues. This was a key step to understand the mechanisms of cross-talk between DNA and spindle formation.

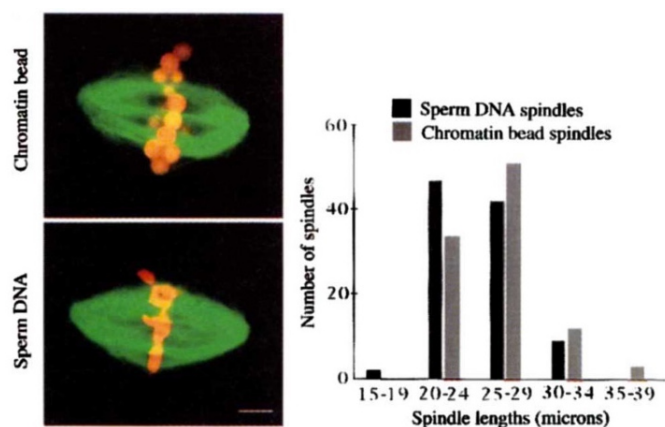


Figure 2.13: Nucleation of bipolar spindles around beads coated with chromatin, acting as artificial chromosomes. *Extracted from [82].*

Interestingly, the egg extract system can give access to systematic studies. For example, Grenfel *et al.* [83] set-up automated image analysis of spindles nucleated in egg extracts. They re-analyzed the morphology of more than 36 000 spindles from 80 independent experiments performed by different experimenters. This method describes spindle characteristics over a large set of data, and it was surprising to see that the spindle length varies in a cyclic manner, given the time of the year.

2.3.2 Actin-intact egg extracts

Classical cell extracts are prepared by following standard protocols [84, 85]. In these protocols, cytochalasin-D is added during the preparation to remove F-actin. Those ex-

tracts are used at room temperature. In these conditions, F-actin undergoes a gelation-contraction event that causes the formation of a contracted gel (Figure 2.14, [86]). This is one of the reasons most researchers excluded F-actin in cell extracts, while focusing on the study of microtubules in those systems. Recently, researchers have found tricks to keep

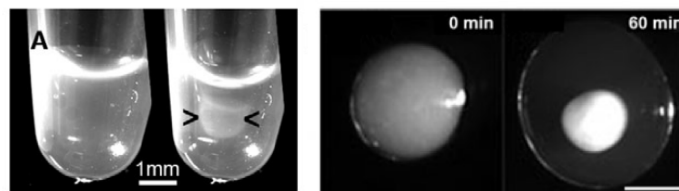


Figure 2.14: Contraction of actin-CSF at room temperature. *Extracted from [86].*

F-actin in the extracts. For example, when driven into interphase, the extract presents an homogeneous F-actin meshwork that is stable for long time periods [87]. Other studies showed that using actin-intact high speed extracts reconstitutes filopodia formation [70]. Encapsulation of M-phase actin-intact egg extracts allows to control the contraction of F-actin and recapitulates several symmetry-breaking processes observed during development [80]. Encapsulation of diluted actin-intact egg extracts and localization of actin to an artificial cortex was also done recently [81].

2.3.3 The mouse oocyte

Mouse is a common model system in labs because it's a vertebrate and therefore close to the human model; it is also very powerful from a genetic point of view. Research on mouse oocytes is very interesting from a fundamental point of view, but also from a medial viewpoint: understanding the divisions of the mouse oocyte helps understand issues related to infertility, for example. Fundamentally, mouse oocyte is an interesting model system because it is an isolated cell; the symmetry breakings observed in the cell only result from intracellular cues. They are convenient to use because of their size (80 μm in diameter, almost visible by naked eye) and their transparency, making microscopy easier (Figure 2.15a). One of the drawbacks is that the harvesting of the eggs requires the sacrifice of the mouse. Some genetic modified strains exist but they are sometimes complicated to maintain (and less robust than the wild-type mice). Otherwise, each experiment requires injection of RNAs (coding for fluorescent proteins for example). Most of the drugs and some organic fluorescent compounds can go through the membrane. Meiosis produces gametes with haploid content; it consists of two asymmetric divisions without DNA replication. In the female vertebrate, the stock of gametes (oocytes) is synthesized during the development of the embryo. Then the whole stock of oocytes is blocked in Prophase I until puberty. At each menstrual cycle, upon hormonal stimulation, a few oocytes undergo meiosis until the end of Metaphase II. This block will stay until the fertilization that will lead to the ejection of the second polar body. Meiotically-arrested oocytes accumulate large quantities of dormant maternal mRNAs that are required at the meiotic resumption. During meiosis the oocyte undergoes a unique prophase-to-metaphase transition. The oocyte normally undergoes a highly asymmetric division that is critical to ensure the formation of a competent resource-rich egg, capable of generating a living descendant after fertilization (Figure 2.15b). There is great interest in understanding chromosome segregation from a medical point of view, since chromosome

non-disjunction can lead to several problems, including developmental arrest, or severe birth defects such as Down's syndrome. The field of mouse oocyte research is very broad:

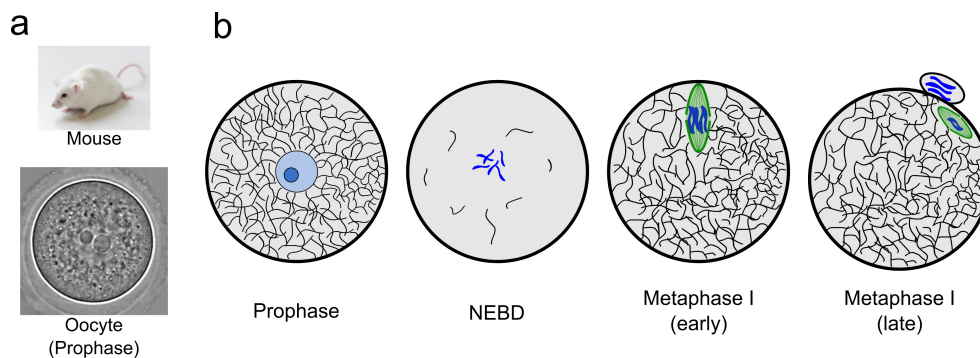


Figure 2.15: (a) The mouse oocyte model. (b) Scheme of meiosis for the mouse oocyte. Actin is represented in black, microtubules in green, DNA in blue.

from fundamental cell division questions to reproductive biology. There are many studies on chromosome recombination, an important step of meiosis. On the reproductive biology side, for example, biophysical studies checked the effect of cryopreservation on the actin cytoskeleton of mouse oocytes [88], and the effect of the viscosity of the oocyte cytoplasm on the development of an embryo after fertilization [89, 90].

In our case, we are interested in the meiosis divisions, and especially the asymmetric division during meiosis I (Prophase and Metaphase steps). It has been known for a while that the cytoplasmic F-actin meshwork plays a predominant role in the highly asymmetric division taking place during meiosis I. It has been possible to observe an "actin cage" around the spindle (Figure 2.16a) [91, 92]. The formation of the network is dependent on Formin-2, that nucleates straight filaments in cooperation with Spire 1 and Spire 2. The symmetry breaking occurring in meiosis I is now known to come from a transient destabilization of the F-actin network, mediated by a down-regulation of the formin-2 activity (Figure 2.16b) [93]. Recent studies showed a role of active diffusion for nucleus positioning [94] and of cortical tension for spindle positioning [95]. These studies will be explained in more details in **Chapter 6**.

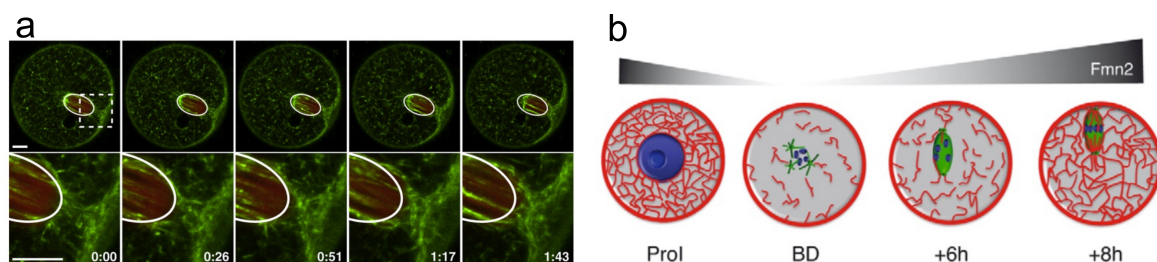


Figure 2.16: (a) Actin cage observed around the spindle during meiosis. *Extracted from [92].* (b) Formin-2 regulation during meiosis. *Extracted from [93].*

Chapter 3

Methods

This chapter describes the experimental methods used during this work. We will first present the protocols to prepare *Xenopus* egg extracts and mouse oocytes. Then, we will briefly present the microscopy techniques we are using and the molecules we used to nucleate, visualize and perturb the cytoskeleton. At the end, we will introduce the automated particle tracking.

Contents

| | | |
|------------|---|-----------|
| 3.1 | <i>Xenopus</i> egg extracts protocols | 40 |
| 3.1.1 | <i>Xenopus</i> egg extracts preparation | 40 |
| 3.1.2 | Cycling of cell extracts | 41 |
| 3.1.3 | Encapsulation of egg extracts | 41 |
| 3.1.4 | Typical experiment in <i>Xenopus</i> egg extracts | 42 |
| 3.2 | Mouse oocytes protocols | 43 |
| 3.2.1 | Extraction of oocytes | 43 |
| 3.2.2 | Injection of oocytes | 43 |
| 3.3 | Visualization with microscopy | 44 |
| 3.4 | Visualization and perturbation of the cytoskeleton | 45 |
| 3.4.1 | Nucleation of F-actin and microtubules in egg extracts | 45 |
| 3.4.2 | Visualization of cytoskeleton in egg extracts and mouse oocytes | 47 |
| 3.4.3 | Perturbation of actin and microtubule cytoskeletons | 48 |
| 3.5 | Particle tracking | 49 |
| 3.5.1 | Introduction to Mean Square Displacement (MSD) | 49 |
| 3.5.2 | Particle tracking to decipher F-actin properties | 50 |
| 3.5.3 | Tools for particle tracking in mouse oocytes | 51 |
| 3.5.4 | Icy tracking | 54 |

3.1 *Xenopus* egg extracts protocols

3.1.1 *Xenopus* egg extracts preparation

Classical cell extracts are prepared by following standard protocols [84, 85, 96]. The main steps of egg extracts preparation are described briefly below. In our case, we prepare actin-intact egg extracts, meaning that we keep the F-actin during the preparation of the egg extracts which is different from what is typically done with *Xenopus* egg extracts.

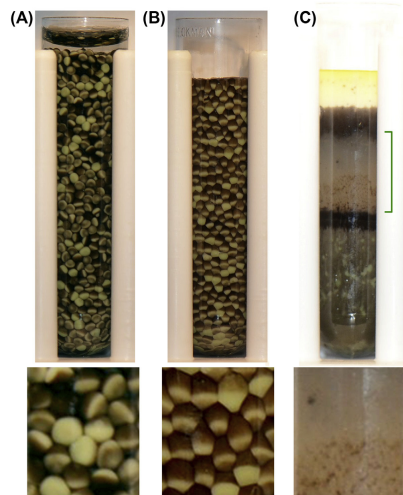


Figure 3.1: Centrifugation steps during the preparation of egg extracts. (A) Eggs before the first the centrifugation. (B) Eggs after the slow centrifugation. All the eggs oriented the same way. (C) Cell extract after the fast centrifugation. The cell extract phase is indicated with the green bracket. *Extracted from [96].*

Preparation of egg laying

To trigger the egg-laying, the *Xenopus* female must be injected with hormones. An injection of PMSG (Pregnant Mare Serum Gonadotrophin) is made three to ten days before the extract preparation. The day before the extract preparation, an injection of HCG (Human Chorionic Gonadotropin) is made and the frogs are put in separated tanks. They lay eggs during the night; it is very important to harvest those eggs between 16 and 18 hours after the HCG injection. The eggs are rinsed with NaCl (110 mM) and with a XB-CSF buffer (HEPES 10 mM, KCl 100 mM, MgCl₂ 1mM, EGTA 5 mM, Sucrose 100 mM, pH = 7.5). A "good" frog usually produces eggs that leads to 0.8 mL of extract.

Rinse and dejellinging

To provoke the dejellinging of eggs, cystein is added, to make the egg mucus more fluid: 2% cystein is added during two minutes and then the eggs are rinsed several times with the NaCl (110 mM), with the XB-CSF buffer and finally with XB-CSF buffer containing 2 μ M of DTT.

Centrifugation steps

For an actin-intact cell extract, all the centrifugations steps must be performed at 4°C and cytochalasin-D should not be added to the preparation (in contrary to classical protocols). After addition of protease inhibitors, a first, slow centrifugation (150 *g*, 1 minute) allows the sedimentation of the eggs (Figure 3.1b). After removal of buffer excess, a fast centrifugation step is carried out (10 000 *g*, 10 minutes). After these centrifugations, three phases can be observed (Figure 3.1c). The top yellow phase contains the lipids, the middle phase contains the cytoplasm and the pellet contains the DNA, some organelles and the membranes. The cytoplasmic phase is harvested and a last centrifugation (10 000 *g*, 10 minutes) is performed to remove the contaminants. The cytoplasmic phase is taken and flash-frozen in aliquots stored at -80°C. The extracts are blocked in metaphase-II (due to the EGTA and EDTA) and do not contain DNA.

3.1.2 Cycling of cell extracts

In classical cell extracts (where actin has been removed during the preparation), cell cycle resumption is possible. Indeed, addition of calcium triggers the interphase in 1h30 and so the replication of DNA. The addition of a new volume of CSF allows the extract to go back in metaphase and to produce bipolar spindles. Triggering of the anaphase is also possible (Figure 3.2).

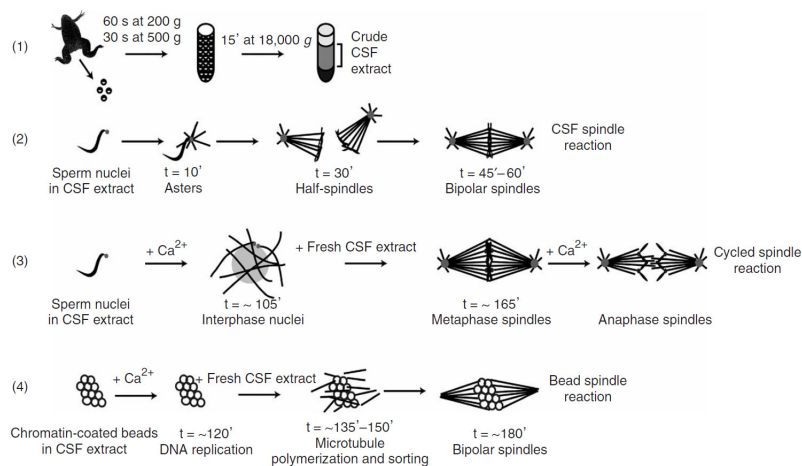


Figure 3.2: Cycling of egg extracts. *Extracted from [84].*

It has been shown that actin-intact CSF can be put in interphase where the F-actin is less contractile [80, 87]. To the best of our knowledge, it was not shown that cycling actin-intact CSF in metaphase is technically possible. Indeed it is a challenge, especially because of the contractile state of the actin in those extracts.

3.1.3 Encapsulation of egg extracts

Jimenez *et al.* [97] showed that it is feasible to encapsulate *Xenopus* egg extracts in a water-in-oil emulsion. Using a flow-focusing device, they generated many droplets and showed that the biological properties of the extracts are conserved after the encapsulation. They also demonstrated that the surfactant choice was important, especially to avoid coalescence of the droplets. They chose a polymeric surfactant (poly-PHS-PEO-PHS,

Arlacel 135) soluble in oil (continuous phase of the emulsion). It is composed of a PEO chain soluble in water. The PHS chain is soluble in oil and therefore provides steric stabilization (Figure 3.3,[98]). poly-PHS-PEO-PHS was the surfactant that we have used in our experiments.

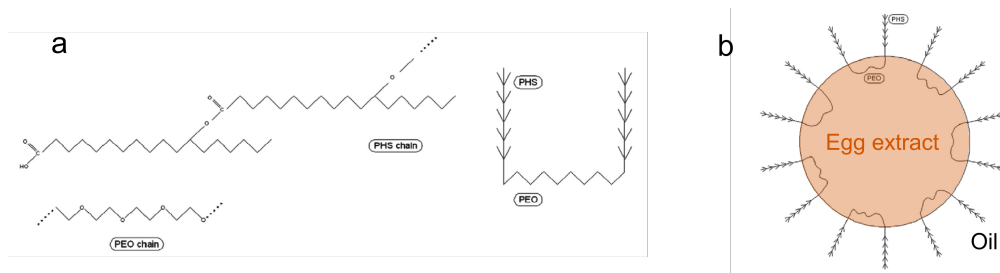


Figure 3.3: (a) Structure of the PHS-PEO-PHS copolymer. (b) Principle of the encapsulation of egg extracts. *Adapted from [98]*.

3.1.4 Typical experiment in *Xenopus* egg extracts

The egg extracts are prepared with eggs that are blocked in Metaphase II. In the extracts, the actin can polymerize spontaneously. To trigger microtubule nucleation, a nucleation factor has to be added. A number of microtubule nucleating factors can be used (Figure 3.4). They will be described in Section 3.4.1.

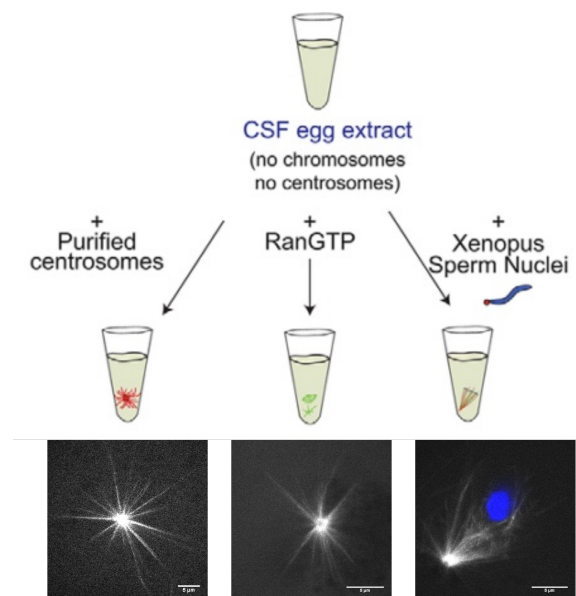


Figure 3.4: Microtubule nucleation in *Xenopus* egg extracts. Microtubules are represented in grey and DNA in blue. *Adapted from [99]*.

A typical experiment is done as follows: the extract is thawed out at 4°C, and the components are added sequentially. The typical volumes and final concentrations of an experiment are given in Table 3.1. Then 1 μL of the mix is added to 80 μL of mineral oil and the emulsion is generated manually. Usually, five emulsions are prepared for one experiment. The emulsions and the rest of the mix ("bulk" control) are incubated at 19°C for 20-30 minutes and then observed with fluorescence microscopy. It is important

| | Volume (μL) | Final Concentration |
|-------------------------|--------------------------|------------------------------------|
| Fluorescent tubulin | 0.5 | 200 nM |
| Cell extract | 10 | |
| ATP regenerating system | 0.2 | ATP: 1 mM |
| Fluorescent utrophin | 0.2 | 80 nM |
| Microtubule nucleator | 0.8 | Ran: between 2 and 8 μM |

Table 3.1: Typical volumes and concentrations for an experiment with *Xenopus* egg extracts.

to observe different emulsions during the experiments because of the intrinsic variability of each emulsion (inherent to the biological nature of the sample), and because the emulsion is warmed up under the microscope; therefore a too long time of exposure of the sample on the microscope can lead to artefacts caused by the warming of the sample under the microscope. With actin-intact egg extracts, it is very important to stay at 4°C during the preparation (until the emulsion formation) and to work quickly; otherwise the F-actin starts to contract in the tube.

3.2 Mouse oocytes protocols

3.2.1 Extraction of oocytes

Before each experiment, the oocytes are "freshly" extracted from a mouse. The protocol is the following: the mouse is sacrificed and dissected to harvest the ovaries. The ovaries are transferred in medium containing milrinone (a drug that will keep the oocytes in prophase and prevents meiosis resumption). Using mechanical shearing, the oocytes are extracted from the ovaries; they are then cleaned from their follicular cells and transferred to clean medium. One mouse yields about 20 oocytes.

3.2.2 Injection of oocytes

The oocytes are injected with an Eppendorf Femtojet microinjector. The typical set-up of injection is shown in Figure 3.5. After injection, the oocytes are imaged through a spinning disk confocal microscope.

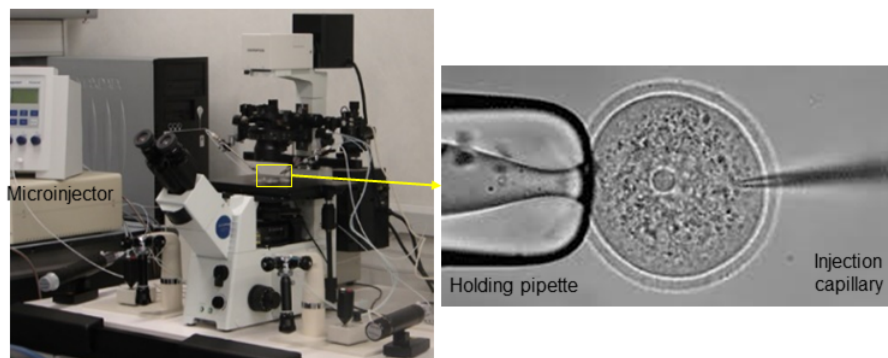


Figure 3.5: Typical set-up for oocytes injection. A microscope is equipped with a microinjector and micromanipulators. The oocyte is blocked with a holding pipette on one side and injected with an injection capillary on the other side.

3.3 Visualization with microscopy

Fluorescence is based on the absorption of light by a specimen and its re-emission at a certain wavelength. The main tool to observe our systems is fluorescence microscopy; we mainly use epifluorescence or confocal microscopy (Figure 3.6). Epifluorescence is very fast, but it lacks spatial resolution, whereas confocal microscopy is slower but has a very good spatial resolution. Confocal microscopy also allows a precise evaluation of the co-localization between two components. The confocal microscope is a conventional microscope, with a laser-beam focused on the sample instead of a lamp. The focus is obtained thanks to a pinhole aperture placed just before the detector. The image is built-up pixel by pixel (which makes the imaging very slow).

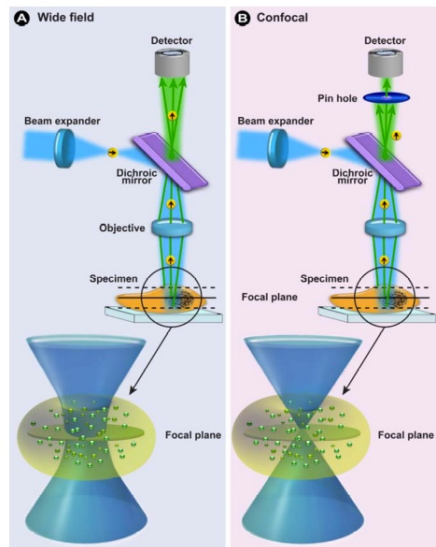


Figure 3.6: Comparison between epifluorescence (wide field) and confocal microscopy. *Extracted from [100].*

One of the problems we faced in our experiments was the problem of spatiotemporal resolution. The temporal resolution can be increased by decreasing the acquisition time of an image. Therefore, the imaging is a compromise between the quality of the image and the temporal resolution. The spatial resolution is given by the optical properties of the set-up. When a specimen is observed, a diffraction pattern is associated (also known as Airy pattern). Indeed, the image of a single point will appear as a diffraction pattern with a shape of concentric rings having decaying intensities as the distance from center increases. Spatial resolution can be defined as the smallest distance between two points in the specimen that can still be discriminated as separate points (Figure 3.7). The expression of this distance d is given in Equation 3.1 (λ is the laser wavelength and $N.A$ the numerical aperture of the objective).

$$d = \frac{\lambda}{2N.A} \quad (3.1)$$

For example, in confocal microscopy, we use a 63X objective with a numerical aperture of 1.4. Therefore, when we obtain a GFP with a 488 nm laser, we have a spatial resolution of 174 nm.

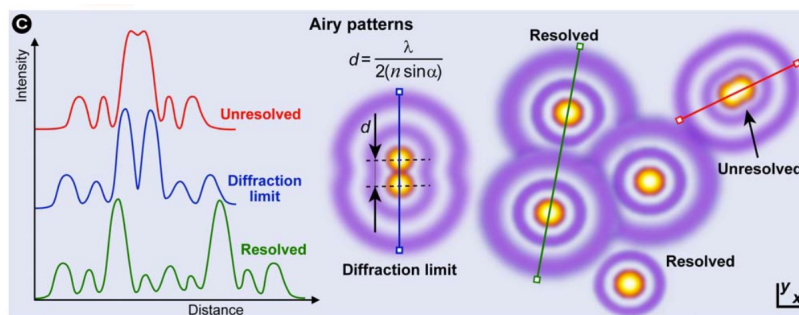


Figure 3.7: Schematic explanation for Airy pattern and diffraction limit. *Extracted from [100]*.

3.4 Visualization and perturbation of the cytoskeleton

In this section we describe the molecules used to nucleate and perturb actin and microtubule cytoskeletons. The precise concentrations used in experiments are given in the "Materials and methods" sections of the articles in the different chapters.

3.4.1 Nucleation of F-actin and microtubules in egg extracts

F-actin nucleation in *Xenopus* egg extracts. In extracts, actin polymerizes spontaneously. Different patterns can be observed when egg extract is confined in droplets.

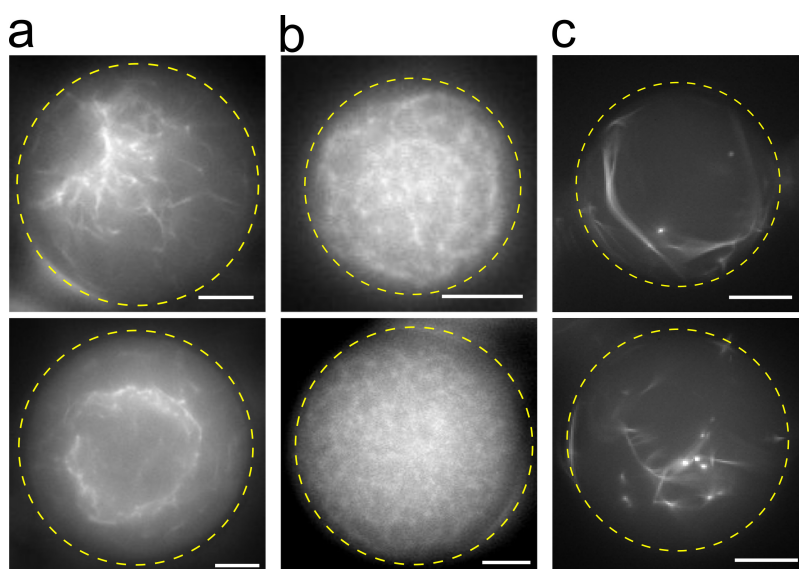


Figure 3.8: Examples of patterns obtained with actin-intact egg extracts confined into droplets. (a) Spontaneous symmetry breaking leading the formation of a ring structure. (b) Extract incubated with $1.3 \mu\text{M}$ of pWA leading to the formation of an homogeneous meshwork in the droplet. (c) Structures obtained when incubating α -actinin (65 nM final concentration) in actin-intact cell extracts. In all cases, actin is labelled with GFP-utrophin and scale bars are $10 \mu\text{m}$.

Spontaneous nucleation in actin-intact cell extracts. In actin-intact cell extracts, the F-actin presents a contractile behavior; in bulk, this contraction can be seen by naked eye. When confined into droplets, the contraction creates a symmetry breaking that leads to the formation of a ring structure that encompasses all the cytoplasmic material (Figure 3.8a).

Homogeneous nucleation: Scar-pWA. In confined cell extracts, the symmetry breaking can be explained by a localization of the actin nucleators at the droplet boundary. To favor an homogeneous nucleation, a nucleator can be introduced that will trigger actin nucleation homogeneously in the droplet (Figure 3.8b). We used Scar-pWA that is an activator of the Arp2/3 pathway.

α -actinin is an actin binding protein that favors the formation of actin bundles. We will not present results with this protein because even though it gave us a very interesting pattern of F-actin in droplets (Figure 3.8c), we were not able to nucleate microtubules in presence of α -actinin in the egg extracts. This phenomenon may have been due to the buffer in which the protein was kept, or a sequestration of the monomers of tubulin by the α -actinin. To the best of our knowledge, nothing has been published on microtubule nucleation in presence of α -actinin *in vitro*.

Microtubule nucleation in *Xenopus* egg extracts. The egg extract is blocked in Metaphase II, a state where there is no spontaneous microtubule nucleation. To trigger microtubule nucleation, we added nucleating factors to our extracts (Figure 3.4). The microtubule nucleating factors that we used in our studies were the following:

RanQ69L. Ran is a guanosine triphosphatase acting as a microtubule nucleator in a gradient existing around the chromosomes. The microtubule nucleation from Ran is dependent on γ -TuRC and XMAP215 [101] and presents a sigmoidal response: indeed, below a certain concentration of Ran, no microtubule nucleation is observed whereas above the threshold concentration, asters can be formed. RanQ69L is a constitutive active form of RanGTP and we use this protein to trigger aster formation. The protocol of purification is given in Appendix 2. **Utrophin-Ran.** For the project presented in Chapter 4 we created a chimera protein that can link both actin and microtubules. We chose to fuse the calponin homology domain of utrophin with Ran. The characterization of this protein is presented in the article of Chapter 4. The protocol of purification is given in Appendix 2.

Sperm Nuclei are highly condensed individual chromosomes extracted from *Xenopus laevis* testis. When incubated in *Xenopus* egg extracts, they trigger the formation of monopolar or bipolar spindles [102]. They can also be replicated by cycling the extract [84]. They are prepared using standard protocols [103].

Centrosomes are the principal MTOC found in eukaryotic cells. They can be purified from HeLa cells [104] and when introduced in *Xenopus* egg extracts they trigger the formation of asters [99]. The centrosomes that we use were kindly provided by M.Théry and J. Sillibourne.

3.4.2 Visualization of cytoskeleton in egg extracts and mouse oocytes

In *Xenopus* egg extracts, the cytoskeleton probes are introduced as purified proteins whereas in the mouse oocyte, they are injected, as coding RNAs that will express the protein, directly in the cell.

F-actin probes. There have been a lot of technical issues related to live imaging of F-actin. Cytoplasmic F-actin was very challenging to detect for a long time, because of the high fluorescence of the cortical actin pool. The development of new probes, like GFP-Utrophin, has been a critical advance in the visualization of cytoplasmic F-actin [105, 106].

Fluorescent G-actin (488) is the historical probe to visualize F-actin; it is a fusion between the monomer of F-actin (G-actin) with a fluorescent dye (protein or organic dye). But due to the large pool of soluble monomers, it tends to give poor contrasts and makes the visualization of structures difficult. However, due to its dynamic exchange between the soluble pool and the filaments pool, this probe is very useful for techniques such as FRAP.

GFP-Utrophin / dsRed-Utrophin. Utrophin probes are based on the calponin homology domain of utrophin (Utr-CH) which binds F-actin *in vitro*. It was shown to bind selectively to actin without stabilizing the filaments [106]. Therefore, the contrast is increased and a better visualization of the cytoplasmic meshwork of F-actin is possible. However, the range of concentration needs to be carefully chosen because at high concentration UtrCH stabilizes actin filaments.

Fluorescent phalloidin is usually used in fixed cells because it stabilizes the actin filaments very strongly. If introduced at very low concentration (≤ 50 nM) in *Xenopus* egg extracts, it can be used to do live imaging of filaments [80].

Microtubule probes

Fluorescent tubulin can be prepared from bovine brain and labeled with fluorescent probe (Alexa for example) [107]. In our case, we obtain it from the company *Cytoskeleton* directly labeled with TAMRA Rhodamine or with HiLyte Fluor 488. It is provided as a lyophilized powder; during the resuspension in the buffer, aggregates of fluorescent tubulin often form; they are removed with a step of ultracentrifugation before flash-freezing the aliquots of tubulin.

EB1-GFP. EB1 (End binding 1) is a plus-end tracking protein that localizes to microtubule plus-ends. Fused with GFP, it is a very convenient probe to sense the polarity of microtubules. We used it in *Xenopus* egg extracts to label microtubules, have information on their polarity, on their dynamic behavior and on their length.

NuMA-GFP antibody can be used to label the pole of asters or spindle. It was kindly provided by J. Pelletier and T.J. Mitchison. The stock aliquot is stored at -20°C ; the antibody is in 50% glycerol at a final concentration of 0.5 mg/mL. We used the antibody at a final concentration of $7.5\ \mu\text{g}/\text{mL}$, to characterize the spindle and asters poles (Figure 3.9).

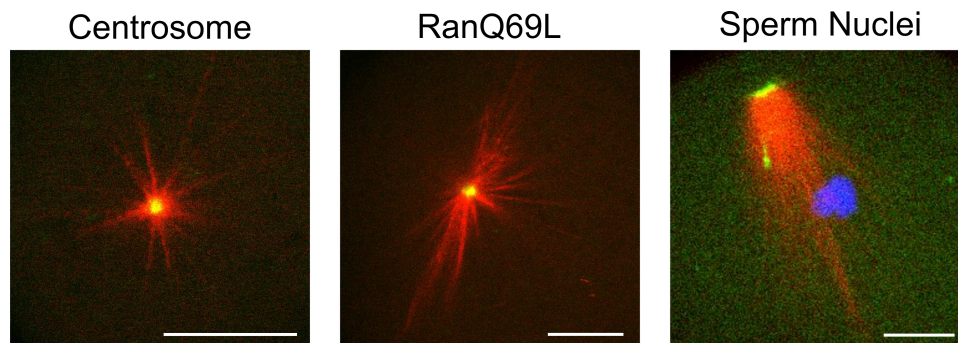


Figure 3.9: Examples of structures nucleated from centrosomes, RanQ69L or sperm nuclei, labelled with fluorescent tubulin (red) and NuMA-GFP antibody (green). All scale bars are $10\ \mu\text{m}$.

3.4.3 Perturbation of actin and microtubule cytoskeletons

F-actin drugs

Cytochalasin-D is an inhibitor of actin polymerization. It promotes favorable conditions for depolymerization of F-actin by binding to the barbed end of the filaments. It is membrane permeable, therefore, it can be used in mouse oocytes to disrupt the F-actin meshwork. In combination with other drugs, it can be used in *Xenopus* egg extracts. The structure is given in Figure 3.10.

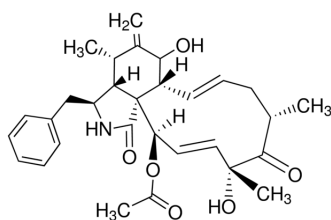


Figure 3.10: Cytochalasin-D structure (*from Sigma website*).

Latrunculin-A is a toxin that disrupts actin filaments by binding the G-actin monomers. The structure is given in Figure 3.11.

Blebbistatin is a cell-permeable inhibitor of the myosin II motor. It blocks the myosin head in a complex that has low affinity for actin; the myosin II is then blocked in an actin-detached state. The structure is given in Figure 3.12. Used in combination with cytochalasin-D or latrunculin-A, it produces the disruption of the F-actin meshwork in *Xenopus* egg extracts.

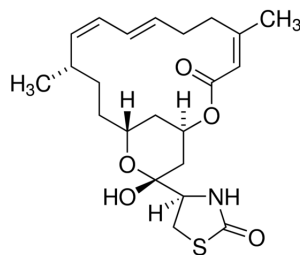


Figure 3.11: Latrunculin-A structure (from Sigma website).

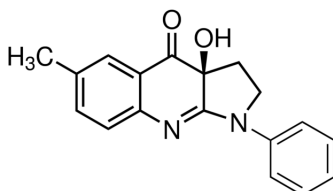


Figure 3.12: Blebbistatin structure (from Sigma website).

Microtubules drugs

Nocodazole is a microtubule drug that acts by binding to β -tubulin. It is cell-permeant and disrupts the microtubule network in cells.

p50 is a protein that inhibits dynein, a motor well-known to interact with microtubules.

3.5 Particle tracking

It is necessary to define the physical properties of a biological medium; for example, the diffusion of a protein depends greatly on the properties of the cytoplasm. Therefore, to understand the spatiotemporal properties of this protein and its participation to the dynamic organization of a cell, it is necessary to understand the physical properties of its surrounding medium. Particle tracking is a powerful tool to study dynamic processes in biology [108]. This technique often relies on a fluorescent reporter. In our case (**Chapter 6**, particle tracking in mouse oocytes), we used fluorescent nanoparticles or vesicles stained with Nile Red. The motion of the reporter is recorded with video-microscopy and then analyzed using image processing tools. The trajectories obtained from the tracking enable the collection of statistical data on spatial displacements, allowing the evaluation of physical properties such as diffusion coefficient, instantaneous velocities *etc.* as a function of time and space.

3.5.1 Introduction to Mean Square Displacement (MSD)

Mean Square Displacement (MSD) is one of the most popular tools used to analyze trajectories obtained from particle tracking [108]. The MSD describes the average space explored by a particle for a given lag time (Figure 3.13a). The mathematical definition of the MSD is given in Equation 3.2 (for a particle j diffusing in 2D, whose position

coordinates $\vec{x}_j = \{x_j, y_j\}$ are sampled at N discrete times $m\Delta t$.

$$MSD(t_{lag} = m\Delta t) = \frac{1}{N-m} \sum_{i=1}^{N-m} [\vec{x}_j(t_i + m\Delta t) - \vec{x}_j(t_i)]^2 \quad (3.2)$$

As the motion of a particle results from the interaction with its surrounding environment, the scaling of MSD with the delay (lag time) gives information about the surrounding medium of the probe (Figure 3.13b,c). If the MSD curve shows a plateau, it means that the particle presents a confined motion (trapped in a mesh, for example). If the MSD curve is straight, it means that the particle has diffusive (brownian) motion (like in water). If the MSD curve has a quadratic shape, then the movement of the particle is directed (particle taken by a motor for example). From the MSD, it is possible to extract the diffusion coefficient of the particle (see explanation later in this section).

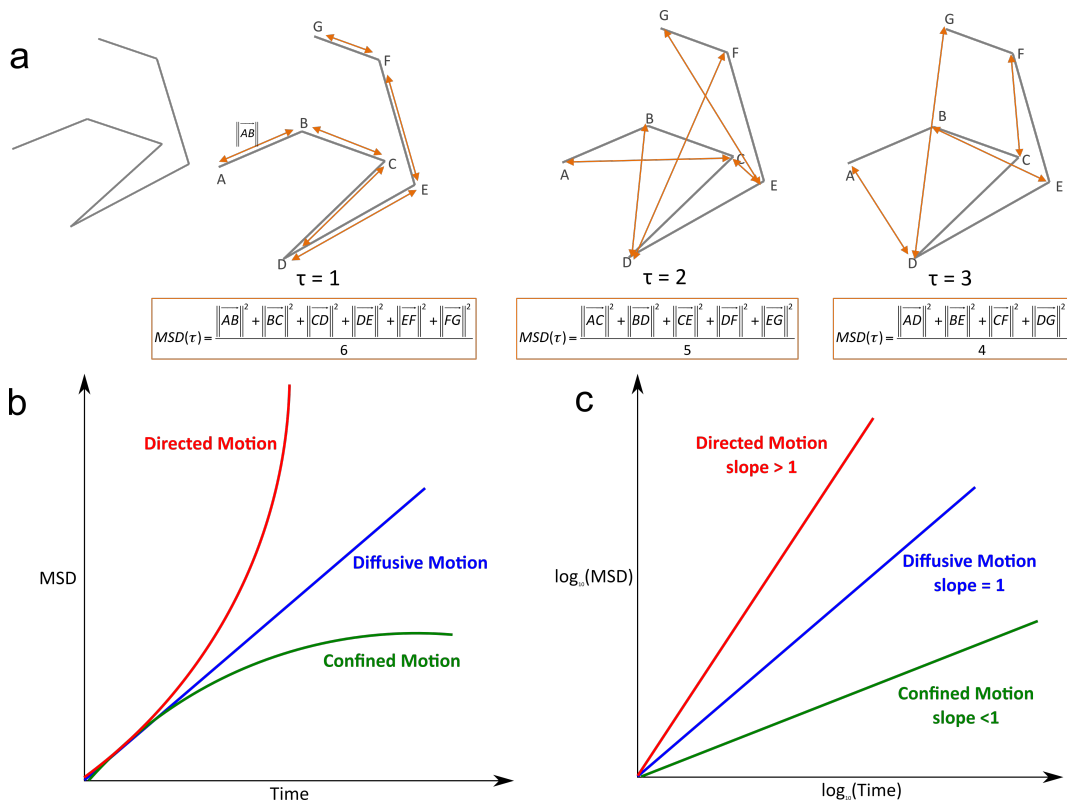


Figure 3.13: Calculation (a) and interpretation (b,c) of Mean Square Displacements.

3.5.2 Particle tracking to decipher F-actin properties

Particle tracking has been widely used to decipher F-actin properties *in vitro*. The tracer displacement is sensitive to local viscous and elastic forces, as well as chemical and steric interactions between the particle and the network. For example, Amblard *et al.* [109] showed that a bead smaller than the meshwork size ($0.3 \mu\text{m}$ in diameter in a $1 \mu\text{m}$ meshwork) will present a brownian motion. On the contrary, a bead larger than the meshwork size ($2.8 \mu\text{m}$ in diameter in a $1 \mu\text{m}$ meshwork) shows a subdiffusive motion (Figure 3.14a). This motion can be explained by the fact that the bead is deforming the filaments of the surrounding cage. In the same spirit, Wong *et al.* [110] checked

the influence of the actin meshwork size on the motion of beads (Figure 3.14b). Many measurements have been made in cells. For example, Caspi *et al.* [111] showed that some particles can present enhanced diffusion, dependent on microtubules but not on F-actin (Figure 3.14c).

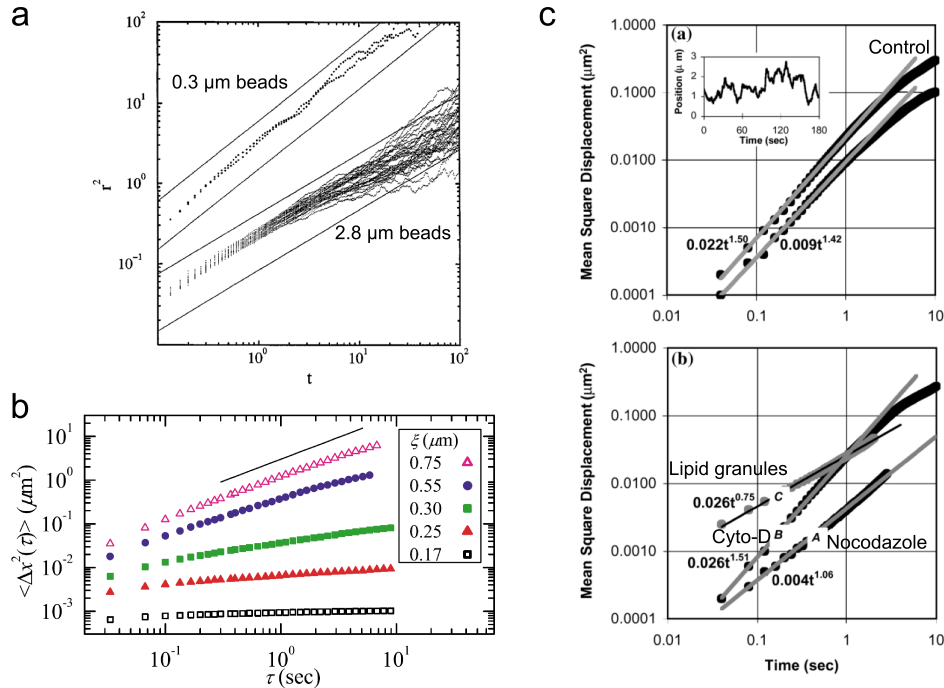


Figure 3.14: Historical studies of particle-tracking in actin networks. (a) MSD as a function of bead size. (b) MSD as a function of actin meshwork size. (c) MSD in cells untreated (top) or treated with various drugs (Cyto-D or Nocodazole) and MSD of lipid granules in cells (bottom). *Extracted from [109, 110, 111].*

More recently, Feric and Brangwynne used particle tracking to probe the nucleoplasm structure in *Xenopus* oocytes [112]. They managed to estimate the nucleoplasmic viscosity (Figure 3.15a). Thanks to particle tracking, they demonstrated that the movement of ribonucleoprotein droplets is supported by the F-actin network. By using carbon nanotubes functionalized with a kinesin, Fakhri *et al.* [113] demonstrated the existence of an intermediate mode of transport between thermal diffusion and directed motor activity in COS-7 cells (Figure 3.15b).

3.5.3 Tools for particle tracking in mouse oocytes

Fluorescent beads

For experiments of particle tracking in mouse oocytes, we used fluorescent latex (polystyrene) beads that were purchased from ThermoFisher. The particles surface is coated with a carboxyl group and they contain fluorescent dye. Their diameter is 100 nm. It is known that the surface properties of nanoparticles are important for their behavior in a (biological) medium [114, 115]. Indeed, it is important to control the surface state of the particle, to avoid non-specific protein adsorption on the surface. Coating the surface with BSA (Bovine Serum Albumin) will prevent other proteins to bind to the surface. Another

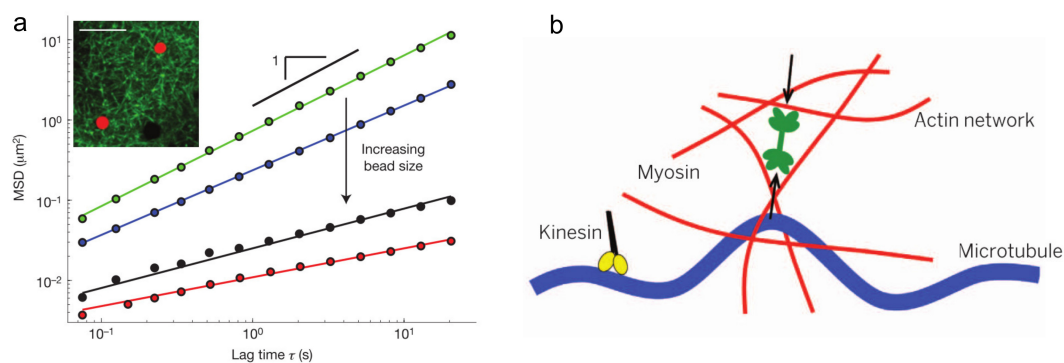


Figure 3.15: (a) MSD of beads of various size injected in the *Xenopus* oocyte nucleus. *Extracted from [112]*. (b) Carbon nanotube functionalized with a kinesin moving along a microtubule embedded in an actin-myosin network. *Extracted from [113]*.

alternative is to coat the particles with a monolayer of polyethylene glycol (PEG) which is known to reduce the adsorption of protein when grafted to the surface of a particle by forming a brush, that creates steric repulsion effects (Figure 3.16a).

Protocol of PEG coating. We used PLL-PEG because the amines of the poly-lysine (PLL) will interact with the carboxyl group of the particles (due to electrostatic charges). The structure of PLL-PEG is given in Figure 3.16b; it is a 20 kDa PLL grafted with a 2 kDa PEG (bought from Susos compagny). Reference [116] was used to define the ratio surface/polymer needed to saturate the particle surface with the polymer. For our 100 nm particles, we needed about 17 000 molecules of PLL-PEG per particle. The coupling was done by placing the particles with the PEG in a HEPES buffer (10 mM final concentration) and by agitating for 1h30 at 500 rpm at 21°C. To characterize the PEG coating, we measured the zeta-potential of the nanoparticles with a ZetaSize (NanoZS, Malvern Instruments). The results for 100 nm nanoparticles coupled with PEG are shown in Figure 3.16c. It can be seen that the PEG reduces the surface charge of the particle and makes it neutral. The coupling was not very stable in time (we did a new coupling for each new experiment).

In the mouse oocyte, we found striking differences of behavior between the particles that were coated with PEG and those that were not. When computing the MSD, we found that the particles coated with PEG were more mobile than the bare ones (Figure 3.17).

Nile Red

Nile Red is an organic compound that was found to be a lipophilic stain, powerful and selective for lipid droplets in cells [117]. It is membrane-permeable in mouse oocyte and can be used to label the total vesicles. Following their movement provides information regarding the physical properties of the mouse oocyte cytoplasm.

Fluoroinert oil

We decided to inject oil in mouse oocyte to study the behavior of a large object in the cytoplasm. The oil is a Fluoroinert FC70 fluorocarbon oil with a density of 1.93 g.ml^{-1} .

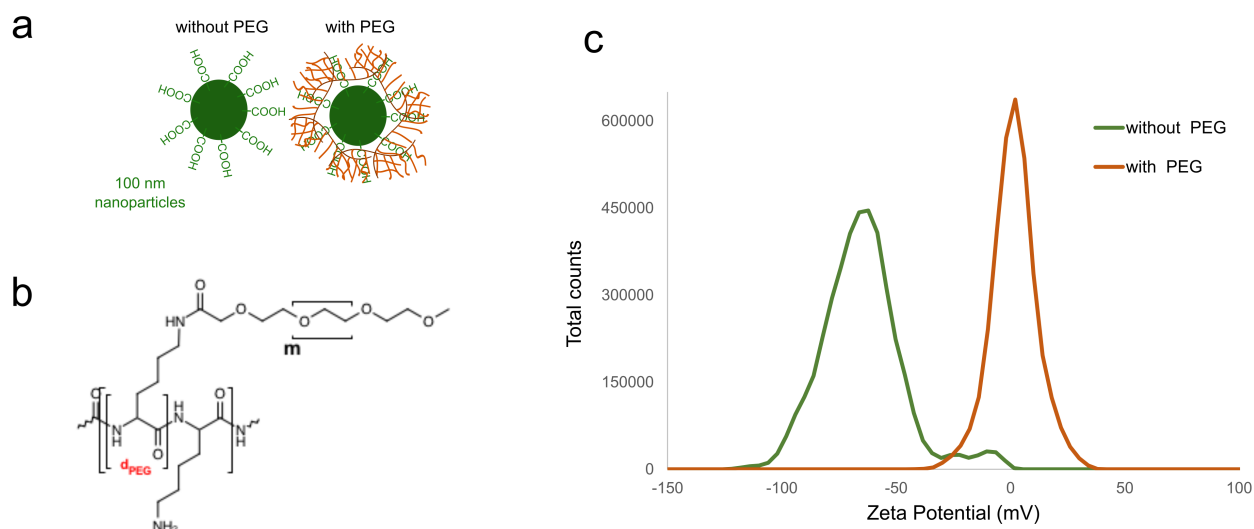


Figure 3.16: (a) Principle of the PLL-PEG coupling. (b) Structure of PLL-PEG. (c) Zeta-potential measurements for bare and coated particles.

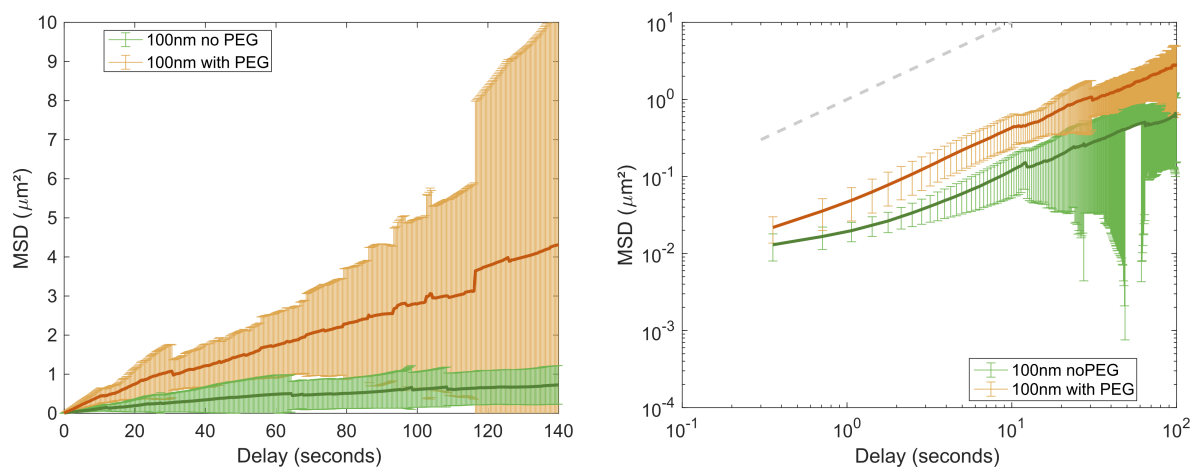


Figure 3.17: Comparison of MSD for 100 nm particles injected in mouse oocytes coated with PEG or bare.

3.5.4 Icy tracking

Icy software

To carry out particle tracking, we used the Icy software developed at Institut Pasteur [118]. The image analysis method is divided in two steps: first, particle detection is made with the Spot Detector plugin (Figure 3.18b). In this step, the spots corresponding to the particles are separated from the background according to certain criteria, and their coordinates are estimated in every frame of the image sequence. The second step is the trajectory reconstitution with the Spot Tracking plugin (Figure 3.18c). In this step, the detection coordinates are connected from frame to frame, to construct a trajectory. The trajectories are then exported in an excel file to be analyzed in Matlab.

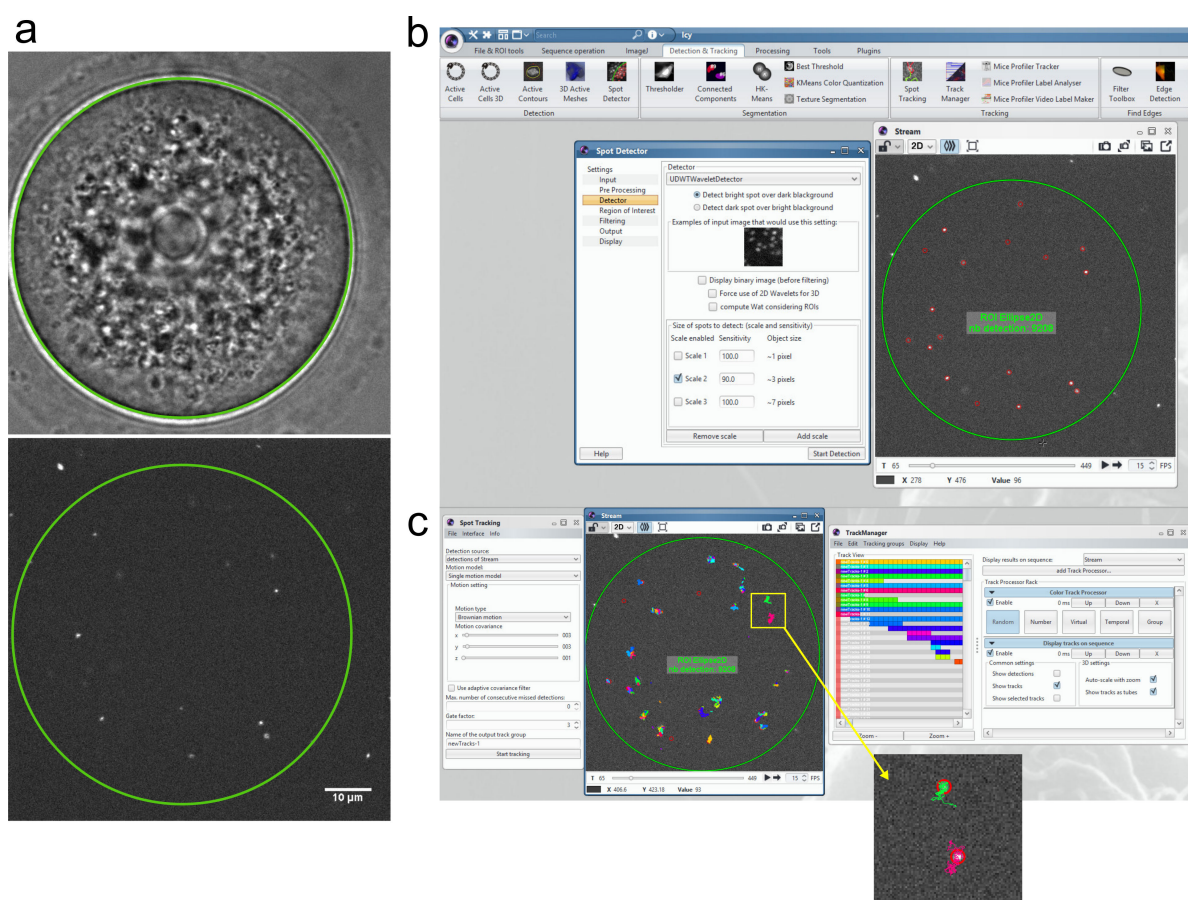


Figure 3.18: Icy procedure for spot detection and tracking. (a) Mouse oocyte in bright field and typical frame extracted from a movie (oocyte injected with nanoparticles). (b) Screen capture of Spot detection (first step of the tracking). (c) Screen capture of Spot Tracking (second step of the tracking).

One of the main problems when dealing with particle tracking is the wrong reconstitution of trajectories. We made two tests to check our tracking. We simulated data that we tracked into Icy software and then checked if the tracking was accurate when compared to the simulated trajectories. We also studied the movement of nanoparticles in a liquid of known viscosity, to see if our tracking gives us coherent results.

Simulated data

We generated data with the "Particle Tracking - Benchmark Generator" plugin of Icy. This plugin generates movies with particles having a mixed behavior between pure and biased diffusion. The switching between the two modes of diffusion is modeled with a Markov process that is known to be a good description of Brownian motion. The Brownian motion is controlled with the standard deviation of the Gaussian distribution associated to the displacement between two frames. The parameters chosen were as close as possible to the parameters of a movie obtained from injection of nanoparticles in mouse oocyte (same length, number of particles...).

We generated trajectories with three different simulations (Figure 3.19a). We saved these data as Tiff files (to have a simulated movie) and as Excel files (to have the exact coordinates of the trajectories). Then the simulated movies were opened in Icy and tracked with the same parameters as the one used for oocytes. At the end of this process, we had two files: one with the "true" trajectories and one with the "tracked" trajectories. We analyzed these two sets of trajectories with Matlab and compared the obtained results. The goal of this experiment was to evaluate the filter to use to know which trajectories we should keep (in order to avoid the detection of false trajectories coming from the noise of the movie).

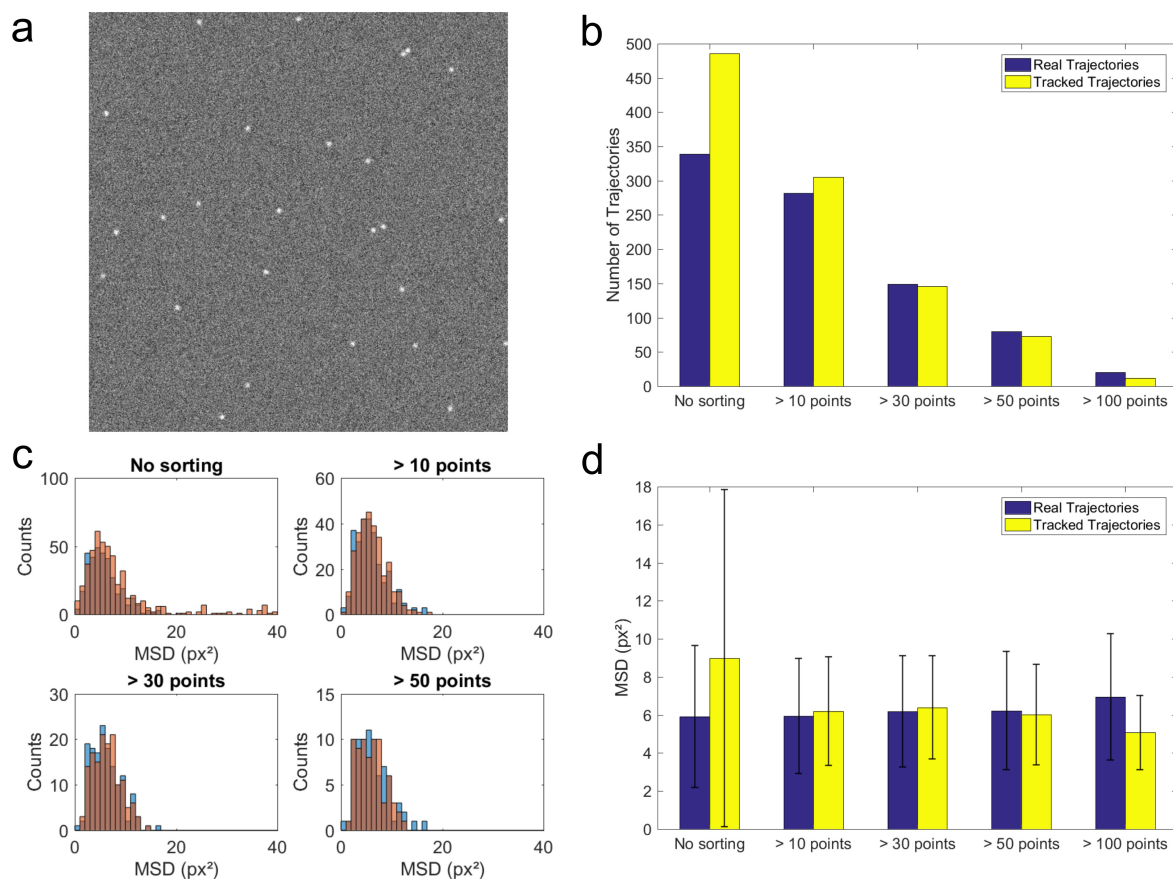


Figure 3.19: (a) Image from a simulated movie. (b) Comparison between the number of real trajectories and tracked trajectories as a function of sorting. (c) Histograms of MSD at $1 \Delta t$ for different sorting. Real trajectories are in blue, tracked trajectories are in orange. (d) Mean and standard deviation of MSD at $1 \Delta t$ for different sorting.

To compare the real trajectories and the one from the tracking, we first compared the number of trajectories obtained. We then selected data on the basis of the length of the trajectory. We see that when we do not sort our trajectories, the number of tracked trajectories is way higher than the number of real trajectories (486 compared to 339 trajectories, Figure 3.19b). Applying filters allows to reduce this difference between the number of tracked and real trajectories. Then, we compared their MSD at a delay of $1 \Delta t$ (Figure 3.19c, d). The goal was to see which sorting was optimal for the tracked trajectories to be as close as possible to the real trajectories.

In conclusion, we see that data sorting is necessary because the tracking yields a lot of "false" trajectories (especially small ones). We see also that sorting should not be too selective: for a sequence length of 450 frames, if only the trajectories with more than 100 points are taken, the data are biased toward the slower particles (smaller MSD). For our data in mouse oocytes, we decided to apply an intermediate sorting and to keep only the trajectories with more than 30 points (sequences of 450 frames).

Particles in glycerol

We used diluted 100 nm fluobeads that we placed in 80% glycerol. We then imaged them under the epifluorescence microscope with an interval of 500 ms between frames. After the tracking in Icy, we analyzed the trajectories in Matlab. Some results of the analysis are shown in Figure 3.20.

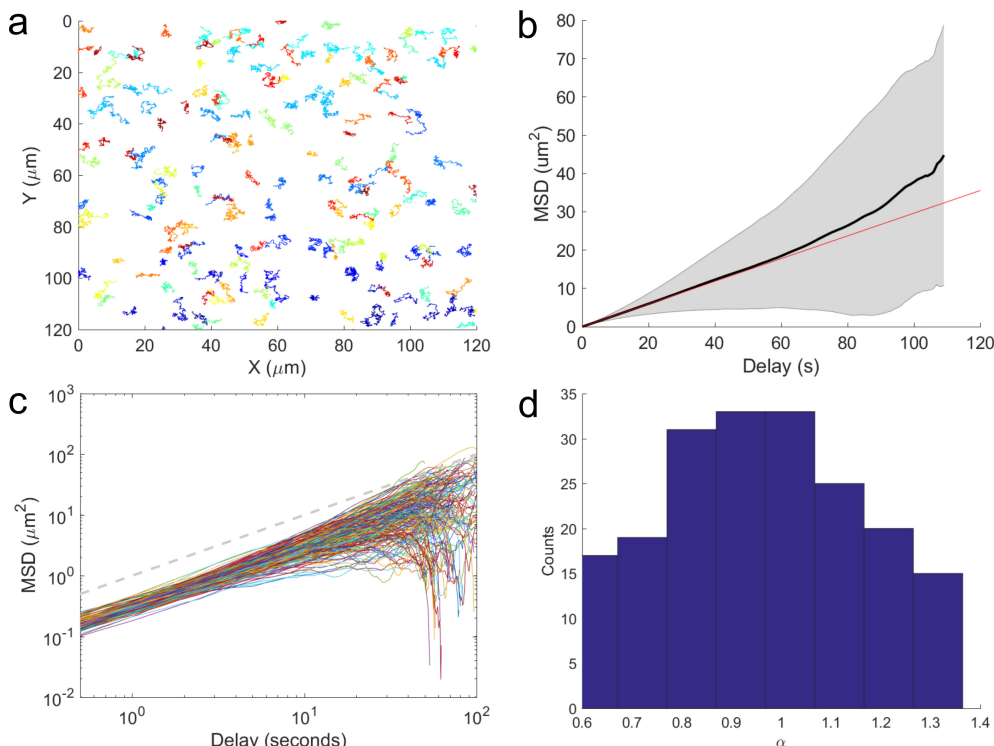


Figure 3.20: Results from glycerol tracking analysis. (a) Tracks obtained from the automated tracking. (b) Black line: average of MSD for all the trajectories. Grey area: standard deviation of MSD for all the trajectories. Red line: Fit on the first 25 % of the curve. (c) Log-log plot of the MSD for individual trajectories shown in (a). The grey dotted line has a slope of 1. (d) Distribution of α (slope of MSD curve in log-log scale).

From the fit of the beginning of the MSD curve, a diffusion coefficient can be extracted (Figure 3.20b). Indeed, it is known that for a 2D diffusion, the diffusion coefficient D scales with the linear part of the MSD slope according to the Equation 3.3.

$$MSD(\tau) = 4D\tau \quad (3.3)$$

This diffusion coefficient can then be related to the viscosity of the medium or to the size of the tracked objects. The Stokes-Einstein relationship 3.4 provides a link between those quantities (k_B is the Boltzmann constant, T the temperature of the medium, η the viscosity of the medium, r the radius of the particle, D the diffusion coefficient).

$$k_B T = 6\pi\eta r D \quad (3.4)$$

In the model case of the particles in glycerol, the viscosity of the medium and the radius of the particles are known. We can use the diffusion coefficient that we measured from MSD to see if it will lead to the correct viscosity (or correct radius of particles). From the data of Figure 3.20b, we estimate a diffusion coefficient $D = 7,4 \cdot 10^{-2} \mu m \cdot s^{-1}$. For this diffusion coefficient and a particle radius of 50 nm, we find a glycerol viscosity $\eta_{glycerol80\%} = 60 \text{ mPa}\cdot\text{s}$ which corresponds to the reported value for the viscosity of 80 % glycerol.

From the MSD plot in the log-log scale the diffusive behavior can be obtained (Figure 3.20c,d). The slope of the MSD curve in log-log representation can be computed for each trajectory. The value of the slope gives information about the diffusive behavior of the particles (Figure 3.13b,c). In the glycerol case we can see that the distribution of the slope α peaks around 1. Therefore we can conclude that the motion of our particles is purely diffusive. This is to be expected for particles in glycerol, and therefore means that our tracking gives us consistent results with what was expected for model systems.

In conclusion, using simulated data and tracking of fluorescent particles in glycerol with a known viscosity, we demonstrated that the tracking procedure in Icy is robust and gives us access to the trajectories of tracked objects. We can therefore use this method to track objects in biological systems. The tracking is used in **Chapter 4** to evaluate the diffusion coefficient of beads in various *Xenopus* egg extracts and in **Chapter 6** to decipher the physical properties of the mouse oocyte.

Chapter 4

Triggering Signaling Pathways Using F-actin Self-organization

The heterogeneous spatiotemporal organization of proteins is essential for cell fate behavior. Although it is known that actin cytoskeleton is vital for numerous functions in cells (cell division, migration...), it remains unclear how F-actin self-organization can control signaling pathways in space and time throughout the cytoplasm. In this project, we constructed a proof-of-concept experiment demonstrating that F-actin can trigger signaling pathways by either confining or scaffolding signalization proteins. The results presented in this chapter were published in *Scientific Reports* in 2016.

Contents

| | | |
|------------|---|-----------|
| 4.1 | Introduction | 60 |
| 4.1.1 | How to build heterogeneity in a cell? | 60 |
| 4.1.2 | Regulation of signaling pathways by F-actin in natural occurring systems | 62 |
| 4.1.3 | Ultrasensitive signaling pathways | 64 |
| 4.2 | Article 1: Triggering signaling pathways using F-actin self-organization | 65 |
| 4.2.1 | Presentation of the article | 65 |
| 4.2.2 | Manuscript | 65 |
| 4.3 | Conclusion | 92 |

4.1 Introduction

4.1.1 How to build heterogeneity in a cell?

A cell can be considered as an out-of-equilibrium system. To maintain this state, the cells needs to be an heterogeneous medium. Different ways to create heterogeneity can be found in cells. Cells can use heterogeneity to control signaling pathways in space and time.

Membrane-based organelles

The first way to create heterogeneity is to create a membrane to separate two compartments. Indeed, a membrane functions as a barrier, allowing to maintain different concentrations in the organelle and in the cytosol. Historically, the organelles with membrane have been well characterized because they could be observed by electron microscopy for example. The lysosomes contain enzymes that can degrade proteins or nucleic acids. These enzymes have an optimal activity at acid pH. Therefore, thanks to their membrane, the lysosomes maintain a small internal pH by pumping of protons from the outside medium. Another example where the internal membranes play a key role is the mitochondria. In those organelles, the membranes are used to maintain the protons gradient that will be used to synthesize ATP by the ATP synthase at the mitochondria membrane (Figure 4.1).

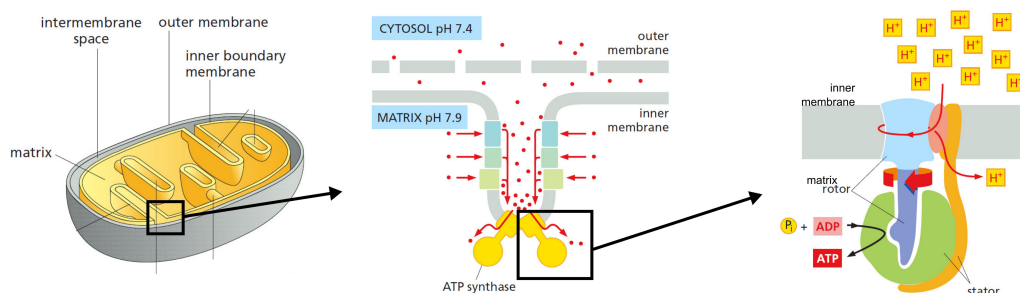


Figure 4.1: ATP synthase uses the protons gradient created by the mitochondria membranes to produce ATP. *Adapted from [119].*

Gradients

Due to the fact that the cytoplasm is a crowded environment, excluded volume effects can lead to the generation of gradients, mostly due to the decrease of diffusion coefficients in the crowded environment. Thanks to a process of reaction-diffusion, signaling proteins can form spatial gradients of signalization for example. Brown and Kholodenko [120] wrote the theory to obtain a concentration gradient of proteins. They considered a molecule that can be in a phosphorylated or dephosphorylated state. The transition between those two states is done by a kinase and a phosphatase. They showed that the necessary condition for the generation of a gradient is to have a spatial separation between the kinase and the phosphatase. An example of gradient generation by Ran will be introduced later in this chapter (Section 4.1.3, Page 64).

Membrane-free compartments

More and more studies emphasize the importance of phase separation of macromolecules in cells. For example, in granules or droplets, the thermodynamic and kinetic properties of proteins are modified. Changes in the equilibrium constant can be observed upon association of molecules in granules or droplets. We will now describe some observations of phase-separation in cells and their role in signaling pathways.

In *C. elegans*, P-granules were shown to behave like liquids [121]. The P-granule distribution vary in the embryo throughout development. They are initially uniformly distributed in the one-cell embryo and upon symmetry breaking, P-granules become localized on the posterior half of the cell. Instead of moving, the granules undergo dissolution and condensation on the other side of the cell (Figure 4.2). This study showed that phase transitions can be a driving force to organize the cytoplasm.

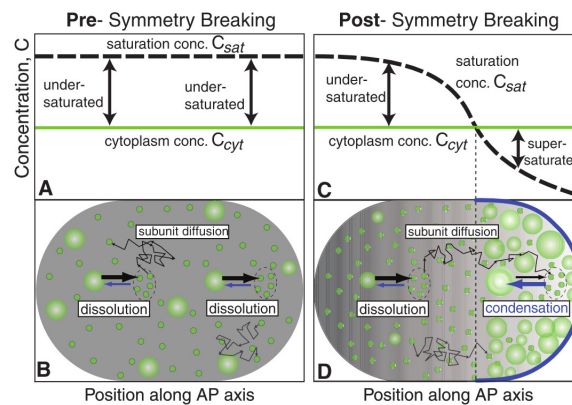


Figure 4.2: Model for dissolution and condensation of P-granules in *C. elegans*. *Extracted from [121]*.

Recently, Woodruff and colleagues [122] proposed that the phase separation of centrosomes proteins mediated by molecular crowding in *C. elegans* drives the formation of microtubule organizing centers. Thanks to the scaffolding of centrosomes proteins, the tubulin was concentrated in droplets by four-folds. This was sufficient to reconstitute microtubule aster nucleation *in vitro*. The inert macromolecules in the cytoplasm can therefore shape the pericentriolar material into a spherical structure.

These phase transitions can have a primordial role in signaling. For example Li *et al.* [123] showed that phase transition of signaling proteins can trigger an increase in proteins activity. Engineered proteins with repetition of precise motifs (multivalent proteins) form droplets that present liquid properties (Figure 4.3a). The authors then studied the Nephritin-NCK-N-WASP system. NCK can bind to a N-WASP region and it was shown that the multivalency of NCK is necessary for proper actin assembly. They saw that the incubation of NCK and N-WASP caused droplet formation (Figure 4.3b). Interestingly, they showed that the phosphorylation state of NCK has an influence on the phase boundary. This is an indication that in cells, kinases could regulate phase transition by controlling the degree of phosphorylation of nephritin. In addition, the droplets containing N-WASP kept the ability to nucleate actin filaments, organized in bundles (Figure 4.3c).

These results show that multivalent interactions can generate non-linearity in signaling pathways.

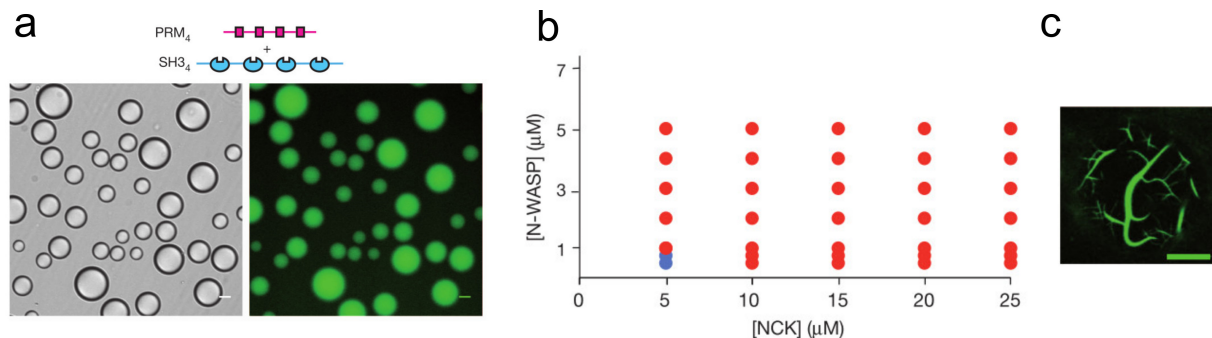


Figure 4.3: Multivalent signalling proteins can induce phase transitions. (a) Principle of the experiment. Two multivalent proteins are mixed; above a certain concentration they form droplets that have liquid properties. (b) Interaction between N-WASP and NCK triggers phase transition (indicated in red in the diagram). (c) Actin nucleation properties are kept in the droplets (actin labeled with phalloidin). *Adapted from [123]*.

Later, Banjade and Rosen [124] used this system with supported lipid bilayers and showed that the clustering of Nephtrin, NCK and N-WASP in presence of Arp2/3 can promote local actin assembly at the membranes. On a supported lipid bilayer, NCK, Nephtrin and N-WASP present a phase transition above a critical concentration and create a micron-sized cluster that can act as a signaling zone. This cluster will act as a coordinator of the actin filaments nucleation (spatial organization and increased biochemical signaling activity). Receptor clustering could be used to control the localization, structure and/or dynamics of actin filament networks. More generally, this concept could be applied to the organization of signaling receptors.

Cytoskeleton

The cytoskeleton can also create heterogeneity in cells by scaffolding or confining proteins. Cytoskeleton is a good candidate for regulation of signaling pathways as a lot of signaling molecules are immobilized or transiently bound on cytoskeleton fibers. Though the cytoskeleton is often considered as a scaffold and not as a potential signaling information carrier. Loverdo *et al.* showed theoretically that the active transport by the cytoskeleton can enhance reactivity of large objects like vesicles [125]. On the other hand, it was shown with synthetic biology that the scaffolding of signaling proteins can convert a simple linear signaling protein into an ultrasensitive switch [126]. Indeed by scaffolding the SH3 domains together, it was shown that even with no cooperativity, the simple fact to increase the number of interactions can increase the ultrasensitivity.

4.1.2 Regulation of signaling pathways by F-actin in natural occurring systems

Since few years, cytoplasmic actin has gained more and more attention [105]. Though, there is still no clear link between actin and signaling pathways. We have seen that

signaling pathways can be regulated by the concentration heterogeneity induced by the intracellular organization; we will now show how F-actin has been shown to regulate signaling pathways in biological systems.

By looking at protein-protein interactions in *Saccharomyces cerevisiae*, Forgacs *et al.* showed that the network of signaling proteins is very related to the cytoskeleton [127]. Indeed the proteome studies demonstrate the existence of a strong correlation between the signaling proteome and the cytoskeleton proteome. This could be either by a direct link between cytoskeleton proteins and signaling proteins. Another hypothesis is that **the cytoskeleton provides a macromolecular scaffold which spatially organizes the components of a signaling cascade.**

In the context of the T cell antigen receptor (TCR) triggering, it was shown that lipid rafts are membrane platforms where the TCR signaling machinery is assembled and where the TCR signaling pathway is orchestrated. Valensin *et al.* showed that the recruitment of TCR to lipid raft requires the F-actin cytoskeleton [128]. As shown in figure 4.4, the actin acts a scaffold for the clustering of TCR. After the clustering, actin regulates T cell signaling by maintaining the association between TCR and other signaling proteins. F-actin plays a role at different steps of T cell activation: at the maintenance of cell-cell contact, for the facilitation of TCR triggering and for the scaffolding and organization of proteins.

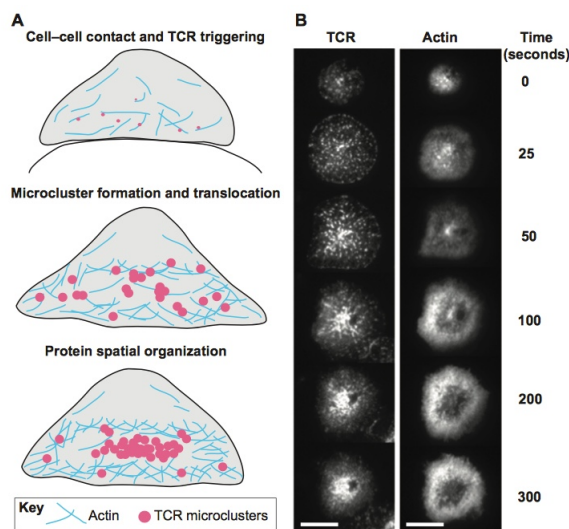


Figure 4.4: Role of actin in T cell clustering and activation. *Extracted from [129].*

It was shown theoretically that active contractility of actin network can result in the focusing of passive molecules into clusters [130]. Therefore, the actin-dependant clustering of cell surface proteins can lead to an increase in the reaction efficiency and output levels (Figure 4.5). Later, it was shown that lipid-anchored proteins can interact with actin and then exhibit anomalous concentration fluctuations [131]. Clusters can be formed by the interaction between a membrane protein and actin; this provides an hypothesis for an active mechanism for molecular organization and regulation of the plasma membrane. In this group, they have the idea of actin asters that would increase reaction rates (polar filaments forming asters that drive bound molecules by active contractile stresses).

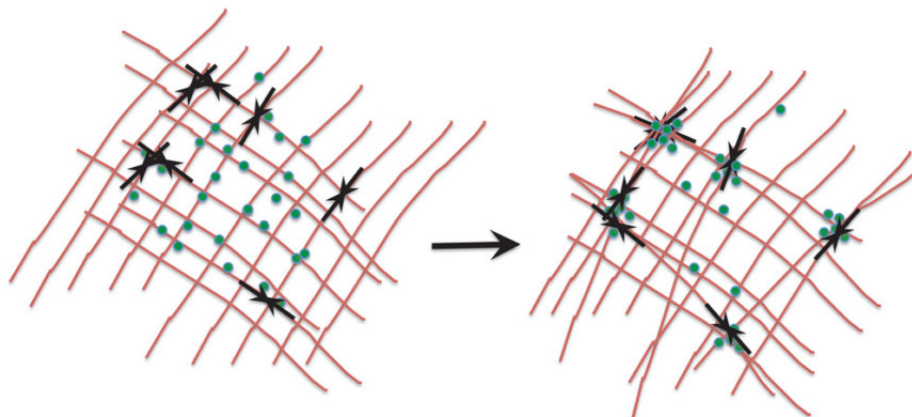


Figure 4.5: Actin contractility can drive the clustering of molecules. *Extracted from [130].*

4.1.3 Ultrasensitive signaling pathways

Ultrasensitive responses are very common in biology [132]. One of the most famous example of sigmoidal response is the oxygen binding by hemoglobin as a function of partial pressure of oxygen. The models showed that this response is due to a cooperativity between the different subunits of the hemoglobin. An ultrasensitive response is often described by the Hill equation (4.1) where K the effective concentration at 50%.

$$Output = \frac{Input^n}{K^n + Input^n} \quad (4.1)$$

As a proof of concept that F-actin self-organization can trigger signaling pathways, we chose to use the Ran signaling pathway known to trigger microtubule nucleation. The guanosine triphosphatase Ran was first identified for its role in nuclear trafficking. Then, Ran in its GTP-bound state was shown to stimulate microtubule nucleation and therefore to be a potential regulator of microtubule structures in mitosis [101]. Microtubule nucleation responds in an ultrasensitive manner to the concentration of Ran-GTP (Figure 4.6a). It was shown that a gradient of Ran (spanning over about 30 micrometers) is present around the chromosomes during mitosis. This gradient is based on two states of Ran: RanGTP and RanGDP. The conversion between those two states is achieved by two enzymes: RCC1 and RanGAP (Figure 4.6b). The gradient is generated thanks to one protein bound to the chromatin (a guanine nucleotide exchange factor, RCC1) and one freely diffusing in the cytoplasm (a GTPase-activating protein, RanGAP). The ultrasensitivity behavior appears when these converting enzymes operate near saturation [132]. The spatial segregation of the two opposing enzymes can generate a gradient of activity [133]. The ultrasensitive response usually generates steep gradients; it is the interaction between RanGTP and importin- β that allows to have a more extended gradient thanks to the prevention of GTP hydrolysis by RanGAP when RanGTP is bound to importin- β [134, 135].

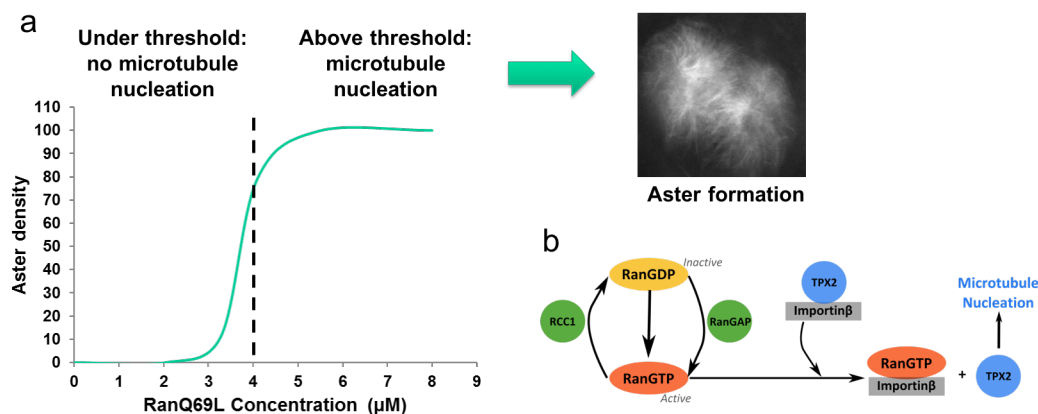


Figure 4.6: (a) Ran GTPase ultrasensitive behavior. (b) Signaling pathway for microtubule nucleation via RanGTP.

4.2 Article 1: Triggering signaling pathways using F-actin self-organization


4.2.1 Presentation of the article

In this project, we report a novel strategy showing how **F-actin self-organization can shape signaling pathways in space and time**. Using an interdisciplinary approach, we show how F-actin self-organization can trigger signaling activity. This highlights novel functions for cytoplasmic F-actin that may be used in cells as well as novel methods of control of biological processes based on cytoskeleton self-organization. **We isolate design principles underlying the control of signaling pathways by cytoplasmic F-actin self-organization**. Even if there are some examples showing how F-actin can act as a signaling molecule, there is still a lack of a general framework explaining of actin can control signaling events. In this study, we show that F-actin can trigger signaling pathways by two different means: the confinement of signaling proteins and the scaffolding of signaling proteins along microfilaments.

We engineered an ultrasensitive switch to trigger microtubule assembly. Although it is known that F-actin and microtubules must be coordinated to achieve essential cellular functions, the mechanisms by the two cytoskeletons interact remain elusive. In this study, we show that F-actin dynamics can enhance signaling activity and promotes the robust assembly of microtubules.

4.2.2 Manuscript

SCIENTIFIC REPORTS



OPEN

Triggering signaling pathways using F-actin self-organization

A. Colin*, L. Bonnemay*, C. Gayraud, J. Gautier & Z. Gueroui

Received: 11 May 2016

Accepted: 16 September 2016

Published: 04 October 2016

The spatiotemporal organization of proteins within cells is essential for cell fate behavior. Although it is known that the cytoskeleton is vital for numerous cellular functions, it remains unclear how cytoskeletal activity can shape and control signaling pathways in space and time throughout the cell cytoplasm.

Here we show that F-actin self-organization can trigger signaling pathways by engineering two novel properties of the microfilament self-organization: (1) the confinement of signaling proteins and (2) their scaffolding along actin polymers. Using *in vitro* reconstitutions of cellular functions, we found that both the confinement of nanoparticle-based signaling platforms powered by F-actin contractility and the scaffolding of engineered signaling proteins along actin microfilaments can drive a signaling switch. Using Ran-dependent microtubule nucleation, we found that F-actin dynamics promotes the robust assembly of microtubules. Our *in vitro* assay is a first step towards the development of novel bottom-up strategies to decipher the interplay between cytoskeleton spatial organization and signaling pathway activity.

To achieve their numerous functionalities, cells have evolved a large variety of strategies to coordinate the spatial organization of intracellular components at multiple scales. The cytoplasm which is a highly crowded environment and heterogeneous at nearly all length scales participates in this spatial organization¹. In particular, the specific physical properties of the cytoplasm have a strong impact on the spatiotemporal organization of signaling networks that are essential for cellular behavior². Spatial heterogeneities in protein concentration can lead to the generation of gradients of enzymatic activities spanning over several micrometers and producing pockets of concentrated enzyme activity involved in cell morphogenesis³. In addition, the isolation of specific proteins into membrane-bound organelles, or their recruitment and immobilization into multiprotein complexes using scaffold proteins, allows the simultaneous binding of signaling proteins enhancing their interactions and promoting specific cellular functions^{4–7}. For instance, recent studies have suggested how multivalency and cooperativity mediated by protein-protein or protein-RNA interactions could generate phase-separated micro-domains to isolate functional biomolecules into localized subcellular regions in the absence of membrane barriers and eventually triggering signaling activity^{8–12}. Other studies describe P granules in *Caenorhabditis elegans* as liquid-like compartments and explain how biochemical reactions can be facilitated within the cytoplasm¹³. These studies provide an emerging picture on how phase transitions can be a driving force to organize the cell cytoplasm⁹.

The cytoskeleton can also organize signaling pathways in space and time by partitioning the cell and providing transient docking sites for proteins^{14,15}. For example, actin microfilament dynamics regulate the clustering of membrane proteins controlling T cell signaling^{16,17} or the positioning of polarity markers during the establishment of the anterior-posterior axis in *C. elegans* embryos¹⁸. In a different context, subcompartmentalization of signaling proteins mediated by the actin cytoskeleton has been proposed to regulate dendritic spines during neuronal plasticity¹⁹. These recent works often describe mechanisms based on the interplay between F-actin operating at the membrane and signaling activity¹⁴. Although recent studies highlight novel roles of cytoplasmic F-actin in various cellular functions^{20–26}, a general framework explaining how such cytoplasmic microfilaments may also coordinate signaling pathways in space and time in the cytoplasm is still missing.

In vitro reconstitutions of cellular processes have provided key breakthroughs for understanding the basic morphogenetic properties of cytoskeleton organizations^{27–36}. These approaches also revealed how the physical and kinetic properties of the cytoskeletal elements determine their spatial self-organization^{29,37–39}. In addition, studies deciphering the effect of the spatial boundaries on these assemblies shed the light on the role of geometric and mechanical parameters on fundamental organizing principles^{36,40–45}. Here we examine how *in vitro* reconstitution of cellular processes can provide novel insights to decipher the interplay between cytoskeleton spatial

Ecole Normale Supérieure, Department of Chemistry PSL Research University-CNRS-ENS-UPMC 24, rue Lhomond, 75005, Paris, France. *These authors contributed equally to this work. Correspondence and requests for materials should be addressed to Z.G. (email: zoher.gueroui@ens.fr)

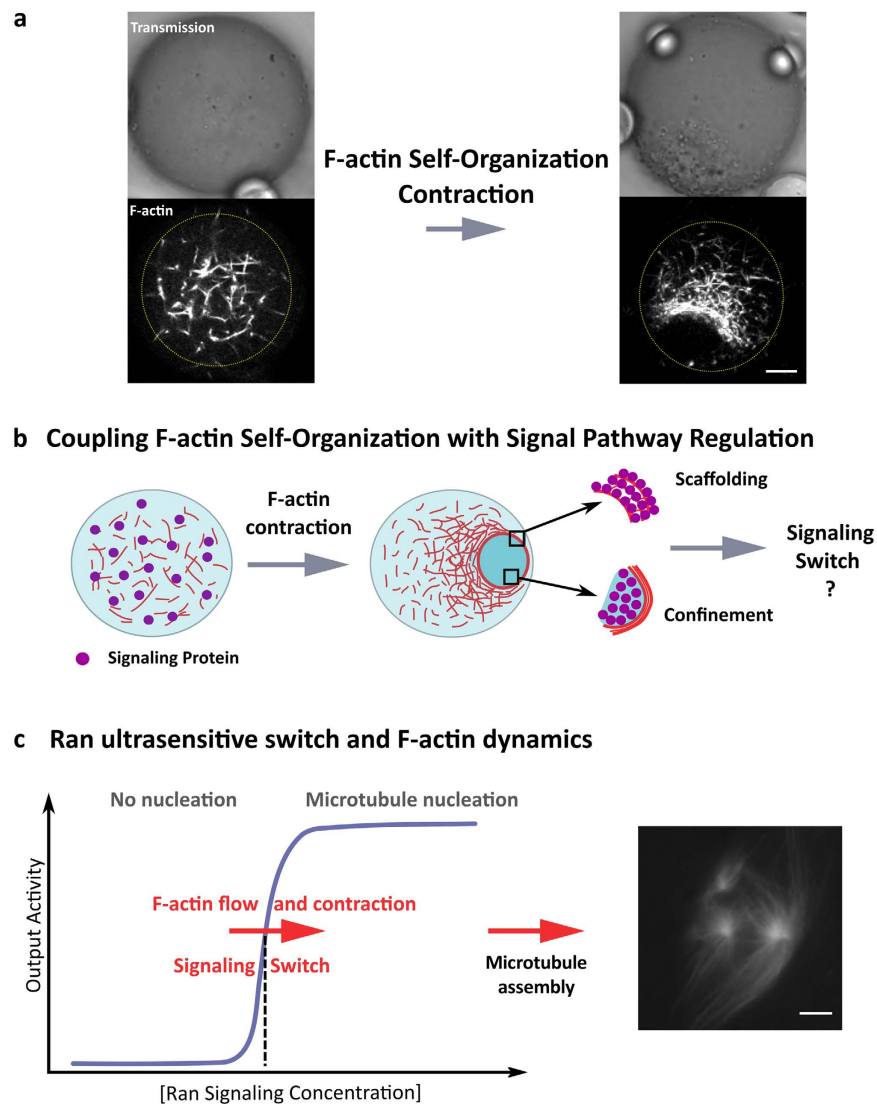


Figure 1. Membrane-free confinement mediated by F-actin self-organization to localize and trigger signaling pathways. (a) The confinement of egg extracts within oil droplets leads to the spontaneous generation of a centripetal F-actin flow that eventually forms a contractile ring-like structure. F-actin flow conveys cytoplasmic materials that are trapped by the filament meshwork. Actin microfilaments were labeled with Utr-GFP. Scale bar is 10 μm . (b) Schematic of the concept of signaling localization and switch: F-actin self-organization powered the active compartmentalization of nanoparticles operating as signaling platforms or the scaffolding of signaling proteins by F-actin polymers. Starting from a homogeneous distribution of signaling proteins, the generation of the F-actin flow drives the concentration enhancement of regulatory elements that could trigger signal pathway. (c) The activity of Ran GTPase is characterized by a non-linear response following a sigmoidal response with the concentration (ultrasensitive switch). The nucleation of microtubules is triggered above a concentration threshold of Ran. Our hypothesis is that the F-actin self-organization into a contractile meshwork will trigger the Ran signaling pathway and the nucleation of microtubules.

organization and signaling pathway activity. In particular, we assess whether high-order organizations of cytoplasmic F-actin meshwork can trigger signaling activity by enhancing regulatory protein concentration. To test these hypotheses, we evaluated the enhancement of signaling activity: first as mediated by the membrane-free compartmentalization of nanoparticles operating as nanometric signaling platforms; and second, by the scaffolding of regulatory proteins by actin microfilaments (F-actin). We devised a bottom-up approach based on *Xenopus* egg extracts that have proven to be a powerful system to examine the self-organizing properties of the cytoskeleton^{31,34,46–52} as well as the spatiotemporal behavior of signaling cascades that regulate cell cycle events^{53–57}.

Using metaphasic egg extracts confined within oil droplets, we can reconstitute the spontaneous generation of centripetal F-actin flow along with the formation of a contractile meshwork that eventually forms a ring-like organization (Fig. 1a). This F-actin flow drives the long-range transport of cytosolic components such as organelle-based structures as well as their partitioning within a confined space encompassed by filaments. To examine how cytoplasmic confinement could impact signaling activity, we first examined nanometric signaling

platforms that are composed of regulatory proteins grafted to nanoparticles (Fig. 1b). As proof of concept we focused on Ran, a GTPase controlling the nucleation of microtubules, with an ultrasensitive switch activity characterized by a sigmoidal concentration dependency^{58–61} (Fig. 1c). RanGTP conjugated to selected nanoparticles was efficiently transported and concentrated by F-actin flow in confined egg extracts. Interestingly, we found that F-actin dynamics activate microtubule assembly after the local accumulation and the cytoplasmic partitioning of Ran-nanoparticles. This illustrates how F-actin self-organization can generate a robust biochemical switch by promoting localized fold increases in nanometric signaling platform concentration. We then evaluated the concept that F-actin operates as a polymeric hub to recruit regulatory proteins. We have engineered Ran to specifically recognize actin microfilaments using an actin binding protein based on utrophin. We found that the formation of a dense F-actin meshwork during contraction recruits Ran and triggers microtubule assembly. Altogether these studies shed the light on how cytoplasmic F-actin self-organization can promote a signaling switch based on concentration enhancement and polymeric scaffolding.

Results

Active confinement of cytoplasmic materials mediated by F-actin dynamics. To examine how cytoplasmic confinement and partitioning can be mediated by cytoskeleton, we investigated the organization of F-actin filaments into dynamic contractile patterns using Metaphase II *Xenopus* egg extracts encapsulated within emulsion droplets. To visualize the F-actin meshwork, we have supplemented *Xenopus* egg extracts with the calponin homology domain of utrophin fused to GFP (Utr-GFP) at sub-stoichiometric conditions (50 nM). Utrophin binds actin filaments with a reduced disturbance of the polymer assembly and dynamics⁶². In bulk extract (unconfined geometry), F-actin organized into a heterogeneous contractile meshwork within a few minutes (Supplementary Figure 1). In extracts confined into droplets, actin assembled into a convergent and centripetal contractile meshwork⁴¹. F-actin eventually formed a ring-like structure within 5 minutes with a dimension which scales to about one third of the droplet diameter for a broad size range (Fig. 1a, Supplementary Figure 2 and ref. 41). We estimated the size of the F-actin meshwork using confocal images of F-actin network (Supplementary Figure 3a). We found an average actin meshsize of about 1.1 μm and a range of interdistances between 0.5 to 4 μm (Supplementary Figure 3a). The F-actin meshsize decreases gradually from the periphery of the droplet to the actin ring and the mean F-actin contractile rate was about 90 $\text{nm}\cdot\text{s}^{-1}$ in agreement with previous results⁴¹ (Supplementary Figure 3b). The F-actin dynamics produced a long-range flow that convey micrometric objects such as microbeads over a distance covering several micrometers, in agreement with observations we previously reported⁴¹. In order to further characterize the system we examined the dynamics of the nanoparticle trapping. First, we analyzed the effect of particle size on the efficiency of accumulation (size ranging from 50 nm to 1 μm). Nanoparticles were covered with PEG-polymers to reduce non-specific interactions with cytoplasmic elements. We found that the majority of nanoparticles with a diameter larger than 100 nm can be trapped and efficiently conveyed by the F-actin flow (Fig. 2a). Small cytoplasmic proteins were not conveyed by F-actin flow, as confirmed by the absence of accumulation of fluorescent proteins within ring-like structures (Supplementary Figure 4). Our observations are reminiscent of cytoplasmic F-actin meshwork observed in starfish oocytes that produce a long-range transport of micrometer particles during chromosome congression²⁵, suggesting a common mechanism of transport powered by cytoplasmic F-actin.

Time-lapse observations revealed that nanoparticle steric trapping occurs within 5 minutes (Fig. 2b and Movie 1). In addition, the use of a fluorescent membrane-tracker confirmed that organelle structures from the *Xenopus* cytoplasm accumulated in F-actin based-structures (Fig. 2c). To further characterize the confinement of nanoparticles, we monitored the spatiotemporal dynamic of individual nanoparticles during F-actin contraction (Supplementary Figure 5). Analysis of the mean orientation of the trajectories showed that the particle movements are directed towards the F-actin ring (Fig. 2d, Supplementary Figure 5a,b,c). The mean velocity of the transported particles is about 9.8 $\text{nm}\cdot\text{s}^{-1}$ (Supplementary Figure 5e), which is an order of magnitude smaller than the mean velocity of the F-actin flow (90 $\text{nm}\cdot\text{s}^{-1}$) (Supplementary Figure 3b). These results suggest that the trajectories of nanoparticles display a directed motion in intermittence with a Brownian-like behavior. Velocity fields along single nanoparticle trajectories are highly heterogeneous within droplets (Supplementary Figure 5d). For instance, the amplitude of the velocity along single tracked nanoparticles spans from approximately 20 $\text{nm}\cdot\text{s}^{-1}$ to approximately 150 $\text{nm}\cdot\text{s}^{-1}$ (Supplementary Figure 5f). In addition the distribution of instantaneous velocity is independent of the nanoparticle localization within the droplets (Supplementary Figure 5f).

Confocal observations showed that the F-actin ring-like structure encompasses the cytoplasmic materials and acts as an efficient membrane-free compartment (Fig. 2c). On the contrary, when F-actin flow was disrupted by perturbing filament polymerization and by inhibiting myosin-II activity, nanoparticles failed to accumulate and were found homogeneously distributed throughout the cytoplasmic space of the droplets (Supplementary Figure 6). To characterize the physical properties of the confined cytoplasmic extracts we monitored the diffusion behavior of passive tracers. We tracked the motion of fluorescent latex beads (300 nm diameter) and extracted their mean square displacements for three conditions of confined egg extracts (Fig. 2e and Methods): meiotic extracts in absence of F-actin growth, egg extracts supporting F-actin growth prior to ring-like formation, and egg extracts after the completion of the ring-like formation (see Movie 2). Beads were freely diffusing within the extract cytoplasm for each condition except for the beads that were trapped within the F-actin ring structures. In this latter case beads were completely immobile reflecting the very dense nature of the cytosolic phase confined within the F-actin ring organization. We next estimated the corresponding diffusion coefficients from the bead mean square displacement and found a value of 0.14 $\mu\text{m}^2\cdot\text{s}^{-1}$ for extracts incompetent for F-actin growth, consistent with previous measurements⁶³, and 0.07 and 0.05 $\mu\text{m}^2\cdot\text{s}^{-1}$ for egg extracts prior to and after ring-like formation, respectively (Fig. 2e and Methods). These results suggest that the physical property of the cytoplasm external to the confined cytoplasmic space behaves the same irrespective of the presence or absence of the F-actin ring, whereas the cytoplasm confined within the actin-ring behaves like a solid phase for micrometric assemblies.

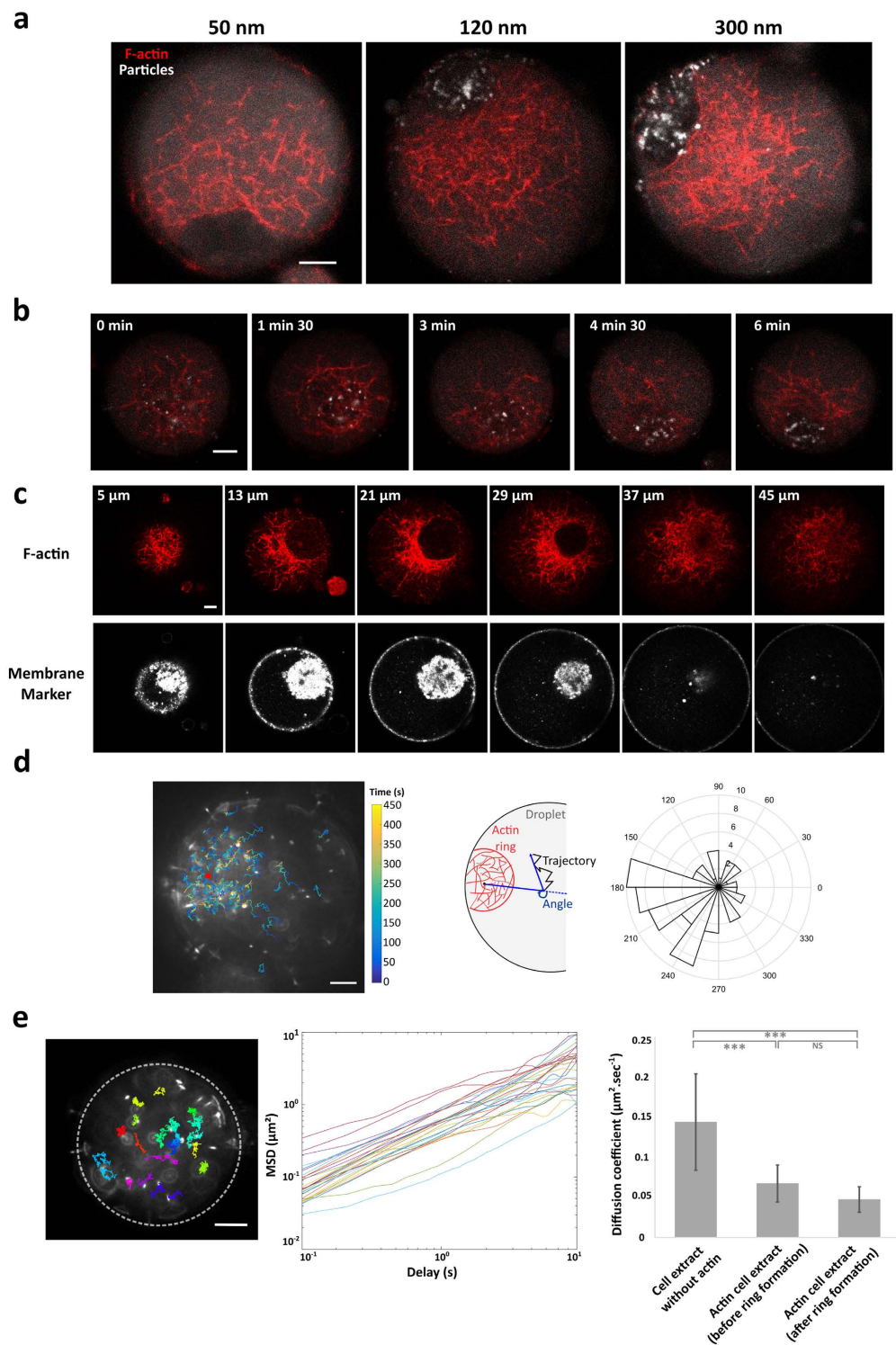


Figure 2. Characteristics of the membrane-free compartmentalization mediated by F-actin flow. (a) F-actin dynamics transport nanoparticles in a size-dependent manner. Accumulation of nanoparticles of different sizes (50 nm, 120 nm, and 300 nm) shows that only nanoparticles above a diameter of 100 nm are transported by F-actin flow. (b) Time-dependent accumulation of 120 nm fluorescent nanoparticles. After 6 minutes, almost all the nanoparticles are gathered at the center of the F-actin ring. (c) Confocal observations of F-actin ring-like structures show that microfilaments encompass cytoplasmic materials stained with membrane marker. Slices of a z-stack; images are $8 \mu\text{m}$ apart (from 5 to $45 \mu\text{m}$ in the droplet). (d) Left: Displacement field of 300 nm-nanoparticles reveals that their motions are highly directed towards the F-actin ring. Right: Angular distribution of tracked trajectories with respect to the actin ring position. (e) Estimation of the cytoplasmic diffusion coefficients in cell extracts incompetent for F-actin organization, and contractile cell extracts at early stage and late stage of F-actin ring organization. Mean and standard deviation are plotted. Scale bars are $10 \mu\text{m}$.

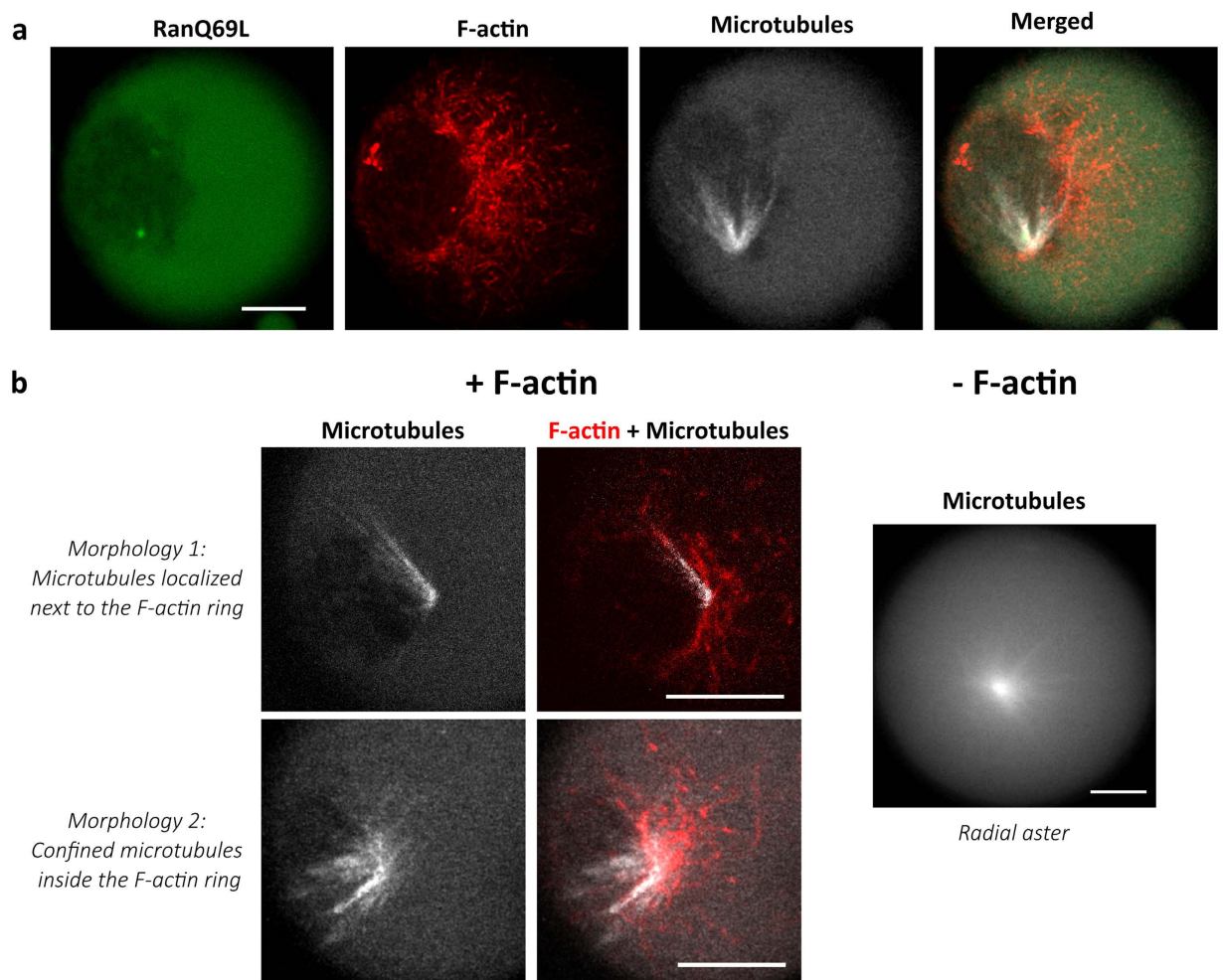


Figure 3. Characterization of asters nucleated with RanQ69L in an F-actin intact cell extract.

(a) Microtubule asters nucleated with $8\ \mu\text{M}$ of RanQ69L. The microtubules are localized and confined within F-actin ring. mCherry-labeled RanQ69L observation indicates an homogenous distribution of Ran within the droplet. (b) Two types of morphologies are observed when microtubule nucleation is triggered in presence of F-actin: asymmetric asters localized inside the F-actin ring and asymmetric asters localized outside the F-actin ring. In absence of F-actin we observed a radial aster. F-actin was labeled with Utr-GFP and fluorescent (TRITC) tubulin was used to visualize microtubules. Scale bars are $10\ \mu\text{m}$.

Altogether our observations within confined egg extracts show that the dynamic state of F-actin meshwork defines two different spatial distributions of nanoparticles and cytoplasmic materials. The nanoparticles were either concentrated by the F-actin meshwork or homogeneously distributed throughout the cytoplasm in cases where F-actin flow was impeded. This membrane-free confinement powered by F-actin flow provides a localized concentration enhancement of nanoparticles, and serves as an active mechanism for the generation and the maintenance of a cytoplasmic partitioning.

Signaling switch mediated by F-actin flow and active confinement to trigger microtubule aster assembly. To evaluate if the mechanism of cytoplasmic confinement could spatiotemporally direct the activation of biochemical signaling pathways, we have designed a proof-of-concept experiment using small GTPase proteins that exhibit ultrasensitivity, e.g. a strong nonlinear input-output relationship (Fig. 1c). We focused our study on the RanGTP pathway and more precisely on RanQ69L, a mutant of Ran locked in the GTP state which promotes the nucleation of microtubule structures into radial asters in *Xenopus* egg extracts⁵⁸. In order to verify that signaling triggered by RanQ69L has the same activation profile in egg extracts supporting F-actin assembly, we monitored the efficiency of aster formation as a function of RanQ69L concentration (0 to $8\ \mu\text{M}$) in both unconfined and confined extracts. In bulk conditions (unconfined extracts), aster formation exhibits a sigmoid dependence on RanQ69L concentration with a concentration threshold around $4\ \mu\text{M}$ both in presence and absence of F-actin flow (Supplementary Figure 7). Experiments performed with confined extracts display a sharper sigmoidal shape than unconfined extracts, but the threshold for polymerization is about 3 to $5\ \mu\text{M}$ for all conditions (Supplementary Figure 7e). Confocal microscopy revealed that asters nucleated with RanQ69L above the nucleation threshold have their pole positioned next to the F-actin ring structure (Fig. 3a, Supplementary Figure 8a). Interestingly, this localization of microtubule based-structures is observed despite the homogeneous spatial

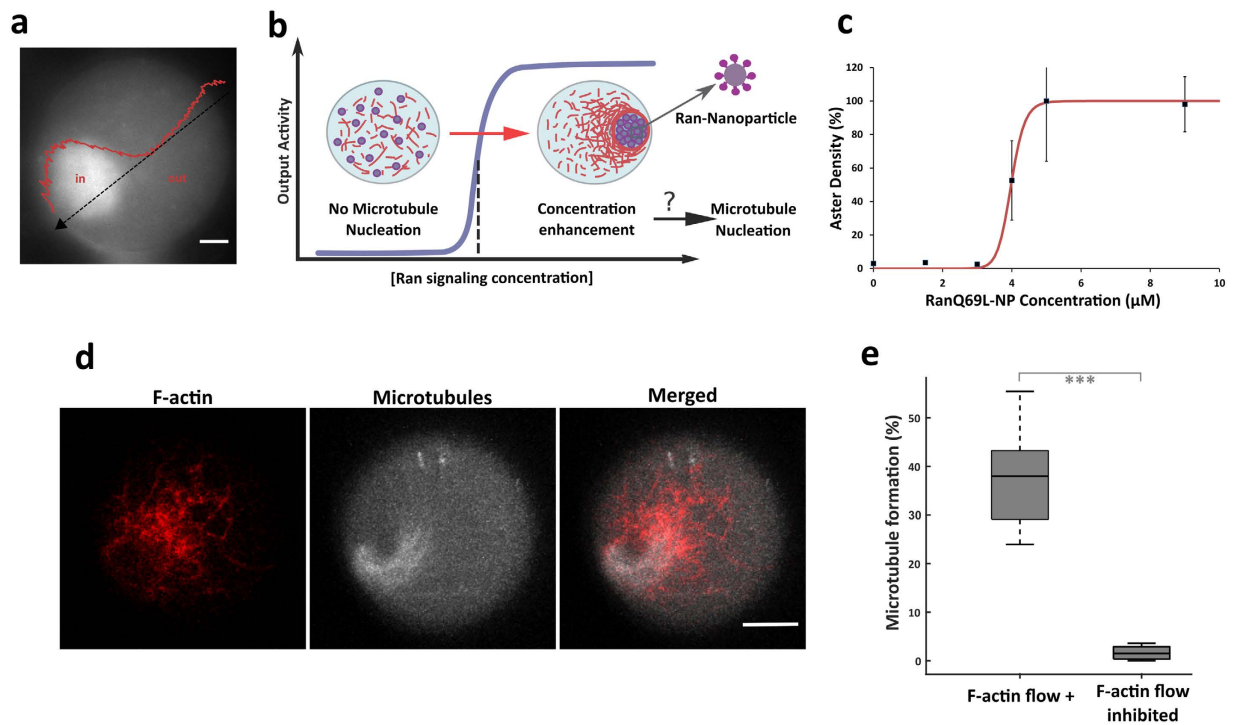


Figure 4. Signaling switch triggered by F-actin flow and by the active confinement of Ran-nanoparticles. (a) Estimation of the concentration enhancement driven by F-actin self-organization by quantifying the lysotracker spatial distribution along the droplet diameter. (b) Schematic of the proof-of-concept experiment. GTPase RanQ69L are grafted on nanoparticles and the complexes are dispersed within cell extract droplets at a concentration level below the threshold required for microtubule growth. The F-actin flow conveys and confines the Ran-nanoparticles within the F-actin ring-structure to eventually induce a concentration enhancement of Ran in a restricted area, which may lead to activate microtubule nucleation. (c) Ran-nanoparticles control microtubule assembly with an activity characterized by a sigmoidal concentration dependency. (d) Confocal observation of a microtubule-aster formation induced by the active confinement of Ran-NPs (initially added at a concentration under nucleation threshold, 500 nM). Microtubules are stained with rhodamine-labeled tubulin, and F-actin with Utr-GFP. (e) Quantification of the efficiency of the signaling switch: percentage of droplets containing an aster in presence or absence of F-actin flow. The box plot shows the median (central mark), the 25th and 75th percentiles (edges of the box); the whiskers extend to the most extreme data points that are not considered as outliers.

distribution of mCherry-labeled RanQ69L within the droplet (Fig. 3a, Method). We were able to detect two types of morphologies in this condition: asymmetric asters localized inside the F-actin ring and asymmetric asters localized outside the F-actin ring (Fig. 3b left). This is in contrast with radial asters observed in extracts incompetent for actin (Fig. 3b right). In addition, both the morphology and the localization of the asters next to the F-actin ring were similar regardless of the concentration of Ran used (4–10 μM) (Supplementary Figure 8b).

Microscopic observations of the concentration increase of acidic organelles during F-actin contraction (2–5 fold) suggest a hypothetical mechanism of concentration enhancement of mesoscopic objects (Fig. 4a). To implement a biochemical switch mediated by F-actin flow, we used 120 nm nanoparticles as platforms to locally concentrate RanQ69L (Fig. 4b). We first conjugated RanQ69L to nanoparticles (Ran-NPs) and verified the functional activity of the proteins grafted at the nanoparticle surface (Fig. 4c, Methods). The formation of microtubule asters triggered by Ran-NPs exhibited a similar sigmoidal dependence on concentration and nucleation threshold, indicating that conjugating RanQ69L to nanoparticles did not perturb aster formation⁵⁶. Next, we examined how local concentration increase of Ran-NPs mediated by F-actin flow impacts microtubule nucleation. Initially, the Ran-NPs were dispersed homogeneously throughout the droplet cytoplasm at a concentration below the microtubule nucleation threshold (between 0.5 and 1.5 μM). Within five minutes, the nanoparticles were transported by the dynamics of F-actin leading to a strong local enrichment of Ran-NPs (Fig. 2b and Movie 1). Remarkably, after 40 minutes we observed the formation of microtubule-based structures (Fig. 4d and Supplementary Figure 9). Confocal observations showed that the microtubules assembled into aster-like structures or polarized arrays localized either within the F-actin contractile ring or in the vicinity of the microfilament structure (Fig. 4d and Supplementary Figure 9). In some cases we observed the bending of microtubule fibers suggesting that F-actin contractility induces a confinement sufficient to constrain microtubule growth. From these observations we estimate that the forces applied on the microtubule fibers by the F-actin are on the order of 10 pN (see Methods). To assess the robustness and efficiency of the signaling switch, we performed systematic studies showing that microtubule fibers were found in more than 35% of the total number of observed contractile droplets (six independent

experiments, $n = 391$ droplets; Fig. 4e), whereas almost no microtubule fibers were detectable in confined extracts when F-actin flow was impeded with cytochalasin-D and blebbistatin (six independent experiments, $n = 458$ droplets; Fig. 4e). This indicates that the accumulation of Ran-NPs was sufficiently efficient to trigger the nucleation of microtubules, therefore surpassing the local Ran concentration threshold. In addition, the cytoplasmic accumulation of unconjugated nanoparticles within extracts failed to trigger aster assembly, ruling out the possibility that the F-actin flow concentrated non-specific microtubule nucleation factors associated with the nanoparticles. Moreover the absence of bright clusters when monitoring fluorescent proteins suggests that protein aggregation, which could serve as a non-specific protein scaffold, is not occurring inside the F-actin ring (Fig. 3a, Supplementary Figure 3). Thus, the active confinement of Ran-NPs by F-actin self-organization induces a robust signaling switch that triggers microtubule assembly.

Signaling switch mediated by F-actin-based polymeric scaffolds. Given the high-order organization and the large density of F-actin meshwork that is assembled during contraction, we next investigated if the direct recruitment of Ran along the microfilaments could trigger sufficient downstream signaling activities to nucleate microtubules (Fig. 5a). Microscopic observations suggest that the density in polymeric actin can reach a 3–8 fold increase during contraction (Fig. 5b), suggesting a hypothetical mechanism of concentration enhancement given that F-actin could act as polymeric scaffold to recruit proteins. To evaluate this concept, we engineered RanQ69L to specifically target F-actin filaments (Fig. 5a) by fusing RanQ69L to the calponin homology domain of utrophin (Utr-RanQ69L). We first verified the capacity of the utrophin domain to bind filaments by co-localizing GFP-Utr-RanQ69L with fluorescent actin filaments (labeled using Alexa-568 Phalloidin, Fig. 5c). We also studied the perturbation of Utr-Ran (500 nM) on the F-actin meshwork structure and dynamics (concentration used in the signaling switch experiments). We found that the ratio between the droplet diameter and the ring diameter was identical in presence or absence of 500 nM of Utr-Ran (Supplementary Figure 2). The size of the F-actin meshwork was also evaluated and found to be slightly increased from 1.1 μm to 1.2 μm in the presence of Utr-Ran supplemented in the extract (Supplementary Figure 3a). On the Supplementary Figure 3b, one can see that the mean F-actin velocity (94 $\text{nm}\cdot\text{s}^{-1}$) in absence of Utr-Ran is slightly smaller in presence of 500 nM of Utr-Ran (72 $\text{nm}\cdot\text{s}^{-1}$). Second, we tested the capacity of the chimera protein Utr-RanQ69L to induce microtubule nucleation. Achieving a homogenous distribution of Utr-RanQ69L in the cytoplasm, by impeding F-actin filament formation and consequently any scaffolding effect of RanQ69L, was a prerequisite for accurately assessing the functionality of Utr-Ran in absence of scaffolding. We then quantified the aster density as a function of Utr-RanQ69L concentration and again found a sigmoidal concentration dependence, with a nucleation threshold of 5 μM (Fig. 5d). The timescale for aster formation was similar between RanQ69L and Utr-RanQ69L (between 20 and 30 minutes) indicating that Utr-RanQ69L remains functional. Finally, to evaluate F-actin scaffolding can mediate a signaling switch, we added Utr-RanQ69L to the egg extract at an initial concentration under the nucleation concentration threshold (500 nM). Remarkably, the assembly of the F-actin meshwork triggered the nucleation of microtubule filaments in less than one hour (Fig. 5e and Supplementary Figure 10a). We quantified this effect and found that microtubule assemblies occurred within 43% of the droplets (7 independent experiments, $n = 246$ droplets), whereas only 17% of the droplets contained microtubules when the F-actin flow was disrupted (7 independent experiments, $n = 259$ droplets) (Fig. 5f). Therefore, almost no microtubule nucleation was observed when F-actin flow was disrupted, showing the specificity of the actin scaffold. This suggests that non-specific protein aggregation is not involved in the microtubule nucleation process. The few microtubule nucleation events observed in absence of F-actin flow could originate from remaining micrometric F-actin patches (despite drug treatment) that could scaffold Utr-RanQ69L (Supplementary Figure 11).

Microtubule filaments appeared to be supported by the actin meshwork. We also generally observed that microtubules assembled into polymeric arrays rather than into asters. These structures were found aligned with F-actin fibers (Supplementary Figure 10b) and co-localized with GFP-labeled Ran-Utr (Fig. 5g). Further characterizations of the microtubule-based structures were performed using EB1-GFP to visualize microtubule plus-end dynamics. A typical example of microtubule dynamics is shown in Movie 3, which suggests that the microtubule arrays mediated by Utr-RanQ69L are polarized with a plus-end dynamic having a growth rate between 5 and 20 $\mu\text{m}\cdot\text{min}^{-1}$; this range of velocity is similar to that obtained with RanQ69L wild type (Fig. 5h).

Altogether we have demonstrated how the artificial scaffolding mediated by F-actin could drive the accumulation of Ran with an enhanced concentration sufficient to trigger the activation of microtubule nucleation, forming an asymmetric polarized array of fibers.

Interestingly, the microtubules organized into two different patterns according to the mode of localization of Ran by F-actin: confinement of Ran-NPs within F-actin ring and scaffolding along actin polymers (Supplementary Figure 12). In the case of Ran-NPs microtubules formed a single asymmetric aster, whereas in the case of Utr-Ran microtubules organized into a polarized array of fibers without pole organization (Fig. 5e). This suggests a mode of spatial organization of microtubules that depend on F-actin state and on the localization of nucleation.

Discussion

F-actin structures and dynamics drive numerous essential functions when they are assembled at the cortex of cells as well as within the cytoplasm. We have shown that the combination of *in vitro* reconstitution of a confined cytoplasm with synthetic strategies imparted two novel functions to F-actin dynamics: first, the membrane-free confinement of signaling proteins, and second, the scaffolding of signaling proteins along actin polymers. In this context, F-actin self-organization into contractile meshwork drives the triggering of the RanGTP pathway, an archetypal of ultrasensitive signaling switch.

From the perspective of synthetic biology, our *in vitro* approach allowed us to explore and implement artificial and novel functions by engineering the F-actin spatial organization and signaling processes^{64–66}. Our bottom-up

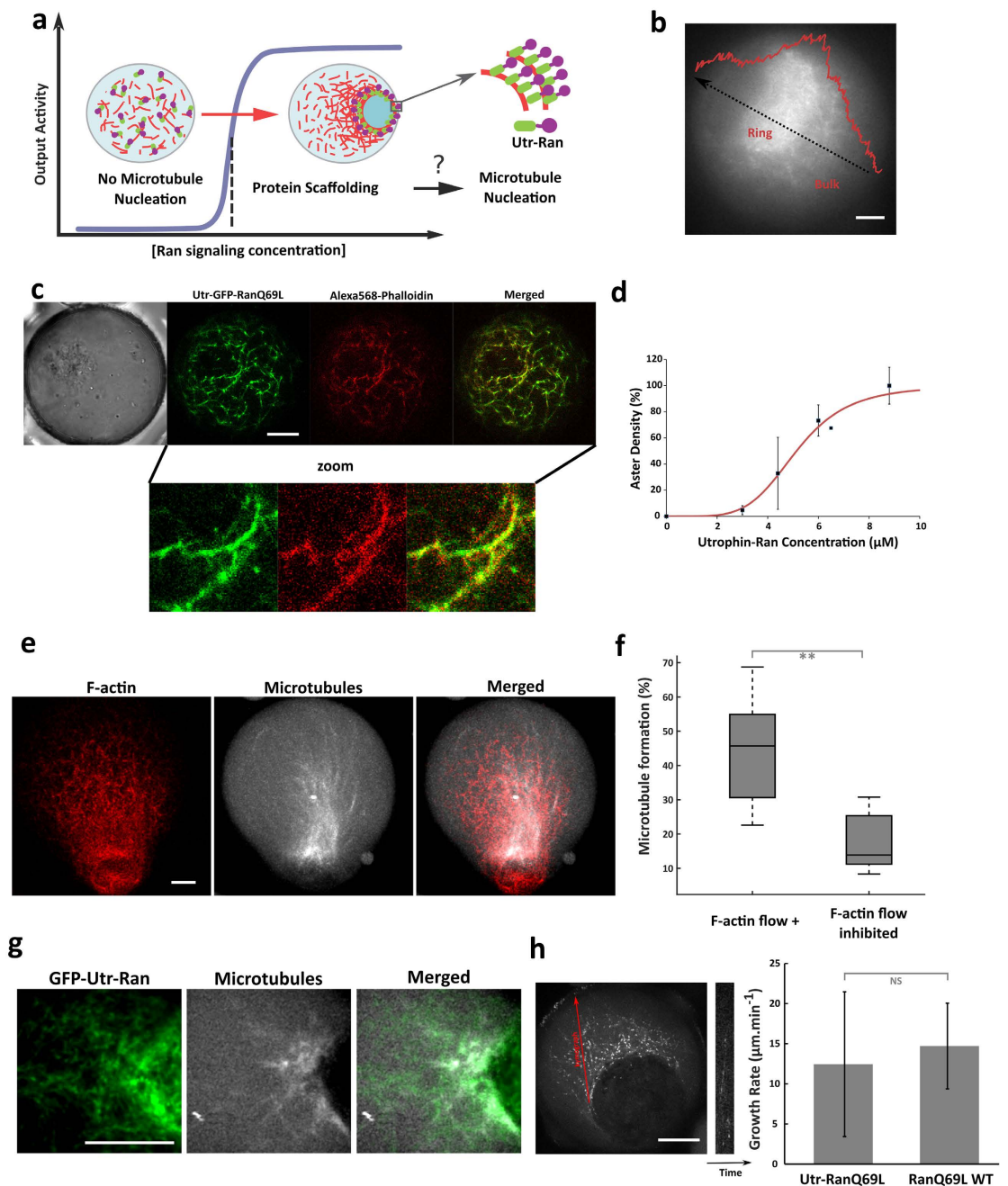


Figure 5. Signaling switch mediated by F-actin polymeric scaffolds. (a) Principle of the proof-of-concept experiment examining how F-actin could act as polymeric scaffold hubs to recruit regulatory proteins. RanQ69L is fused to the CH domain of utrophin to target F-actin filaments. Contraction and F-actin density increase may drive the concentration increase of Utr-Ran in a restricted area to trigger microtubule polymerization. (b) Evaluation of the fold increase in density of F-actin meshwork after contraction. (c) Co-localization of Utrophin-emGFP-RanQ69L (green) with F-actin meshwork (Alexa-568 Phalloidin, red). (d) Utr-RanQ69L induces microtubule assembly in confined extracts with a sigmoidal concentration dependency. (e) Confocal observation of microtubule formation induced by Utr-RanQ69L under nucleation threshold (500 nM) in confined extract. Microtubules are stained with rhodamine-labeled tubulin, and F-actin with Utr-GFP. (f) Quantification of the efficiency of the signaling switch mediated by F-actin flow: number of droplets containing microtubule arrays with F-actin flow and with the inhibition of F-actin flow. Observations were done with confocal microscopy. (g) Confocal observation of microtubules induced by GFP-Utr-Ran under nucleation threshold (500 nM). Microtubules are stained with rhodamine-labeled tubulin. (h) Left: typical kymograph extracted from Movie 3. Microtubules are labeled with EB1-GFP. Right: quantitative analysis of the growth rate extracted from the kymographs. Growth rates were measured for microtubules assembled using Utr-RanQ69L that are recruited to F-actin scaffolds (initial concentration at 500 nM) and using RanQ69L (6 μM). Mean and standard deviation are plotted. The measured growth rates are similar between these two pathways for growth (Utr-RanQ69L and RanQ69L). Scale bars are 10 μm .

approach is generic, versatile and modular, and could be extended to other signaling proteins, such as kinases, that exhibit non-trivial dynamics through collective effects.

One important difference between our *in vitro* system and living systems concerns the regulation of actin cytoskeleton, which occurs in cells in a reversible manner, thus providing a richer dynamic of control. An improvement of our assay from droplets of egg extracts to vesicles of egg extracts made of a lipid bilayer may allow the use of drugs to assess more precisely the dynamic properties of such signaling switches induced by F-actin self-organization. F-actin dependent-formation of microdomains in dendritic spines and during T cell signaling are some of the many possible roles for microfilament control of signaling pathways in living cells^{17,19}. Our *in vitro* assay isolates simple design principles underlying the control of signaling pathways by cytoplasmic F-actin self-organization to tune signaling processes: either by docking signaling proteins to a mesoscopic-like structure sufficiently large to be non-specifically confined by a contractile meshwork, or the specific recruitment of signaling proteins along actin microfilaments, which serve as linear and rigid scaffolding polymers. One perspective will be the implementation of the strategy into living cells in order to artificially couple F-actin spatiotemporal organization and signaling events. This may help to examine if the widespread occurrence of F-actin structures throughout living cells could be used to shape signaling events.

Furthermore, there are mounting interests in studying how phase transitions generate membrane-free micro-domains in the cytoplasm that eventually regulate functions or signaling pathways^{8,9,12,13}. These mechanisms generally operate near thermodynamic equilibrium, and interestingly we found that out-of-equilibrium structures powered by F-actin organization can contribute in partitioning the cytoplasm and in shaping signaling processes in space and time.

Finally our minimal system could be extended to examine possible mechanisms of crosstalk between actin and microtubules, which could be reconstituted in a controlled manner.

Material and Methods

Expression and purification of recombinant proteins. The plasmids for *E. coli* expression of RanQ69L (pQE32-Ran, 6His Tag) and EB1-GFP were kindly provided by Iain Mattaj (EMBL) and Ron Vale (UCSF) respectively. The plasmids Utr-Ran, Utr-GFP, and GFP-Utr-Ran for *E. coli* expression were cloned from pSPE3 GFP Utrophin plasmid²¹ in a pET28. Expression of plasmids and purification of recombinant proteins (RanQ69L, EB1-GFP, Utr-Ran, Utr-GFP, Utr-GFP-Ran) were realized using standard protocols.

Reagents. ATP, DTT, creatine phosphate, cytochalasin D, latrunculin-A, blebbistatin, creatine phosphokinase and mineral oil (M5904) were purchased from Sigma-Aldrich (St Louis, MO). Poly(12-hydroxystearic acid) (PHS) and poly(ethylene oxide) (PEO-30) are commercially available (Arlacel P135) and were purchased from UNIQEMA. Tubulins, labeled with Rhodamin or with FITC, were ordered from Cytoskeleton Inc. (Denver, CO). Membrane tracker, lysotracker and Alexa-fluor 568 Phalloidin were purchased from Life Technologies. 120 nm and 300 nm nanoparticles were purchased from Ademtech. 50 nm nanoparticles were purchased from Micromod.

Cytostatic-factor-arrested (CSF) *Xenopus laevis* egg extracts, which correspond to active cytoplasm of oocytes arrested in metaphase II of meiosis, were prepared as previously described⁶⁷, with the following modifications: no cytochalasin D was added and all steps were carried at 4 °C^{41,68}. All reagents for buffer preparation were purchased from Sigma-Aldrich.

Microtubule and actin assembly. Microtubule structures were assembled using metaphase *Xenopus laevis* egg extracts, containing an ATP regenerating system (1 mM ATP, 10 mM creatine phosphate, 100 µg/µL creatine phosphokinase, final concentrations), incubated in the presence of RanQ69L, Ran-NP complexes, or UtrCH-RanQ69L, at the final concentration indicated in the manuscript for 30 min at 19 °C. Microtubules were labeled either with Rhodamin-labeled tubulin at 100 nM final (Cytoskeleton Inc.), Fluorescein-labeled tubulin at 100 nM final (Cytoskeleton Inc.), or EB1-GFP at 150 nM.

Actin structures were assembled using metaphase *Xenopus laevis* egg extracts, containing an ATP regenerating system (1 mM ATP, 10 mM creatine phosphate, 100 µg/µL creatine phosphokinase, final concentrations). The actin flow was disturbed using blebbistatin at 130 nM final and cytochalasin D at 2 µg/mL final or latrunculin at 25 µM final. Actin was labeled with GFP-utrophin at 110 nM final or Alexa-Fluor 568 Phalloidin at 50 nM final.

Imaging and Data Analysis. Fluorescence imaging of microtubule asters and actin network was performed using an IX81 (Olympus) and X60 (PlanApo, NA 1,42) oil objective, equipped with an EM-CCD camera (electron multiplying CCD, C9100-02, Hamamatsu, Corporation), and a LED system of illumination (Spectra X, Lumencor). Microscope settings and functions were controlled using Simple PCI software (Hamamatsu). Image analysis was performed using ImageJ Software, Matlab, and Simple PCI software. Confocal microscopy was performed with a Zeiss LSM 710 META laser scanning confocal microscope using X63 (PlanApoChromatic, NA 1,4) objective. Image analysis was performed using LSM Software Zen 2009 and ImageJ.

To quantify the concentration enhancement of organelles within the F-actin ring-like structures, contractile cell extracts were supplemented with lysotracker (Lysotracker Green DND-26 final concentration 2 µM, Fig. 4a). We first monitored F-actin droplets and computed the intensity profile to quantify the lysotracker spatial distribution along the droplet axis for both contractile and non-contractile F-actin states. After normalization and averaging, we obtained fluorescent profiles that were deconvoluted to correct the volume contribution. Then the concentration enhancement was estimated by computing the ratio between the maximum and the minimum of the intensity profile. The same procedure was applied for computing the concentration enhancement of labeled F-actin at late F-actin contraction (Fig. 5b).

To estimate viscosity of cell extracts in different conditions, we monitored the Brownian motion of latex beads (328 nm diameter, Estapor). The trajectories of the beads were then recovered thanks to IcY software⁶⁹.

Mean Square Displacement (MSD) analysis was computed using Matlab and the diffusion coefficient of the beads was obtained from the 25 first percent of the MSD slope. For the experiments performed after ring formation, the motions of immobile particles within the F-actin ring have not been considered for the estimation of the viscosity.

We estimated the meshsize of the network from confocal images. We plotted intensity profiles and then measured the distance between two fibers. We only took the values that were above the diffraction limit of our optical system (500 nm).

Student's t-tests were performed with Matlab. For the interpretation of the p-values: NS means there is no significant difference between the two distributions. One star means pvalue <0,05, two stars means pvalue <0,01, three stars means pvalue <0,001.

To quantitatively assess the degree of colocalization between the actin and microtubule structures we used the ImageJ plugin "Coloc 2" to plot the 2d-histograms and get the Pearson's coefficients for the two representative images in Supplementary Figure 10b.

Visualization of Ran using mCherry reporters. In order to see how RanQ69L is distributed within the droplet, we generated a dimer between Ran and mCherry using FRB and FKBP dimerizing system. Briefly, we formed dimers with FKBP-Ran and FRB-mCherry in a premix during 5 minutes at room temperature ([FKBP-Ran]=112 μ M; [FRB-mCherry]=11,2 μ M; [Rapamycin]=100 μ M). We performed extract experiments with a final concentration of Ran of 8 μ M.

Conjugation of Ran proteins to nanoparticles. Carboxylic acid nanoparticles (iron oxide core, 120 nm diameter) were purchased from Ademtech. The nanoparticles/RanQ69L conjugation was performed as previously described⁵⁶. Conjugation stoichiometry was determined by a semi-quantitative assay using SDS-PAGE electrophoresis.

Extract-in-Oil Droplet Formations. Cellular extract was encapsulated in droplets via water-in-oil emulsion process. Mineral oil contains a biocompatible block copolymer in order to stabilize emulsion and facilitate observations. This method has been previously described and allows the formation of microtubule asters and active actin meshworks in droplets^{40,70}. PHS-PEO-PHS block copolymer (Arlacel P135) was first dissolved in mineral oil (0.4 mg.mL⁻¹). The *Xenopus laevis* egg extracts containing fluorescently labeled tubulin and/or utrophin-GFP was then added to the block copolymer solution (1% (v CSF/v Oil)) at room temperature. The mixture is gently sheared, by pipetting up and down the solution during few seconds, to generate extract-in-oil droplets. The mechanical dispersion of the biphasic solution formed micrometer-sized extract-in-oil droplets within few seconds. The emulsion is incubated for 20–30 minutes at 19 °C. Then droplets were observed in a time frame comprised between 20 and 60 minutes after mixing of the components. The droplets presenting microtubule formation had a diameter comprised between 10 and 55 μ m. Observations were done maximum one hour after the beginning of the incubation. After one hour of incubation, some spontaneous microtubule nucleation could be sometimes observed.

Estimation of the forces applied on microtubules. Two mechanisms of force generation could explain the bending of microtubules observed in our observations (Fig. 3d and Fig. 3 – figure supplement 1). First, the forces applied on elongated microtubules could be directly produced by the F-actin meshwork during contraction through both the polymerization of actin microfilaments and the myosin II activity. Second, microtubule fibers during growth can encounter the F-actin ring-like structure that can be considered as a rigid confinement boundary. Consequently when growing microtubules encounter the F-actin ring-like structure, normal compression forces are exerted. These compressive forces eventually cause microtubules to buckle. This buckling instability appears when a critical force, F_c , is reached. F_c scales with N^2B/l^2 ; l is the microtubule length, N the number of filaments composing the bundle (the filaments are cross-linked together), and B the bending modulus characterizing the stiffness of the microtubule (25 pN. μ m²). N is found to vary between 3 to 7 microtubules in egg extracts⁷⁰. Therefore, typical observations indicate that forces of the order of 10 pN are applied on microtubules.

References

1. Luby-Phelps, K. The physical chemistry of cytoplasm and its influence on cell function: an update. *Mol. Biol. Cell* **24**, 2593–2596 (2013).
2. Kinkhabwala, A. & Bastiaens, P. I. Spatial aspects of intracellular information processing. *Curr Opin Genet Dev* **20**, 31–40 (2010).
3. Kholodenko, B. N., Hancock, J. F. & Kolch, W. Signalling ballet in space and time. *Nat Rev Mol Cell Biol* **11**, 414–426 (2010).
4. Bashor, C. J., Helman, N. C., Yan, S. & Lim, W. A. Using engineered scaffold interactions to reshape MAP kinase pathway signaling dynamics. *Science (80-.)*. **319**, 1539–1543 (2008).
5. Good, M. C., Zalatan, J. G. & Lim, W. A. Scaffold proteins: hubs for controlling the flow of cellular information. *Science (80-.)*. **332**, 680–686 (2011).
6. Kiel, C., Yus, E. & Serrano, L. Engineering signal transduction pathways. *Cell* **140**, 33–47 (2010).
7. Albertazzi, L. *et al.* Spatiotemporal control and superselectivity in supramolecular polymers using multivalency. *Proc. Natl. Acad. Sci. USA*. **110**, 12203–12208 (2013).
8. Li, P. *et al.* Phase transitions in the assembly of multivalent signalling proteins. *Nature* **483**, 336–340 (2012).
9. Weber, S. C. & Brangwynne, C. P. Getting RNA and protein in phase. *Cell* **149**, 1188–1191 (2012).
10. Banjade, S. & Rosen, M. K. Phase transitions of multivalent proteins can promote clustering of membrane receptors. *Elife* **3**, 1–24 (2014).
11. Kato, M. *et al.* Cell-free formation of RNA granules: Low complexity sequence domains form dynamic fibers within hydrogels. *Cell* **149**, 753–767 (2012).
12. Wu, H. Higher-order assemblies in a new paradigm of signal transduction. *Cell* **153**, 287–292 (2013).
13. Brangwynne, C. P. C. *et al.* Germline P granules are liquid droplets that localize by controlled dissolution/condensation. *Science* **324**, 1729–1732 (2009).
14. Forgacs, G., Yook, S. H., Janmey, P. a., Jeong, H. & Burd, C. G. Role of the cytoskeleton in signaling networks. *J. Cell Sci.* **117**, 2769–2775 (2004).

15. Janmey, P. a. & Lindberg, U. Cytoskeletal regulation: rich in lipids. *Nat. Rev. Mol. Cell Biol.* **5**, 658–666 (2004).
16. Valensin, S. *et al.* F-actin dynamics control segregation of the TCR signaling cascade to clustered lipid rafts. *Eur. J. Immunol.* **32**, 435–446 (2002).
17. Chichili, G. R., Westmuckett, A. D. & Rodgers, W. T cell signal regulation by the actin cytoskeleton. *J. Biol. Chem.* **285**, 14737–14746 (2010).
18. Munro, E., Nance, J. & Priess, J. R. Cortical flows powered by asymmetrical contraction transport PAR proteins to establish and maintain anterior-posterior polarity in the early *C. elegans* embryo. *Dev. Cell* **7**, 413–424 (2004).
19. Colgan, L. A. & Yasuda, R. Plasticity of Dendritic Spines: Subcompartmentalization of Signaling. *Annu. Rev. Physiol.* **76**, 365–385 (2014).
20. Field, C. M. & Lenart, P. Bulk cytoplasmic actin and its functions in meiosis and mitosis. *Curr Biol* **21**, R825–R830 (2011).
21. Azoury, J. *et al.* Spindle positioning in mouse oocytes relies on a dynamic meshwork of actin filaments. *Curr Biol* **18**, 1514–1519 (2008).
22. Niwayama, R., Shinohara, K. & Kimura, A. Hydrodynamic property of the cytoplasm is sufficient to mediate cytoplasmic streaming in the *Caenorhabditis elegans* embryo. *Proc. Natl. Acad. Sci. USA.* **108**, 11900–11905 (2011).
23. Schuh, M. & Ellenberg, J. A new model for asymmetric spindle positioning in mouse oocytes. *Curr Biol* **18**, 1986–1992 (2008).
24. Li, H., Guo, F., Rubinstein, B. & Li, R. Actin-driven chromosomal motility leads to symmetry breaking in mammalian meiotic oocytes. *Nat Cell Biol* **10**, 1301–1308 (2008).
25. Mori, M. *et al.* Intracellular transport by an anchored homogeneously contracting F-actin meshwork. *Curr Biol* **21**, 606–611 (2011).
26. Maiuri, P. *et al.* Actin Flows Mediate a Universal Coupling between Cell Speed and Cell Persistence. *Cell* **161**, 374–386 (2015).
27. Lee, K., Gallop, J. L., Rambani, K. & Kirschner, M. W. Self-assembly of filopodia-like structures on supported lipid bilayers. *Science* (80-.). **329**, 1341–1345 (2010).
28. Reymann, A. C. *et al.* Nucleation geometry governs ordered actin networks structures. *Nat Mater* **9**, 827–832 (2010).
29. Bernheim-Groswasser, A., Wiesner, S., Golsteyn, R. M., Carlier, M. F. & Sykes, C. The dynamics of actin-based motility depend on surface parameters. *Nature* **417**, 308–311 (2002).
30. Paluch, E., van der Gucht, J., Joanny, J. F. & Sykes, C. Deformations in actin comets from rocketing beads. *Biophys J* **91**, 3113–3122 (2006).
31. Heald, R. *et al.* Self-organization of microtubules into bipolar spindles around artificial chromosomes in *Xenopus* egg extracts. *Nature* **382**, 420–425 (1996).
32. Liu, A. P. & Fletcher, D. A. Biology under construction: *in vitro* reconstitution of cellular function. *Nat Rev Mol Cell Biol* **10**, 644–650 (2009).
33. Preciado López, M. *et al.* Actin-microtubule coordination at growing microtubule ends. *Nat. Commun.* **5**, 4778 (2014).
34. Nguyen, P. a. *et al.* Spatial organization of cytokinesis signaling reconstituted in a cell-free system. *Science* (80-.). **346**, 244–247 (2014).
35. Ciobanasi, C., Faivre, B. & Le Clainche, C. Actomyosin-dependent formation of the mechanosensitive talin-vinculin complex reinforces actin anchoring. *Nat. Commun.* **5**, 3095 (2014).
36. Roostalu, J., Cade, N. I. & Surrey, T. Motor-mediated cortical versus astral microtubule organization in lipid-monolayered droplets. *Nat. Cell Biol.* **17**, 1422–1434 (2015).
37. Surrey, T., Nedelec, F., Leibler, S. & Karsenti, E. Physical properties determining self-organization of motors and microtubules. *Science* (80-.). **292**, 1167–1171 (2001).
38. Köhler, S., Schmolter, K. M., Crevenna, A. H. & Bausch, A. R. Regulating contractility of the actomyosin cytoskeleton by pH. *Cell Rep.* **2**, 433–439 (2012).
39. Falzone, T. T., Lenz, M., Kovar, D. R. & Gardel, M. L. Assembly kinetics determine the architecture of α -actinin crosslinked F-actin networks. *Nat. Commun.* **3**, 861 (2012).
40. Pinot, M. *et al.* Effects of Confinement on the Self-Organization of Microtubules and Motors. *Curr. Biol.* **19**, 954–960 (2009).
41. Pinot, M. *et al.* Confinement induces actin flow in a meiotic cytoplasm. *Proc. Natl. Acad. Sci. USA.* **109**, 11705–11710 (2012).
42. Reymann, A. C. *et al.* Actin network architecture can determine myosin motor activity. *Science* (80-.). **336**, 1310–1314 (2012).
43. Vignaud, T., Blanchoin, L. & Thery, M. Directed cytoskeleton self-organization. *Trends Cell Biol* **22**, 671–682 (2012).
44. Good, M. C., Vahey, M. D., Skandarajah, a., Fletcher, D. a. & Heald, R. Cytoplasmic Volume Modulates Spindle Size During Embryogenesis. *Science* (80-.). **342**, 856–860 (2013).
45. Laan, L., Roth, S. & Dogterom, M. End-on microtubule-dynein interactions and pulling-based positioning of microtubule organizing centers. *Cell Cycle* **11**, 3750–3757 (2012).
46. Salman, H. *et al.* Nuclear localization signal peptides induce molecular delivery along microtubules. *Biophys. J.* **89**, 2134–2145 (2005).
47. Gaetz, J., Gueroui, Z., Libchaber, A. & Kapoor, T. M. Examining how the spatial organization of chromatin signals influences metaphase spindle assembly. *Nat Cell Biol* **8**, 924–932 (2006).
48. Yoo, B.-K., Buguin, A. & Gueroui, Z. Biochemical perturbations of the mitotic spindle in *Xenopus* extracts using a diffusion-based microfluidic assay. *Biomicrofluidics* **9**, 044101 (2015).
49. Dinarina, A. *et al.* Chromatin Shapes the Mitotic Spindle. *Cell* **138**, 502–513 (2009).
50. Field, C. M. *et al.* Actin behavior in bulk cytoplasm is cell cycle regulated in early vertebrate embryos. *J Cell Sci* **124**, 2086–2095 (2011).
51. Hara, Y. & Merten, C. A. Dynein-Based Accumulation of Membranes Regulates Nuclear Expansion in *Xenopus laevis* Egg Extracts. *Dev. Cell* **33**, 562–575 (2015).
52. Scrofani, J., Sardon, T., Meunier, S. & Vernos, I. Microtubule nucleation in mitosis by a RanGTP-dependent protein complex. *Curr. Biol.* **25**, 131–140 (2015).
53. Kim, S. Y. & Ferrell, J. E. Substrate competition as a source of ultrasensitivity in the inactivation of Wee1. *Cell* **128**, 1133–1145 (2007).
54. Chang, J. B. & Ferrell, J. E. Mitotic trigger waves and the spatial coordination of the *Xenopus* cell cycle. *Nature* **500**, 603–607 (2013).
55. Halpin, D., Kalab, P., Wang, J., Weis, K. & Heald, R. Mitotic spindle assembly around RCC1-coated beads in *xenopus* egg extracts. *PLoS Biol.* **9**, e1001225. doi: 10.1371/journal.pbio.1001225 (2011).
56. Hoffmann, C. *et al.* Spatiotemporal control of microtubule nucleation and assembly using magnetic nanoparticles. *Nat. Nanotechnol.* **8**, 199–205 (2013).
57. Bonnemay, L., Hostachy, S., Hoffmann, C., Gautier, J. & Gueroui, Z. Engineering spatial gradients of signaling proteins using magnetic nanoparticles. *Nano Lett.* **13**, 5147–5152 (2013).
58. Caudron, M., Bunt, G., Bastiaens, P. & Karsenti, E. Spatial coordination of spindle assembly by chromosome-mediated signaling gradients. *Science* **309**, 1373–1376 (2005).
59. Clarke, P. R. & Zhang, C. Spatial and temporal coordination of mitosis by Ran GTPase. *Nat. Rev. Mol. Cell Biol.* **9**, 464–477 (2008).
60. Ferrell, J. E. & Ha, S. H. Ultrasensitivity part I: Michaelian responses and zero-order ultrasensitivity. *Trends Biochem. Sci.* **39**, 496–503 (2014).
61. Cavazza, T. & Vernos, I. The RanGTP Pathway: From Nucleo-Cytoplasmic Transport to Spindle Assembly and Beyond. *Front. cell Dev. Biol.* **3**, 82 (2015).
62. Burkel, B. M., Von Dassow, G. & Bement, W. M. Versatile fluorescent probes for actin filaments based on the actin-binding domain of utrophin. *Cell Motil. Cytoskeleton* **64**, 822–832 (2007).

63. Valentine, M. T., Perlman, Z. E., Mitchison, T. J. & Weitz, D. A. Mechanical properties of *Xenopus* egg cytoplasmic extracts. *Biophys. J.* **88**, 680–689 (2005).
64. Kim, A. K. *et al.* Toward total synthesis of cell function: Reconstituting cell dynamics with synthetic biology. *Sci. Signal.* **9**, re1–re1 (2016).
65. Goodman, B. S., Derr, N. D. & Reck-Peterson, S. L. Engineered, harnessed, and hijacked: Synthetic uses for cytoskeletal systems. *Trends in Cell Biology* **22**, 644–652 (2012).
66. Lim, W. A. Designing customized cell signalling circuits. *Nat Rev Mol Cell Biol* **11**, 393–403 (2010).
67. Hannak, E. & Heald, R. Investigating mitotic spindle assembly and function in vitro using *Xenopus laevis* egg extracts. *Nat. Protoc.* **1**, 2305–2314 (2006).
68. Field, C. M., Nguyen, P. a., Ishihara, K., Groen, A. C. & Mitchison, T. J. *Xenopus* egg cytoplasm with intact actin. *Methods Enzymol.* **540**, 399–415 (2014).
69. de Chaumont, F. *et al.* Icy: an open bioimage informatics platform for extended reproducible research. *Nat. Methods* **9**, 690–696 (2012).
70. Pinot, M. *et al.* Effects of confinement on the self-organization of microtubules and motors. *Curr. Biol.* **19**, 954–960 (2009).

Acknowledgements

We thank Marina Garcia-Jove Navarro and Alison G. Tebo for reading carefully the manuscript. A.C. and L.B. were supported by a “Ministère de la Recherche” predoctoral fellowship. This work was supported by the CNRS, Ville de Paris “Emergence(s)”, and Ecole Normale Supérieure.

Author Contributions

A.C., L.B. and Z.G. conceived and designed the experiments. A.C., L.B., C.G., J.G. and Z.G. performed and analyzed the experiments. A.C., L.B. and Z.G. wrote the manuscript.

Additional Information

Supplementary information accompanies this paper at <http://www.nature.com/srep>

Competing financial interests: The authors declare no competing financial interests.

How to cite this article: Colin, A. *et al.* Triggering signaling pathways using F-actin self-organization. *Sci. Rep.* **6**, 34657; doi: 10.1038/srep34657 (2016).



This work is licensed under a Creative Commons Attribution 4.0 International License. The images or other third party material in this article are included in the article’s Creative Commons license, unless indicated otherwise in the credit line; if the material is not included under the Creative Commons license, users will need to obtain permission from the license holder to reproduce the material. To view a copy of this license, visit <http://creativecommons.org/licenses/by/4.0/>

© The Author(s) 2016

Supplementary Information

Triggering signaling pathways using F-actin self-organization

*A. Colin#, L. Bonnemay#, C. Gayraud, J. Gautier, and Z. Gueroui**

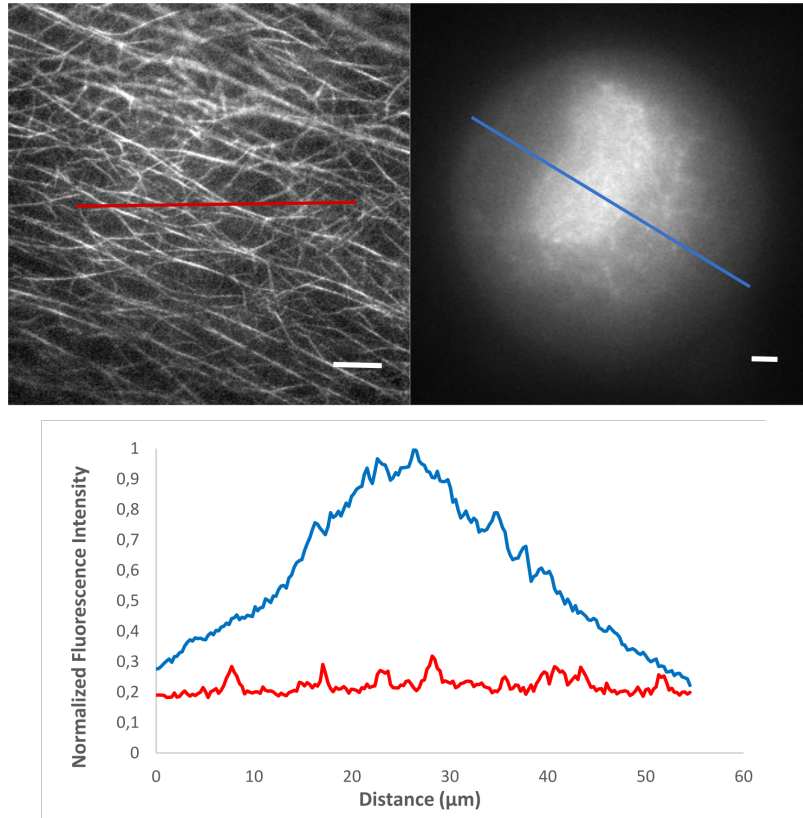
Ecole Normale Supérieure, Department of Chemistry
PSL Research University-CNRS-ENS-UPMC
24, rue Lhomond, 75005, Paris, France.

12 Supplementary Figures, 3 Supplementary movies

Correspondence:

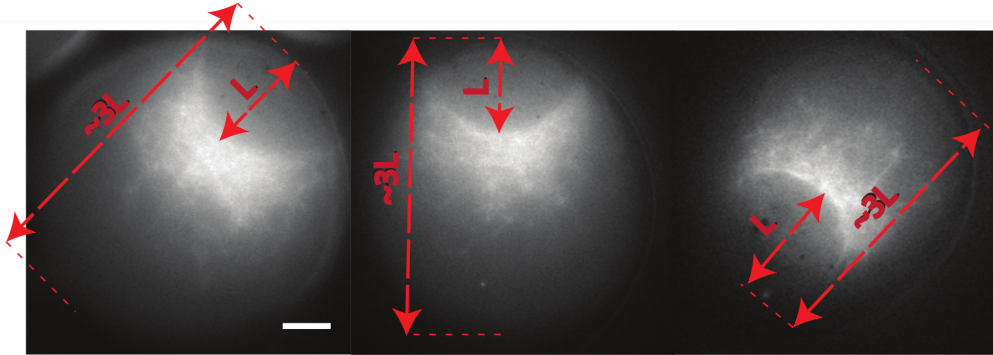
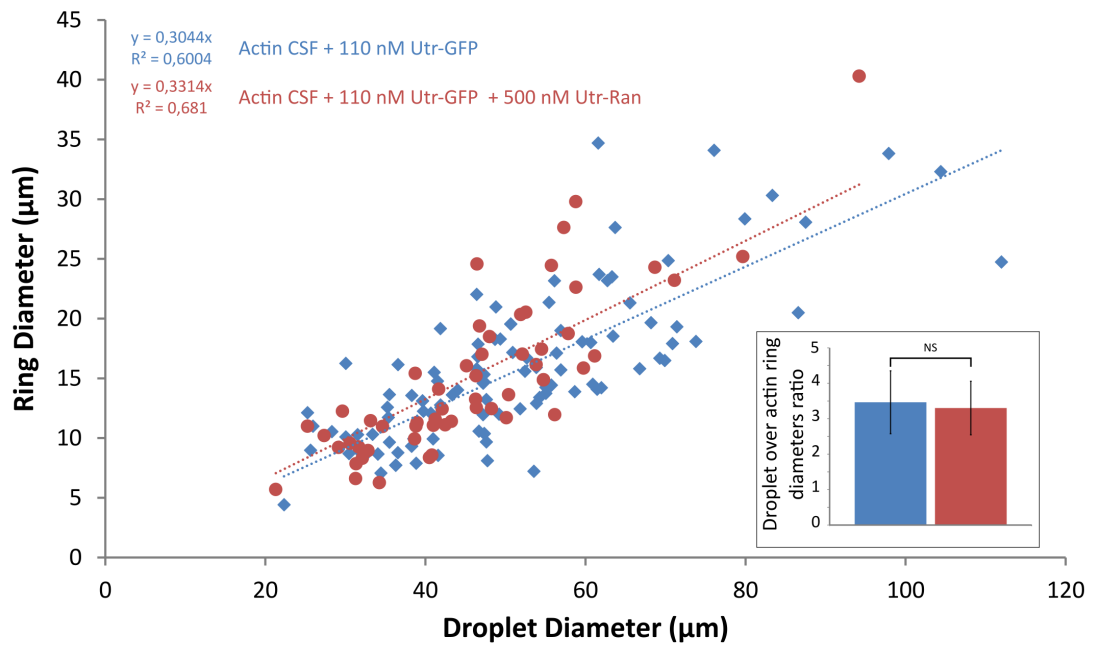
Zoher GUEROUI

Phone: +33 1 44 32 24 09

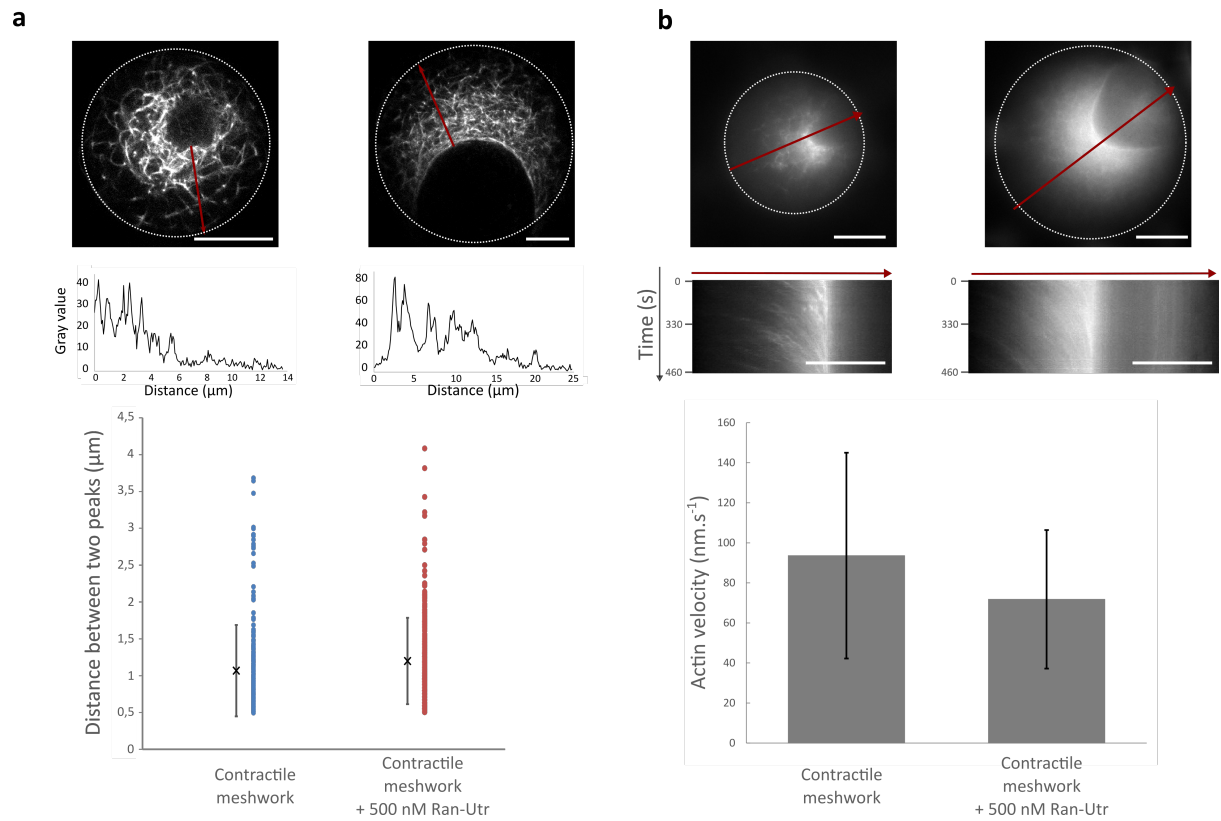


Supplementary Figure 1. F-actin meshwork morphology observed in bulk and in confined droplet.

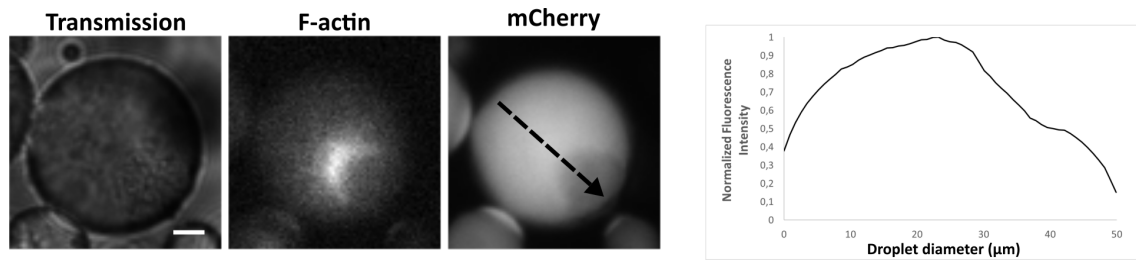
On the left, F-actin meshwork formation polymerized in bulk. On the right, F-actin meshwork formation confined in a droplet. Microfilaments were labeled with Utr-GFP. Intensity profiles quantifying the F-actin spatial density and highlighting the strong enrichment of fibers when F-actin meshwork is contracted. Scale bars are 10 μm .



Supplementary Figure 2. The size of the actin ring scales with a ratio of 3 with the size of the droplet. Top: Plot of the F-actin ring structure diameter as a function of the droplet diameter showing a ratio of 3 in ratio between these two diameters. The ratio between the droplet diameter and the ring diameter was identical in presence or absence of 500 nM of Utr-Ran. Bottom part: examples of F-actin ring structures. Scale bar is 10 μm .

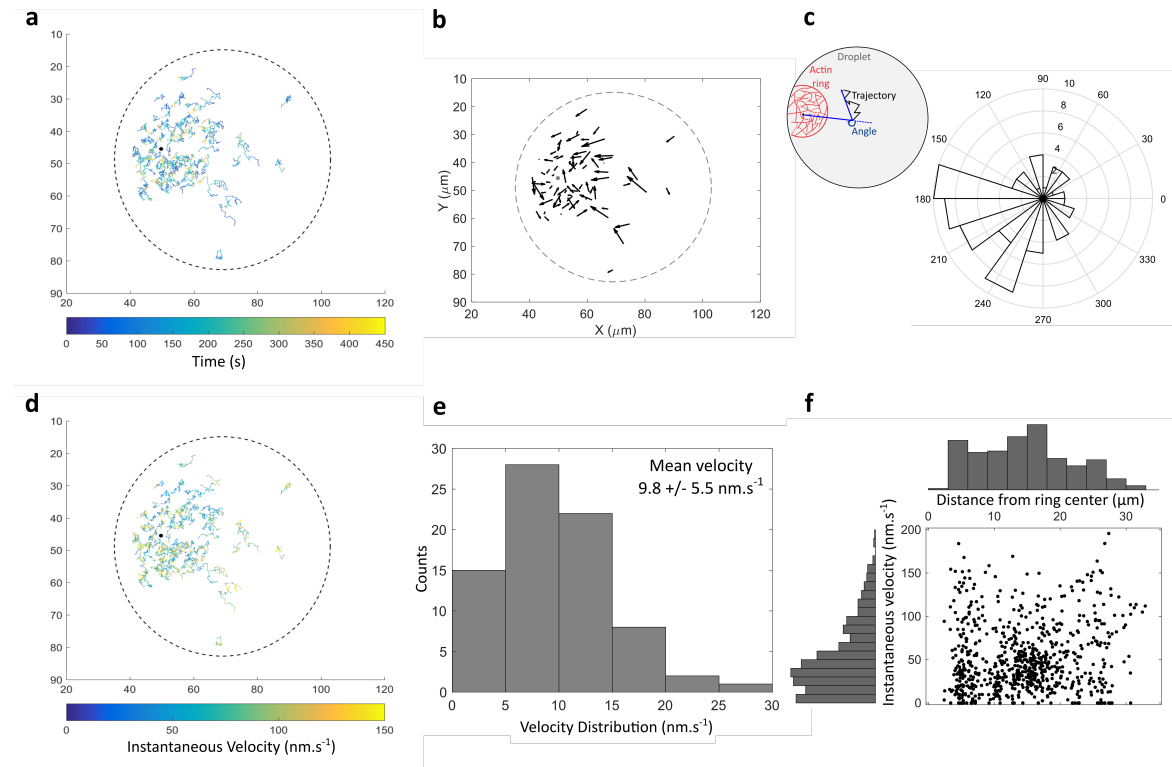


Supplementary Figure 3. Characterization of the F-actin meshwork structure and dynamics. a. Top: Confocal images of F-actin rings obtained in absence (left) or presence (right) of 500 nM Utr-Ran. The plots represent the intensity profiles taken along the red line. To measure the distance between two fibers of the F-actin meshwork, we extracted from the intensity profiles the distances that were larger than the diffraction limit (500 nm). Bottom: Plot of the distribution of distances, mean, and standard deviation (351 and 355 respectively for each case). **b.** Comparison of F-actin flow dynamics in presence or in absence of 500 nM of Ran-Utr. Representative kymographs illustrating the contractile behavior of F-actin. The mean F-actin velocity in absence of Utr-Ran is $94 \text{ nm}\cdot\text{s}^{-1}$. In presence of 500 nM of Utr-Ran, the mean F-actin velocity is $72 \text{ nm}\cdot\text{s}^{-1}$. F-actin was labelled with 110 nM of Utr-GFP in both cases. Scale bars are $10 \mu\text{m}$.



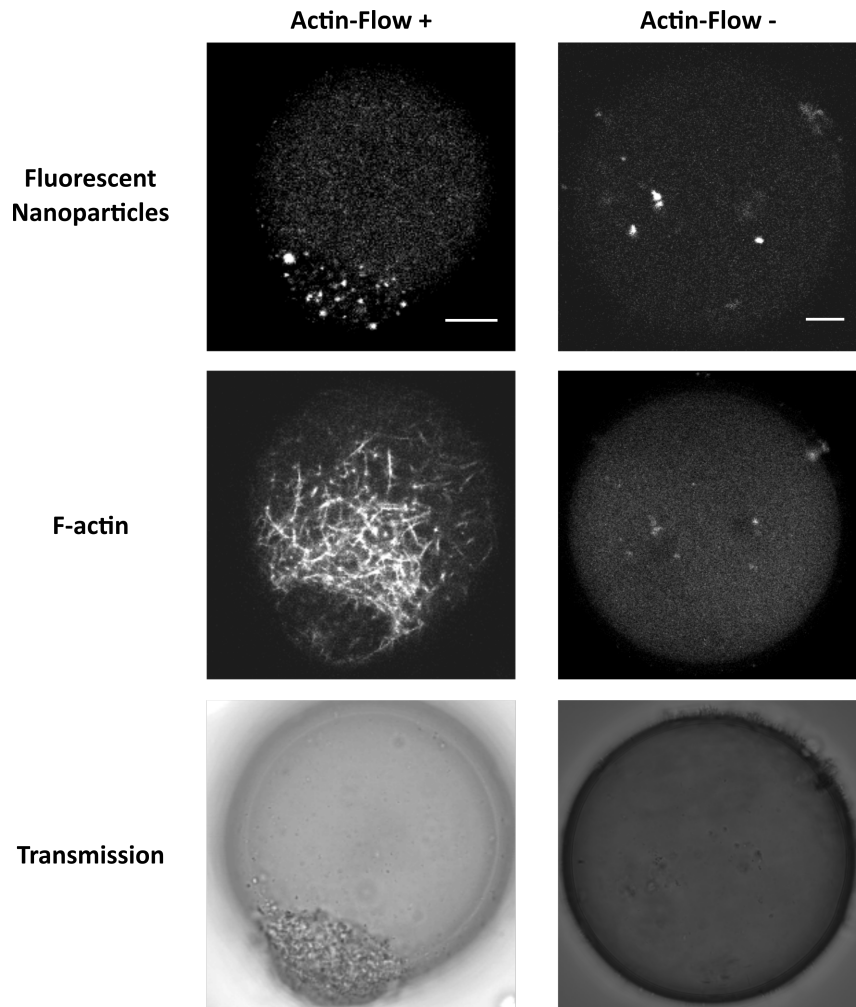
Supplementary Figure 4. The actin ring conveys the cytoplasmic organelle-like materials but not small proteins.

Spatial repartition of cytoplasmic fluorescent proteins within droplets with contractile activity. On the left, we selected examples of droplets containing fluorescent proteins (mCherry). Actin is labeled with utrophin-GFP. On the right, we represent the intensity profile of the fluorescence protein along the droplet diameter (dotted arrow). The distribution of mCherry shows that it is mostly excluded from the ring. Scale bar is 10 μm .

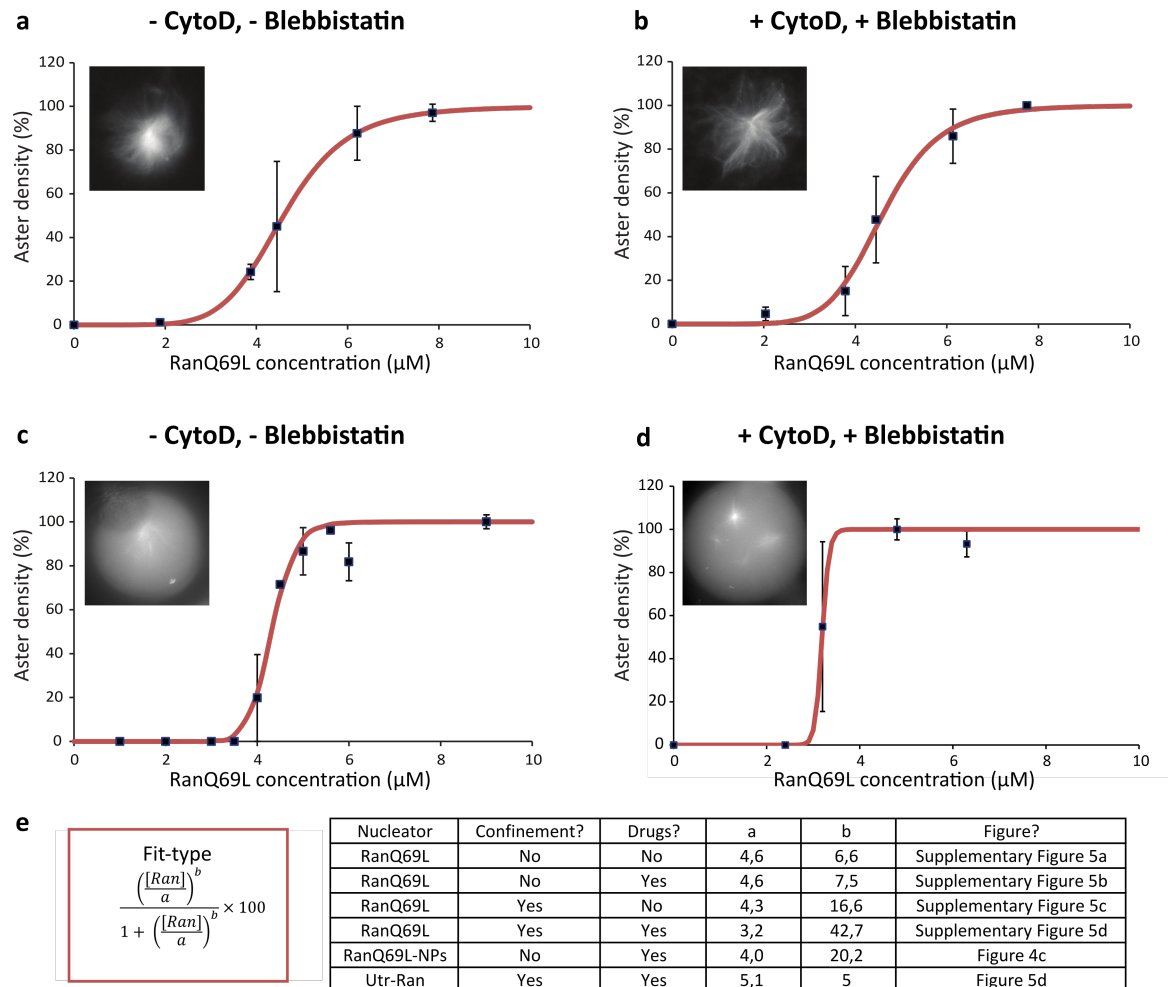


Supplementary Figure 5. Multiple particle tracking to characterize the spatiotemporal dynamics of the nanoparticles during F-actin self-organization.

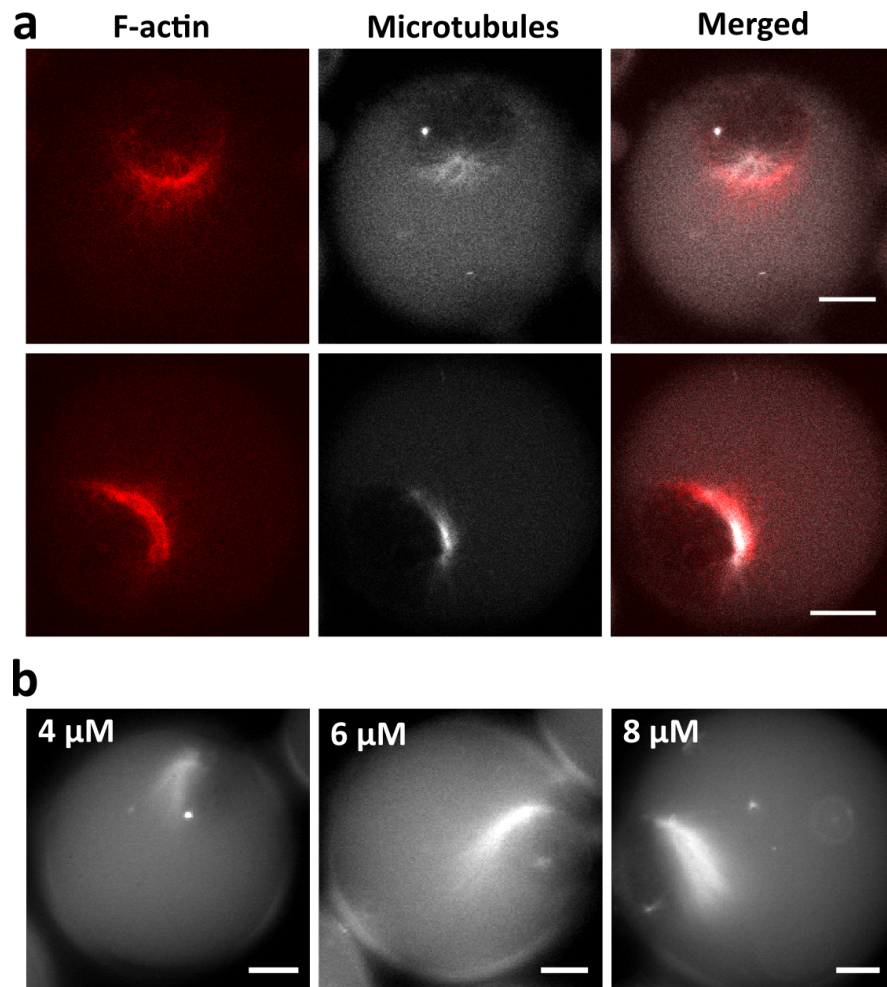
a. Displacement fields of 300 nm nanoparticles reveal a directed motion toward the F-actin ring. **b.** Mean orientation for each nanoparticle trajectories within the droplet. **c.** Angular distribution of tracked trajectories with respect to the actin ring position. **d.** Velocity field distribution computed for the trajectories of nanoparticles shows that instantaneous velocities are heterogeneous along single tracked trajectories. **e.** Distribution of the mean velocities of each nanoparticle trajectories (mean = 9.8 nm.s⁻¹). **f.** The distribution of instantaneous velocity is independent of the nanoparticle localization within the droplets.



Supplementary Figure 6. The nanoparticles are homogeneously distributed in the droplet in absence of the F-actin flow. Nanoparticles fail in accumulating in a restricted area when F-actin flow is disrupted (using blebbistatin and cytochalasin-D). The nanoparticles are found randomly distributed within the cytoplasm. Scale bars are 10 μm .

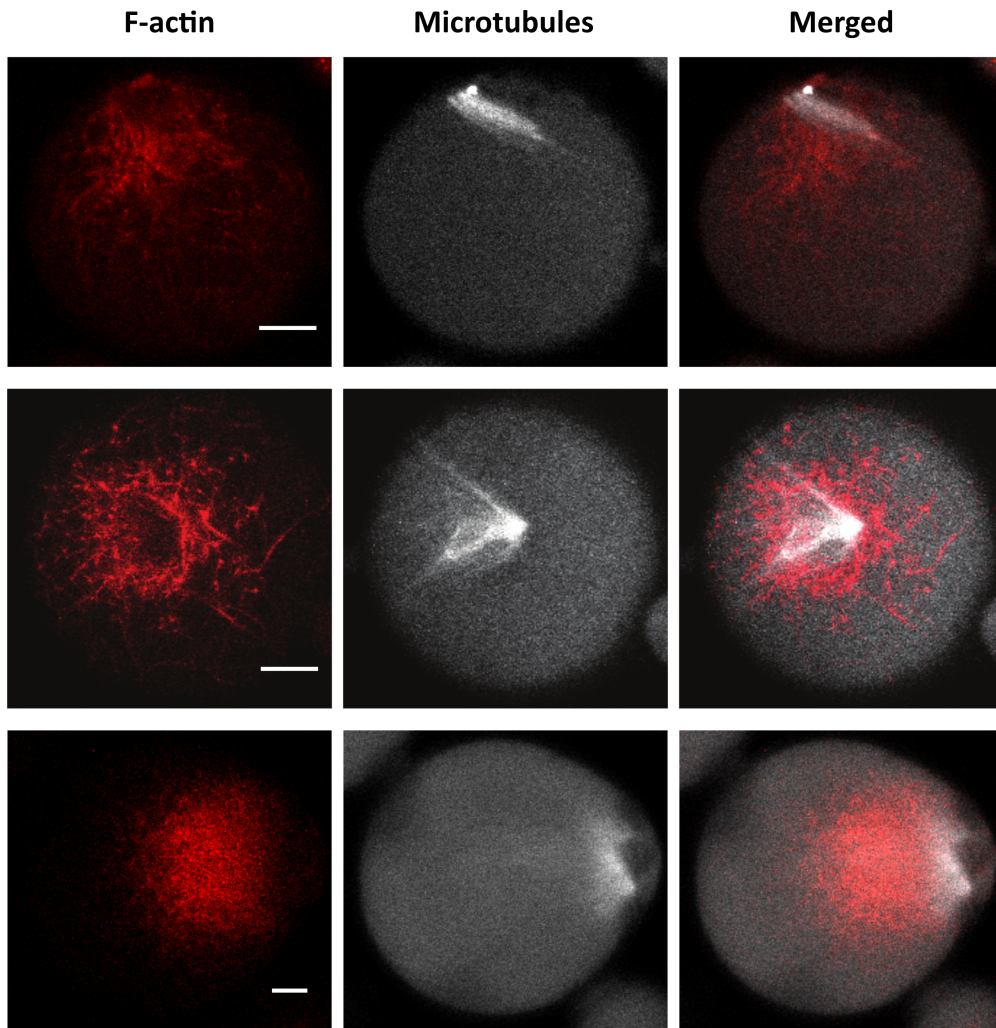


Supplementary Figure 7. The sigmoidal response of the Ran pathway is conserved in extracts supporting F-actin meshwork formation. Microtubule nucleation is ultrasensitive to the concentration of RanQ69L-GTP in bulk extracts and confined extracts, either in presence or in absence of F-actin contraction. Aster density was quantified by fluorescence microscopy and normalized to reach 100% for the plateau at the highest RanGTP concentration. **a,b.** Aster efficient for experiments performed with unconfined extracts in presence (a) or absence (b) of F-actin contractile activity. **c,d.** Aster efficient for experiments performed with confined extracts in presence (c) or absence (d) of F-actin contractile activity. Thus, the confinement and the F-actin dynamics are not modifying the concentration threshold for aster assembly. **e.** Fitting values of the sigmoidal response of microtubule polymerization as function of RanQ69L concentration. The parameter *a* represents the concentration threshold, whereas *b* represents the slope of the fitted curve (Hill factor).



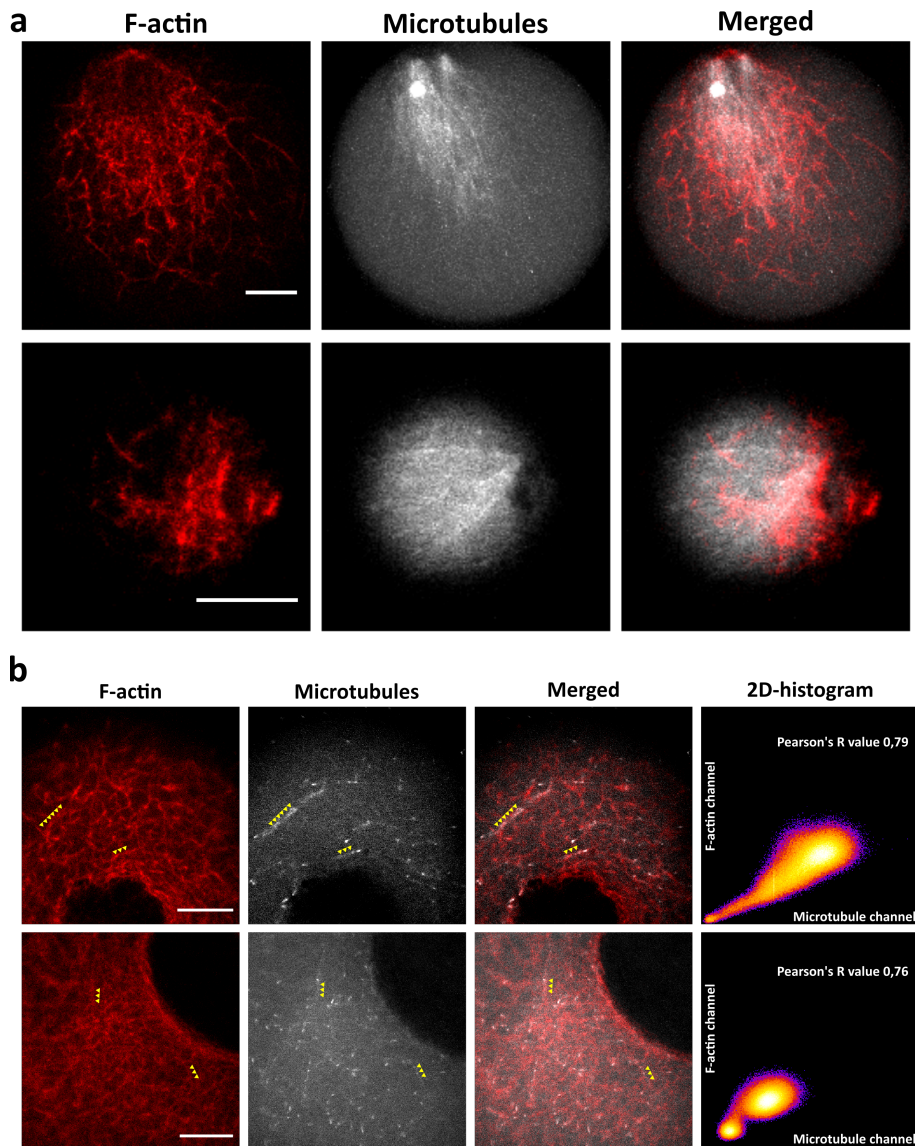
Supplementary Figure 8. Microtubule fibers nucleated with Ran during F-actin meshwork formation are localized next to the microfilaments.

a. Examples of confocal observations showing that microtubule arrays are nucleated next to F-actin ring-like structures. Asters were nucleated from an extract containing 10 μM of RanQ69L. F-actin filaments are labeled with Alexa-Fluor 568 Phalloidin (red channel) and microtubules are labeled with FITC-tubulin (gray channel). **b.** Observations of the morphology of the microtubules nucleated for various concentrations of RanQ69L in an F-actin intact cell extract. Microtubules are labeled with TRITC tubulin. Scale bars are 10 μm .



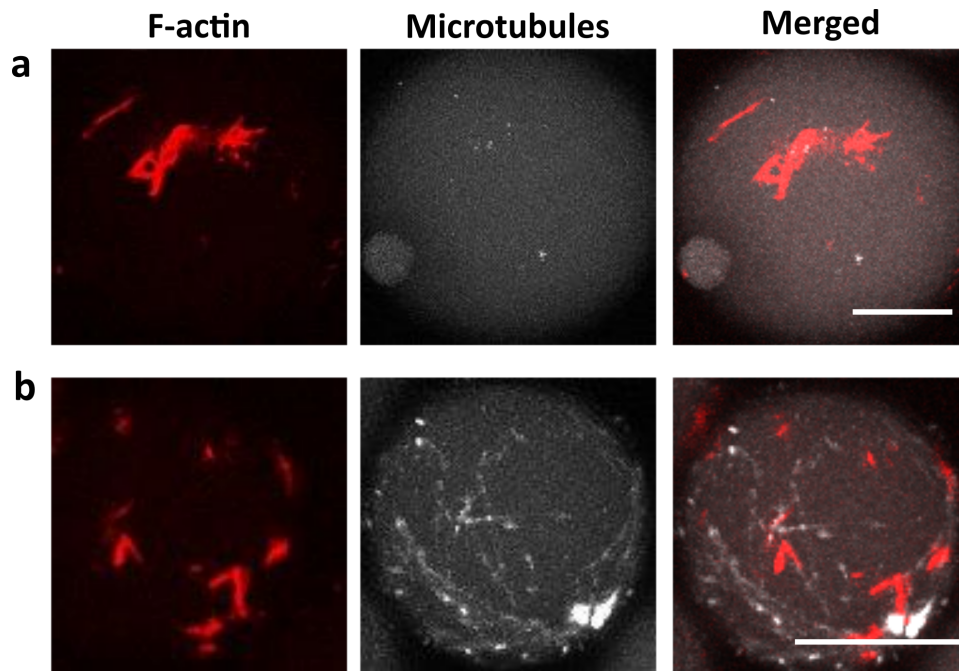
Supplementary Figure 9. Examples of microtubule organizations triggered by F-actin flow and by the active confinement of Ran-nanoparticles

Confocal observations of contractile extract droplets illustrating the colocalization of microtubule arrays with F-actin meshwork. F-actin filaments are represented in red and are labeled with Utr-GFP. Microtubules are represented in gray and are labeled with TRITC-tubulin. Scale bars are 10 μm .

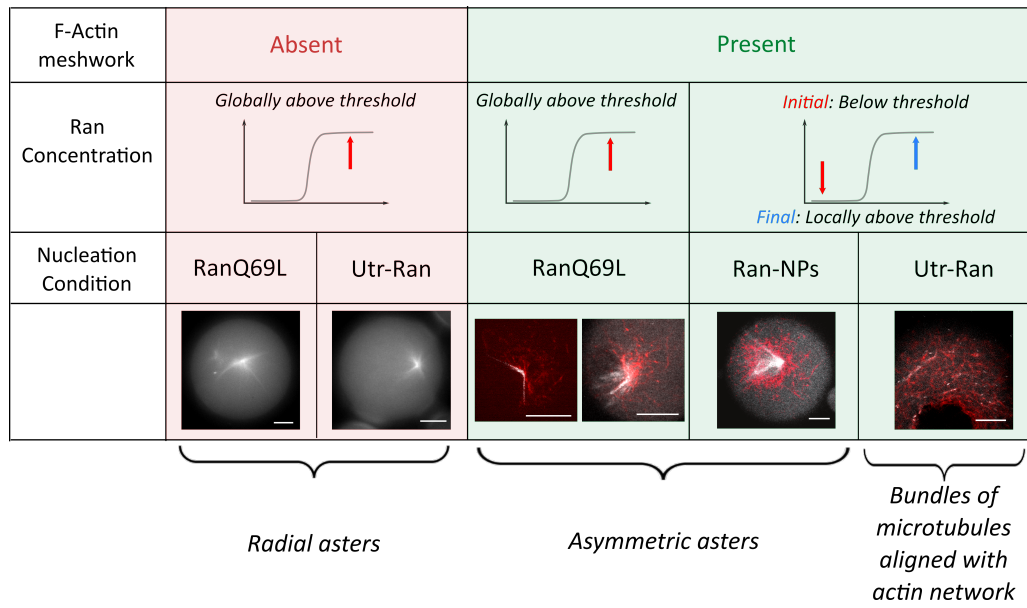


Supplementary Figure 10. Examples of morphologies of microtubule arrays assembled with Utr-Ran scaffolded on F-actin meshwork.

a. Confocal co-localization between microtubule arrays (TRITC-tubulin, gray) and F-actin ring-like structures (Utr-GFP, red). **b.** Left: example of events of co-alignments between microtubules and F-actin fibers (yellow triangles). Microtubules are labelled with EB1-GFP and FITC-tubulin; F-actin is labelled with Utr-dsRed. Scale bars are 10 μm . Right: 2D-histograms representing the quantification of the co-localization between F-actin and microtubule fluorescence channels. Pearson's coefficient is indicating the degree of correlation.



Supplementary Figure 11. Examples of confocal observations of control experiments in confined extracts when F-actin contraction is inhibited. Co-localization of F-actin and microtubules mainly shows an absence of microtubule nucleation within droplets (a) and in some few cases droplets with spontaneous microtubule fibers (b). F-actin is labeled with Alexa-Fluor-568-phalloidin; microtubules are labeled with FITC-tubulin and EB1-GFP. The images presented are Z-projection of confocal images. Scale bars are 10 μm .



Supplementary Figure 12. Comparison of the microtubule morphologies obtained for different nucleation conditions.

Legends for Supplementary Movies

Supplementary Movie 1

The dynamic accumulation of nanoparticles (300 nm in diameter) during F-actin meshwork contraction occurs in less than 5 minutes. Frames are 10 seconds apart.

Supplementary Movie 2

Examples of movies displaying the motion of fluorescent latex beads (300 nm diameter) that were used for the estimation of the diffusion coefficient of tracers in the cell extract. From left to right: meiotic extracts in absence of F-actin growth, egg extracts supporting F-actin growth prior to ring-like formation, and egg extracts after the completion of the ring-like formation. Movies were recorded with the stream mode of the microscope and frames are 120 ms apart.

Supplementary Movie 3

Time-lapse movie showing the dynamic of microtubule plus-end growth using EB1-GFP. Frames are 5 seconds apart.

4.3 Conclusion

In this study, we showed that F-actin contractility and scaffolding can promote the robust assembly of microtubules structures. The large occurrence of F-actin structures throughout living cells suggests that confinement or scaffolding of signaling proteins may be used in natural systems. It would be interesting to test if other signaling pathways can be triggered through the scaffolding or the confinement mediated by F-actin. In addition, we saw that the organelles are confined inside the F-actin ring, it would therefore be instructive to couple a microtubule nucleation factor to organelles and see if the microtubule nucleation can be triggered as well. It would be also interesting to see if this concept is applicable in living cells, for example by studying the behavior of the Utrophin-Ran protein in cells as a function of the F-actin state.

This *in vitro* assay is a first step toward the development of novel bottom-up strategies to decipher the interplay between cytoskeleton spatial organization and signaling pathway activity. The synthetic biology has been mainly based on genetic systems. Here we propose a protein-based systems engineering. One drawback of our system is that the control of actin morphology in space and time is not possible once the droplet is generated. This could be improved by the use of microfluidics system or by the improvement of our assay from droplets to vesicles (with the boundary of the compartment made of a lipid bilayer).

Our minimal reconstituted system could also be extended to examine possible mechanisms of cross talks between actin and microtubules, which could be reconstituted in a controlled manner. Indeed, we saw that without creating a link between F-actin and microtubules (RanQ69L in the contractile egg extract, Figure 3), the aster is positioned at the vicinity of the contractile ring of F-actin. This suggest that without having a specific molecular link, actin and microtubule structures can be linked.

In the next chapter, we present an application of our reconstituted system to study F-actin/microtubule interaction in the context of the formation of a half-spindle.

Chapter 5

Probing the Physical Constraints Induced by Cytoplasmic F-actin on Microtubule Dynamics of Asters and Spindle-like Organizations

It is known that the interaction between F-actin and microtubules is critical to control various aspects of metaphase spindles. Though, in *Xenopus* egg extracts, microtubules and metaphase spindles have mainly been studied in absence of F-actin. In this chapter, we study the influence of dense actin networks on microtubule assemblies (asters and spindles).

Contents

| | | |
|------------|--|------------|
| 5.1 | Introduction | 94 |
| 5.1.1 | Context | 94 |
| 5.1.2 | Outlook on studies about actin-microtubule interactions | 94 |
| 5.2 | Article 2: Probing the physical constraints induced by cytoplasmic F-actin on microtubule dynamics of asters and spindle-like organizations | 98 |
| 5.2.1 | Presentation of the article | 98 |
| 5.2.2 | Manuscript | 98 |
| 5.3 | Discussion | 126 |
| 5.3.1 | Perspectives of the work | 126 |
| 5.3.2 | Regulation of F-actin through the cell cycle | 127 |
| 5.3.3 | F-actin misregulation in pathological cases | 127 |
| 5.3.4 | Conclusion | 128 |

5.1 Introduction

5.1.1 Context

There is mounting interest in identifying the physical and biochemical parameters that control microtubules spatial organizations. For instance, the morphogenetic properties of microtubule spindles depend drastically on their intrinsic elements, such as the biophysical characteristics of the mitotic motors [136, 137, 138], the microtubule dynamics [139, 140, 141], the molecular actuators [142, 143, 144], and the spatial organization of the chromosome [145, 146]. By contrast, extrinsic factors such as the geometry of the cell envelope [147, 47, 148], the volume confining the spindle [79, 77, 78, 149], and extracellular forces influence spindle formation, orientation, and position [150, 151]. Finally, the spindle is resistant to mechanical perturbations [152, 153, 154].

In meiotic systems, cytoplasmic F-actin dynamics plays important roles. For example for the spindle migration in Meiosis I (MI) division in mouse oocytes [91, 92] or for the gathering of the chromosomes to ensure proper spindle formation in starfish oocytes [35, 36] or in the stabilization of the nucleus against gravitational forces in *Xenopus* oocytes [112].

Although the mechanisms controlling the properties of spindle morphogenesis are now being uncovered, much less is known about how F-actin architecture and dynamics are involved in microtubule organizations like asters or spindle.

5.1.2 Outlook on studies about actin-microtubule interactions

Even if they are not extensively studied, actin-microtubule interactions have been described in a lot of systems. For example, in migrating cells, it was shown that actin can affect microtubule movement and assembly and therefore create a polarized gradient of microtubule dynamic instability (microtubule growth at the leading edge and microtubule shortening in the cell body). The joint movement of the two filaments during retrograde flow suggests that they are linked during cell migration [155].

Coordination between actin and microtubules is also of a primary importance in the neuron growth [156]. Indeed, the axon growth cone is a dynamic structure with filopodia that probe the environment (usually a gradient of chemical cue). F-actin and microtubules can be found in the growth cone; they co-exist and are often found to co-align (Figure 5.1). Their coordination is important for a directed outgrowth of the cone that will guide the neuron during its development.

Technical difficulties of studies about actin and microtubules

Studying interactions between actin and microtubules was not easy, first for technical reasons. Indeed, the cytoplasmic pool of F-actin has been hidden by the cortical pool for a long time. As discussed in Chapter 3, the development of new probes allows to have a better view on this cytoplasmic pool [106, 105].

Identified molecular motors between actin and microtubules

In the past decade, much emphasis has been placed in identifying molecular linkers between actin and microtubules. We will now present some identified molecular motors linking actin and microtubules and playing a role during cell division. The following

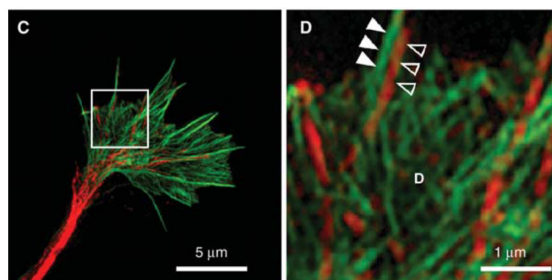


Figure 5.1: Actin (green) and microtubules (red) distribution in axon growth cone. Right: a co-alignment between an actin filament and a microtubule is indicated with the arrowheads. F-actin is labelled with fluorescent phalloidin and microtubules with an antibody to tyrosinated tubulin. *Extracted from [156]*.

examples do not provide an exhaustive review of all the linkers identified; we picked up the examples that were pertinent compared to our studies.

Myosin X was already described in Chapter 1 (see section 1.4.3, page 16).

Myosin-1C binds to microtubules and stabilizes the spindle in *Dictyostelium* during mitosis ([157], Figure 5.2a). The molecule was shown to be necessary for spindle integrity by being localized mainly at spindle poles. Thanks to *in vitro* reconstitutions, it was shown that myosin-1C has a stabilizing effect on microtubules and can serve as a dynamic linker between the two cytoskeletons.

Myosin VIII guides the axis of cell division in plants and especially the tip growth. It interacts with actin and microtubules to guide the formation of the new cell plate during cytokinesis. When the myosin VIII is impaired, the tip growth is less persistent [158].

Nabkin (Nuclear and meiotic actin-bundling Kinesin) was identified in *Xenopus* oocytes. It directly links microtubules with actin and was shown to be necessary for the attachment of spindle to cortex during meiosis (Figure 5.2b) and for cytokinesis [159]. Interestingly, the interaction between NabKin and actin is favoured by RanGTP which is also involved in other meiotic processes.

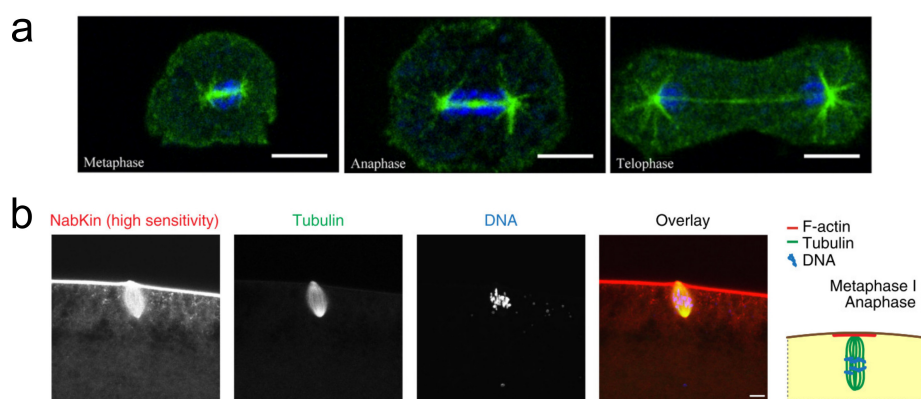


Figure 5.2: Examples of molecular motors identified to link actin and microtubules during cell division. (a) Myosin-1C localizes to spindle poles during mitosis. (b) Nabkin co-localizes with both actin and microtubules during spindle anchoring in *Xenopus* oocytes. *Adapted from [157, 159]*.

Actin-microtubule reconstitutions *in vitro*

As we showed in Chapter 2, *in vitro* reconstitutions are very useful to evaluate key parameters of a system. In the following, we will describe some examples where F-actin/microtubules interactions have been reconstituted *in vitro* and have provided insights into the biochemical and biophysical links between actin and microtubules. The reconstitutions allow to evaluate the impact of a cross-linker on the kinetics, the assembly or the geometry of filaments for example.

A first approach of *in vitro* reconstitution was performed by Griffith and Pollard [160] by using a viscometer and electron microscopy. They incubated actin, microtubules and MAPs (Microtubule Associated Proteins) and found that this mixture was forming a gel. They hypothesize the existence of an interaction between actin and microtubule mediated by MAPs. By characterizing this gel, they found the existence of a specific interaction between actin and microtubule, mediated by MAPs. The identification of the responsible MAP was complicated, mainly due to the lack of resolution of the techniques used.

As soon as the MAPs were identified, they have been studied individually, as well as their effect on actin and microtubule mix. For example, the protein tau (a microtubule-associated protein usually found in neurons) was shown to be a molecular linker between actin and microtubules networks *in vitro* [161]. The protein co-aligns actin and microtubule filaments *via* a coupled co-polymerization, without changing the growth rate of the two polymers (Figure 5.3a). Though, a straightening of actin with microtubule filaments was observed. This study gives hints about mechanisms that play a crucial role in synapses during neuronal development. CLIP-170, another well-known microtubule plus-end-associated protein was studied and found to have a direct effect on actin assembly kinetics [162]. Indeed, CLIP-170 was found to bind to mDia1 and to accelerate actin filament elongation to 200 subunits/sec/ μM in comparison to 55 subunits/sec/ μM with just mDia on the filament (Figure 5.3b). The elucidation of the mechanism showed that CLIP-170 increases formin duration at barbed end in presence of capping proteins. Once again, this reconstitution can be related to what is happening in neurons (for the dendritic branching for example).

A more "synthetic" reconstitution was done by engineering TipAct, a protein that links growing microtubule ends *via* end-binding proteins to actin filaments [163]. The results of this study show that a simple crosslinker can generate a mechanical feedback between actin and microtubule organizations. Arrays of actin can impose their organization on microtubules or conversely (Figure 5.3c).

Actin-microtubules interactions in *Xenopus* egg extracts

Historically, the team of W. Bement performed the first observations of actin-microtubules interactions in *Xenopus* egg extracts. The work of Sider *et al.* [164] was the first to provide direct evidence for association between microtubules and actin *in vitro*. By using interphase extracts, they observed co-localization between actin and microtubule asters in a lengthwise manner (Figure 5.4). This interaction is mediated by microtubule binding proteins. In addition, they showed that this interaction was correlated with bending, letting them hypothesize that microtubules can exert forces on the F-actin cytoskeleton. Later, Waterman-Storer *et al.* [165] analyzed the dynamics of the microtubule-actin interaction and found that microtubules can remodel actin networks. Since those studies, F-actin/microtubule interaction has been poorly studied in *Xenopus* egg extracts.

5.2 Article 2: Probing the physical constraints induced by cytoplasmic F-actin on microtubule dynamics of asters and spindle-like organizations

5.2.1 Presentation of the article

In this project, we wanted to reconstitute spindle formation in presence of an actin network. Spindle was never studied in presence of F-actin in *Xenopus* egg extracts. For that, **we used our *in vitro* assay to probe the physical constraints induced by F-actin on the meiotic spindle self-organization.** As presented above, much emphasis has been placed on the role of molecular components linking F-actin and microtubules. However, the influence of physical parameters such as mechanical constraints remains unexplored. In this article, we demonstrate that *Xenopus* actin-intact egg extracts, encapsulated into droplets, can be used to reconstitute the self-organization of microtubule structures (asters, spindles) interacting with actin. As a result, we found that **cytoplasmic F-actin meshwork modulates microtubule dynamics.** F-actin filaments, acting as elastic and stiff biopolymers, directly reduce microtubule polymerization rate. This illustrates how F-actin meshwork elasticity can modulate microtubule dynamics by physical constraints. Reciprocally, we observed that microtubules locally dictate F-actin geometry by inducing their organization into aster-like structures at the spindle poles. Our results suggest how non-biochemical regulations can coordinate large-scale organizations between microtubules and F-actin. In addition, we found that **the dynamic and elastic properties of F-actin meshwork are critical for a proper spindle formation.** Indeed, we found that in a static meshwork, the spindle elongation is drastically perturbed. To the contrary, proper spindle elongation is restored in a dynamic meshwork. These results illustrate how the regulation of cytoplasmic F-actin architecture and dynamic can impact metaphase spindle organization through purely physical and mechanical effects.

This manuscript is currently in revisions in *Current Biology*.

5.2.2 Manuscript

Probing the Physical Constraints induced by Cytoplasmic F-actin on Microtubule Dynamics of Asters and Spindle-like Organizations

*A. Colin and Z. Gueroui**

École Normale Supérieure, PSL Research University, CNRS, UPMC,
Department of Chemistry,
24 rue Lhomond, 75005 Paris, France

Correspondance:

Zoher GUEROUI

Phone: +33 1 44 32 24 09

Email: zoher.gueroui@ens.fr

Summary

Coordination between F-actin and microtubules is critical to complete important steps in cell division during mitosis and meiosis. For instance, cytoplasmic F-actin dynamics plays an active role in positioning the spindle off-centre during MI division in mouse oocytes[1–3] or in gathering the chromosomes to ensure proper spindle formation [4,5], whereas cortical F-actin controls spindle rotation and positioning[6–9]. Several molecular effectors such as Myosin-10 have been found to facilitate anchoring between the meiotic spindle and the F-actin cortex[10–14]. In addition, *in vitro* reconstitutions have provided detailed insights in the biochemical and physical interactions between microtubules and F-actin[15–20]. Yet, how F-actin architecture and dynamics affect microtubule dynamic and self-organization is still unclear. Using *Xenopus* actin-intact egg extracts that were encapsulated into droplets of variable size, we reconstituted microtubule aster assembly in F-actin meshworks of different dynamics. We found that a dense F-actin meshwork, independently of its dynamic state, impacts the lengths and the growth rate of microtubules in centrosome and Ran-nucleated asters and constrain the aster mobility. In addition, we examined the impact of cytoplasmic F-actin meshwork on the formation of aster spindles. For a static F-actin meshwork, we found that the aster spindle assembly process is perturbed, with monopolar spindle 35%-shorter than normal. By contrast, proper aster spindle assembly was restored in a dynamic meshwork. We propose that F-actin meshwork provides physical barriers that affect microtubule dynamics, a key parameter for the proper assembly of complex organizations.

RESULTS

Microtubule aster assembly in a cytoplasmic F-actin meshwork

Xenopus egg extracts provide a powerful model system to unravel the general principle of microtubule assembly during metaphase spindle organization[21–24]. However, until now, this cell-free system has been used mainly to study isolated microtubule spindle assemblies devoid of F-actin structures. To examine the interplay between cytoplasmic F-actin and microtubule self-organization, we used F-actin intact *Xenopus laevis* egg extracts (actin Cytostatic Factors extracts hereafter referred to as actin-CSF), which correspond to Metaphase II-arrested extracts that have been prepared without inhibiting the growth of endogenous F-actin[25,26] (Methods). We encapsulated these extracts in spherical compartments corresponding to droplets of egg extracts dispersed in mineral oil (Methods). This technique generates droplets ranging from a few micrometres up to 100 μm in size, with rigid boundaries, which are well suited for quantitatively studying the effect of such confinement on actin self-organization[27,28] or on microtubule and spindle self-organization[29–31]. To reconstitute F-actin meshworks in droplets we added to the actin-CSF extract a cellular activator of Arp2/3, pWA, in order to trigger the nucleation of F-actin (Methods). In absence of pWA, we observed a highly dynamic and contractile meshwork that eventually assembles into a F-actin ring structure[20,27] (**Figure S1a Left, Movie 1**). With 250 nM pWA, a dense and homogeneous F-actin meshwork formed rapidly and entirely in the droplets (**Figure S1a Middle, Figure S1b Movie S1**), with an average contractile rate of 30 $\text{nm}\cdot\text{s}^{-1}$ (**Figure S1c, green data, Movie 1**). At high concentration of pWA (1.3 μM), the resulting F-actin meshwork had an apparent morphology similar to the one obtained for 250 nM of pWA

(**Figure S1a Right**) but, in contrast, this meshwork was static (**Figure S1c, grey data, Movie 1**). Because F-actin meshwork assembles much faster than microtubule structures, we can use pre-assembled F-actin meshwork to study aster formation.

During spindle formation, microtubules can nucleate at the centrosome sites or they can assemble in the vicinity of the chromosomes using spindle assembly factors (SAFs), which are regulated by a Ran-dependent pathway[32]. We studied aster self-organization in the absence of chromosomes, using purified RanGTP or centrosomes. Aster assembly was induced in actin-CSF droplets in the presence of F-actin depolymerization factors, and with a dynamic or with a static F-actin meshwork (**Figure 1a**). Microtubule structures were first induced by adding RanQ69L, a constitutively active form of RanGTP, to the extract (Methods). We monitored aster assembly using encapsulated actin-CSF extracts, microtubules labelled with FITC-Tubulin or EB1-GFP, and F-actin labelled with Utrophin-dsRed (**Figure 1a, Movie S2**). In actin-CSF devoid of F-actin, we observed that radial microtubules had an average length of $10.8 \pm 5.5 \mu\text{m}$ (**Figure 1b, 1c, Methods**). In presence of dense F-actin meshwork, microtubules organised into asters morphologically similar to those observed in absence of F-actin (**Figure 1a**). Co-alignments were observed between F-actin and microtubules, resulting in the remodelling of F-actin into aster-like organizations (**Figure S2**). For a dynamic F-actin meshwork, we found that the length of microtubules dropped on average from $10.8 \mu\text{m}$ to $8.8 \mu\text{m}$ (19% of reduction, **Figure 1c, green**). For a static F-actin meshwork, the microtubule length dropped from $10.8 \mu\text{m}$ to $7.8 \mu\text{m}$ (**Figure 1c, grey, 27%** of reduction). This decrease in microtubule length was correlated with a slower growth rate of microtubules in both dynamic and static meshworks (**Figure 1b, 1d left, Methods**).

We next examined microtubule dynamics of centrosome-induced asters where co-alignments between F-actin and radial microtubules were also observed (**Figure S2**). In a dynamic F-actin meshwork, we found that microtubule length and growth rate decreased on average by about 19% and 30%, respectively, compared with structures formed in the absence of F-actin meshwork (**Figure 1c, 1d**). This reduction of microtubule length and growth rate was also observed in a static F-actin meshwork. Therefore, in Ran- and centrosome- nucleated asters, microtubule lengths and dynamics are significantly reduced in a dense F-actin meshwork, independently of its dynamic state.

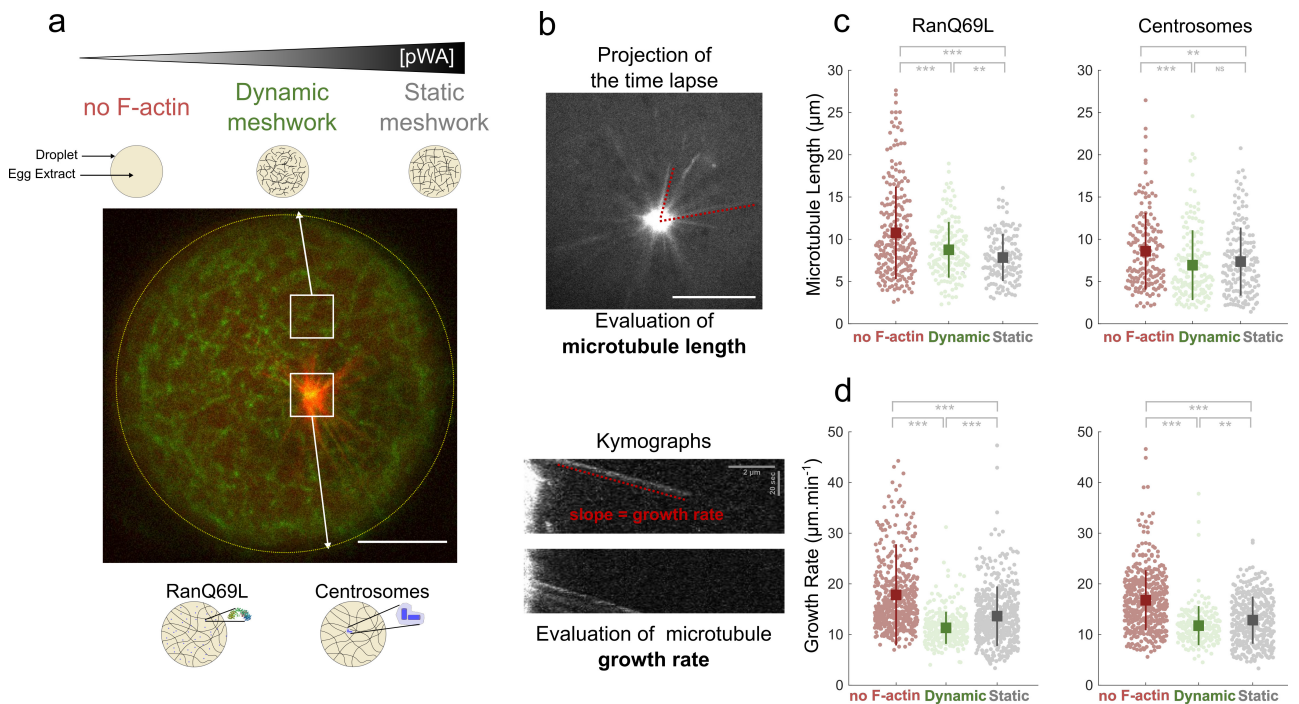


Figure 1. Microtubule aster assembly in a cytoplasmic F-actin meshwork

a. Principle of the experiment: observation of microtubule formation in dense F-actin meshworks with various dynamics. Asters are formed from two nucleation pathways: RanQ69L or centrosomes. F-actin is labelled with GFP-Utrophin, microtubules with TRITC-tubulin. Scale bar is 10 μm . **b.** Microtubule length was evaluated by measuring EB1 traces. Growth rate was evaluated from kymographs (Methods). **c-d.** Quantitative analysis of microtubule length (**c**) and

growth rate (**d**) for RanQ69L and centrosome-nucleated asters in various F-actin meshworks. Each point represents a single measurement for one microtubule. Mean and standard deviation are superimposed.

Aster pole mobility is strongly reduced in static or dynamic F-actin meshwork.

A dense and homogeneous F-actin meshwork could also act as a physical barrier by constraining and trapping the aster poles in an elastic gel. To examine this point, we monitored the motion of radial asters triggered by the Ran-dependent pathway in a static or dynamic meshwork. In droplet extracts devoid of F-actin, the aster poles are very dynamic and explore a large part of the droplet space (**Figure 2a left, Movie 3**). By contrast, both static and dynamic F-actin meshworks induced a drastic reduction of the aster motion (**Figure 2a middle and right, Movie 3**). The reduction of aster motion is confirmed by the quantification of the mean square displacement (MSD), which indicates the surface explored by the aster poles (**Figure 2b**). In the absence of F-actin, the mobility of asters is comparable with the passive diffusion of a micrometric object, suggesting that thermal energy could be sufficient to drive their motion. In the presence of F-actin, the pole asters exhibited a confined motion, as they were entrapped within a dense meshwork (with an estimated mesh size of 2.7 μm). This was confirmed by their directional transport at a velocity similar to the contraction rate of the F-actin meshwork (**Figure 2c, Movie 4**). Both co-alignments of F-actin and microtubules, and co-localization of microfilaments with microtubule poles (as previously observed[15,33]) suggest a strong enrichment of F-actin surrounding the pole (**Figure S3**). The local architecture of the F-actin correlates with the confined motion of aster poles in static or dynamic F-actin meshworks, illustrating how the meshwork traps the microtubule structures.

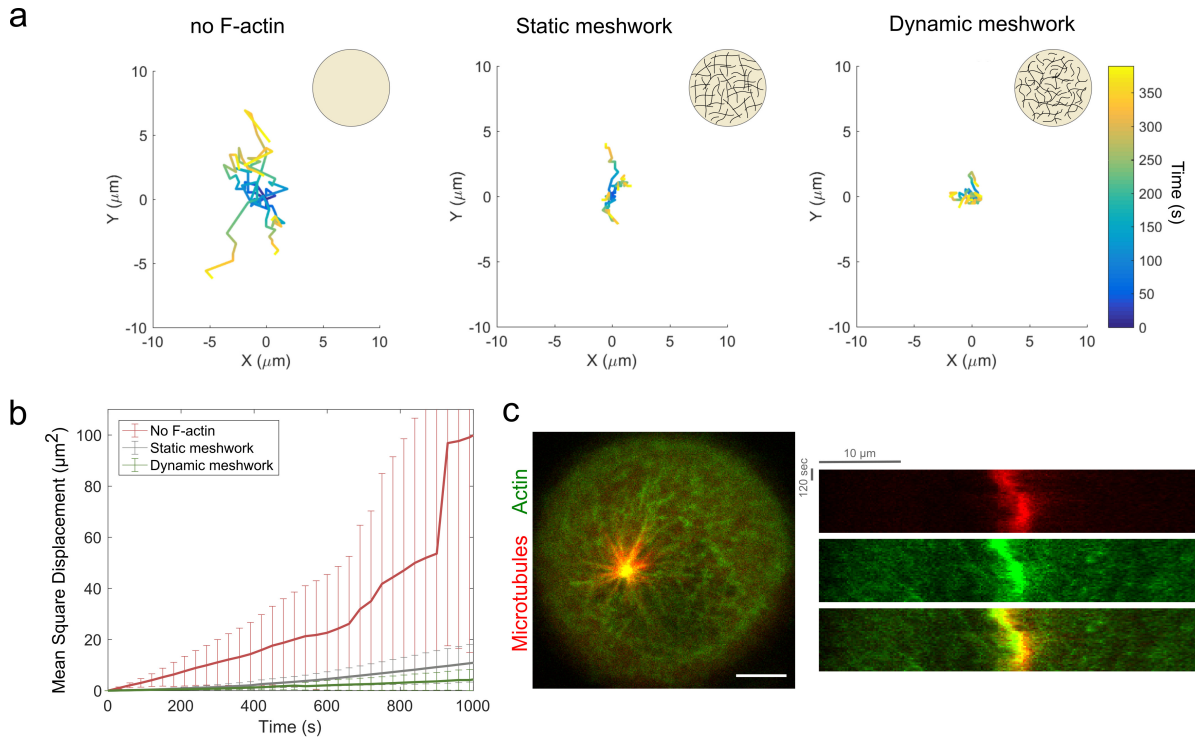


Figure 2. Aster pole mobility in F-actin meshworks with different dynamic properties

a. Trajectories of Ran-aster poles nucleated for three cases: in absence of F-actin, in a static F-actin meshwork, and in a dynamic F-actin meshwork. Normalized trajectories in space are represented and time is encoded in colour. **b.** Quantification of mean square displacements. **c.** Representative kymograph showing that aster pole is transported by the F-actin meshwork contraction. F-actin is labelled with GFP-utrophin and microtubules are labelled with TRITC-tubulin. Scale bars are 10 μm .

Aster spindle self-organization in F-actin-intact egg extracts confined in droplets.

To study spindle self-organization in actin-CSF extracts, we used sperm nuclei (hereafter referred to as chromosomes), which drive the formation of meiotic monopolar spindles in classical CSF extracts[22,34]. These structures correspond to focused asters with microtubules asymmetrically distributed from the pole to the chromosomes. Before examining the effect of F-actin architecture and dynamics on spindle formation, we first characterized microtubule self-organization from chromosomes in actin-CSF in absence of filaments, e.g. by adding F-actin depolymerizing drug and myosin-II inhibitors to the

extracts (Methods). We observed monopolar spindle organizations characteristic of those obtained in classic CSF extracts (**Figure 3a**). Using a fluorescent antibody directed against nuclear mitotic apparatus protein (NuMA), we found that NuMA is recruited at the poles (**Figure 3b** and methods). We also found that the pole-to-chromosome distance becomes smaller as droplet diameter decreases (**Figure 3c**). These measured distances and this scaling are in agreement with previous studies that examined spindle assembly in confined droplets[30,31]. This recapitulates observations made during *Xenopus* embryogenesis, and suggests that a limited amount of important spindle assembly factors modulates spindle size[30,31,35]. In presence of F-actin meshwork, we observed that microtubules nucleated from chromosomes organized into morphologies that were different given the dynamic state of F-actin. Indeed, we found that in dynamic meshwork, the structures acquired a monopolar spindle morphology (**Figure 3d, 3e**) with a pole-to-chromosome distance similar to the one found in an actin-CSF extract devoid of filaments ($9.3 \pm 4 \mu\text{m}$ in both cases, **Figure 4a**). On the contrary, microtubules nucleated in a dense and static F-actin meshwork organized into asters in the vicinity of the chromosomes, suggesting that the spindle formation is arrested at early stage and did not undergo to steady state (**Figure 3g**). The measured pole-to-chromosome distance was of $6.1 \pm 3 \mu\text{m}$ on average, which corresponds to a 35% decrease compared to spindle nucleated in absence of F-actin or in presence of a dense and dynamic F-actin meshwork (**Figure 4a**). In all cases, NuMA was recruited to the pole, illustrating that the monopolar spindle nucleated in presence of F-actin share similar biochemical characteristics with aster poles formed in absence of F-actin (**Figure 3b, 3e, 3h**). In the dynamic actin meshwork, the scaling between the pole-to-chromosome distance and the droplet

diameter was conserved (**Figure 3f**). Interestingly, in the static meshwork, we observed no dependency of the pole-to-chromosome distance on droplet size (**Figure 3i**). Confocal microscopy also revealed that microtubules dictate F-actin geometry locally by guiding microfilament organization into aster-like structures at the spindle poles (**Figure S4**).

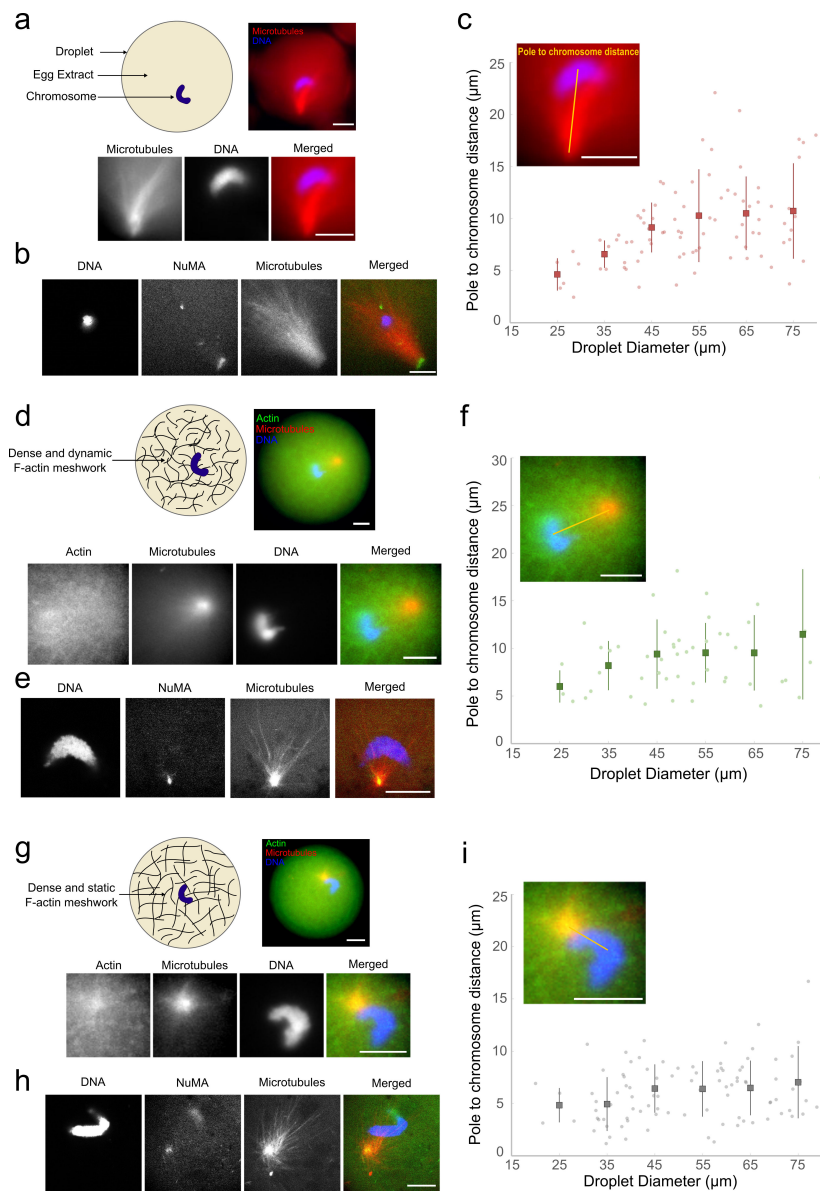


Figure 3. Aster spindle self-organization in F-actin-intact egg extracts confined in droplets

a. Monopolar spindle formed in confined extracts in the absence of F-actin. **b.** NuMA is recruited at the poles in extract droplets devoid of F-actin structures. **c.** Pole-to-chromosome distance as a function of the droplet diameter for confined extracts without F-actin. **d.** Monopolar spindle formed in confined extracts in presence of a dynamic F-actin meshwork. **e.** NuMA is recruited at the spindle poles formed in a dynamic F-actin meshwork. **f.** Pole-to-chromosome distance as a function of the droplet diameter in the case of a dynamic F-actin meshwork. **g.** Microtubule self-organization in a static F-actin meshwork leads to aster formation at the vicinity of chromosomes. **h.** NuMA is recruited at the spindle poles in extract droplets in a static F-actin meshwork. **i.** Pole-to-chromosome distance as a function of the droplet diameter for confined extracts with static F-actin meshwork. In all the images, chromosomes were labelled with DAPI, microtubules with TRITC-tubulin, pole with NuMA-GFP antibody, and F-actin with GFP-Utrophin. All scale bars are 10 μm .

We then ask how microtubule aster dynamics in a chromosome-assembly pathways are impacted depending on the dynamic properties of F-actin. We found that microtubule length and growth were roughly the same in a dynamic F-actin meshwork ($14 \pm 7 \mu\text{m}$) and in absence of F-actin ($13 \pm 6 \mu\text{m}$) (**Figure 4b**). To the contrary, in the presence of a static F-actin meshwork, the average length dropped to $11 \pm 5 \mu\text{m}$ (11% reduction; **Figure 4b**) as well as the growth rate. This difference in microtubule dynamics between chromosome-nucleated asters and Ran or centrosome-nucleated asters could be explained by the presence of the RanGTP gradient generated by chromosomes, which is known to favor the local stabilization of growing microtubules in the vicinity of the chromatin[36,37].

Altogether these data suggest that the spindle formation is arrested at an early stage of self-organization in a static F-actin meshwork, whereas it can assemble properly in a dynamic meshwork.

In the contractile actin meshwork, our observations showed that the chromosomes were always located inside the F-actin ring structure after being transported by F-actin flow in less than 10 minutes (**Figure 4c**). The microtubules that were nucleated from the chromosomes succeeded in self-organizing into monopolar or bipolar structures despite their active confinement within the F-actin structures (**Figure 4c**). We observed that the F-actin boundary remained mainly unperturbed and that it constrained the microtubule-based structures. In a few cases, we observed the deformation of microtubules by F-actin as well as the deformation of F-actin by microtubules. In this condition, the F-actin acts as a geometrical boundary within which chromosomes can still trigger microtubule nucleation.

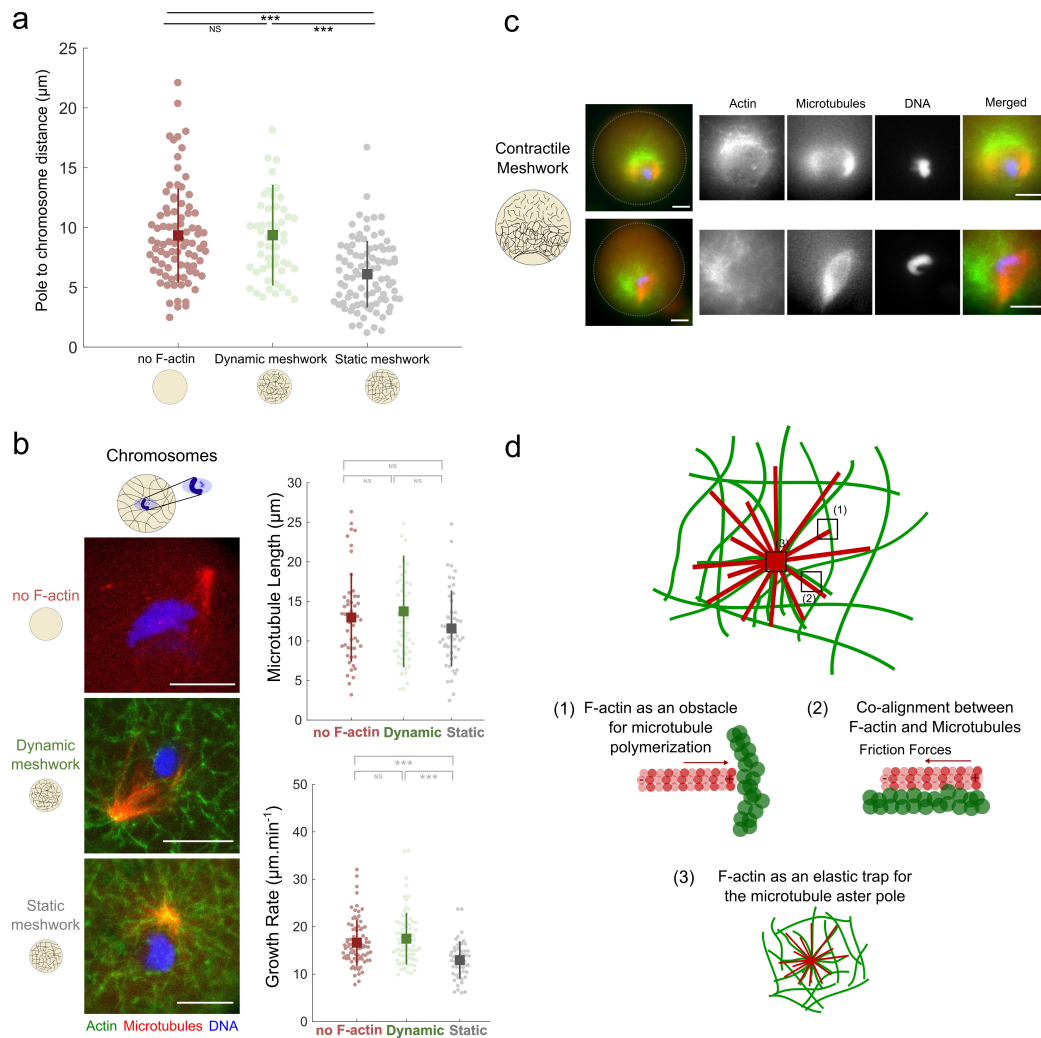


Figure 4. Aster spindle formation in F-actin meshworks with different dynamic properties

a. Pole-to-chromosome distance for three cases: no F-actin meshwork, dynamic meshwork, and static meshwork. **b.** Length and growth rate of chromosome-nucleated microtubules. The procedure of measurement is the same as described in Figure 1. In all the images, chromosomes were labelled with DAPI, microtubules with TRITC-tubulin, pole with NuMA-GFP antibody, and F-actin with GFP-Utrophin. All scale bars are 10 μm . **c.** Microtubule nucleation in a contractile F-actin meshwork. Chromosomes and microtubules are entrapped in the F-actin ring structure. **d.** Schematic of hypothetical explanations of the effect of F-actin meshwork on microtubule growth: F-actin filaments, acting as elastic and stiff biopolymers, reduce microtubule dynamics by acting as obstacles. Co-alignments between microtubules and F-actin could induce friction forces opposing microtubule growth. Additionally, the cytoplasmic F-actin meshwork constrains the motion of the aster poles by trapping them in an elastic gel.

DISCUSSION

Our *in vitro* assay examined how microtubule assembly and dynamics are affected in the presence of a dense F-actin meshwork. For Ran- and centrosome-nucleated microtubules, the aster morphology was conserved but length and dynamics of microtubules were reduced, independently of the dynamic state of F-actin. To explain these observations, we hypothesize that the F-actin meshwork provides physical constraints that perturb microtubule dynamics. We propose that F-actin filaments, acting as elastic and stiff biopolymers, are obstacles for growing microtubules and reduce their polymerization velocity by generating opposing forces (**Figure 4d**). The regulation of microtubule growth by mechanical forces has previously been demonstrated using *in vitro* assays [38,39]. Conversely, microtubules locally dictate F-actin geometry by guiding the microfilament organization into aster-like structures at the spindle poles (**Figures S2, S4**). This finding is in agreement with observations showing that microtubule organisation can constrain F-actin alignment *in vitro*[15,18] or *in vivo*[1,2]. The co-alignments between microtubules and F-actin also correlate with the reduction of growth velocity. These co-alignments suggest an alternative mechanism involved in the change of microtubule dynamics. The multiple contacts between microtubules and F-actin, probably mediated by the presence of cross-linkers, could generate friction forces opposing microtubule growth (**Figure 4d**). Such mechanical regulations of microtubules by F-actin may play a role in living cells, complementary to biochemical regulations controlling the coordination between F-actin and microtubules[40].

For the chromosome-nucleated microtubules, the monopolar spindle formation was arrested at an early stage in static F-actin meshwork, whereas it can assemble

properly in a dynamic meshwork. In the case of the static meshwork, stalling forces that are induced by the F-actin meshwork could prevent proper spindle formation by trapping the pole in an elastic gel (**Figure 4d**). In this case, the cytoplasmic F-actin could modulate the motion of the aster poles outward from the chromosomes. This difference in monopolar spindle formation as a function of the dynamic state of F-actin can be explained by the different elastic properties between static and the dynamic meshworks. Indeed, the modulus of elasticity of semi-flexible F-actin polymer networks is expected to increase non-linearly with local actin concentration[41], and increasing the branching concentration also stiffens the meshwork[42]. These characteristics suggest that the static F-actin meshwork has greater elasticity than the dynamic one. This is consistent with the existence of a larger resistive force that is induced by the static F-actin meshwork and that opposes to the force-generating elements driving the outward growth of the spindle pole. In a dynamic meshwork, the force-generating elements of the spindle apparatus, which powered the motion of the pole outward from the chromosomes, are thus sufficient to drive spindle formation and elongation.

Our reconstituted system examined how F-actin meshwork can affect complex morphogenetic processes such as spindle aster assembly. F-actin spatiotemporal dynamics are tightly regulated in cells and vary strongly throughout the cell cycle[43,44]. For instance, studies in mouse oocytes reveal the importance of F-actin regulation and the meshwork mechanical properties in controlling spindle migration[8,9]. Therefore, the spatial regulation of cytoplasmic F-actin architecture and dynamics can affect microtubule self-organization in many pathways, such as through purely physical and mechanical effects.

COMPETING INTERESTS

The authors declare that they have no competing interests.

AUTHOR'S CONTRIBUTIONS

A.C performed the experiments. A.C and Z.G conceived and analyzed the experiments.

A.C and Z.G wrote the manuscript.

ACKNOWLEDGMENTS

We thank L. Blanchoin and C. Guerin for providing the Scar-pWA constructs; J.Pelletier and T.J.Mitchison for providing the antibody NuMA-GFP; and M.They and J. Sillibourne for providing the purified centrosomes. We thank M.H. Verlhac and M.E. Terret for careful reading of the manuscript. We also thank all the members of the “Pole de Chimie Biophysique” and F.Robin for fruitful discussions. A.C was supported by a “Ministère de la Recherche” predoctoral fellowship. This work was supported by the CNRS, Ville de Paris “Emergence(s)”, and Ecole Normale Supérieure.

REFERENCES

1. Azoury, J., Lee, K.W., Georget, V., Rassinier, P., Leader, B., and Verlhac, M.-H. (2008). Spindle positioning in mouse oocytes relies on a dynamic meshwork of actin filaments. *Curr. Biol.* *18*, 1514–9.
2. Schuh, M., and Ellenberg, J. (2008). A new model for asymmetric spindle positioning in mouse oocytes. *Curr. Biol.* *18*, 1986–92.
3. Li, H., Guo, F., Rubinstein, B., and Li, R. (2008). Actin-driven chromosomal motility leads to symmetry breaking in mammalian meiotic oocytes. *Nat. Cell Biol.* *10*, 1301–8.
4. Lénárt, P., Bacher, C.P., Daigle, N., Hand, A.R., Eils, R., Terasaki, M., and Ellenberg, J. (2005). A contractile nuclear actin network drives chromosome congression in oocytes. *Nature* *436*, 812–818.
5. Mori, M., Monnier, N., Daigle, N., Bathe, M., Ellenberg, J., and Lénárt, P. (2011). Intracellular transport by an anchored homogeneously contracting F-actin meshwork. *Curr. Biol.* *21*, 606–11.
6. Kunda, P., and Baum, B. (2009). The actin cytoskeleton in spindle assembly and positioning. *Trends Cell Biol.* *19*, 174–179.
7. Morin, X., and Bellaïche, Y. (2011). Mitotic spindle orientation in asymmetric and symmetric cell divisions during animal development. *Dev. Cell* *21*, 102–19.
8. Chaigne, A., Campillo, C., Gov, N.S., Voituriez, R., Azoury, J., Umaña-Díaz, C., Almonacid, M., Queguiner, I., Nassoy, P., Sykes, C., *et al.* (2013). A soft cortex is essential for asymmetric spindle positioning in mouse oocytes. *Nat. Cell Biol.* *15*, 958–66.
9. Chaigne, A., Campillo, C., Voituriez, R., Gov, N.S., Sykes, C., Verlhac, M.-H., and Terret, M.-E. (2016). F-actin mechanics control spindle centring in the mouse zygote. *Nat. Commun.* *7*, 10253.
10. Rump, A., Scholz, T., Thiel, C., Hartmann, F.K., Uta, P., Hinrichs, M.H., Taft, M.H., and Tsiavalariis, G. (2011). Myosin-1C associates with microtubules and stabilizes the mitotic spindle during cell division. *J. Cell Sci.* *124*, 2521–2528.
11. Wu, S.Z., and Bezanilla, M. (2014). Myosin VIII associates with microtubule ends and together with actin plays a role in guiding plant cell division. *Elife* *3*, 1–20.
12. Weber, K.L., Sokac, A.M., Berg, J.S., Cheney, R.E., and Bement, W.M. (2004). A microtubule-binding myosin required for nuclear anchoring and spindle assembly. *Nature* *431*, 325–329.
13. Woolner, S., O'Brien, L.L., Wiese, C., and Bement, W.M. (2008). Myosin-10 and actin filaments are essential for mitotic spindle function. *J. Cell Biol.* *182*, 77–88.
14. Kwon, M., Bagonis, M., Danuser, G., and Pellman, D. (2015). Direct Microtubule-Binding by Myosin-10 Orients Centrosomes toward Retraction Fibers and Subcortical Actin Clouds. *Dev. Cell* *34*, 323–337.
15. Magdalena, P.L., Huber, F., Grigoriev, I., Steinmetz, M.O., Akhmanova, A., Koenderink, G.H., and Dogterom, M. (2014). Actin-microtubule coordination at growing microtubule ends. *Nat. Commun.*, 1–9.
16. Henty-Ridilla, J.L., Rankova, A., Eskin, J.A., Kenny, K., and Goode, B.L. (2016). Accelerated actin filament polymerization from microtubule plus ends. *Science* (80-.). *352*, 1004–1009.

17. Sider, J.R., Mandato, C. a, Weber, K.L., Zandy, a J., Beach, D., Finst, R.J., Skoble, J., and Bement, W.M. (1999). Direct observation of microtubule-f-actin interaction in cell free lysates. *J. Cell Sci. 112 (Pt 1)*, 1947–1956.
18. Waterman-Storer, C., Duey, D.Y., Weber, K.L., Keech, J., Cheney, R.E., Salmon, E.D., and Bement, W.M. (2000). Microtubules remodel actomyosin networks in *Xenopus* egg extracts via two mechanisms of F-actin transport. *J. Cell Biol. 150*, 361–376.
19. Nguyen, P.A., Groen, A.C., Loose, M., Ishihara, K., Wuhr, M., Field, C.M., and Mitchison, T.J. (2014). Spatial organization of cytokinesis signaling reconstituted in a cell-free system. *Science (80-)*. *50*, 244–247.
20. Colin, A., Bonnemay, L., Gayrard, C., Gautier, J., and Gueroui, Z. (2016). Triggering signaling pathways using F-actin self-organization. *Sci. Rep. 6*, 34657.
21. Heald, R., Tournebize, R., Blank, T., Sandaltzopoulos, R., Becker, P., Hyman, a, and Karsenti, E. (1996). Self-organization of microtubules into bipolar spindles around artificial chromosomes in *Xenopus* egg extracts. *Nature 382*, 420–425.
22. Mitchison, T.J., Maddox, P., Groen, A., Cameron, L., Perlman, Z.E., Ohi, R., Desai, A., Salmon, E.D., and Kapoor, T.M. (2004). Bipolarization and Poleward Flux correlate during *Xenopus* Extract Spindle Assembly. *Mol. Biol. Cell 15*, 5603–5615.
23. Caudron, M., Bunt, G., Bastiaens, P., and Karsenti, E. (2005). Spatial coordination of spindle assembly by chromosome-mediated signaling gradients. *Science (80-)*. *309*, 1373–1376.
24. Brugués, J., Nuzzo, V., Mazur, E., and Needleman, D.J. (2012). Nucleation and transport organize microtubules in metaphase spindles. *Cell 149*, 554–564.
25. Field, C.M., Nguyen, P. a., Ishihara, K., Groen, A.C., and Mitchison, T.J. (2014). *Xenopus* egg cytoplasm with intact actin. *Methods Enzymol. 540*, 399–415.
26. Field, C.M., Pelletier, J.F., and Mitchison, T.J. (2017). *Xenopus* extract approaches to studying microtubule organization and signaling in cytokinesis. *Methods Cell Biol. 137*, 395–435.
27. Pinot, M., Steiner, V., Dehapiot, B., Yoo, B.-K., Chesnel, F., Blanchoin, L., Kervrann, C., and Gueroui, Z. (2012). Confinement induces actin flow in a meiotic cytoplasm. *Proc. Natl. Acad. Sci. U. S. A. 109*, 11705–10.
28. Abu Shah, E., and Keren, K. (2014). Symmetry breaking in reconstituted actin cortices. *Elife 2014*, 1–15.
29. Pinot, M., Chesnel, F., Kubiak, J.Z., Arnal, I., Nedelec, F.J., and Gueroui, Z. (2009). Effects of confinement on the self-organization of microtubules and motors. *Curr. Biol. 19*, 954–60.
30. Hazel, J., Krutkramelis, K., Mooney, P., Tomschik, M., Gerow, K., Oakey, J., and Gatlin, J. (2013). Changes in Cytoplasmic Volume Are sufficient to drive spindle scaling. *Science (80-)*., 853–856.
31. Good, M.C., Vahey, M.D., Skandarajah, A., Fletcher, D. a., and Heald, R. (2013). SI Cytoplasmic Volume Modulates Spindle Size During Embryogenesis. *Science (80-)*. *342*, 856–860.
32. Wilde, A., and Zheng, Y. (1999). Stimulation of microtubule aster formation and spindle assembly by the small GTPase Ran. *Science (80-)*. *284*, 1359–1362.
33. Farina, F., Gaillard, J., Guérin, C., Couté, Y., Sillibourne, J., Blanchoin, L., and

- Théry, M. (2016). The centrosome is an actin-organizing centre. *Nat. Cell Biol.* *18*, 65–75.
34. Cavazza, T., Peset, I., and Vernos, I. (2016). From meiosis to mitosis : the sperm centrosome defines the kinetics of spindle assembly after fertilization in *Xenopus*. *J. Cell Sci.* *129*, 2538–2547.
 35. Wühr, M., Chen, Y., Dumont, S., Groen, A.C., Needleman, D.J., Salic, A., and Mitchison, T.J. (2008). Evidence for an Upper Limit to Mitotic Spindle Length. *Curr. Biol.* *18*, 1256–1261.
 36. Athale, C.A., Dinarina, A., Mora-Coral, M., Pugieux, C., Nedelec, F., and Karsenti, E. (2008). Regulation of microtubule dynamics by reaction cascades around chromosomes. *Science* *322*, 1243–7.
 37. Yokoyama, H., Gruss, O.J., Rybina, S., Caudron, M., Schelder, M., Wilm, M., Mattaj, I.W., and Karsenti, E. (2008). Cdk11 is a RanGTP-dependent microtubule stabilization factor that regulates spindle assembly rate. *J. Cell Biol.* *180*, 867–875.
 38. Dogterom, M., and Yurke, B. (1997). Measurement of the Force-Velocity Relation for Growing Microtubules. *Science* (80-.). *278*, 856–860.
 39. Janson, M.E., De Dood, M.E., and Dogterom, M. (2003). Dynamic instability of microtubules is regulated by force. *J. Cell Biol.* *161*, 1029–1034.
 40. Nejedla, M., Sadi, S., Sulimenko, V., de Almeida, F.N., Blom, H., Draber, P., Aspenstrom, P., and Karlsson, R. (2016). Profilin connects actin assembly with microtubule dynamics. *Mol. Biol. Cell* *27*, 2381–2393.
 41. MacKintosh, F.C., Kas, J., and Janmey, P.A. (1995). Elasticity of semiflexible biopolymer networks. *Phys Rev Lett* *75*, 4425–4428.
 42. Pujol, T., du Roure, O., Fermigier, M., and Heuvingsh, J. (2012). Impact of branching on the elasticity of actin networks. *Proc. Natl. Acad. Sci.* *109*, 10364–10369.
 43. Azoury, J., Lee, K.W., Georget, V., Hikal, P., and Verlhac, M.-H. (2011). Symmetry breaking in mouse oocytes requires transient F-actin meshwork destabilization. *Development* *138*, 2903–8.
 44. Field, C.M., Wühr, M., Anderson, G. a, Kueh, H.Y., Strickland, D., and Mitchison, T.J. (2011). Actin behavior in bulk cytoplasm is cell cycle regulated in early vertebrate embryos. *J. Cell Sci.* *124*, 2086–2095.

Supplementary Information for
Probing the Physical Constraints induced by Cytoplasmic F-actin on
Microtubule Dynamics of Asters and Spindle-like Organizations

*A. Colin and Z. Gueroui**

École Normale Supérieure, PSL Research University, CNRS, UPMC,
Department of Chemistry,
24 rue Lhomond, 75005 Paris, France

Supplemental Figures

Legends for Supplementary Movies

Supplemental Experimental Procedures

Correspondence:

Zoher GUEROUI

Phone: +33 1 44 32 24 09

Email: zoher.gueroui@ens.fr

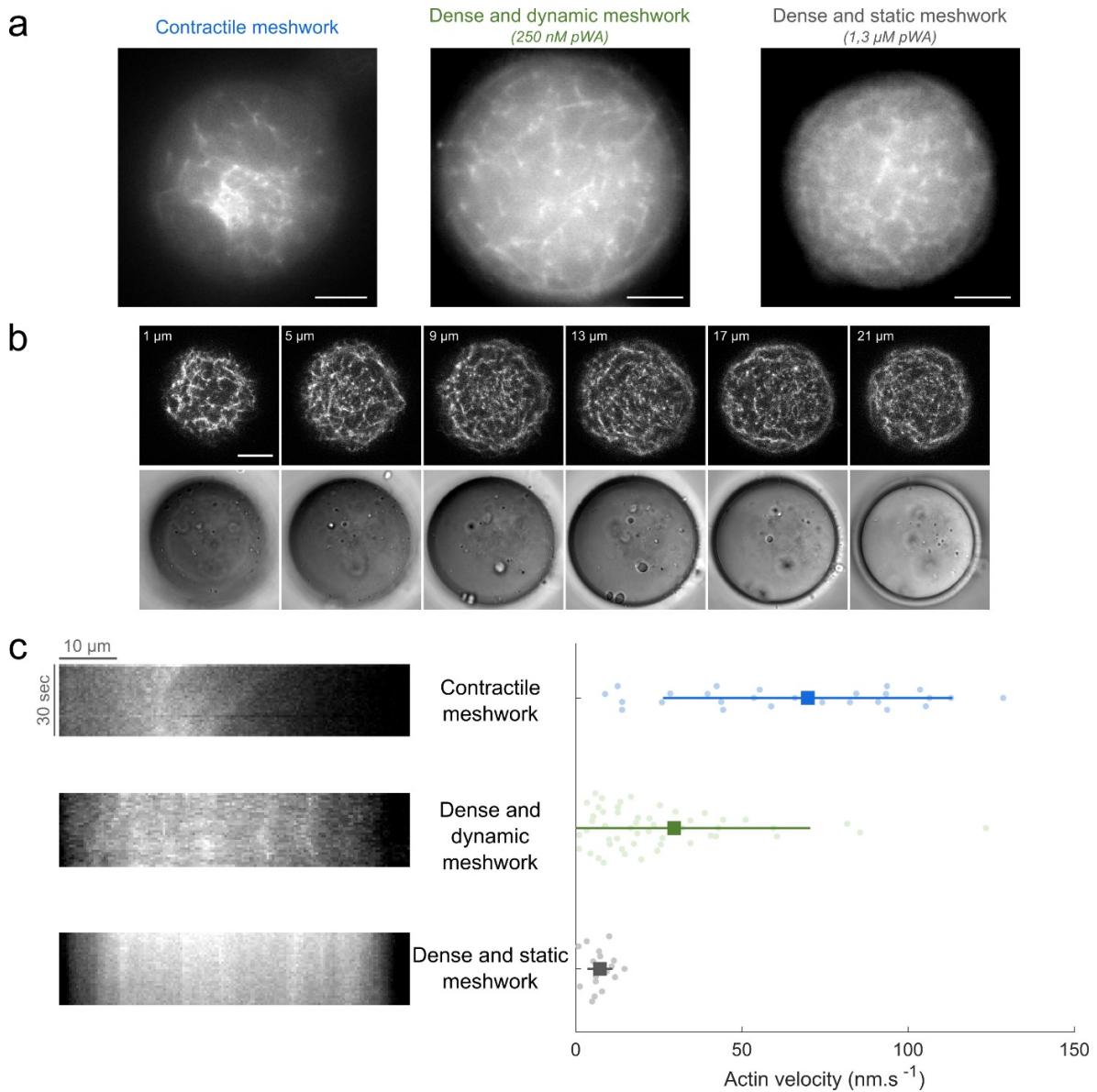


Figure S1. Characterization of the F-actin meshwork. (Related to Figure 1)

a. Examples of different types of meshworks obtained with actin-intact cell extracts confined in droplets. **b.** Confocal z-scan of a droplet with a F-actin meshwork nucleated with pWA (250 nM). z-scan were taken every 4 μm. **c.** Analysis of the actin flow velocity. Velocity was measured from kymographs extracted from dynamics that were taken with a time interval of 3 seconds for the blue and green cases, and 30 seconds for the grey case. In all cases, F-actin was labelled with GFP-utrophin. All scale bars are 10 μm.

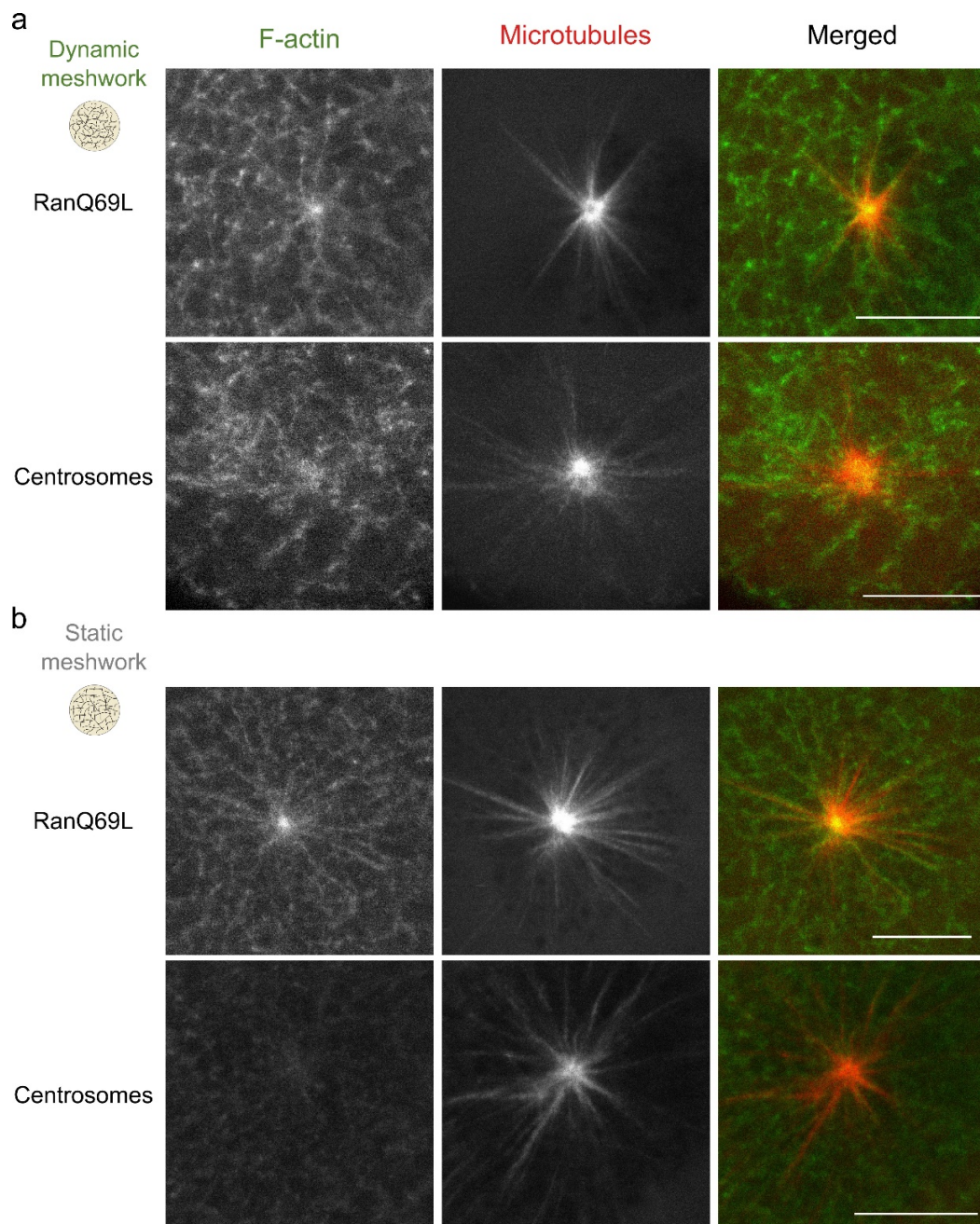


Figure S2. Examples of co-alignments between F-actin and microtubules. (Related to Figure 1)

Ran and centrosome-nucleated asters in dynamic (a) or static (b) F-actin meshwork. F-actin is labelled with GFP-utrophin, microtubules with TRITC-tubulin.

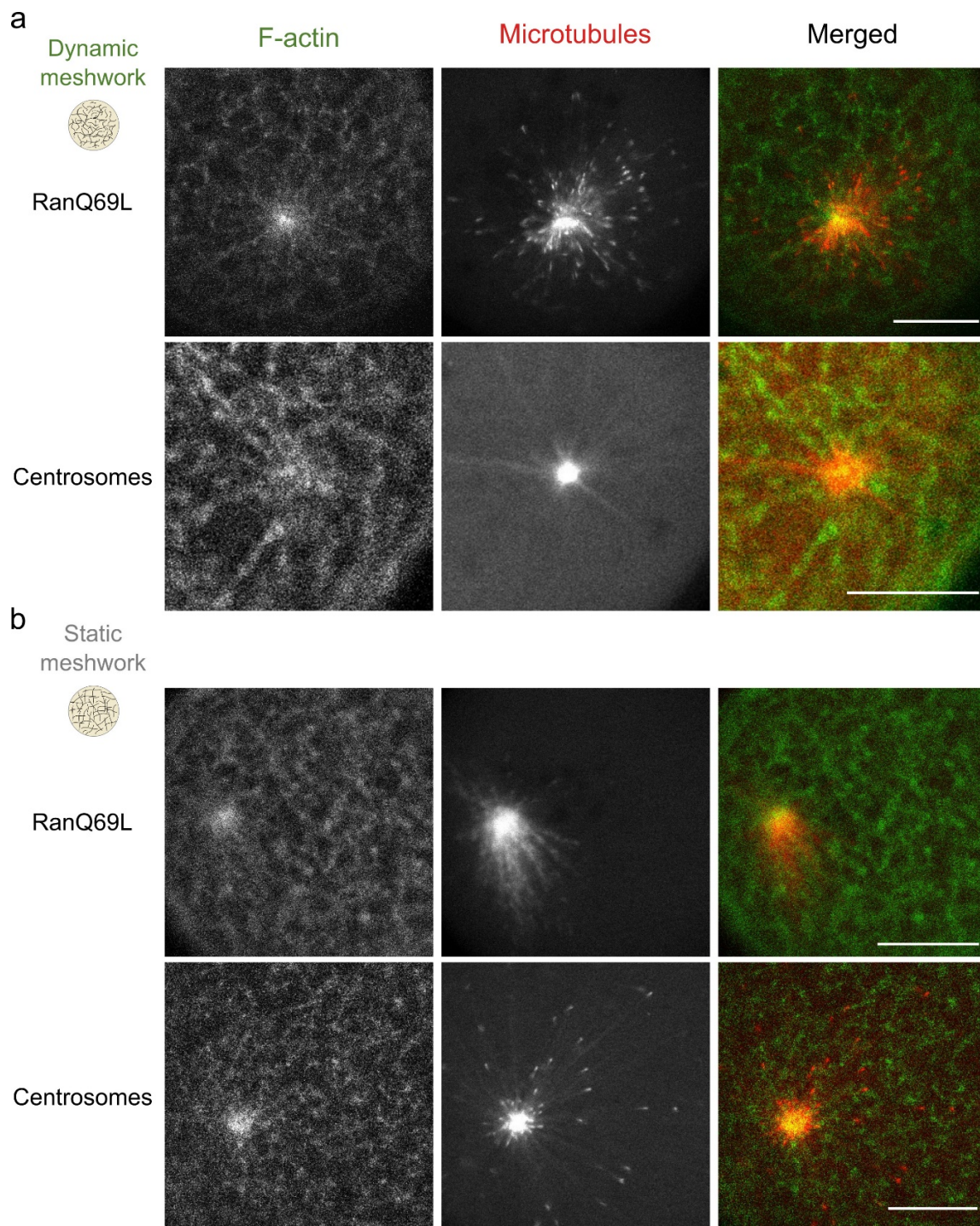


Figure S3. Co-localisation of F-actin at the level of the spindle aster pole. (Related to Figures 1,2) a.b. Confocal observations of the co-localisation in the case of (a) a dynamic meshwork (250 nM pWA), and (b) a static one (1.3 μ M pWA). All scale bars are 10 μ m.

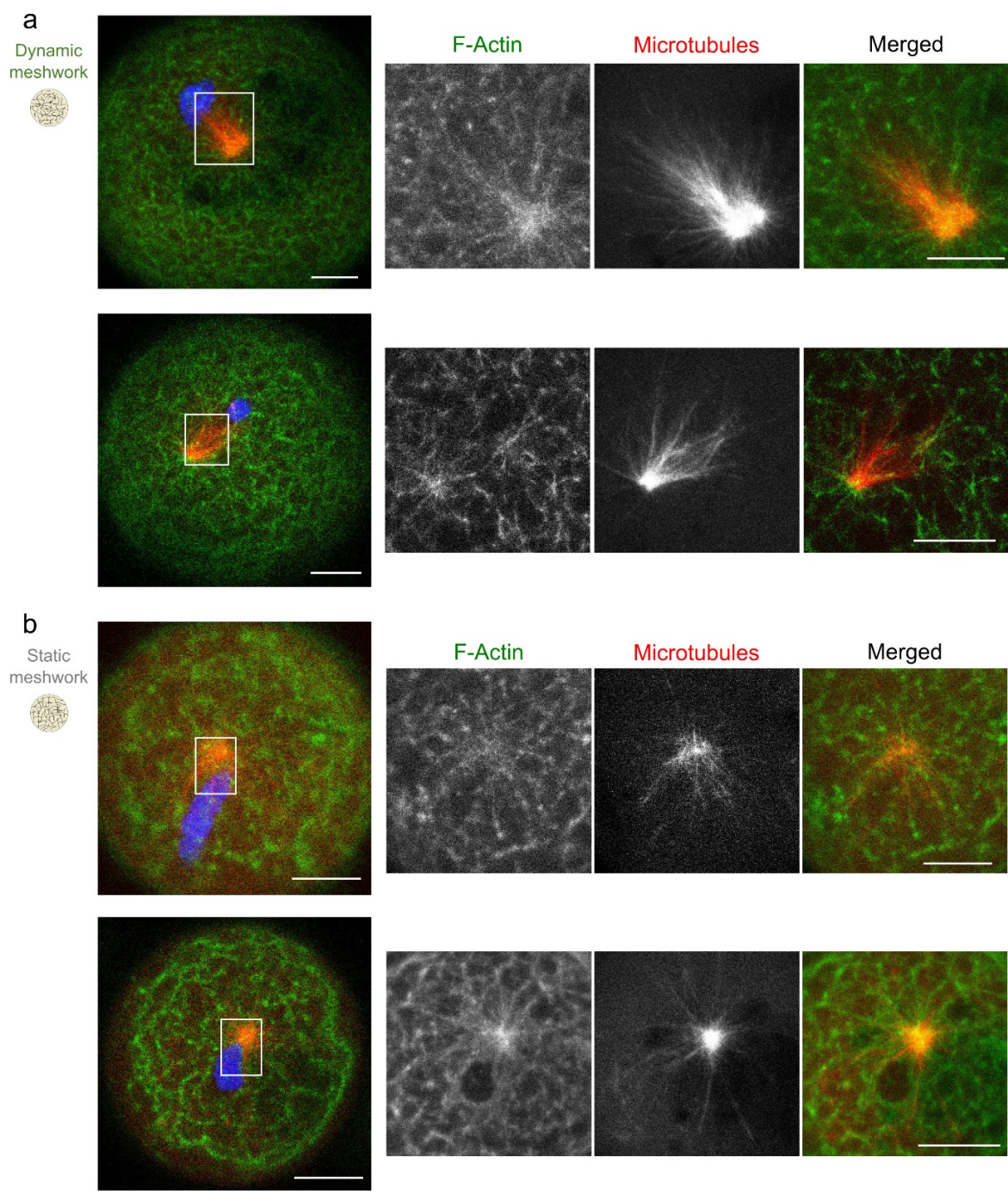


Figure S4. Examples of co-alignments between F-actin and microtubules. (Related to Figures 3,4)

Chromosomes-nucleated asters in (a) dynamic meshwork or (b) static meshwork.

Legends for Supplementary Movies

Supplementary Movie 1.

Various dynamics of F-actin meshworks in confined egg extracts. From left to right: contractile meshwork (native meshwork), static meshwork (1.3 μ M pWA), dynamic meshwork (250 nM pWA). F-actin is labelled with GFP-Utrophin. Frames are 3 seconds apart.

Supplementary Movie 2.

Time-lapse observation of a centrosome-nucleated aster labelled with EB1-GFP. Frames are 1 second apart.

Supplementary Movie 3.

Aster pole motion in meshworks with different F-actin dynamic properties. F-actin is labelled with GFP-Utrophin and microtubules with TRITC-tubulin. Frames are 30 seconds apart.

Supplementary Movie 4.

Confocal observation of the transport of a RanQ69L-nucleated aster by the contraction of F-actin. Recruitment of F-actin at the level of the microtubule pole is also detectable. F-actin (green) is labeled with GFP-Utrophin and microtubules (red) with TRITC-tubulin. Frames are 15 seconds apart.

Supplemental Experimental Procedures

Actin-intact *Xenopus* egg extract preparation

Xenopus laevis egg extracts were prepared as previously described[1], [2]. ATP regenerating system (1 mM ATP, 10 mM creatine phosphate, 80 µg/mL creatine phosphokinase, final concentrations) was added at the beginning of each experiment. All reagents for buffer preparation were purchased from Sigma-Aldrich. Sperm nuclei were prepared as previously described[3].

Protein production and purification

Recombinant pWA (Scar-WA) proteins were produced as previously described[4]. RanQ69L, EB1-GFP, Utr-GFP, and Utr-dsRed were expressed from plasmids and purified using standard protocols. Centrosomes were kindly provided by M. They and J. Sillibourne.

Microtubule nucleation and observation

Microtubules were nucleated from several assembly pathways, mediated by sperm nuclei, centrosomes, or RanQ69L. Depending on the requirements of the experiments, microtubules were labelled with FITC-tubulin or TRITC-tubulin (Cytoskeleton Inc.) at a final concentration of 300 nM or with EB1-GFP at a final concentration of 200 nM. The antibody NuMA-GFP was used at a final concentration of 7.5 µg/mL to characterize the spindle pole and was a gift of J. Pelletier and T.J. Mitchison. Asters nucleated from Ran were nucleated in the presence of 8 µM RanQ69L (final concentration).

Actin nucleation and observation

Actin was labelled with GFP-Utrophin or dsRed-Utrophin at a final concentration of 80 nM. To impede F-actin meshwork formation, we depolymerized F-actin by adding Latrunculin-A (Sigma) and block myosin-II activity using Blebbistatin (Sigma) to the extract at final concentrations of 25 µM and 70 µM, respectively. To promote homogeneous nucleation of F-actin in the droplets, pWA was used at final concentrations of 1.3 µM or 250 nM.

Generation of emulsion droplets/encapsulated extracts

Cell extract was encapsulated in droplets using a water-in-oil emulsion process. A biocompatible block copolymer (Arlacel P135) is added to mineral oil (Sigma) to stabilize emulsion and facilitate observations. This method, which has previously been described allows the formation of microtubule asters in droplets[5]. The *Xenopus laevis* egg extracts were added to the block copolymer solution (1% (v CSF/v

Oil)) at room temperature. The mixture was then gently sheared by pipetting the solution up and down for a few seconds to generate extract-in-oil droplets. The mechanical dispersion of the biphasic solution formed micrometre-sized extract-in-oil droplets within a few seconds. The emulsion was incubated for 30 minutes at 19°C and then observed under the microscope for 45 minutes. The droplets presenting microtubule formation had a diameter comprised between 10 and 120 µm.

Image and data analysis

Fluorescence imaging was performed using IX71 and IX81 Microscopes (Olympus) equipped with an EM-CCD camera (electron multiplying CCD, C9100-02, Hamamatsu, Corporation) or an ImageEM (X2 EM-CCD C9100-23B, Hamamatsu Corporation) respectively. An X60 (PlanApo, NA 1.42) oil objective and a LED system of illumination (Spectra X, Lumencor) were used. Microscope settings and functions were controlled using Simple PCI software (Hamamatsu) or Micro-Manager. Confocal microscopy was performed with a Zeiss LSM 710 META laser scanning confocal microscope using an X63 (PlanApochromatic, NA 1.4) objective. Image analysis was performed using ImageJ and Matlab. The pole-to-chromosome distance was measured by taking the distance between the microtubule pole (maximum of fluorescence of the microtubule fluorescence channel) and the chromosome centroid.

Kymographs analysis: for dynamic meshworks, we measured the F-actin velocity on movies with a 3 second interval whereas for the static meshwork, it was measured on movies with a 30 second interval (to obtain the necessary resolution for the velocity measurement). Kymographs were traced and analysed with ImageJ software. Quantitative analysis of EB1-GFP dynamics: movies were acquired with one image every second for one minute. Time projection of the movies allowed the measurement of microtubule length. Kymographs following the path of microtubules were traced and growth rate was extracted from those kymographs. For each condition described, two independent experiments were performed with two different cell extracts. In each experiment, three to six asters were monitored and analysed.

For pole mobility, movies were acquired between 30 and 75 minutes after the beginning of the incubation. Droplets with only one pole were imaged at 30 seconds intervals for about 10-15 minutes. For movie analysis, tracking was done manually using the Manual Tracking plugin from ImageJ.

Data treatment was performed with Excel and Matlab. Student's t-tests were performed with Matlab. For the interpretation of the p-values, NS means there is no significant difference between the two distributions. One star means p-value < 0.05, two stars means p-value < 0.01, and three stars means p-value < 0.001.

Supplemental References

- [1] E. Hannak and R. Heald, “Investigating mitotic spindle assembly and function in vitro using *Xenopus laevis* egg extracts.,” *Nat. Protoc.*, vol. 1, no. 5, pp. 2305–2314, 2006.
- [2] C. M. Field, J. F. Pelletier, and T. J. Mitchison, “*Xenopus* extract approaches to studying microtubule organization and signaling in cytokinesis,” *Methods Cell Biol.*, vol. 137, pp. 395–435, 2017.
- [3] P. J. Gillespie, A. Gambus, and J. J. Blow, “Preparation and use of *Xenopus* egg extracts to study DNA replication and chromatin associated proteins,” *Methods*, vol. 57, no. 2, pp. 203–213, 2012.
- [4] L. M. Machesky *et al.*, “Scar, a WASp-related protein, activates nucleation of actin filaments by the Arp2/3 complex.,” *Proc. Natl. Acad. Sci. U. S. A.*, vol. 96, no. 7, pp. 3739–3744, 1999.
- [5] a M. Jimenez, M. Roché, M. Pinot, P. Panizza, L. Courbin, and Z. Gueroui, “Towards high throughput production of artificial egg oocytes using microfluidics.,” *Lab Chip*, vol. 11, pp. 429–434, 2011.

5.3 Discussion

5.3.1 Perspectives of the work

There would have been more work to do on this project. Some experiments can be seen as "short-term" experiments and others would need another dedicated project. We will try to list the experiments missing and that would have helped to have a better understanding of our system.

Short-term experiments

In these experiments presented in this chapter, we did not try to decipher if the effect of F-actin on microtubules was biochemical or non-biochemical. In particular, we did not rule out that the change in F-actin meshwork dynamics can trigger the spatial re-localization of biochemical microtubule factors.

We could have checked the distribution of myosin X in our droplets. This can be done with an antibody directed against myosin X [32]. This would allow us to see if myosin X is reorganized in the droplets. We could also confirm that what we are observing is a real effect of the actin on microtubule dynamics and not just a reorganization of molecular actors. Immunodepletion of myosin X would also have been possible and allowed us to show the role of myosin X in our system and confirm the multipolar phenotypes already observed [33].

We did not try to differentiate the distinct role of architecture or dynamics of F-actin on microtubules. We did not really change the dynamics of the actin meshwork as we just played on the concentration of the activator of the Arp2/3 complex. We could have played on the capping proteins by adding cofilin to the extracts and see what was the effect of a more or less dynamic F-actin meshwork on the microtubule dynamics.

Long-term experiments

We did not try to cycle the actin-intact egg extract because it was a technical challenge. Though, it would be interesting to be able to replicate DNA in an actin-intact egg extracts. Therefore, we would be able to nucleate bipole spindle in those extracts. Thus we could see if the effect of a dense F-actin meshwork is the same on a bipole as on a monopole.

In the project, we changed the actin dynamics only by playing on the recruitment of Arp2/3. Though, it was shown that the cytoplasmic F-actin meshwork is often based on formins; therefore, it would have been interesting to obtain other meshwork morphology with formin nucleators (mDial1 for example).

Another idea comes from the work of Abu Shah and Keren (Figure 2.11b, page 35, [81]); they showed that it was possible to reconstitute an actin cortex with egg extracts confined in droplets. In addition, this cortex undergoes spontaneous polarization under certain conditions. An interesting idea would be to couple this actin cortex with the cytoplasmic meshwork that we have generated and see the influence of these two networks on spindle positioning in the droplet for example (Figure 5.5).

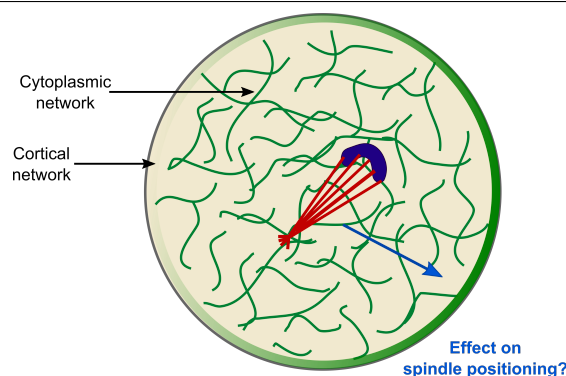


Figure 5.5: Scheme of a droplet with two actin meshworks reconstituted: a cortical and a cytoplasmic meshwork. The positioning of a spindle in this environment could be studied.

An important question is to see if those results make sense physiologically and if it is meaningful to study dense static meshwork for example. In the following, we will present example in cell cycle or pathological cases where the regulation of F-actin dynamics is very important.

5.3.2 Regulation of F-actin through the cell cycle

Studying the influence of F-actin on microtubule and spindle nucleation is important because F-actin is regulated through cell cycle. Indeed, cells change of shape during the cell cycle is due to a change of cortical tension mediated by F-actin and myosin II. It was also shown that differences in the organization of actin can be seen in metaphase and interphase [86]. The hypothesis is that embryos nucleate more actin during metaphase and that this nucleation could be important for vesicle trafficking, mitotic spindle assembly or mechanics of bulk cytoplasm.

5.3.3 F-actin misregulation in pathological cases

The results we obtained are interesting because they suggest that the actin regulation is important for microtubule morphological properties. One case where the microtubule morphology has been shown to be impacted by a change of actin morphology is found in cases of Alzheimer's disease. Indeed, by analyzing affected brains, researchers found that the frontal cortex presents a lot of actin rods. These rods can be induced by an ATP depletion in the medium (Figure 5.6). They co-localize with ADF and cofilin, actin-associated proteins (that are important for F-actin turnover *in vivo*). Interestingly, those rods were shown to be able to disrupt the microtubules in the neurites in some cases (by occluding the neurite). Therefore, if microtubules are disrupted, the axonal transport is not working anymore. The authors conclude that these actin rods compromise the function of the neurite without causing neuron death [166, 167].

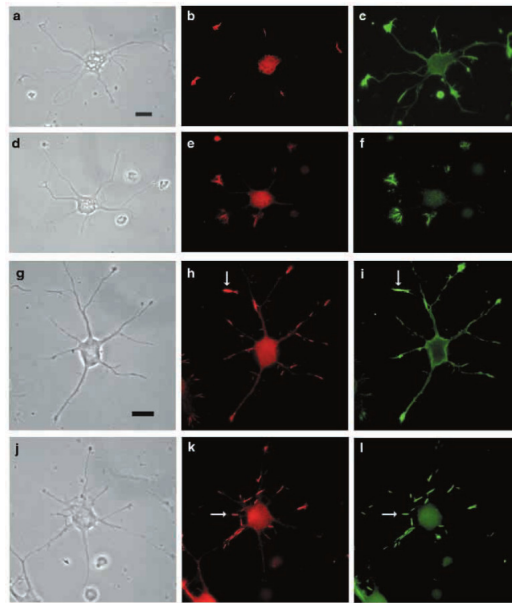


Figure 5.6: Actin-rods (ADF in red, actin in green). *Extracted from [166].*

5.3.4 Conclusion

This study provides a proof of concept that encapsulated *Xenopus* egg extracts are a useful tool to study F-actin/microtubules interactions. The parameters can be easily tuned (concentration in actin nucleators for example) and the droplet volume mimics well the cell volume. We also saw that cytoplasmic actin was shown to have more and more roles in cells. Therefore, it is important to study what can be the effect of such a network on microtubules structures.

Chapter 6

Spatiotemporal Characterization of the Active Diffusion Driving Nucleus Centering in Mouse Oocytes

During meiosis, the mouse oocyte undergoes two asymmetric divisions to keep as much as possible reserves (cytoplasmic stores, organelles, RNAs) for the beginning of the embryo development. Interestingly, the oocyte uses the same molecular actors to center or off-center large objects (nucleus or spindle) at different states of meiosis. In this chapter, we introduce a project where we studied the nucleus centering in mouse oocyte during meiosis.

Contents

| | | |
|------------|--|------------|
| 6.1 | Introduction | 130 |
| 6.1.1 | Context | 130 |
| 6.1.2 | How a cell can find its geometric center? Nucleus and spindle positioning in various organisms | 130 |
| 6.1.3 | Spindle migration mechanism in mouse oocytes | 134 |
| 6.2 | Article 3: Spatiotemporal characterization of the active diffusion driving nucleus centering in mouse oocytes | 135 |
| 6.2.1 | Presentation of the article | 135 |
| 6.2.2 | Manuscript | 135 |
| 6.3 | Discussion | 163 |
| 6.3.1 | Oil droplets as biomimetic objects and force sensors | 163 |
| 6.3.2 | Homeostasis of actin networks | 163 |
| 6.3.3 | Conclusion | 164 |

6.1 Introduction

6.1.1 Context

In the classical textbooks, the nucleus is often drawn at the center of the cell. But the nucleus position is highly dependent on the cell type and cell fate. Depending on the organisms, the nucleus can determine the location of the division. For example, in sea-cucumbers or in *Xenopus*, it is the nucleus that migrates to determine the place of the asymmetric division [168, 169]. In *C. elegans* oocytes, the germinal vesicle is in the center of the immature oocyte. The microtubules are used to asymmetrically position the germinal vesicle during oocyte maturation (Figure 6.1).

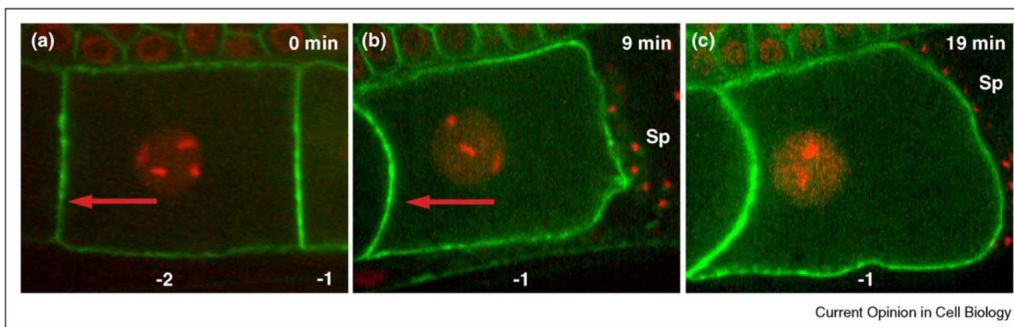


Figure 6.1: Images showing the migration of germinal vesicle in *C. elegans* during oocyte maturation. *Extracted from [170].*

In mouse oocytes, the positioning of the nucleus is related to the further capacity of development of the oocyte. Indeed, the position of the nucleus defines the starting point of spindle migration, therefore its positioning seems to be an important parameter to check. Brunet and Maro [171] showed that incompetent oocytes possess a peripheral nucleus whereas competent oocytes present a centered germinal vesicle. They showed that the position of the nucleus is related with the ability to undergo spindle migration and polar body exclusion. Oocytes with a centered nucleus have more chances to undergo proper meiosis than the ones with an off-centered nucleus. In addition, they found that old mice presented oocytes with nucleus less centered and so with a weaker ability to progress through meiosis.

6.1.2 How a cell can find its geometric center? Nucleus and spindle positioning in various organisms

In biology, organisms often need to find their center to achieve the further symmetric division of the cell. Depending on their size, organisms have various ways of finding their center. Small organisms ($1\ \mu\text{m}$ in diameter) use diffusion to deliver molecules whereas larger organisms ($10\text{-}30\ \mu\text{m}$ in diameter) use active transport. We will go through some examples from bacteria that find their center thanks to reaction-diffusion processes to mouse oocytes that find their center thanks to a long range transport via cytoplasmic actin.

Bacteria use a reaction-diffusion system to find their center

The bacteria have a length of about $1 \mu\text{m}$. At this length scale, the diffusion is not limited. Diffusive transport is powered by thermal noise and gives rise to a flux that is proportional to the local concentration gradient. From Fick equations, the characteristic time of diffusion τ_D can be expressed as following: $\frac{L^2}{D}$. Therefore, in bacteria, the diffusion time for a GFP will be 0.13 seconds with $D_{GFP} = 7.7 \mu\text{m}^2.\text{s}^{-1}$ [172, 173].

In bacteria, cell segregation is done by the contractile "Z ring", composed of FtsZ, a tubulin homologue. *E. coli* locates the Z ring (and therefore the division plane) with a very high precision [173]. The position of the Z ring results from a reaction-diffusion involving the Min proteins (introduced in Section 2.2.2, page 29). Briefly, the MinD protein oscillate between the bacteria poles; MinD is associated with MinC, an inhibitor of cell division. Because of the pole-to-pole oscillations, the concentration of MinC is the lowest at the middle of the cell, allowing the division to happen at this location precisely [174] (Figure 6.2).

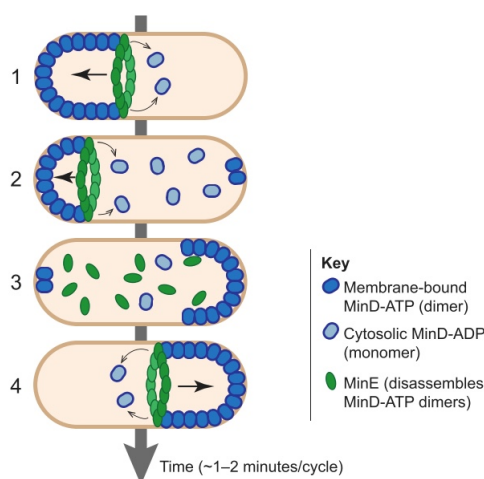


Figure 6.2: MinD oscillations to position the Z ring in bacteria. *Extracted from [174].*

In larger organisms, diffusion is not sufficient anymore to transport objects. Cells rely on active transport, mediated by the cytoskeleton. For example, microtubules can generate either pushing forces, generated by microtubule polymerization or pulling forces mediated by microtubule motors or microtubule depolymerization.

Microtubule-based pushing forces promotes nucleus and spindle centering in *S. pombe*

Schizosaccharomyces pombe, also called fission yeast has a size of 3 to 4 μm in diameter and 7 to 14 μm in length. During interphase, the nucleus of *S. pombe* maintains its position at the geometrical center of the cell. It was shown that interaction of growing microtubules with the periphery of the cell generates pushing forces that maintain the nucleus in the middle of the cell [175]. The microtubule plus-end polymerization exerts forces that are able to push the nucleus. A balance of these pushing forces allows to position the nucleus at the middle of the cell. During mitosis, the spindle also aligns with the cell axis [176]. It was shown that astral microtubules push on the mitotic spindle in *S. pombe*. They generate forces of about 1 to 10 pN consistent with a process based on

microtubule polymerization. Astral microtubules extend from spindle pole body into the cytoplasm and exert a force upon contact with the cell cortex.

The difference between the two states is that during interphase, the pushing forces are exerted along the long axis of the cell, whereas in mitosis, the force acts on the short axis of the cell (Figure 6.3).

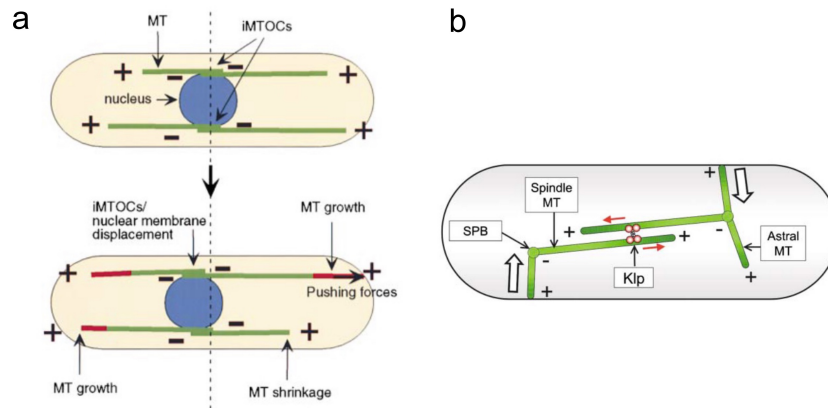


Figure 6.3: Growing microtubules generate pushing forces to position either the nucleus (a) or the spindle (b) at the center of the cell in *S. pombe*. *Extracted from [175, 176]*.

Aster positioning with pulling forces mediated by membrane-anchored dyneins

Pushing forces are generally associated with systems where short distances are involved because longer microtubules can not withstand compressive forces. Indeed, the force exerted decreases with the square of microtubule length because of buckling [177, 178]. The *Caenorhabditis elegans* embryo has a size of $30\ \mu\text{m}$ in diameter and $50\ \mu\text{m}$ in length, a scale at which pulling forces are inefficient. The first division of the *C. elegans* embryo is asymmetric. It is well-known that the asymmetric spindle positioning is driven by cortical dynein-mediated pulling forces generated by the astral microtubules at the cell cortex [179].

In HeLa cells, Kiyomitsu and Cheeseman [180] found the dynein is attached to the cortex *via* a LGN/NuMA complex. The spindle-pole-localized polo-like kinase (Plk1) regulates dynein localization by controlling the interaction between dynein and the LGN/NuMA complex. When the spindle pole is close to the cortex, Plk1 (localized on the pole) provokes the dissociation of dynein and LGN-NuMA complex. This leads to the displacement of the spindle toward the other side of the cell, because of the force imbalance. The same phenomenon will happen when the spindle will arrive on the other side of the cell (Figure 6.4). In addition, the RanGTP gradient emanating from the chromosomes restricts the localization of NuMA-LGN to the lateral cortex, therefore maintaining the spindle orientation axis.

Aster transport can be dependent on cytoplasmic pulling forces

In large cells, a model of cytoplasmic pulling was proposed by Kimura and Kimura [181, 182]. The viscous drag of organelles transported toward the minus ends of astral microtubules (anchored at the centrosome) by cytoplasmic dynein generates a force in the opposite direction toward the cortex. This mechanism might predominate in very

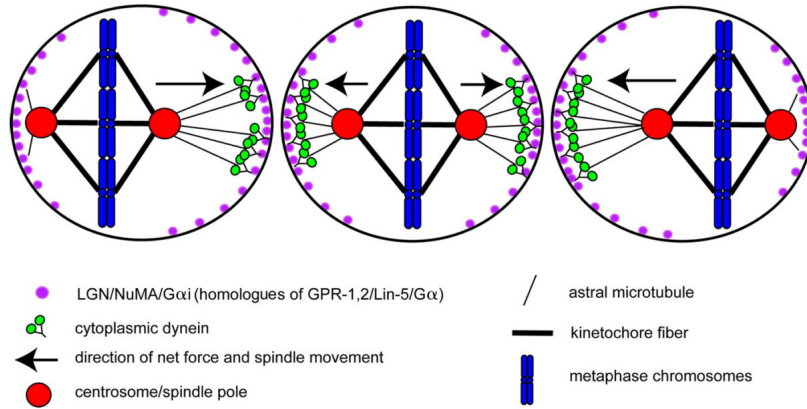


Figure 6.4: Spindle centering in HeLa cells mediated by dynein pulling forces regulated by Plk1 and LGN/NuMA complex. *Extracted from [180].*

large cells where astral microtubules can not reach the cortex. Wühr *et al.* also showed the existence of such a mechanism in *Xenopus* (diameter of about 1 mm) and zebrafish embryos [183]. In sea urchin oocyte (100 μ m in diameter), the centration of sperm asters represents a ubiquitous and stereotypical aster long-range movement. Indeed, the sperm pronucleus shows a very persistent movement of centration, strictly dependent on microtubules. Tanimoto *et al.* showed that the centering of the aster is driven by microtubule-length-dependent pulling forces mediated by the dynein in the cytoplasm [184].

Cytoplasmic actin for long range transport in mouse oocytes

Interestingly, in large oocytes like mouse oocytes or starfish oocytes, long-range transport has been shown to be highly dependent on cytoplasmic F-actin. Because mouse oocytes lack centrosomes and astral microtubules, cytoplasmic F-actin networks play a key role in the positioning of the spindle by transmitting forces over long distances. It was shown recently that the nucleus centering is also dependent on the cytoplasmic F-actin meshwork, showing again the importance of this network for the long-range transport (Figure 6.5, [94]).

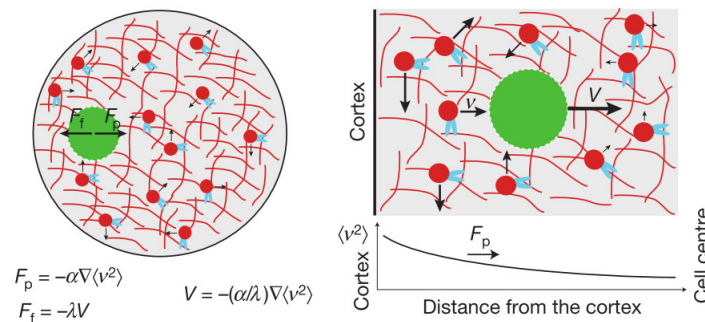


Figure 6.5: Model for nucleus centering in mouse oocytes. The nucleus is represented in green and cytoplasmic actin in red. *Extracted from [94].*

6.1.3 Spindle migration mechanism in mouse oocytes

We will now detail the molecular mechanisms of spindle migration in mouse oocytes that have been widely studied in these last years. The positioning of the spindle mainly depends on actin filaments and formin-2. The spindle migrates toward the closest pole with a velocity of $0.12 \mu\text{m}\cdot\text{min}^{-1}$ for 2-3 hours.

Azoury *et al.* [91] studied the morphology of the actin network in mouse oocytes thanks to a Utrophin-GFP probe. They showed that the actin organize in a cage surrounding the spindle (actin-spindle structure). This organization is lost in absence of microtubules, showing the influence of the microtubules on the actin organization. Concomitantly Schuh and Ellenberg [92] showed that myosin II was required for the actin filament pulling toward the spindle poles as well as for spindle relocation.

Azoury *et al.* [93] then studied the variation of actin meshwork density during the first meiotic division and showed that the meshwork remodeling correlates with the formin regulation (Figure 2.16b). They showed that the F-actin remodeling upon meiosis entry is essential for symmetry breaking in mouse oocytes. The amount of formin-2 controls the density of the meshwork and the extent of external forces applied on the nucleus: the more formin-2, the denser the meshwork, the greater the forces. In presence of continuous forces (applied by the actin meshwork on the nucleus), the symmetry breaking is not possible.

Schuh [27] showed the existence of actin vesicles coated with Spire1, Spire2 and formin-2. Those vesicles are connected and form an actin network that allows the long range transport in the mouse oocyte cytoplasm. This vesicles move thanks to myosin Vb. Holubcova *et al.* [185] studied the function of Rab11a-positive vesicles in mouse oocytes. They showed that these vesicles drive the dynamics of actin meshwork by recruiting myosin Vb to reorganize the filaments and that they are required for asymmetric spindle positioning. Depletion of Rab11a-positive vesicles prevented asymmetric spindle positioning; in absence of Rab11a, the actin network was very static.

Chaigne *et al.* [95] showed that a soft cortex is necessary for spindle migration. They described the existence of an Arp2/3 dependent cortical F-actin thickening during spindle migration, coupled with a reduction in cortical tension and a release of myosin II from the cortex of the oocyte. Later they showed [186] that a window of cortical tension allows spindle migration; indeed, the cortex should not be too soft or too stiff. These results are coherent with measures done on the capacity of development of human oocytes [90].

Interestingly, the positioning of the zygotic spindle after fertilization and before first mitotic division relies on the same molecular actors (there is no centrosomes before the 64-cell stage). Two steps are important: the pronuclei centering and then the fine centering of the metaphase plate. Chaigne *et al.* [187] showed that F-actin and myosin Vb cytoplasmic flows drive the centering of the two pronuclei (as in prophase I when the oocytes center their nucleus [94]). The fine chromosome centering in the perfect center of the cell is based on myosin II and on the high cortical tension associated with the presence of myosin II at the cortex (this high cortical tension defines the exact embryo center where the maternal and paternal chromosomes will merge).

6.2 Article 3: Spatiotemporal characterization of the active diffusion driving nucleus centering in mouse oocytes

6.2.1 Presentation of the article

The goal of this project was to have a better understanding of the nucleus centering mechanism in prophase. Indeed, if a model of pressure gradient has been proposed in mouse oocytes [94], its specificity for the nucleus was not established.

First, we wanted to address the specificity of the centering mechanism. We also wanted to see if there was an influence of the size of the objects to be centered. We managed to demonstrate that **the centering mechanism is non-specific**: oil droplets of the nucleus size (20-30 μm) can also be centered by an F-actin-dependent mechanism. We showed that above a certain size threshold (1.5 μm), injected objects have a biased diffusion toward the center of the oocyte.

As presented above, the molecular actors driving the spindle off-centering have been widely studied and some of those molecular actors are the same for spindle off-centering and for nucleus centering, such as myosin V. We demonstrated that **in meiosis I, the centering mechanism is still in action**. Therefore in meiosis I, there is coexistence between a non-specific centering mechanism and a specific off-centering mechanism for the spindle (driven by myosin II). The same molecular actors can have two opposite roles: centering and off-centering of large objects.

The results of this chapter are presented in a manuscript in preparation for submission. Therefore some conclusions are not completely arrested yet.

6.2.2 Manuscript

Spatiotemporal characterization of the active diffusion driving nucleus centring in mouse oocytes.

Authors: Alexandra Colin¹, Maria Almonacid², Wylie Ahmed³, Timo Betz⁴, Marie-Emilie Terret², Raphaël Voituriez⁵, Zoher Gueroui^{1,*}, Marie-Hélène Verlhac^{2,*}

Affiliations:

¹ Ecole Normale Supérieure, Department of Chemistry PSL Research University-CNRS-ENS-UPMC 24, rue Lhomond, 75005, Paris, France.

² CIRB, Collège de France, and CNRS-UMR7241 and INSERM-U1050, Equipe Labellisée FRM, Paris F-75005, France.

³ Department of Physics, College of Natural Sciences & Mathematics California State University, Fullerton, USA.

⁴ Institute of Cell Biology, ZMBE, Von-Esmarch-Straße 56, D-48149 Münster, Germany.

⁵ UMR7600-CNRS/UPMC, 4 Place Jussieu, Paris F-75005, France.

* Correspondence should be addressed to MHV (marie-helene.verlhac@college-de-france.fr) and to ZG (zoher.gueroui@ens.fr)

Abstract

An original mechanism controls nucleus centration in mouse oocytes by a potential pressure gradient generated by actin positive vesicles. Using oil droplets micro-injection, fluorescently-coated latex beads micro-injection and vesicle trapping with optical tweezers, we probe the spatiotemporal properties of this unusual actin mesh. Oil droplets become centred with velocities comparable to nuclear ones and their behaviour phenocopies the nuclear envelope in terms of actin filament recruitment. At high temporal resolution, inert objects (particles or oil droplets) above 1.5 μm experience a centring mechanism and are biased in their diffusion. Their size has no influence over longer time scales, arguing that friction counteracts propulsion of large objects. A similar mechanism, able to non-specifically centre organelles, co-exists in meiosis I with a specific one, which promotes spindle off centring. In this article, we reconcile how the same molecular actors can have two opposite functions (centring versus off-centring of objects).

Introduction

The position of the nucleus in a cell can instruct morphogenesis in some cases, conveying spatial and temporal information. Abnormal nuclear positioning can lead to disease (Gundersen and Worman 2013). In mammals, the oocyte nucleus is centred via actin-based mechanisms (Almonacid et al. 2015). Importantly an off-centre of the nucleus correlates with poor outcomes for mouse and human oocyte development (Brunet and Maro 2007; Levi et al. 2013). This is surprising since oocytes further undergo two extremely asymmetric divisions in terms of the size of the daughter cells (enabling polar body extrusion), requiring an off-centring of their chromosomes (Azoury et al. 2008; Dumont et al. 2007; Verlhac, Lefebvre, Guillaud, et al. 2000).

Thanks to a multidisciplinary approach, we recently discovered how the nucleus robustly localizes in a unique manner at the centre of mouse oocytes (Almonacid et al. 2015). We observed that oocytes derived from Formin 2 (*Fmn2*) knockout mice, which lack microfilaments in their cytoplasm, present off-centred nuclei (Azoury et al. 2011; Dumont et al. 2007). Formin 2 is a straight microfilament nucleator and also an essential maternal gene (Leader et al. 2002). The re-introduction of Formin 2 into *Fmn2*^{-/-} oocytes, that harbour initially off-centred nuclei, induces a directional motion of the nucleus toward the centre in about 5 hours in 100 % of the cases (Almonacid et al. 2015). We proposed the existence of a pressure gradient, exerted by the actin mesh, that acts on the nucleus to move it from the periphery to the centre (Almonacid et al. 2015). Nevertheless, first the existence of a pressure gradient has never been formally demonstrated, second its specificity and mode of action were never addressed. This is precisely what we have addressed in this manuscript. Using micro-injection of oil droplets as well as fluorescently-coated latex beads of various sizes, we probe the spatiotemporal properties of this unusual actin mesh. We show here, that oil droplets become centred with velocities comparable to nuclear ones and their behaviour phenocopies the nuclear envelope in terms of actin filament recruitment. This argues that the gradient acts non-specifically and is able to centre other objects than the oocyte nucleus. At high temporal resolution, we show that objects above 1.5 μm in diameter experience a biased movement toward the centre of the oocyte. These observations are coherent with the existence of a gradient of pressure. Importantly the size of oil droplets has no influence over longer time scales.

In addition, it has remained an unresolved question in the field how the same molecules, namely Formin 2, Spire 1-2 and Myosin Vb are able to promote two opposite motions: centring of

chromosomes enclosed inside a nucleus in Prophase I (Almonacid et al. 2015) and off-centring of chromosomes enclosed inside a meiotic spindle later in meiosis I (Azoury et al. 2008; Chaigne et al. 2013; Holubcová, Howard, and Schuh 2013; Pfender et al. 2011; Schuh 2011; Schuh and Ellenberg 2008). We offer here an explanation to this long-standing question. Indeed, oil droplet injected in meiosis I are also being centred, albeit with a slightly reduced efficiency, that cannot be due to a change in cytoplasmic viscosity. Optical measurements show no difference between prophase and meiosis I in terms of elastic and viscous moduli. We discuss here the origin of this difference in centration of oil droplets. Nevertheless, we demonstrate that a similar mechanism, able to non-specifically centre organelles, co-exists in meiosis I with a specific one, dependent on myosin II promoting spindle off centring. We reconcile here how the same molecular actors can have two opposite functions (centring versus off-centring of objects).

Results

The centring mechanism is not specific to the biological nature of the nucleus

We used oil droplets as passive objects to test whether the centring mechanism is specific or not to the nucleus. For that, we injected oil droplets in prophase I and observed them on short time scale (minute). The injected droplets maintain a round shape indicating that the forces generated in the cytoplasm are not large enough to deform them. These droplets present a 1.9 g cm^3 density and could be injected only with maximal pressure (7000 hPa) of the microinjector (see Methods). We recorded movies with one image every 500 ms and saw that the oil droplet was moving in the cytoplasm (Figure 1a, Movie 1). Interestingly, when the oocyte is treated with cytochalasin D, the droplet does not move anymore (Movie 2). To further quantify the movement, we tracked the oil droplets (Methods) and computed the Mean Squared Displacement (hereafter called MSD) from the obtained trajectories. From the MSD, we can see that in presence of F-actin, the droplets present an active diffusion motion (Figure 1b) with a diffusion coefficient of $0.072 \text{ } \mu\text{m}^2 \text{ min}^{-1}$ and a slope of 1 (Figure S1). On the contrary, in oocytes treated with cytochalasin D, the droplets are almost immobile. This confirms the presence of active diffusion due to the F-actin cytoplasmic mesh, as observed in Almonacid et al. We then checked whether the droplets display a biased movement toward the oocyte centre (where the nucleus is positioned), during the time of observation. For that, we computed the angle between the trajectory and the oocyte centre for each time point Δt (Figure 1c). For $1 \Delta t$ (500 ms) we did not see a biased movement toward the centre neither in oocytes with an F-actin mesh nor in those treated with cytochalasin D (Figure S2). On the contrary, when observing the angles between the trajectory and the oocyte centre for longer time scales, $50 \Delta t$ (25 seconds), we observed that the droplets presented a biased movement toward the centre of the cell in the presence of F-actin (Figure 1c). On the contrary, in oocytes treated with cytochalasin D, the angles of the trajectories were almost randomly distributed, indicating a non-biased motion inside the cell (Figure 1c). In conclusion, the oil droplet is transported by the F-actin meshwork at short time scales and this transport is biased toward the centre of the cell.

We then observed oil droplets injected in oocytes at longer time scales (15 hours). We saw that the oil droplet is being centred (Figure 1d, Movie 3). Once it is at the oocyte centre, it stays there and fluctuates around this position (most probably due to a competition between the nucleus and the oil droplet for the central position inside the cell) (Figure S3). The oil droplet injection allows to

have a wide range of sizes. In our case, we managed to produce droplets with diameters comprised between 5 and 30 μm (Figure S4), a size that mimics well the size of the oocyte nucleus (25 μm). When observing the trajectories of these droplets, we could see that almost all of them are centred (Figure 1e). We computed that 76% of the droplets were centred during the 15 hours-long observation (Figure 1f, Methods). This is similar to the rate of nucleus centring in *Fmn2*^{-/-} oocytes reinjected with formin 2; indeed, 74% of the oocytes reached the centre during the observation time (Almonacid et al. 2015). Even if all droplets don't end-up in the centre, they all presented a biased movement toward the central area of the oocyte, as observed for nucleus centring (Almonacid et al. 2015). Our results demonstrate the non-specific nature of the F-actin dependent centring mechanism in the mouse oocytes in Prophase I.

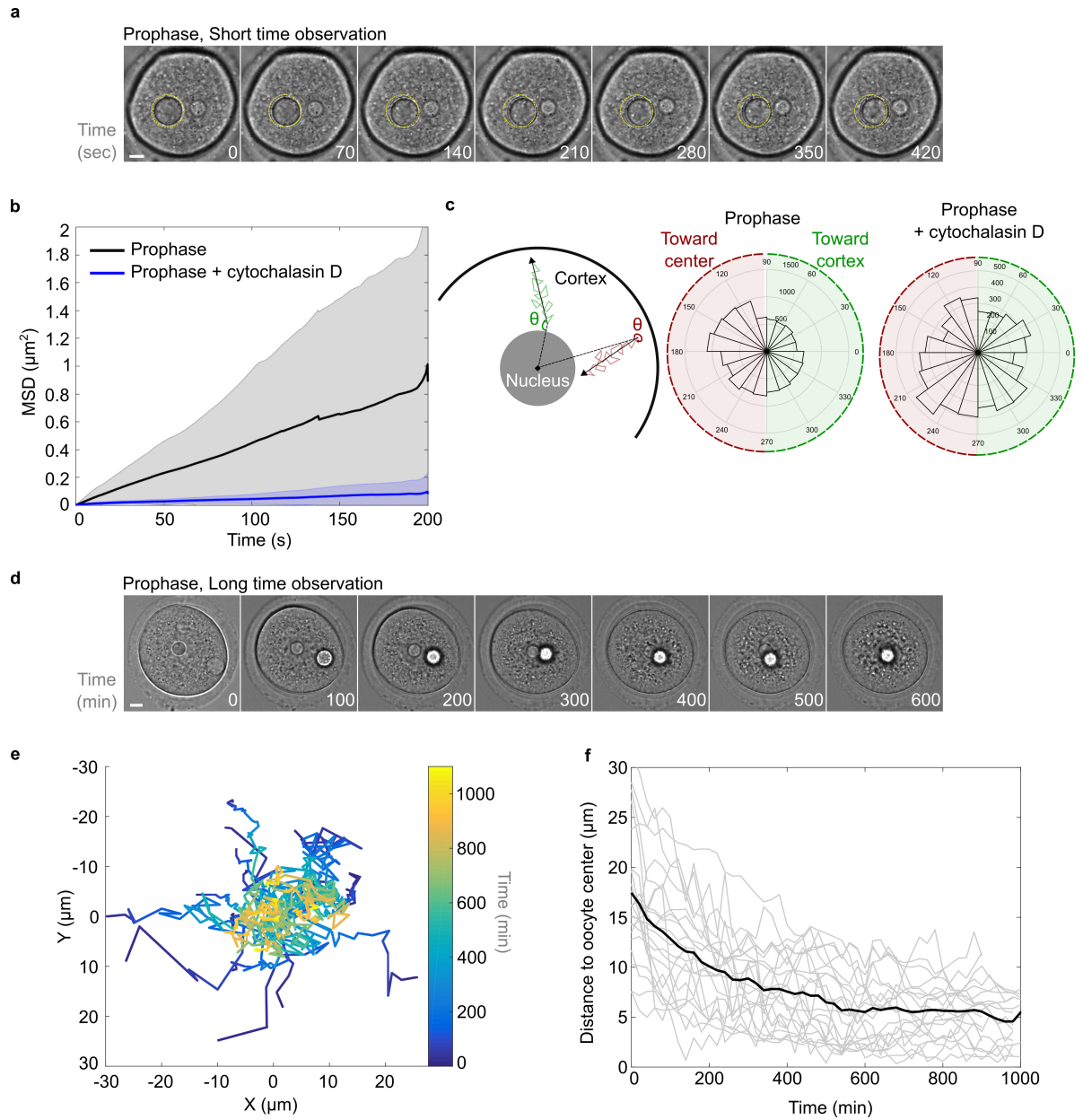


Figure 1. Oil droplets get centred in oocytes maintained in Prophase

(a) Oil droplet moving in an oocyte (observation at short time scale). The images are corresponding to Movie 1. One frame is shown every 70 seconds. Scale bar is $10\ \mu\text{m}$. **(b)** Quantification of the Mean Square Displacement (MSD) as a function of time for the droplets observed at short time scale. Mean and standard deviation are represented. **(c)** Left: angle evaluation and interpretation. Right: distribution of angles at $50\ \Delta t$ for oil droplets observed at short time scale in presence or absence of F-actin. **(d)** Oil droplet getting centred in an oocyte. The images are corresponding to Movie 3. One frame is shown every 100 minutes. Scale bar is $10\ \mu\text{m}$. **(e)** Trajectories of droplets that get centred during the observation. Time is encoded in colour. The

coordinates of the droplets are given in the oocyte referential where (0,0) is the centre of the oocyte. **(f)** Grey: distance to oocyte centre as a function of time for all the droplets that are getting centred during the observation. Black line: the mean over all the trajectories is represented.

The oil droplet recapitulates the nucleus movement

When oil droplets were injected in presence of an F-actin probe (GFP-UtrCH, (Burkel, Von Dassow, and Bement 2007)), we observed bright actin filaments around the droplet and around the nucleus. The meshwork around the droplet was as dense as the meshwork around the nucleus, dependent on the level of expression of the F-actin probe (Figure 2a). We then compared the instantaneous velocities of droplets having a diameter between 20 and 30 μm (black dots and black error bars on Figure 2b) to the instantaneous velocities computed for nucleus velocity in Formin 2 knockout (*Fmn2*^{-/-}) oocytes re-expressing Formin 2 (Almonacid et al. 2015). We observed that the instantaneous velocities are slightly higher for oil droplets (Figure 2b). In both cases we observed a decrease of velocity at the centre, probably due to a balance of forces at the cell centre. The instantaneous velocities for droplets have a larger variability than the one measured for the nucleus. This can be explained as follows: first, in the case of the nucleus, the cRNA encoding Formin 2 was injected into *Fmn2*^{-/-} oocytes and thus in a context of F-actin mesh progressive reformation, while we are injecting the oil droplets at steady state in a control oocytes already presenting an actin mesh. Second, the droplet is void of a nuclear matrix and chromatin inside, it is a more coherent and more rigid object than the nucleus (cannot be easily deformed) and thus propelled more efficiently than the later. Nevertheless our results tend to suggest that oil droplets are good objects mimicking the nucleus and allowing us to probe the spatio-temporal properties of the F-actin mesh in mouse oocytes.

We then wanted to test the impact of the size of objects on their centring efficiency. We studied objects with different ranges of sizes. First we used the oil droplets to have large objects (between 5 and 40 μm in diameter). Second we used fluorescent particles; when injected at a high concentration (Methods), they aggregate in the cytoplasm of the oocyte (Figure 2c). We took advantage of this aggregation because it produces objects with sizes between 100 nm to 2 μm (measured with the fluorescence intensity of the detected spot; see Methods). For each trajectory, we computed the MSD at 25 seconds (50 Δt). Interestingly, for large objects like oil droplets, the

MSD inversely scales with the object diameter (Figure 2c). For the small objects (aggregates of particles), the MSD does not depend on the object diameter. We then looked at the directionality of the objects to see if we can observe a bias toward the centre of the cell. We computed the angle distribution of the trajectory with the centre of the oocyte at $50 \Delta t$ (Figure 2d). For small objects (below $1.5 \mu\text{m}$) there is no biased movement toward the centre. On the contrary, for objects larger than $1.5 \mu\text{m}$, we can observe a bias toward the centre of the oocyte at $50 \Delta t$. These results argue that there is a cut-off size of $1.5 \mu\text{m}$ for the centring mechanism at short time scale.

The MSD at 25 seconds suggest that objects larger than $5 \mu\text{m}$ in diameter are more restricted in their motion than smaller objects. This could be either due to size dependence of the friction in a viscous regime and/or to the capacity of large objects to sense more rapidly the boundaries of the actin mesh. The fact that objects larger than $1.5 \mu\text{m}$ are biased in their motion towards the centre strongly demonstrates the existence of a non-specific centring mechanism that is being sensed by relatively large organelles, but totally not seen by objects smaller than $1.5 \mu\text{m}$ (on the time scales at which we are watching: at prophase + 18 hours, a lot of objects seem to have accumulate at the centre of the oocyte (Almonacid et al. 2015)).

Interestingly, for oil droplets (objects larger than $5 \mu\text{m}$ in diameter) at long time scale, the centring velocity does not depend on their diameter anymore (Figure S5, Discussion).

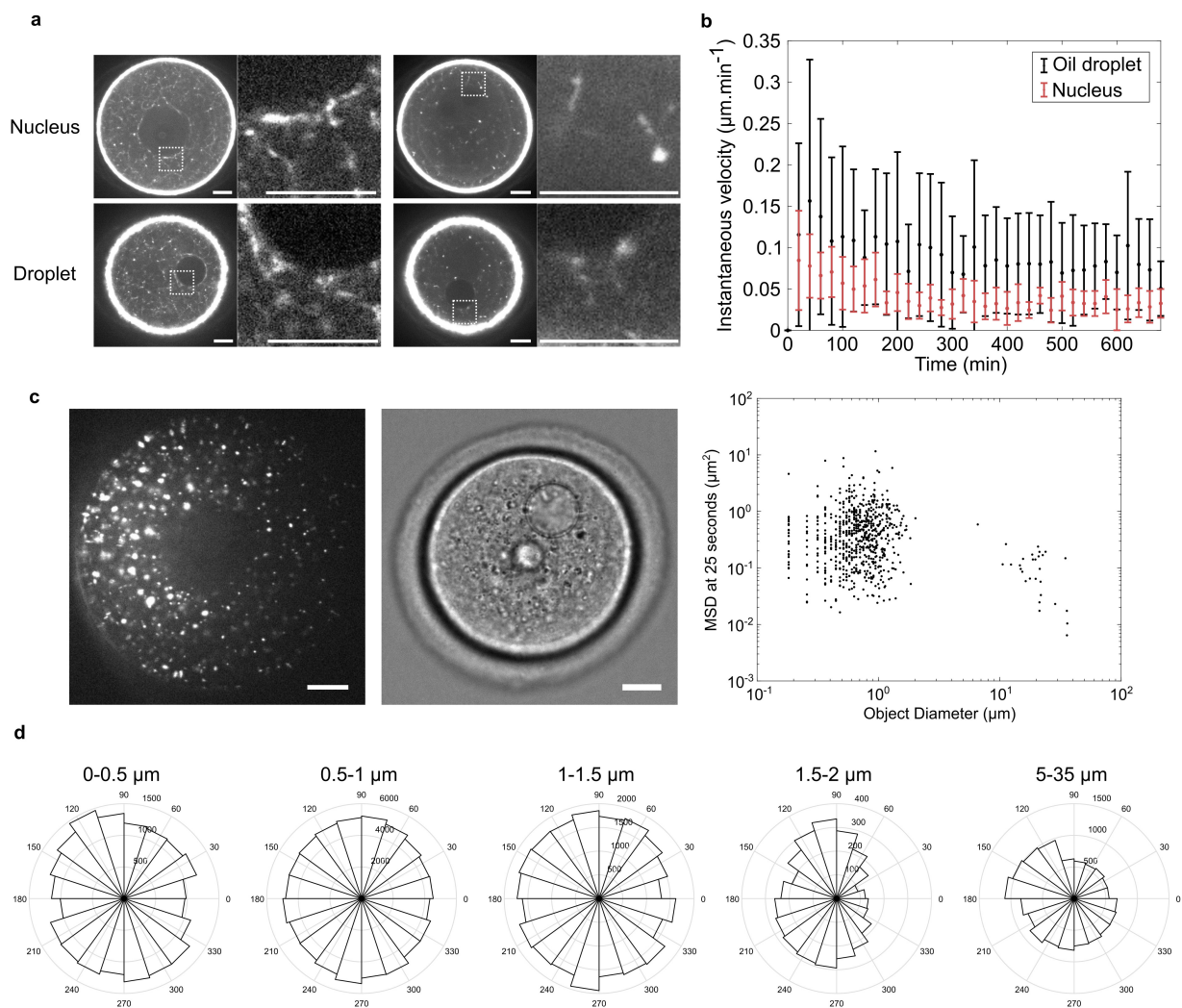


Figure 2. Oil droplets recapitulate nucleus behaviour

(a) Visualization of F-actin around droplets and nucleus. F-actin is labelled with GFP-UtrCH that is either highly-expressed (left) or low-expressed (right). The square dashed zone is zoomed on the right. Scale bars are $10\ \mu\text{m}$. **(b)** (Black) Instantaneous velocity as a function of time for droplets having a diameter comprised between 20 and $30\ \mu\text{m}$. (Red) Instantaneous velocity for nuclei getting centred in $Fmn2^{-/-}$ oocytes rescued with Fmn2. Mean and standard deviation are represented. **(c)** Left: Images of fluorescence particles aggregated in oocyte and corresponding to objects with a diameter between $100\ \text{nm}$ and $2\ \mu\text{m}$. Example of oil droplet injected in an oocyte. Oil droplets correspond to objects between 5 and $35\ \mu\text{m}$ in diameter. Right: Representation of the MSD at 25 seconds ($50\ \Delta t$) for each object's trajectory as a function of its diameter. **(d)** Distribution of angles at $50\ \Delta t$ for objects with various diameters. The first four categories correspond to aggregates of particles. The last category corresponds to oil droplets. When angles are comprised between 90 and 270° , the movement is directed toward the cell centre.

Oil droplets are centred in oocytes that undergo meiosis I

As introduced previously, a question unresolved in the field is how the same molecules (Formin 2, Spire 1-2 and myosin Vb) promote two opposite motions: centring of chromosomes in prophase I (Almonacid et al. 2015) and off-centring of chromosomes later in meiosis I (Azoury et al. 2008; Chaigne et al. 2013; Holubcová, Howard, and Schuh 2013; Pfender et al. 2011; Schuh 2011; Schuh and Ellenberg 2008). We thus decided to address whether the centring mechanism was maintained during meiosis I. For that, we injected oil droplets in oocytes undergoing meiosis I. First we saw that the oocytes succeed in first polar body extrusion (PBE), arguing that the oil droplet is not toxic for the development of the oocyte (Figure 3a). It also showed that the oil droplet could co-exist in the cytoplasm with the mechanism that promotes off-centring of the first meiotic spindle, a prerequisite for the first asymmetric division, i.e. first polar body extrusion (Verlhac, Lefebvre, Guillaud, et al. 2000). Second, we observed that the oil droplet is being centred during the process of meiosis I (Figure 3a, Movie 4). Interestingly, 92% (11 out of 12 droplets) of the droplets were centred before the extrusion of the first polar body (Figure 3b, 3c). When the actin network is dismantled (cytochalasin D was added to culture medium) no movement of the droplets was observed, suggesting that the centring is a consequence of the presence of actin (Figure 3d, 3e, 3f, Movie 5). This phenomenon is interesting because it means that during meiosis I, when the spindle is migrating towards the cortex, a centring mechanism is still present. Interestingly, the same molecular actors are in action as Myosin Vb was shown to play a key role in the centring mechanism (Almonacid et al. 2015) and in the spindle migration (Holubcová, Howard, and Schuh 2013). These results show the co-existence of two mechanisms: a specific mechanism that allows the migration of the spindle to the cortex and a non-specific mechanism that allows the centring of big objects on long time scales. To have a better understanding of the process, we compared the characteristics of droplets centring in prophase I and in meiosis I.

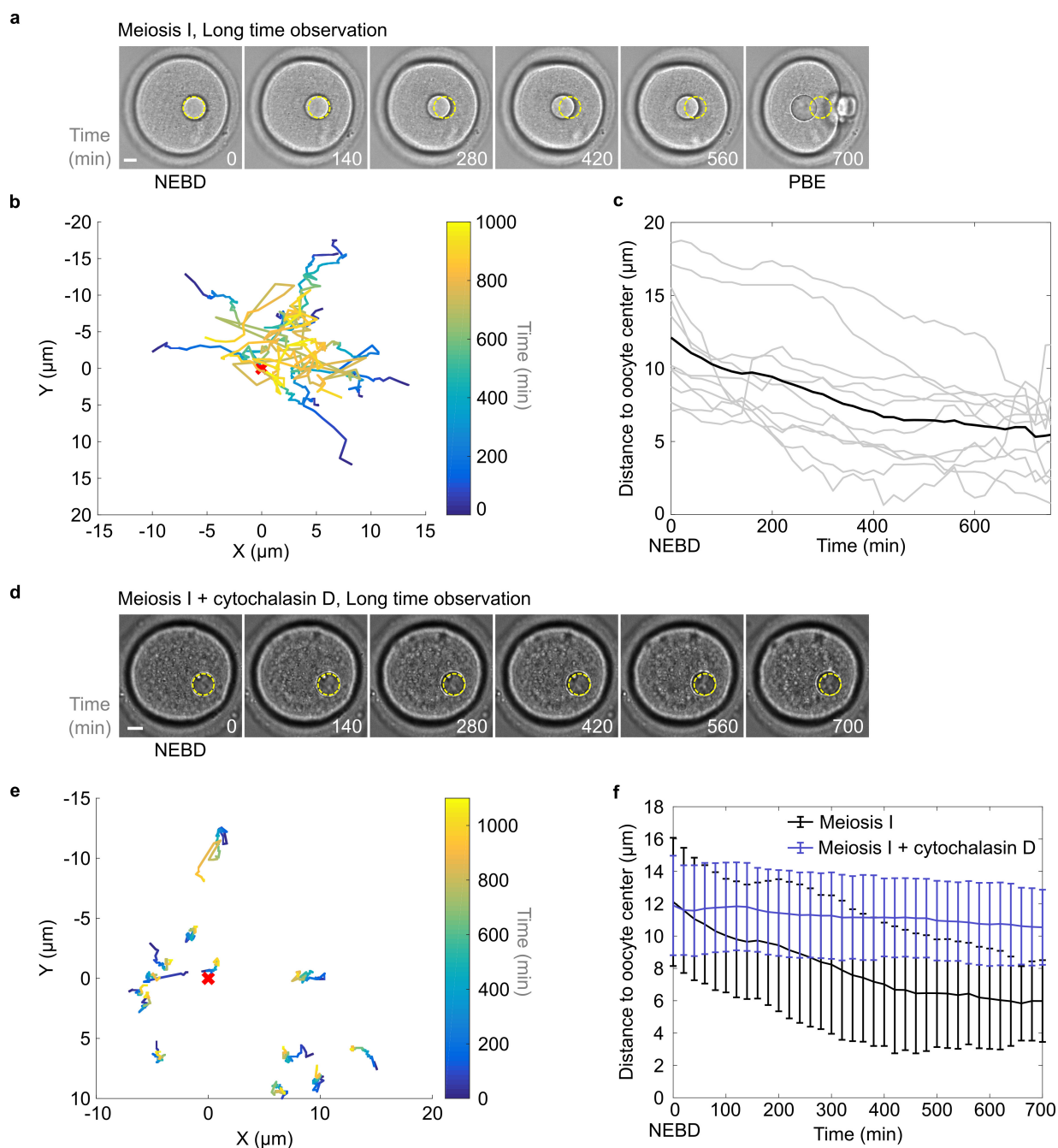


Figure 3. Oil droplets also get centred in oocytes undergoing meiosis

(a) Oil droplet getting centred in an oocyte undergoing meiosis. The images are corresponding to Movie 4. One frame is shown every 140 minutes. The first frame corresponds to NEBD (Nuclear Envelope Breakdown) and the last one to PBE (Polar Body Extrusion). Scale bar is $10\ \mu\text{m}$. **(b)** Trajectories of droplets that get centred during the observation. Time is encoded in colour. The coordinates of the droplets are given in the oocyte referential where (0,0) is the centre of the oocyte. **(c)** Grey: distance to oocyte centre as a

function of time for all the droplets that are getting centred during the observation. Black line: the mean over all the trajectories is represented. **(d)** Oil droplet in an oocyte treated with cytochalasin D. The images are corresponding to Movie 5. One frame is shown every 140 minutes. The first frame corresponds to NEBD. Scale bar is 10 μm . **(e)** Trajectories of droplets that are not centred at the beginning of the observation for oocytes treated with cytochalasin D. Time is encoded in colour. The coordinates of the droplets are given in the oocyte referential where (0,0) is the centre of the oocyte. **(f)** Average of distance to oocyte centre as a function of time for all the droplets that are not centred at the beginning of the experiment. Mean and standard deviation are represented.

Comparison of droplets centring in prophase I versus meiosis I

We first compared the distance to oocyte centre as a function of time for oocytes in prophase I or in meiosis I. For oil droplets injected in oocytes undergoing meiosis I, we can see that the distance to the oocyte centre is decreasing more slowly than for oocytes maintained in prophase I (Figure 4a). To have a good characterization of the centring, we computed a mean centring velocity (Methods; Figure 4b). We saw that the mean centring velocity was 3 times smaller in meiosis I than in prophase I ($0.060 \mu\text{m min}^{-1}$ in prophase I compared to $0.020 \mu\text{m min}^{-1}$ in meiosis I). The higher dispersion of data in prophase I can be explained by the larger diameter range of droplets injected in prophase I than in meiosis I (Figure S5). Interestingly, the instantaneous velocities also show the same behaviour. When looking at instantaneous velocities as a function of time, we observe that in meiosis I, the instantaneous velocities of droplets are slower than in prophase I (Figure 4c). Therefore, even if droplets were centred in both cases, the characteristics of centring are not exactly similar. In prophase I, the centring is more noisy but also faster. In meiosis I, the centring is slower but more directed.

We next checked if we were able to link those data with the physical state of the cytoplasm. We first performed optical tweezers experiments to have access to the mechanical properties of the oocyte cytoplasm in prophase I and meiosis I (Figure S6). We saw that there was no significant difference in the elastic modulus between prophase I and meiosis I oocytes. For the viscous modulus, there is a slight difference between prophase I and meiosis I oocytes, but not large enough to explain the differences of centring velocities with a difference in viscosity between prophase I and meiosis I. From these data, we can extract a viscosity of 1 Pa.s for the cytoplasm of the oocytes

maintained in prophase I, similar to what was previously found with magnetic tweezers measurements (Hosu et al. 2008).

Then, to have access to the cytoplasmic activity of the oocyte cytoplasm, we performed particle tracking in the oocytes. We used two different systems: fluorescent nanoparticles and labelled vesicles of the oocytes (Nile Red, see methods). First, we followed the movement of fluorescent particles in oocytes maintained in prophase and treated or not with cytochalasin D. We injected fluorescent beads of 100 nm in diameter, coated with a PEG on the surface to decrease the non-specific interactions with the surrounding environment. First, we can see that the particles are less mobile in absence of F-actin (Movie 6). To follow the movement of the objects, we used an automated tracking that we performed with the software IcY (Methods). We computed the MSD and found that in presence of F-actin, the beads have a confined movement with a diffusion coefficient of $0.36 \mu\text{m}^2 \cdot \text{min}^{-1}$ whereas in absence of F-actin, the particles are immobile (Figure S7). This shows that F-actin is responsible for cytoplasmic activity in prophase.

To understand the differences of behaviours we see between the prophase and meiosis I states, we followed the movement of total vesicles labelled with fluorescent dye (Movie 7, Figure 4d). We computed different values that we compared between the different states. We first computed MSD and extracted diffusion coefficients for the total vesicles (Figure 4b, Figure S8c). In prophase, the vesicles have a diffusion coefficient of $0.23 \mu\text{m}^2 \cdot \text{min}^{-1}$ whereas in meiosis I, they have a diffusion coefficient of $0.12 \mu\text{m}^2 \cdot \text{min}^{-1}$ at NEBD+1h (actin meshwork dismantled) and $0.09 \mu\text{m}^2 \cdot \text{min}^{-1}$ at NEBD +7h (actin meshwork reassembled). During meiosis, we observe less cytoplasmic activity; thus those results are coherent with the slower centring mechanism in meiosis I. There is less cytoplasmic activity so the centring is slower.

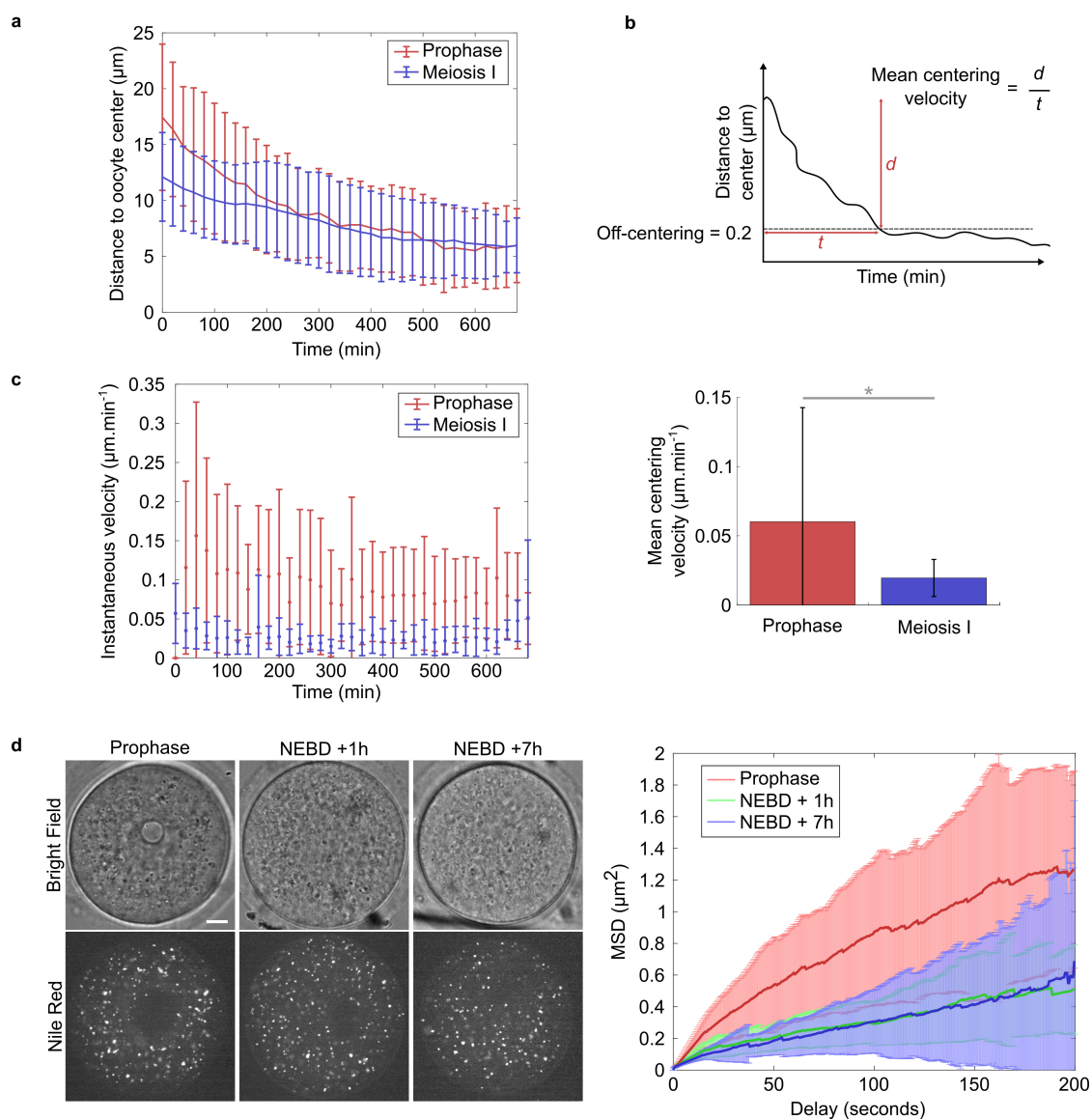


Figure 4. Comparison of droplets centring in Prophase and Meiosis I

(a) Average of distance to oocyte centre as a function of time for droplets that get centred (i.e. that achieve off centring below 0.2 during the observation) in Prophase and Meiosis I. Mean and standard deviation are represented. **(b)** Top: computation of the mean centring velocity that is defined as the time necessary for the droplet to have an off-centring of 0.2. Bottom: Average of mean centring velocity for droplets getting centred during the observation in Prophase and Meiosis I. **(c)** Comparison of instantaneous velocities for droplets getting centred in Prophase and Meiosis I. Mean and standard deviation are represented. **(d)** Left: labelling of total vesicles in oocytes with Nile Red in Prophase and Meiosis I early (NEBD 1h) or late (NEBD 7h). Scale bar is 10 μm . Right: calculation of MSD for the various conditions. Mean and standard deviation are represented.

Discussion

By using oil droplets that mimic the nucleus (size and shape), we showed that the centring mechanism is non-specific to the biological nature of the nucleus. In prophase I, oil droplet and nucleus centring have the same characteristics (time, velocity *etc.*). We also showed that the centring mechanism is still present in meiosis I, with slower kinetics than in prophase I.

We showed the influence of the object size on the centring mechanism. Indeed, large objects (above 1.5 μm) show a biased movement toward the oocyte centre at short time scale (25 seconds). Interestingly this cut-off is on the same order of magnitude than the estimated meshwork size for oocytes maintained in prophase (Azoury et al. 2011; Schuh and Ellenberg 2008). At short time scale, large objects show a displacement more restricted compared the small objects, probably due to a friction effect. At long time scale, for oil droplets (objects between 5 and 35 μm in diameter), the centring velocity does not depend on the oil droplet size (Figure S5). This can be counterintuitive with the proposed pressure-based model (Almonacid et al. 2015) that predicts a velocity that scales with the squared radius, meaning that large objects should move faster than small objects. However, the range of sizes probed at long time scale might not be sufficient. Therefore, having a track of smaller objects (particles aggregates of few μm) at long time scale might help to have a scaling velocity with the size.

The slower droplet centring in meiosis I could be explained by the fact that at this state, the oocyte needs to share the actin resources for two processes: a non-specific centring mechanism and a specific off-centring of the meiotic spindle. Sharing of resources for actin networks has been widely studied in fission yeast (Burke et al. 2014; Michelot and Drubin 2011). It is also interesting to think about the centring mechanism during meiosis I as a mechanism that counteract the spindle migration. Indeed, if the spindle migration was dragging all the maternal stores in the polar body, then the asymmetric division would not make sense anymore. We can think of the centring mechanism in meiosis I as a mechanism to keep the organelles and the granules in the centre of the oocyte.

In conclusion, we demonstrated that the centring mechanism was non-specific in prophase I and still existing in meiosis I. This non-specify of centring can be explained by the fact that in meiosis I, during spindle migration, the oocyte needs to keep the maximum of maternal stores in the cell that will undergo the following divisions.

Methods

Oocyte collection, culture and microinjection

Oocytes were collected from 11 week-old OF1 mice as previously described (Verlhac, Lefebvre, Guillaud, et al. 2000) and maintained in Prophase I arrest in M2+BSA medium supplemented with 1 μ M Milrinone (Reis et al. 2006). All live cultures and imaging were carried out under oil at 37°C. We used the following pspe3-GFP-UtrCH (Azoury et al. 2008) construct to produce cRNA. *In vitro* synthesis of capped cRNAs was performed as previously described (Verlhac, Lefebvre, Guillaud, et al. 2000). cRNAs were centrifuged at 4°C during 45 minutes at 13000 rpm before microinjection. The cRNA encoding GFP-UtrCH were injected first and then oocytes were injected with oil droplets. We injected Fluorinert FC-70 (Sigma, Ref. F9880) with a density of 1.9 g cm³ at the maximal pressure of the microinjector (Clean mode at 7000 hPa). The size of the oil droplets was visually adjusted by manual control of the time of the microinjection pulse. Microinjection were performed using an Eppendorf Femtojet microinjector at 37°C as in (Verlhac, Lefebvre, Kubiak, et al. 2000).

Drug treatments

Cytochalasin D (Life Technologies, Ref. PHZ1063) was diluted at 10 mg ml⁻¹ in DMSO and stored at -20°C. It was used on oocytes at 1 μ g ml⁻¹. Nile Red stain (Sigma, Ref. N3013) was used to label the total pool of vesicles. It was diluted at 5 mg ml⁻¹ in DMSO and stored at room temperature. It was used on oocytes at 10 μ g ml⁻¹. Latex fluorescent beads (0.1 μ m; Life Technologies, F8803) were injected in two different ways: for the injection at high concentration (to have aggregates formation), the beads were rinsed several time in nuclease-free water before use to remove traces of sodium azide and diluted 10 times before injection. For the probing of the cytoplasm physical properties, we coated the particles with PEG to reduce the non-specific interactions with the cytoplasm proteins. The 100 nm-particles were coated with 10 000 PLL-PEG (PLL(20)-g[3.5]-PEG(2), Susos) per particle; the coating was verified with zeta-potential measurement. The particles were diluted 500 times before injection.

Live imaging

Spinning disk images were acquired at 37°C in M2 + BSA +1 μ M Milrinone using a Plan-APO 40x/1.25 NA objective on a Leica DMI6000B microscope enclosed in a thermostatic chamber (Life Imaging Service) equipped with a CoolSnap HQ2/CCD-camera (Princeton Instruments) coupled to a Sutter filter wheel (Roper Scientific) and a Yokogawa CSU-X1-M1 spinning disk. For imaging oil droplets, we either acquired using the stream mode of the camera on Metamorph (one image every 500 ms) or one image every 20 min to follow the whole motion towards the oocyte center. The actin cytoplasmic meshwork decorated with GFP-UtrCH and total vesicles stained with Nile Red were imaged every 500 ms with the stream acquisition mode of Metamorph upon excitation at 491 nm.

Optical tweezer experimental setup

The single-beam gradient force optical trap system uses a near infrared fiber laser ($\lambda= 1064$ nm, YLM-1-1064-LP, IPG, Germany) that passes through a pair of acousto-optical modulators (AA-Optoelectronics, France) to control the intensity and deflection of the trapping beam. The laser is coupled into the beam path *via* dichroic mirrors (Thor Labs) and focused into the object plane by a water immersion objective (60x, 1.2 NA, Olympus). The condenser is replaced by a long distance water immersion objective (40x, 0.9 NA, Olympus) to collect the light and imaged by a 1:4 telescope on an InGaAs quadrant photodiode (QPD) (G6849, Hamamatsu). The resulting signal is amplified by a custom built amplifier system (Oeffner Electronics, Germany) and digitized at a 500 kHz sampling rate and 16 bit using an analog input card (6353, National Instruments, Austin, TX, USA). The position of the trapped particle is measured by back focal plane interferometry (Gittes and Schmidt 1998). All control of the experimental hardware is executed using LabVIEW (National Instruments). Optical trapping of endogenous vesicles was calibrated similarly as in (Mas et al. 2013), where the high-frequency fluctuations ($f > 300$ Hz) are thermal in origin. The mechanical response was measured by applying a sinusoidal force to a vesicle and observing the subsequent displacement. The shear modulus was calculated from the mechanical response using the generalized Stokes-Einstein relation as done previously (Mizuno et al. 2007).

Image Analysis. Image analysis was performed using ImageJ, Icy and Matlab. When needed, movies were realigned with the stackreg plugin of ImageJ. For all the automated tracking the software Icy was used (de Chaumont et al. 2012). Droplet tracking in bright field at short time scale was done with the Active Contours Plugin. Fluorescent particles and total vesicles tracking was done with the Spot Detector plugin combined with the Spot Tracking and Track Manager plugins. The trajectories were exported in Excel files and analysed with Matlab software. The tracks were filtered to keep only the tracks with more than 30 points (movies of 400 frames). This threshold was determined with simulated data, to avoid the tracking of false trajectories coming from the noise of the movie. Mean square displacement analysis was done with the msdalyzer class in Matlab (Tarantino et al. 2014). For the aggregated fluorescent particles, we computed the apparent diameter based on the intensity of the detected spot.

Estimation of centring: we defined that a droplet is centred when its off-centring is below 0.2, with the off-centring being the normalized distance compared to the oocyte radius (the off-centring is equal to 1 at the cortex and to 0 at the centre of the oocyte). To compute the mean centring velocity, we first defined the centring time as the time needed by a droplet to have an off-centring below 0.2. The mean centring velocity is then the net distance travelled by the droplet during this time over this time.

Student's t-tests were performed with Matlab. For the interpretation of the p-values, NS means there is no significant difference between the two distributions. One star means p-value < 0.05, two stars means p-value < 0.01, and three stars means p-value < 0.001.

References

- Almonacid, Maria et al. 2015. "Active Diffusion Positions the Nucleus in Mouse Oocytes." *Nature Cell Biology* (August 2014).
- Azoury, Jessica et al. 2008. "Spindle Positioning in Mouse Oocytes Relies on a Dynamic Meshwork of Actin Filaments." *Current Biology* 18(19): 1514–19.
- . 2011. "Symmetry Breaking in Mouse Oocytes Requires Transient F-Actin Meshwork Destabilization." *Development (Cambridge, England)* 138(14): 2903–8.
- Brunet, Stéphane, and Bernard Maro. 2007. "Germinal Vesicle Position and Meiotic Maturation in Mouse Oocyte." *Reproduction* 133(6): 1069–72.
- Burke, Thomas A. et al. 2014. "Homeostatic Actin Cytoskeleton Networks Are Regulated by

- Assembly Factor Competition for Monomers." *Current Biology* 24(5): 579–85.
- Burkel, Brian M., George Von Dassow, and William M. Bement. 2007. "Versatile Fluorescent Probes for Actin Filaments Based on the Actin-Binding Domain of Utrophin." *Cell Motility and the Cytoskeleton* 64(August): 822–32.
- Chaigne, Agathe et al. 2013. "A Soft Cortex Is Essential for Asymmetric Spindle Positioning in Mouse Oocytes." *Nature cell biology* 15(8): 958–66.
- de Chaumont, Fabrice et al. 2012. "Icy: An Open Bioimage Informatics Platform for Extended Reproducible Research." *Nature Methods* 9(7): 690–96.
- Dumont, Julien et al. 2007. "Formin-2 Is Required for Spindle Migration and for the Late Steps of Cytokinesis in Mouse Oocytes." *Developmental biology* 301(1): 254–65.
- Gittes, F, and C F Schmidt. 1998. "Interference Model for Back-Focal-Plane Displacement Detection in Optical Tweezers." *Optics letters* 23(1): 7–9.
- Gundersen, Gregg G, and Howard J Worman. 2013. "Nuclear Positioning." *Cell* 152: 1376–89.
- Holubcová, Zuzana, Gillian Howard, and Melina Schuh. 2013. "Vesicles Modulate an Actin Network for Asymmetric Spindle Positioning." *Nature cell biology* 15(8): 937–47.
- Hosu, Basarab G, Steven F Mullen, John K Critser, and Gabor Forgacs. 2008. "Reversible Disassembly of the Actin Cytoskeleton Improves the Survival Rate and Developmental Competence of Cryopreserved Mouse Oocytes." *PloS one* 3(7): e2787.
- Leader, Benjamin et al. 2002. "Formin-2, Polyploidy, Hypofertility and Positioning of the Meiotic Spindle in Mouse Oocytes." *Nature Cell Biology* 4(12): 921–28.
- Levi, M., Y. Ghetler, A. Shulman, and R. Shalgi. 2013. "Morphological and Molecular Markers Are Correlated with Maturation-Competence of Human Oocytes." *Human Reproduction (Oxford, England)* 28(9): 2482–89.
- Mas, Josep et al. 2013. "Quantitative Determination of Optical Trapping Strength and Viscoelastic Moduli inside Living Cells." *Physical biology* 10(4): 46006.
- Michelot, Alphée, and David G. Drubin. 2011. "Building Distinct Actin Filament Networks in a Common Cytoplasm." *Current Biology* 21(14): 560–69.
- Mizuno, Daisuke, Catherine Tardin, C. F. Schmidt, and F. C. Mackintosh. 2007. "Nonequilibrium Mechanics of Active Cytoskeletal Networks." *Science (New York, N.Y.)* 315(5810): 370–73.
- Pfender, Sybille et al. 2011. "Spire-Type Actin Nucleators Cooperate with Formin-2 to Drive Asymmetric Oocyte Division." *Current Biology* 21(11): 955–60.
- Reis, Alexandra, Heng-Yu Chang, Mark Levasseur, and Keith T. Jones. 2006. "APCcdh1

- Activity in Mouse Oocytes Prevents Entry into the First Meiotic Division." *Nature Cell Biology* 8(5): 539–40.
- Schuh, Melina. 2011. "An Actin-Dependent Mechanism for Long-Range Vesicle Transport." *Nature Cell Biology* 13(12): 1431–36.
- Schuh, Melina, and Jan Ellenberg. 2008. "A New Model for Asymmetric Spindle Positioning in Mouse Oocytes." *Current biology* 18(24): 1986–92.
- Tarantino, Nadine et al. 2014. "Tnf and Il-1 Exhibit Distinct Ubiquitin Requirements for Inducing NEMO-IKK Supramolecular Structures." *Journal of Cell Biology* 204(2): 231–45.
- Verlhac, M H, C Lefebvre, P Guillaud, et al. 2000. "Asymmetric Division in Mouse Oocytes: With or without Mos." *Current biology : CB* 10(20): 1303–6.
- Verlhac, M H, C Lefebvre, J Z Kubiak, et al. 2000. "Mos Activates MAP Kinase in Mouse Oocytes through Two Opposite Pathways." *The EMBO journal* 19(22): 6065–74.

Supplementary Information

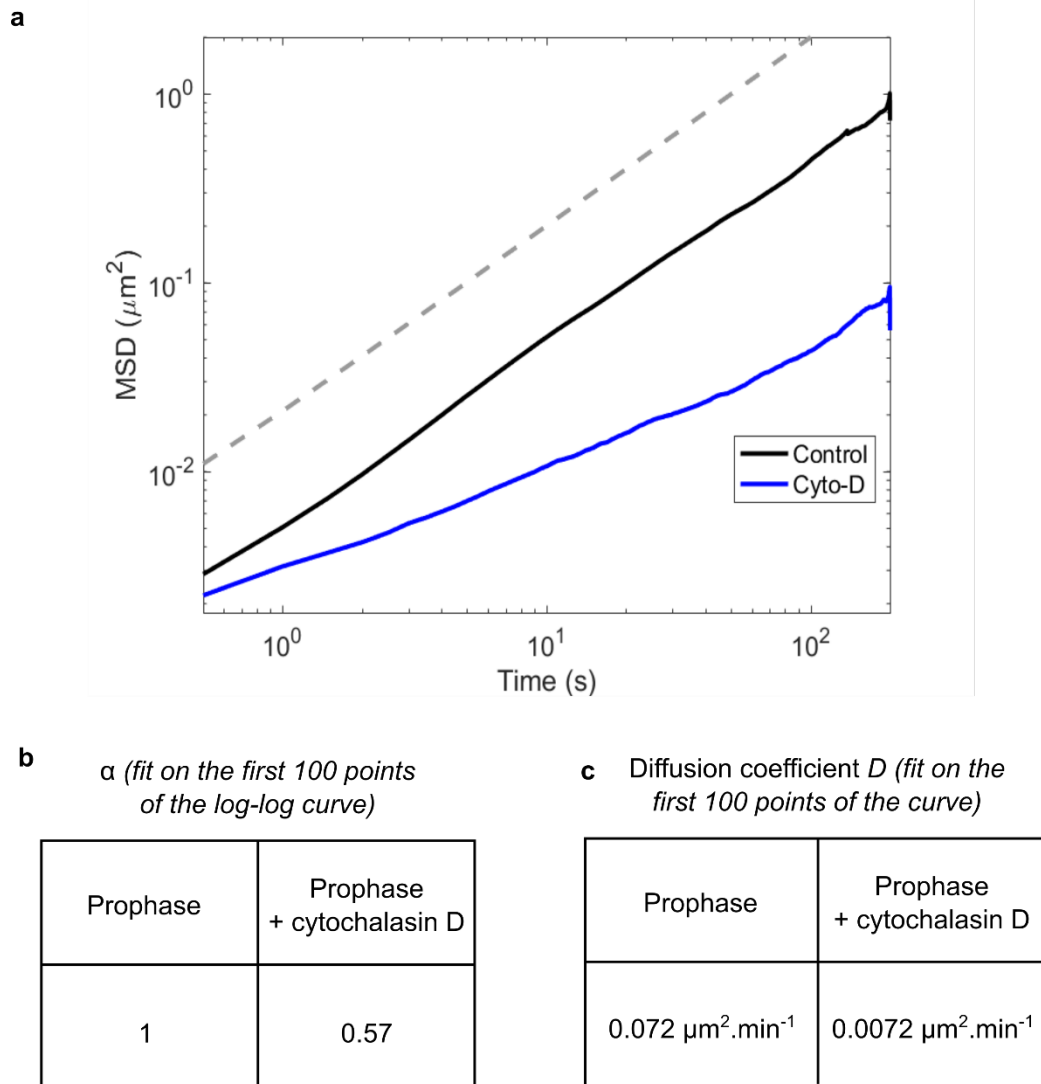


Figure S1. MSD interpretation for oil droplets observed at short time scales. (a) MSD for oil droplets observed at short time scale in a log-log scale. The dotted line represents a slope of 1. **(b)** Results from fitting of the MSD in log-log scale. α represents the slope of the curve (here fit on the first 100 points of the curve). **(c)** Results from fitting of the MSD to extract the diffusion coefficient. Indeed the expression $\text{MSD} = 4D \cdot t$ allows to extract the diffusion coefficient.

N.B: for the cytochalasin-D case, we need to carefully estimate the diffraction limit to see if we really detect a movement of the oil droplets.

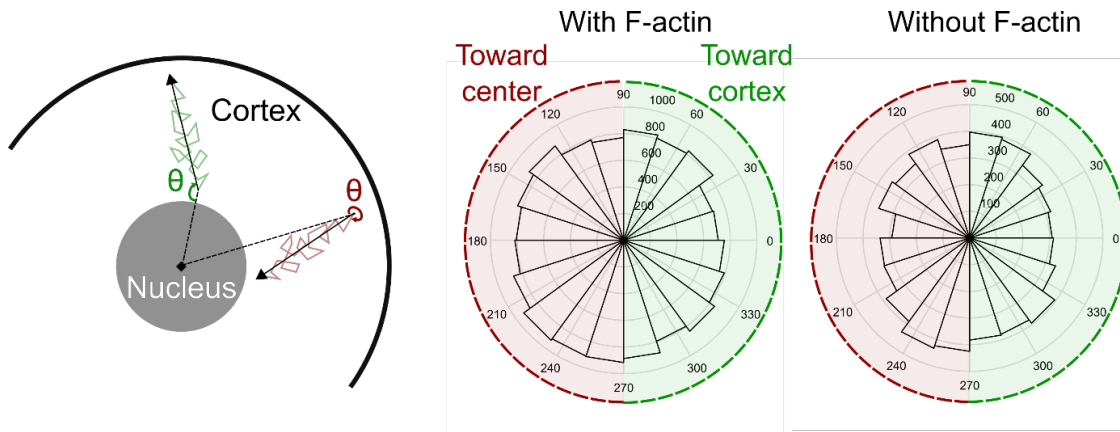


Figure S2. Angle Distribution at 1 Δt for oil droplets observed at short time scales. The distribution corresponds to the angles at 1 Δt for 29 oocytes with F-actin and 14 oocytes without F-actin.

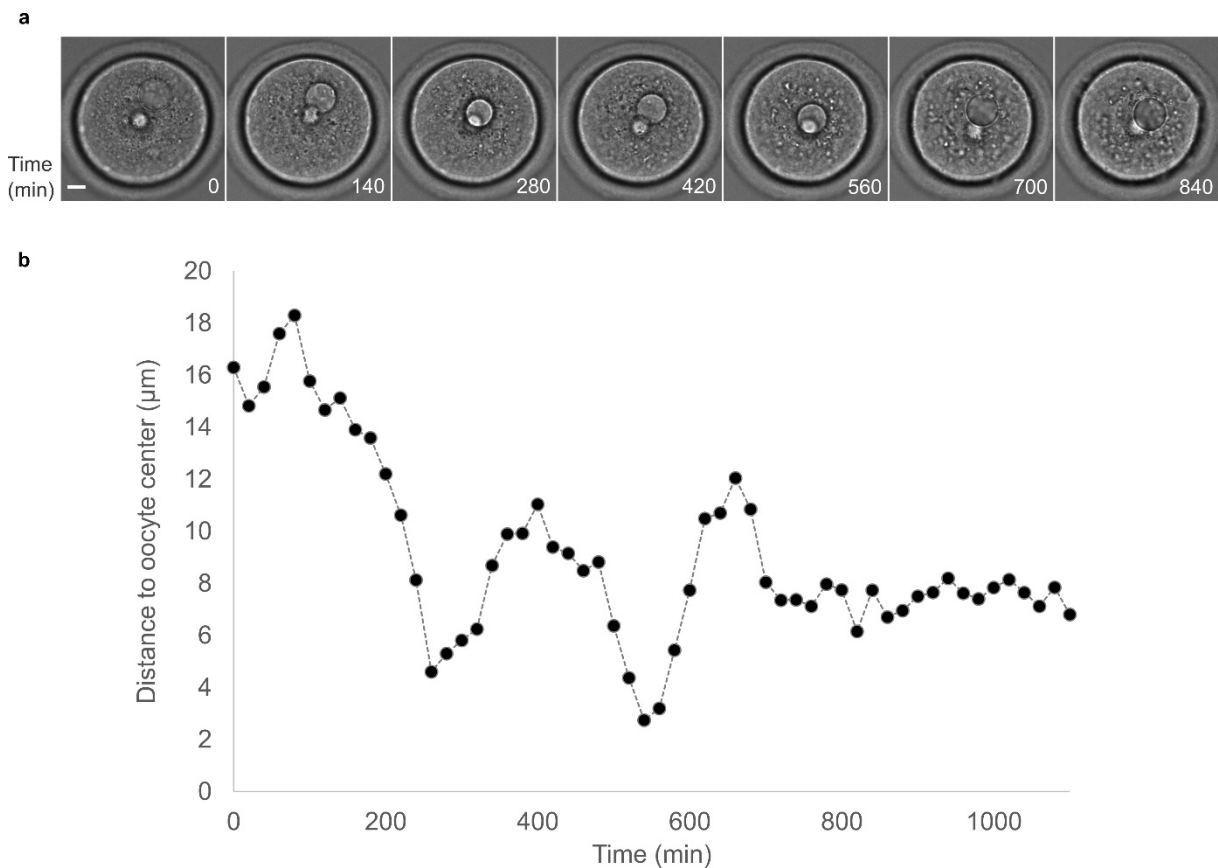


Figure S3. Example of droplet oscillation around the oocyte centre. (a) Images of a droplet getting centred in an oocyte maintained in Prophase. One image is shown every 140 minutes. Scale bar is 10 μm . (b) Distance to oocyte centre as a function of the time for the images shown in (a). Two oscillations from the centre can be seen at 200 and 600 minutes.

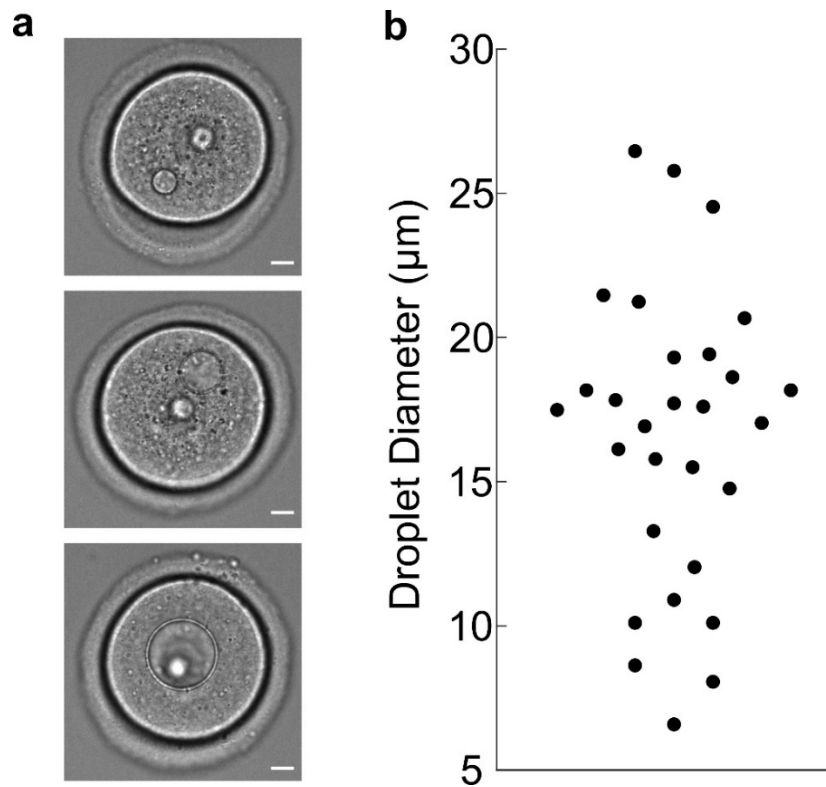


Figure S4. Oil droplets injected in mouse oocytes. (a) Examples of droplets in mouse oocytes. Scale bar is $10\ \mu\text{m}$. (b) Distribution of diameter length for all the droplets that are not centred at the beginning of the observation.

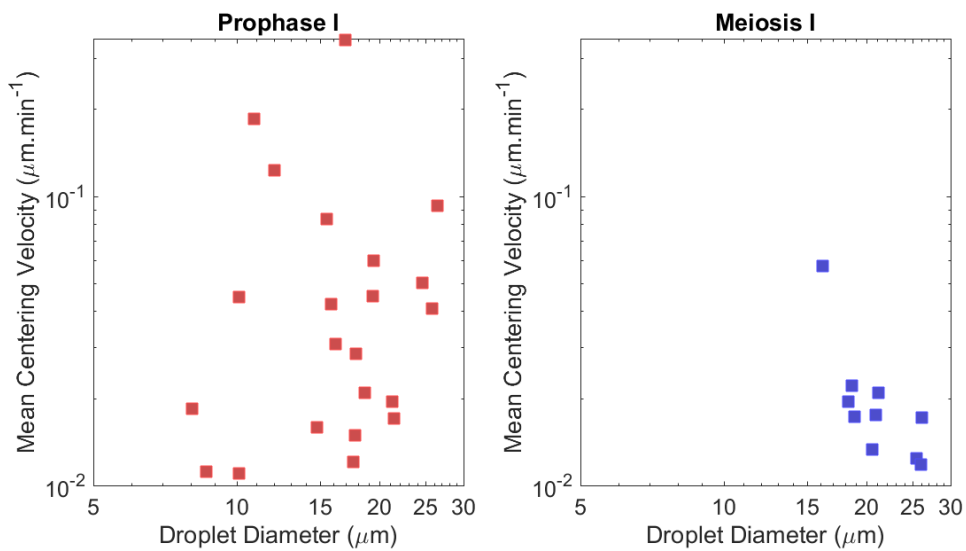


Figure S5. Mean centring velocity as a function of droplet diameter in prophase I. The mean centring velocity is computed as explained in Figure 4b.

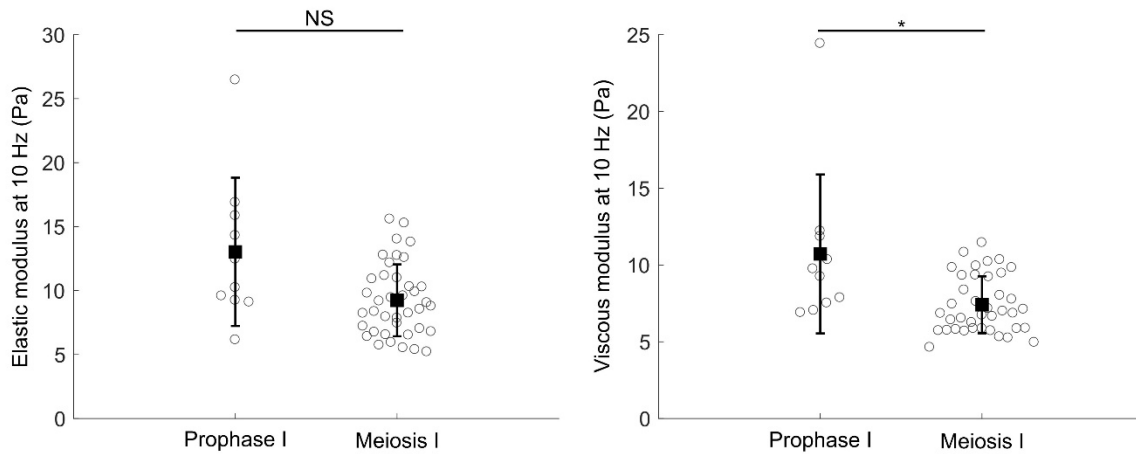


Figure S6. Optical tweezers measurements. Evaluation of elastic and viscous moduli at 10 Hz for oocytes maintained in prophase I and oocytes undergoing meiosis I. For oocytes undergoing meiosis I, the measures were taken at NEBD +6h.

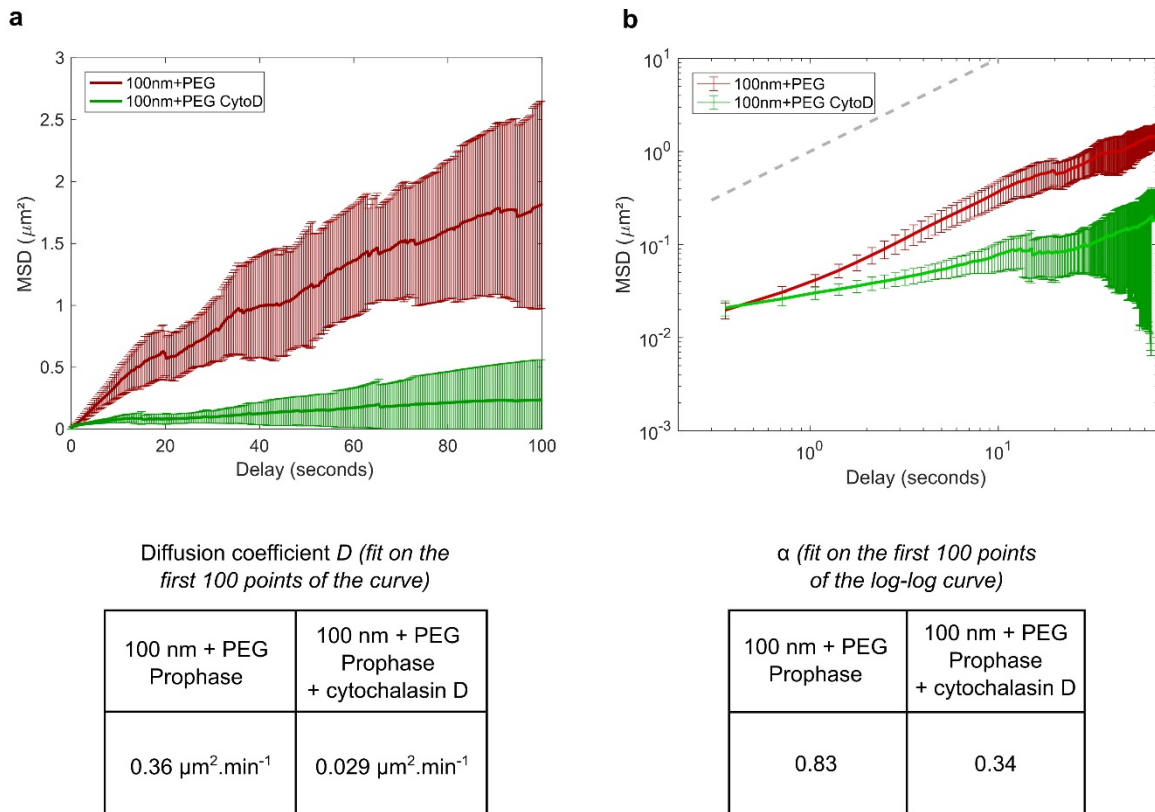
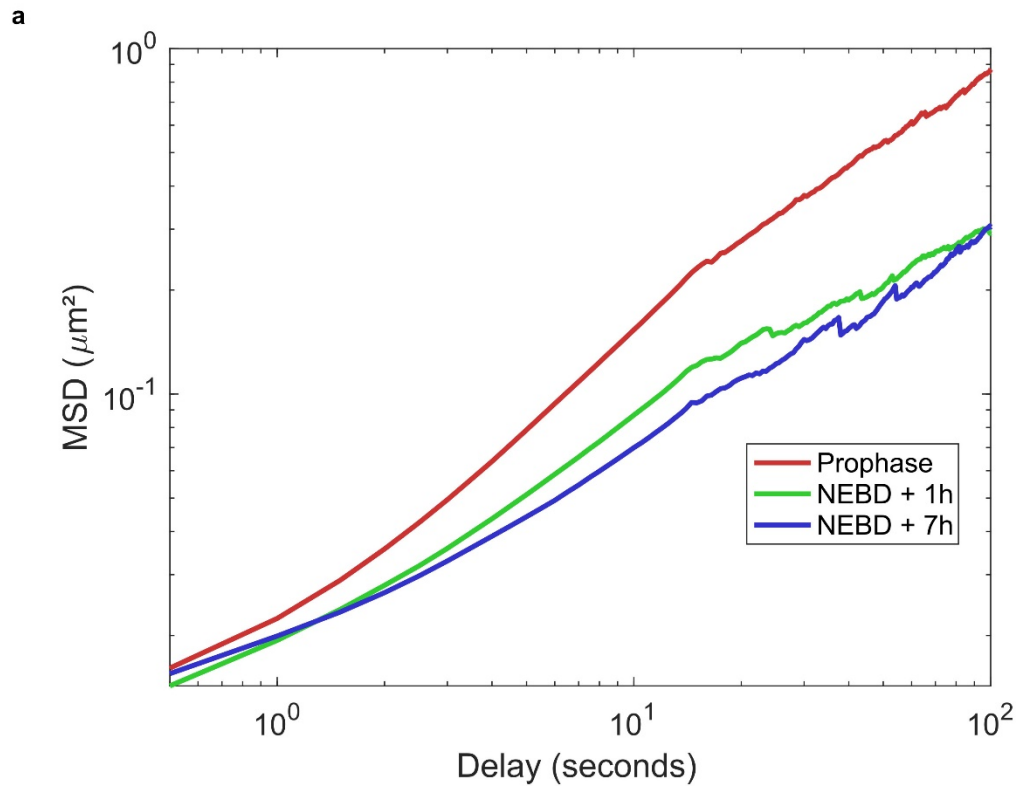


Figure S7. MSD for 100 nm beads injected in oocytes maintained in prophase. (a) Red: MSD computed for 100 nm beads injected in oocytes maintained in prophase. Green: MSD computed for 100 nm beads injected in oocytes maintained in prophase and treated with cytochalasin D. The diffusion coefficients computed from the MSD are given in the table below the curves. (b) Log-log representation of the MSD showed in (a). The α coefficients corresponding to the slope are given in the table below the curves.



b α (fit on the first 100 points of the log-log curve)

| Prophase | NEBD + 1h | NEBD + 7h |
|----------|-----------|-----------|
| 0.81 | 0.61 | 0.59 |

c Diffusion coefficient D (fit on the first 20 points of the curve)

| Prophase | NEBD + 1h | NEBD + 7h |
|---|---|---|
| 0.23 $\mu\text{m}^2.\text{min}^{-1}$ | 0.12 $\mu\text{m}^2.\text{min}^{-1}$ | 0.09 $\mu\text{m}^2.\text{min}^{-1}$ |

Figure S8. MSD for total vesicles during meiosis. (a) Log-log representation of the MSD showed in Figure 4d. The mean for of MSD for 10 oocytes in Prophase and 12 oocytes at NEBD +1h and NEBD + 7h is represented. **(b)** Results from fitting of the MSD in log-log scale. α represents the slope of the curve (here fit on the first 100 points of the curve). **(c)** Results from fitting of the MSD to extract the diffusion coefficient. Indeed, the expression $\text{MSD} = 4D \cdot t$ allows to extract the diffusion coefficient.

Supplementary movies legends.

Movie 1. Oil droplet in an oocyte maintained in prophase I at short time scale. Time lapse movie of an oocyte injected with oil droplet in prophase I. Frames are taken every 500 ms. Movie duration is 500 seconds.

Movie 2. Oil droplet in an oocyte maintained in prophase I treated with cytochalasin D at short time scale. Time lapse movie of an oocyte injected with oil droplet in prophase I and treated with cytochalasin D. Frames are taken every 500 ms. Movie duration is 300 seconds.

Movie 3. Oil droplet in an oocyte maintained in prophase I at long time scale. Time lapse movie of an oocyte injected with oil droplet in prophase I. Frames are taken every 20 min. Movie duration is 16 hours.

Movie 4. Oil droplet in an oocyte undergoing meiosis I at long time scale. Time lapse movie of an oocyte injected with oil droplet and undergoing meiosis I. Frames are taken every 20 min. Movie duration is 14 hours.

Movie 5. Oil droplet in an oocyte undergoing meiosis I and treated with cytochalasin D at long time scale. Time lapse movie of an oocyte injected with oil droplet, treated with cytochalasin D and undergoing meiosis I. Frames are taken every 20 min. Movie duration is 14 hours.

Movie 6. 100 nm beads in oocytes maintained in prophase I without or with cytochalasin D treatment. Time lapse movie of oocytes injected with 100 nm fluorescent beads coated with PEG and maintained in prophase I. Left: oocytes with intact F-actin mesh. Right: oocyte treated with cytochalasin D. Frames are taken every 350 ms. Movie duration is 155 seconds.

Movie 7. Total vesicles observed at different states of meiosis. Time lapse movies of oocytes stained with Nile red at various states of meiosis (from left to right): Prophase, Meiosis I early (NEBD+1h) and Meiosis I late (NEBD+6h). Frames are taken every 500 ms. Movie duration is 150 seconds.

6.3 Discussion

6.3.1 Oil droplets as biomimetic objects and force sensors

Using oil droplets or vesicles to study the forces applied by the cytoskeleton has been known for a long time [50, 188]. Injection of oil droplets in living embryonic tissues was introduced recently (Figure 6.6a, [189]) and was a breakthrough for the direct quantification of endogenous cellular forces *in situ*. The local stresses applied in the tissue can be inferred from the droplet deformation (Figure 6.6b). The advantage of this technique is that the droplet can be coated with specific molecules, adhesion receptor ligands for example. It is even possible to coat the droplets with a ferrofluid. By applying a deformation on the magnetic droplet and monitoring the tissue response, it was possible to have a readout of the local mechanical properties of the tissue [190]. The ferrofluid droplet is then acting as a micro-rheometer.

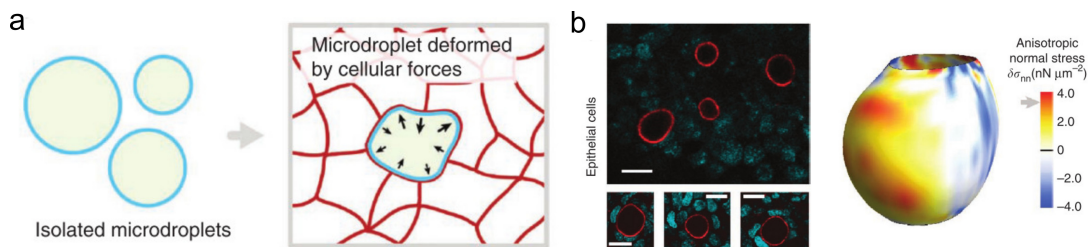


Figure 6.6: Oil droplets in tissues to quantify cell-generated mechanical forces. (a) Principle of the experiment. (b) Example of oil droplets (red) injected in an aggregate of epithelial cells (blue). The anisotropic normal stress computed from the droplet deformation is represented on the right. *Adapted from [189].*

In the mouse oocyte, injection of oil allowed to inject large objects (above $5 \mu\text{m}$ in diameter), which was not possible with the particles injection. We did not see a deformation of the droplet, probably because it was too rigid for the forces applied by the oocyte cytoplasm. This is probably due to their surface tension, which is extremely high. Indeed, the interfacial tension between oil and water is about $10 \text{ mN}\cdot\text{m}^{-1}$, therefore to observe a deformation of 500 nm , a force of 30 nN should be applied. This force might be applied by the oocyte cytoplasm. To observe the deformation, we should label the droplet with fluorescence, to have a better resolution of the interface.

We did not try to functionalize the droplet surface. We could have done it for several reasons: first, we could have add a polymer to passivate the droplet and make sure that there was not non-specific interactions between the droplet and the cytoplasm. Second, we could have try to change the droplet rigidity to make it softer and potentially observe deformations of the droplet. Change of rigidity can be done with adding a phospholipid along with a cosurfactant to the oil droplet. For example, small fluorocarbon-hydrocarbon diblocks have been shown to considerably lower the surface tension when combined with phospholipids [191]. Change of the interfacial tension can also be done by changing the fluorocarbon oil [191].

6.3.2 Homeostasis of actin networks

The idea of having the same molecular actors to do opposite movements (centering and off-centering in our case) is interesting in terms of actin network homeostasis. There have

been a lot of studies dealing with this issue. For example, Burke *et al.* [192] showed that in fission yeast, the actin assembly factors compete for actin monomers (that is in limited quantity in the cell), leading to homeostasis between different actin networks. Indeed, the yeast nucleate Arp2/3 endocytic patches and at the same time, the formins nucleate actin cables and the cytokinetic ring (Figure 6.7). They showed that inhibition of one actin factor enhance the activity of the other.

Lomakin *et al.* [193] showed the existence of similar mechanism with competition between Arp2/3 and myosin-dependent F-actin networks in epithelial cells. This competition defines a mechanism for cell polarization and motility initiation. Myosin stabilizes actin in contractile actomyosin structures. In both cases, an analogy can be done with species fighting for food in an ecological system.

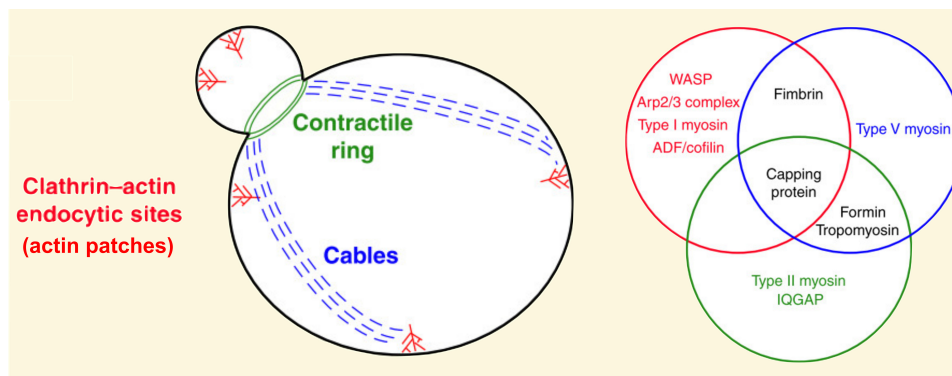


Figure 6.7: Different actin networks nucleated in fission yeast. *Adapted from [194].*

This homeostasis of actin network is interesting in our case since in meiosis I, we showed the coexistence of two mechanisms with opposite effects. Therefore, we can imagine that two actin networks are nucleated with almost the same molecular actors but with completely different effects.

6.3.3 Conclusion

Thanks to biophysical approaches, we managed to have a better understanding of the physical properties of the mouse oocyte cytoplasm. One interesting idea would also be to functionalize the injected objects (particles or oil droplets) and to be able to manipulate them in the cell (*via* a magnetic control for example). In the Appendix A, we present preliminary results about the magnetic control of magnetic nanoparticles in mouse oocytes.

Conclusion

In this PhD, we presented results about the set-up of new experimental and analytical tools to study the role of cytoplasmic F-actin self-organization. For that, we used two model systems: *Xenopus* egg extracts and mouse oocytes. We showed that cytoplasmic F-actin can play various roles in a biological system: first, we showed that actin self-organization can trigger signaling pathways. Then, we demonstrated that cytoplasmic F-actin can modulate microtubules length and dynamics. Finally, we confirmed that F-actin network can mediate the long-range transport of large objects in mouse oocytes.

In confined *Xenopus* egg extracts, endogenous F-actin has a contractile behavior that leads to the self-organization of an F-actin ring (encompassing most of the cytoplasmic material). By artificially engineering two properties of F-actin (confinement and scaffolding), we showed that this self-organization of F-actin can trigger signaling pathways (Chapter 4).

In a second set of experiments, we reconstituted various actin dynamics that allowed us to study the microtubules properties in a dense F-actin meshwork (Chapter 5). By tuning actin density and architecture, we proposed a model in which actin self-organization can regulate microtubule length and dynamics.

The cell extract system is very powerful to explore the parameter space. Indeed, changing the concentration of one component is very simple to perform. We did not do it in those studies but playing on the combination between different actin promoting factors/actin binding proteins would have been possible and very simple to do. In addition, we showed that *Xenopus* egg extracts are perfectly adapted for the study of actin-microtubule interactions (Chapters 4 and 5). In chapter 4, we engineered a new protein to create an artificial link between actin and microtubules. In chapter 5, without creating any biochemical link between actin and microtubules, we saw a co-alignment between actin and microtubules as well as a reorganization of actin at the level of the microtubule pole.

Our encapsulated egg extracts allows us to reconstitute the cellular volume. This makes it an interesting tool to study actin-microtubule interaction by being an intermediate between *in vitro* and *in vivo* systems. Our droplet-based assay could be improved by transforming the droplets in vesicles for example. This would allow to perturb the system in real time.

In chapter 6, we studied the cytoplasmic F-actin meshwork that was shown to be necessary for nucleus centering in mouse oocytes. The injection of objects of various sizes: particles (nanometer scale) or oil droplets (micrometer scale) allowed us to gain a better understanding in the centering mechanism taking place during prophase. In mouse oocytes, the structure visualization is complicated; for example, it was not possible yet to perform super-resolution. Thanks to the particle tracking, we managed to have a better understanding of the actin network properties. In addition, injection of oil droplets gave

us the possibility to mimic a large object like the nucleus and therefore showing that the centering mechanism in prophase is not specific to the nucleus. It was also a surprise to find that the mechanism was conserved during the rest of meiosis I. The centering mechanism could have a physiological role by maintaining the organelles at the center of the oocyte and therefore avoiding an asymmetrisation of the cell during the spindle migration.

Working with those two model systems made me realize their strengths and weaknesses. Indeed, the *Xenopus* egg extracts provide a very plastic system in which numerous parameters can be varied and therefore numerous conditions can be tested. Although the system is very well characterized for few stereotyped assays (spindle assembly, cell cycle control, DNA replication), it remains an *in vitro* assay with some limitations: no membrane, no long-term development. In the mouse oocyte, the experiments are very heavy: injection is necessary for each experiment (except for the membrane-permeable components). This leads to low-throughput experiments. But the system is physiological and is a canonical model of development. In conclusion, both top-down and bottom-up approaches are necessary to have a better understanding of cytoplasmic F-actin self-organization.

Appendix A

Magnetophoresis in Biological Systems

In the last years, the development of new tools to perturb biological systems has been very productive with new methods based on microfluidics (to control the cell environment) or on optogenetics (to activate a specific biological activity with light). One of the main drawback of these methods is the poor spatiotemporal control of the different elements. Though, the concept of information of position is crucial to understand the different processes associated with a signaling pathway. In the lab, there is an expertise about the reversible magnetic control of local concentration in biomolecules. The spatiotemporal resolution permits to localize an activity over a range of few micrometers and a time scale going from seconds to minutes [75].

In this appendix, we present results about magnetophoresis in biological systems (*Xenopus* egg extract and mouse oocytes).

Contents

| | |
|---|------------|
| A.1 Introduction | 168 |
| A.2 Description of the objects used for magnetophoresis | 168 |
| A.2.1 Magnetic nanoparticles | 168 |
| A.2.2 Ferritin clusters | 169 |
| A.2.3 Magnetic manipulation | 170 |
| A.3 Nanoparticles manipulation in mouse oocytes | 172 |
| A.4 Magnetophoresis of ferritin clusters in water and egg extracts | 173 |
| A.4.1 Magnetophoresis in water droplets | 173 |
| A.4.2 Magnetophoresis of an aster in egg extracts | 175 |

A.1 Introduction

We present here two independent projects aiming to use magnetic forces to trigger biological activity (Figure A.1). In mouse oocytes, the idea is to use magnetic nanoparticles coupled with biomolecules. Once injected in the oocyte, the nanoparticles could be manipulated thanks to a magnetic field and the biological response can be observed. In *Xenopus* egg extracts, we showed that ferritin clusters can act as artificial MTOCs. They can be manipulated with magnetic field.

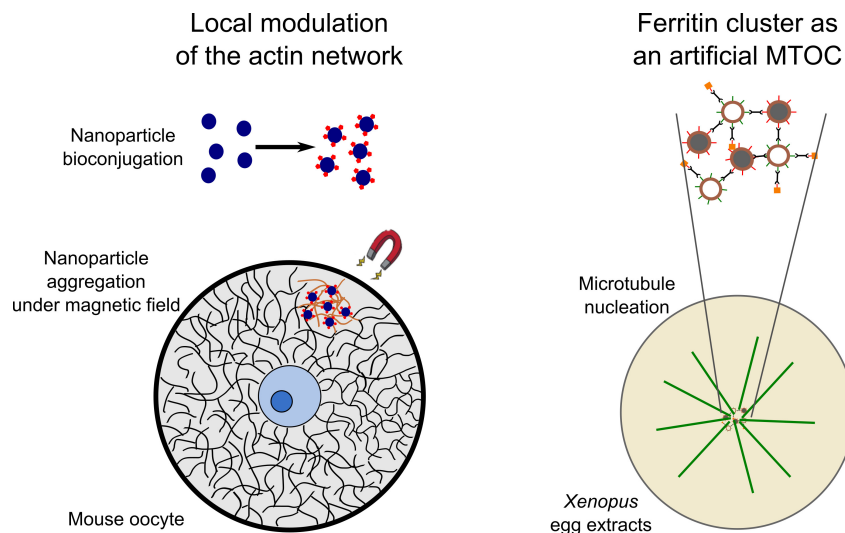


Figure A.1: Schematic of the use of magnetic forces in biological systems. Left: local modulation of the actin network in mouse oocytes thanks to nanoparticles conjugated with actin nucleation factors. Right: use of ferritin mineralized clusters as artificial MicroTubule Organizing Centers (MTOCs) in *Xenopus* egg extracts.

We will first present the objects used for magnetophoresis (nanoparticles, ferritin clusters). Then, we will present preliminary results of nanoparticle manipulation in mouse oocytes. Last, we will present results of ferritin clusters magnetophoresis in *Xenopus* egg extracts.

A.2 Description of the objects used for magnetophoresis

A.2.1 Magnetic nanoparticles

We use magnetic nanoparticles with a Fe_2O_3 (magnetite) core. We buy them from different companies (AdemTech, Micromod, Life Technologies). We used particles of various sizes: 120 nm, 300 nm, 1 μm , 3 μm . They all have a carboxyl group on their surface. Depending of their size, the nanoparticles do not have the same magnetic properties.

Coupling of magnetic nanoparticles with fluorescence

For their use in biological medium, we need to functionalize the nanoparticles with biomolecules (fluorescent molecule or cytoskeleton factor). We used two different types of coupling; electrostatic coupling and covalent coupling.

Electrostatic coupling The electrostatic coupling is based on the electrostatic interaction between the carboxyl group of the nanoparticle and the lysines of the polymer that we add to our nanoparticles. The polymer that we use is a PLL-PEG, already described in section 3.5.3 (page 52). For the fluorescence, we use an organic compound: Alexa568-NHS. The coupling is done in two steps. First, the PLL-PEG and the Alexa are mixed at room temperature during 30 minutes; this will allow the NHS groups of Alexa to react with the poly-lysine amines. At the end of this step, we obtain a fluorescent PLL-PEG. Then the fluorescent PEG is mixed with the nanoparticles during 30 minutes at room temperature. The amines of the poly-lysine will react with the carboxyl groups of the nanoparticles. The excess of fluorescent PEG is washed with a magnet. The advantage of this coupling is that it is very easy to prepare. But the drawback is that it is not very stable in time. In addition, for the specific case of mouse oocytes, we do not know if the coupling is resistant to the pressure put by the micro-injector during the injection in cells.

Covalent coupling The covalent coupling is based on EDC-NHS chemistry. Once again, it is based on the carboxyl surface of the nanoparticle and on the primary amines of the protein that will be coupled to the nanoparticle. In this coupling, we couple a protein with the nanoparticle. We chose to use mCherry. The principle of the coupling is shown in figure A.2. Briefly, the nanoparticles (and more precisely the carboxyl group) are mixed with the EDC in a MES buffer at pH 6. The NHS is then quickly added to the mix that is let for incubation during 10/15 minutes with agitation. The particles are then rinsed for the excess of EDC and NHS with a magnet. Then the proteins to couple with the particles are added to the particles in a NaHCO_3 buffer at pH 8 (for the amines to be in the NH_2 form). The proteins and the particles are incubated for one to two hours at room temperature with agitation. The particles are rinsed to remove the excess of protein and kept in a PBS buffer at pH 7.4. The coupling is kept at 4°C and is stable for several months.

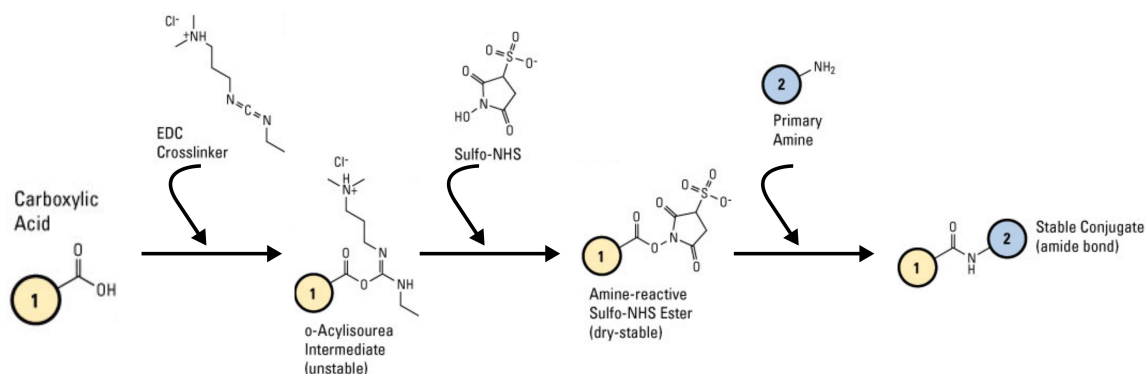


Figure A.2: Principle of the EDC-NHS coupling. *Adapted from thermofischer website scheme.*

A.2.2 Ferritin clusters

One of the drawback of the nanoparticles is that they are not always biocompatible. In addition, their size is complicated to control during their synthesis. This is why since few years, researchers got interested in the ferritin, a protein with a primordial role in the iron homeostasis in living cells. Ferritin presents 24 subunits that assemble to form a protein

shell. Each subunit has two sites: one to catalyze the oxidation of iron(II) in iron(III) and one that guides the mineralization inside the ferritin protein shell. The protein shell has a diameter of 15 nm. The mineralized phase that can have a diameter of 6 nm can be magnetic depending on the conditions of mineralization. Ferritin nanocages provide interesting features as templates for direct nanoparticle synthesis. In the lab, a project has been conducted to design genetically encoded protein-based scaffolds with modular biochemical and magnetic functions. I have been involved in the magnetic characterization of those scaffolds.

The scaffolds are formed with a chemical dimerization based on the FRB-FKBP system. Different proteins have been used with FRB and FKBP to allow the formation of 3D assemblies. For the characterization of the magnetic properties of the scaffolds the following proteins were used: FKBP-ferritin (used as a linker), FRB-ferritin (mineralized, with the protocol described in the methods of the manuscript) and FRB-mCherry to visualize the clusters with fluorescence microscopy (Figure A.3). The precise protocol of cluster formation is described in the Methods section of the manuscript.



Figure A.3: (a) Molecular actors necessary to form clusters. (b) Principle of the clusters formation. The FKBP-ferritin serves as a linker for FRB-ferritin mineralized and FRB-mCherry.

A.2.3 Magnetic manipulation

The magnetic nanoparticles that we use are superparamagnetic. When they are submitted to a magnetic gradient, the particles encounter a force F_{mag} which is described in Equation A.1 where $\frac{dB_x}{dx}$ is the magnetic gradient and \vec{m} the magnetic moment of the nanoparticle.

$$F_{mag} = \vec{m} \frac{dB_x}{dx} \quad (\text{A.1})$$

Therefore, in our experiments, it is the magnetic field gradient that is important. To have a good control of the gradient, we work with magnetic tips. The magnetic tip is made from the outside part of a guitar string. By stretching the string on the top of a flame, we can obtain a tip that has a diameter of about 100 μm (Figure A.4a). This tip is then put on the top of a squared permanent magnet in the north-south axis (NdFeB, Supermagnete, 3x3x3 mm). This set-up allows to strongly increase the magnetic field gradient (4.10⁴ T.m⁻¹ at the tip compared to 2.10³ T.m⁻¹ for the magnet alone). The diameter of the magnetic tip is roughly the distance on which the gradient spans. Therefore the diameter of the tip is important depending on the applications.

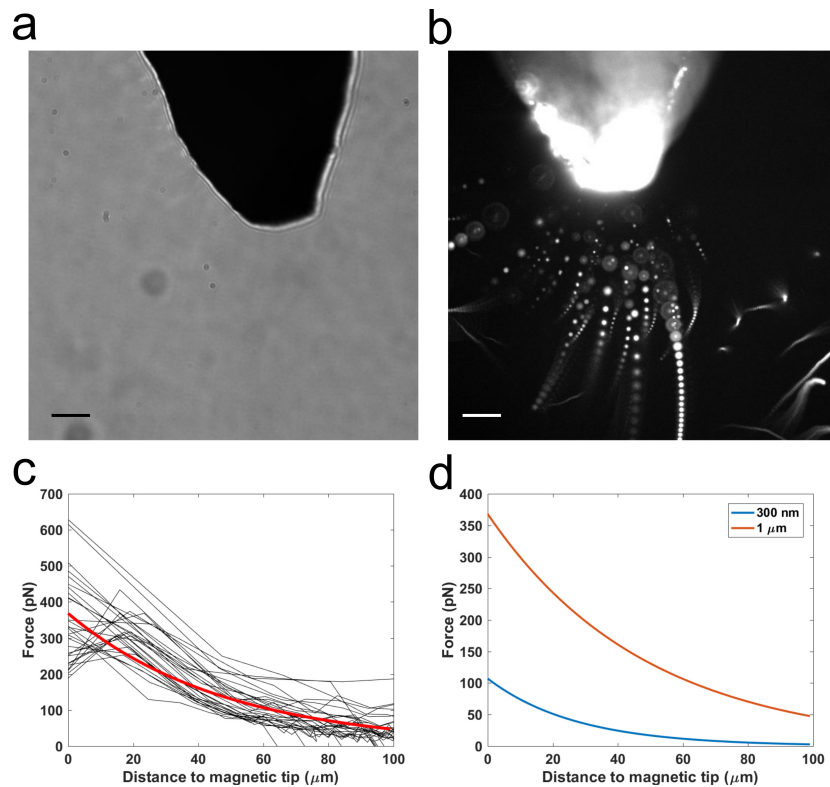


Figure A.4: Magnetophoresis of nanoparticles in glycerol. (a) Bright field image of a magnetic tip elongated from a guitar string. (b) Time projection of a movie of nanoparticles attracted by the magnetic tip. a-b: Scales bars are $20 \mu\text{m}$. (c) Force as a function of distance for $1 \mu\text{m}$ nanoparticles in 80 % glycerol. Black curves are results for individual nanoparticles, red curve is the result of the fit. (d) Comparison of force as a function of distance for 300 nm and $1 \mu\text{m}$ nanoparticles in 80 % glycerol.

Magnetophoresis of nanoparticles in glycerol. To characterize the magnetic force associated with the tip, we performed magnetophoresis of nanoparticles in a medium of known viscosity. By recording their position as a function of the time and computing the speed, we can apply the Stokes law (Equation A.2, η is the viscosity of the medium, r is the radius of the particle, v is the instantaneous velocity of the particle) to evaluate the magnetic force.

$$F = 6\pi\eta rv \quad (\text{A.2})$$

By computing this force at different distances from the magnetic tip, we will be able to characterize the magnetic field generated by the magnetic tip. An example of movie is given in Movie 1. The projection of all the images of this movie is given in Figure A.4b. After a manual tracking, the instantaneous velocity is computed as a distance from the magnetic tip for each individual nanoparticle. The force is then computed as a function of the distance to the magnetic tip. Each curve of force as a function of distance is fitted with the equation given in Equation A.3, where a and b are the parameters of the fit.

$$F_{mag} = a \exp^{-bx} \quad (\text{A.3})$$

The results for particles of $1 \mu\text{m}$ in diameter are shown in Figure A.4c. When comparing results for particles of different sizes, we can see that the bigger particles feel a bigger force close to the tip (Figure A.4d). Indeed, $1 \mu\text{m}$ nanoparticles feel a force of 300 pN at

10 μm of the tip, whereas 300 nm nanoparticles feel a force of 74 pN at the same distance (Figure A.4d and Table A.1).

A.3 Nanoparticles manipulation in mouse oocytes

In mouse oocytes, the idea was to use nanoparticles coupled with proteins to have a better understanding on the properties of the cytoplasm. Coupling nanoparticles with actin nucleators (for example formins) would allow to examine how the morphology and the kinetics of actin networks are dependent of the local concentration on actin nucleators. The advantage of coupling proteins on nanoparticles is that the stoichiometry of the protein on the nanoparticle can be controlled. The magnetic control of nanoparticles coupled with actin nucleators would allow to modulate the local concentration of actin nucleators in the cytoplasm. It would also allow to quantify the spatiotemporal dynamics of actin network. An interesting question would be to see if a local perturbation can change the global polarity of the oocyte. Biochemical perturbations could be added to see the robustness of the asymmetric division process as a function of a spatial perturbation in actin nucleators. The magnetic control of protein localization should bring a new method for protein perturbation in oocytes. This kind of approach could also be applied to numerous other systems.

First step: injection of nanoparticles in the oocytes and checking of the cell viability after injection. In oocytes, it is more usual to inject coding RNAs. Before functionalizing the nanoparticles, we need to be sure that the nanoparticle injection does not perturb the oocyte development.

We had a lot of technical issues to inject nanoparticles in mouse oocytes. We will not detail all the problems encountered but there was troubles with the concentration of nanoparticles, the coupling of fluorescence on the nanoparticles or the viability of the oocytes after injection. It was also complicated to have the oocytes not moving when approaching the magnetic tip. The solution we found was to work with a holding capillary, that allows to maintain the oocytes at a certain position (same process as the one used for injection). When an oocyte was stabilized with the holding capillary, the magnetic tip was brought next to the oocyte (Figure A.5). This method was not always successful.

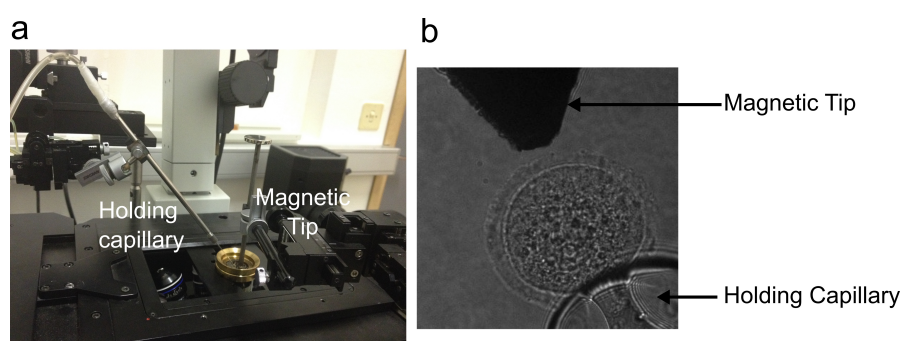


Figure A.5: Set-up used to do magnetic manipulation of nanoparticles in mouse oocytes.

Few times, we managed to inject and visualize nanoparticles in mouse oocytes. It was mostly for 1 μm particles, covalently coupled with mCherry protein in meiosis II oocytes (more resistant to injection). Some images of nanoparticles inside oocytes are shown in Figure A.6. In very few cases, we managed to see some particles moving toward the

magnetic tip. Though this movement was very limited and stopped after a few frames. In addition, it was not reproducible in all the oocytes we were observing. Some examples of particles moving in oocytes are shown in figure A.6b, c.

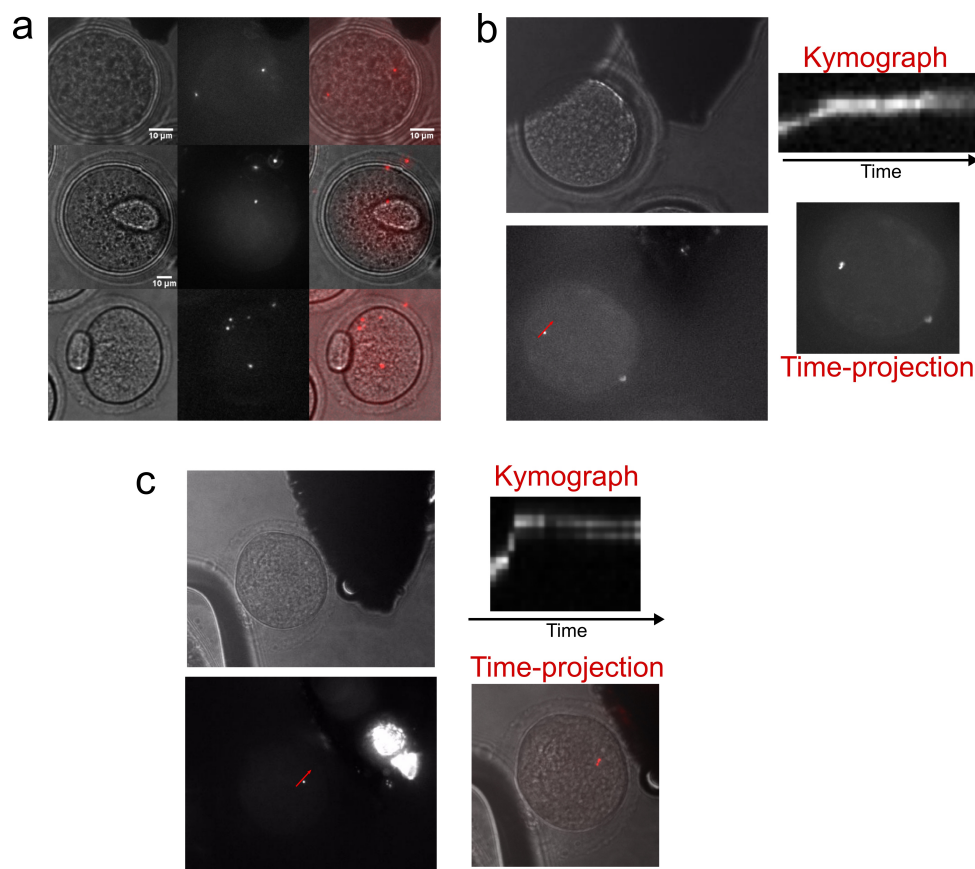


Figure A.6: Injection of nanoparticles in mouse oocytes. (a) $1 \mu\text{m}$ particles observed in mouse oocytes. (b-c) Examples of particles moving toward a magnetic tip. The bright field image shows where is the magnetic tip. The kymograph is traced along the red line.

A.4 Magnetophoresis of ferritin clusters in water and egg extracts

We will now describe the magnetophoresis measurements done on ferritin clusters (introduced in Section A.2.2).

A.4.1 Magnetophoresis in water droplets

Before being able to manipulate biological objects (aster in our case) with magnetic forces, we need to characterize the properties of the ferritin clusters when they are subjected to a magnetic force. For that, we applied the same procedure as we described in Section A.2.3 for the nanoparticles in glycerol. The problem for the clusters was that the magnetic properties of our mineralized ferritins are weaker than the ones of nanoparticles. Therefore, if we put the clusters in glycerol, they are more subjected to hydrodynamic flow than magnetic force. The solution to this problem was to insert the clusters in droplets.

The confined space limits the hydrodynamic flow. In addition, the confining volume allows to be in a viscous regime even if we are in water. We performed measurements for different percentages of mineralized ferritins (Figure A.7). We see that the more there is mineralized ferritin in the cluster, the more the force is felt by the cluster. Interestingly, when comparing the force at a certain distance of the tip for clusters and for commercial nanoparticles, we can see that the clusters are less magnetic than the nanoparticles (Table A.1). *Since those experiments, the protocol of mineralization has been optimized to make the ferritins more magnetic.*

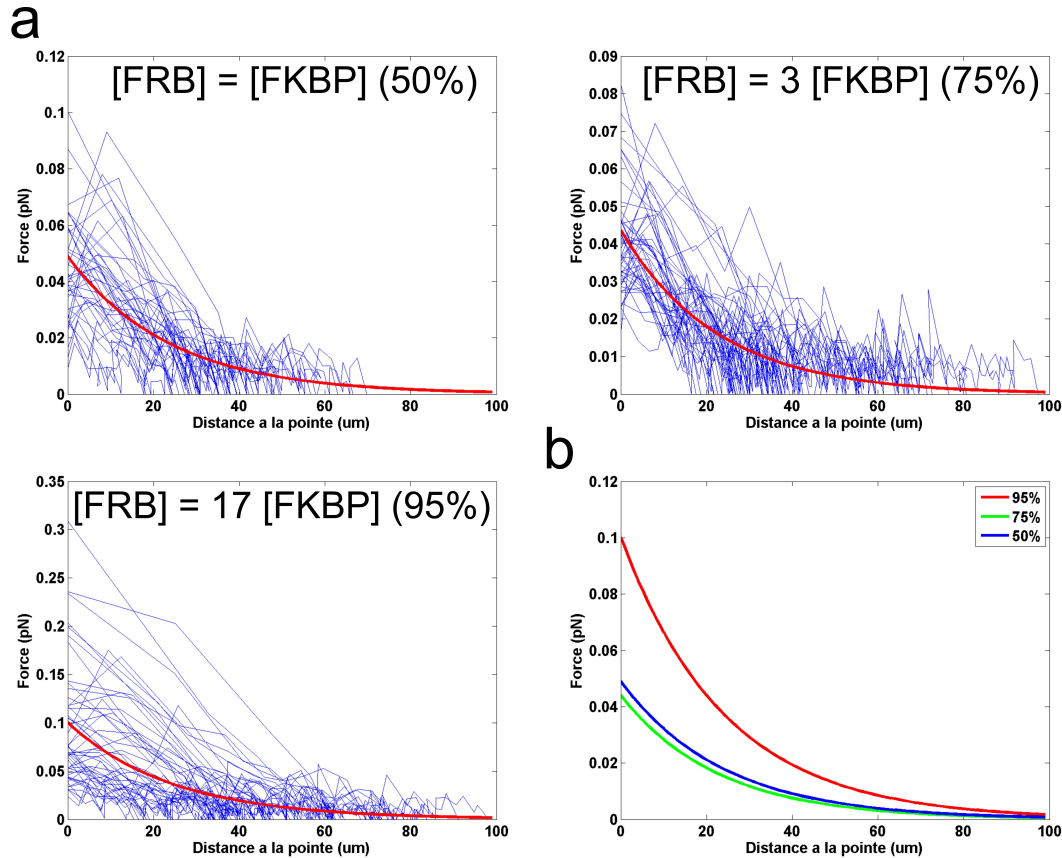


Figure A.7: Magnetophoresis in ferritin clusters. (a) Magnetophoresis for clusters with various percentages of mineralized ferritin in the cluster. Blue curves correspond to individual clusters, red curve to the fit. (b) Superposition of the fits for the three different percentages of mineralized ferritin in the clusters.

| | | |
|---------------------------|----------|------------------|
| | Tip | 10 μm |
| 300 nm particles | 107 | 74 pN |
| 1 μm particles | 368 | 300 pN |
| [FRB] = [FKBP] | 0.049 pN | 0.032 pN |
| [FRB] = 3 [FKBP] | 0.044 pN | 0.028 pN |
| [FRB] = 17 [FKBP] | 0.10 pN | 0.066 pN |

Table A.1: Forces exerted on magnetic objects at various distances from the magnetic tip.

A.4.2 Magnetophoresis of an aster in egg extracts

In addition of their magnetic properties, the clusters can also serve as microtubule nucleating center if a microtubule nucleating factor fused to FRB or FKBP is added to the mix. An aster is then formed around the cluster (Figure 4 of the manuscript). We performed magnetophoresis of these clusters surrounded with microtubules. The explanations of this experiment can be found in the manuscript (Figure 4). This manuscript is currently in revisions in *Scientific Reports*.

Programmed Self-Assembly of a Biochemical and Magnetic Scaffold to Trigger and Manipulate Microtubule Structures

*Rémi Ducasse*¹, Wei-An Wang*¹, Marina Garcia-Jove Navarro*¹, Nicolas Debons¹,
Alexandra Colin¹, Jérémie Gautier¹, Jean-Michel Guigner², François Guyot², and
Zoher Gueroui¹*

¹ École Normale Supérieure, PSL Research University, CNRS, UPMC,
Department of Chemistry,
24 rue Lhomond, 75005 Paris, France

² IMPMC. Sorbonne Université. CNRS. UPMC. MNHN. IRD.
4, place Jussieu, 75005 Paris, France

* R.D, W.A.W, and M.GJ.N contributed equally to this work.

Correspondence:

Zoher Gueroui

Phone: +33 1 44 32 24 09

Email: zoher.gueroui@ens.fr

Abstract

Artificial bio-based scaffolds offer broad applications in bioinspired chemistry, nanomedicine, and material science. One current challenge is to understand how the programmed self-assembly of biomolecules at the nanometre level can dictate the emergence of new functional properties at the mesoscopic scale. Here we report a general approach to design genetically encoded protein-based scaffolds with modular biochemical and magnetic functions. By combining chemically induced dimerization strategies and biomineralisation, we engineered ferritin nanocages to nucleate and manipulate microtubule structures upon magnetic actuation. Triggering the self-assembly of engineered ferritins into micrometric scaffolds mimics the function of centrosomes, the microtubule organizing centres of cells, and provides unique magnetic and self-organizing properties. We anticipate that our approach could be transposed to control various biological processes and extend to broader applications in biotechnology or material chemistry.

Introduction

In living systems, proteins self-organize into macromolecular assemblies at various length scales to ensure the coordination of numerous biological functions in space and time^{1,2}. For instance, at the nanometer scale, protein scaffolds are central to trigger by proximity the activation of proteins involved in signal transduction^{3,4}. At the micrometric scales, multimeric interactions or repetitive interacting domains drive the organization of numerous functional structures, such as cytoskeleton fibres or organelles, with specific functional properties usually not found at the single molecule level^{2,5,6}. Numerous studies are now engaged to establish a clear link between biological multiscale assemblies and emergent functional properties. From this perspective the development of bio-based nanomaterials, produced from the programmed assembly of biomolecules as DNA, RNA, and proteins, offers novel tools to analyse and control the spatiotemporal properties of molecular and cellular processes, but also to engineer novel synthetic functionalities^{7,8}. For instance, DNA-based scaffolds, which provide very precise biomolecule spatial positioning, have been used to elucidate biophysical mechanisms underlying cytoskeleton motor activity⁹⁻¹¹ or as fluorescent biosensors to probe the internal environment of living cells^{12,13}. Complementary, pioneer studies have demonstrated how synthetic protein scaffolds can modulate the cooperativity of ensembles of molecular motors¹⁴, and artificially control metabolic flux¹⁵ or signalling pathways¹⁶⁻¹⁸.

In this study we present a synthetic protein scaffold that combines specific features found in natural systems, such as multimeric interactions and multiscale assemblies, with novel properties provided by an artificial approach, such as stimulus-triggered assembly¹⁹ and magnetic control²⁰⁻²⁶. In this regard, our synthetic protein scaffold, bioengineered from ferritin nanocages, recapitulates several

remarkable characteristics: (i) upon chemical stimulation it self-organizes into micrometric structures *in vitro*, (ii) it can be functionalized with regulatory proteins to trigger specific biochemical responses, and (iii) it displays magnetic properties that could be useful for detection or for magnetic actuation. To illustrate the versatility of our synthetic scaffold, we devised an *in vitro* assay to study specific features of cytoskeleton spatial organizations, by focusing on the nucleation and the magnetic manipulation of microtubule structures. In particular, the generation of 3D micrometric scaffolds from single functionalized and biomineralised ferritins enables us to mimic Microtubule Organizing Centres, such as the centrosome, and to examine an emergent function of these resulting artificial organelles: the centring property, which is essential to define the polarity of cells^{27,28}.

The iron storage ferritin is a protein that assembles into a nanocage composed of 24-subunits. The capacity of ferritin to catalyse the precipitation of inorganic condensed phases within its internal cavity allows living organisms to control the availability of iron²⁹. Several studies have reported modifications of the ferritin cage surface by non-covalent interactions in response to electrostatic interactions^{30,31} or metal coordination³². The oligomeric state of the ferritins has been further exploited to generate controlled multi-scale assemblies^{30,31,33-35}. On the other hand, the catalytic activity of the ferritin has been used for developing novel contrast agents in living organisms (magnetic resonance imaging, electron microscopy), nanoheaters for hyperthermia, nanoproboscopes for biosensing and cell markers, and magnetic actuators for gene expression control (magnetogenetics)³⁶⁻⁴³. In this study, we exploit both the multivalent and catalytic properties of ferritin. Our first goal was to engineer ferritin nanocages as building blocks for the production of inducible micrometric protein scaffolds sharing a specific biochemical activity and magnetic properties. To do so, we have designed a strategy for the controlled functionalization of the

nanocage surface, by multivalent protein-protein interactions. We have genetically modified the ferritin monomer to use chemically inducible dimerization strategies based on the heterodimerization of FKBP and FRB (Figure 1)⁴⁴⁻⁴⁶. Then, the catalytic activity of ferritin, by synthesising monodispersed ferric condensed nanoparticles within its cavity, provides specific magnetic properties to the scaffold^{42,47-49}. This modular strategy permits the targeting of proteins of interest at the nanocage surface (Figure 1a), but also the formation of 3D clusters of ferritins by triggering multimeric interactions between FKBP- and FRB-ferritin cages and magnetically manipulating them, upon biomineralisation of the participating ferritins (Figures 1b, c).

We next examined how ferritin nanocages can serve as biochemical scaffolds to control specific biological processes using *Xenopus* egg extracts, a powerful cell-free system well suited to study the morphogenetic properties of cytoskeleton networks⁵⁰⁻⁵³. We showed that the nucleation of microtubule fibres and formation into asters can be triggered by individual ferritin nanocages when TPX2, a nucleating promoting factor, is recruited to their surface. Moreover, when organized into micrometric clusters, the TPX2-ferritin scaffolds are integrated into the microtubule asters and localized at their pole centre, which confers the ability to manipulate the aster position with magnetic forces. Our observations also suggest the emergence of different biophysical and self-organizing properties of microtubule asters, depending on the scale of ferritin organization, from single cages (nanometre) to clusters (micrometre). Finally, these results illustrate how TPX2-ferritin scaffolds share some similarities with Microtubule Organizing Centres, found in eukaryotic cells, and suggest their utilization as artificial magnetic centrosomes to manipulate microtubule-based structures.

RESULTS

Modular Approach to Functionalize and Organize Ferritin Nanocages

In order to functionalize the ferritin, we used chemically inducible dimerization to target a protein of interest at the surface of the ferritin nanocages (Figure 1a). For this purpose, we selected the proteins FRB (the rapamycin-binding domain of mTOR) and FKBP (the FK506 binding protein) that are able to heterodimerize on fast time-scales upon interaction with the molecule Rapamycin⁵⁴. We genetically fused FRB and FKBP, respectively, to the N terminus of ferritin monomer from the extremophile archaea *Pyrococcus furiosus*. This approach offers several advantages as a result of the multivalency of the ferritin. For instance, each ferritin nanocage fused to FRB can interact with up to 24 FKBP fused to a protein of interest (and symmetrically FKBP-ferritins with up to 24 FRB-Protein of interest, Figure 1a). This anticipates a possible control of the number of proteins being recruited per nanocage or the co-recruitment of different protein families. Furthermore, this approach can also be extended to organize micrometric clusters of protein nanocages by inducing local interactions between FRB- and FKBP-ferritin cages upon Rapamycin addition (Figure 1b).

To validate our strategy, we produced and purified recombinant FRB- and FKBP- ferritins and characterized their assembly (see Methods). Transmission electron microscopy (TEM) was used to characterize single ferritin nanocages at the nanometer scale. TEM images of negatively stained FRB-ferritins and FKBP-ferritins show a majority of monodispersed spherical objects characterized by an average diameter of 11.3 ± 1.5 nm and 12.3 ± 0.7 nm respectively (Figure 2a,b). These data are in agreement with images acquired on native ferritins (11.5 ± 0.7 nm, Figure 2c), suggesting that FRB- and FKBP-ferritin monomers are able to self-

assemble into nanocages in solution. TEM images of negatively stained ferritin clusters, formed by mixing FRB-ferritin, FKBP-ferritin, and Rapamycin, revealed more complex morphologies. The clusters are organized into dense protein meshwork, as shown in Figure 2d, and displayed a broad range of characteristic sizes (150 nm to 2 μ m) (Figure S1a).

To confirm that chemically induced dimerization could be used to functionalize ferritin nanocages with a protein of interest, we examined the formation of complexes of FKBP-ferritin and FRB-eGFP by performing a gel mobility retardation assay (Figure 2e). The electrophoretic migration of complexes formed by different ratios of FKBP-ferritin and FRB-eGFP proteins was analysed and compared to single protein mobility. FKBP-ferritin concentration was fixed at 10 μ M, and the formation of eGFP-ferritin cages was followed in absence or presence of Rapamycin, at increasing concentrations of FRB-eGFP, to reach ratios of 1:0.1, 1:0.25, 1:0.5, 1:1, and 1:1.5 between the FKBP-ferritin monomer and FRB-eGFP (Figure 2e). In absence of Rapamycin, no change in the migration patterns of FKBP-ferritin and FRB-eGFP was observed compared to the mobility of the free protein (Figure 2e, lane 15 vs. control lanes 11, 12, 13, and 14). On the contrary, in presence of an excess of Rapamycin (20 μ M), we noted the disappearance of the free FRB-eGFP band, both in fluorescence and Coomassie-blue observations, that was correlated with the appearance of an eGFP fluorescent signal at the level of the ferritin migration band (Figure 2e, lane 7 vs. lane 15). Moreover, changing the FRB-eGFP concentration allowed us to tune the number of recruited proteins of interest per nanocage (Figure 2e, lanes 6 to 10). This demonstrates the specificity and controlled binding in the recruitment of FRB-eGFP to FKBP-ferritin nanocages upon Rapamycin interaction.

Fluorescence microscopy was used to describe the behaviour of fluorescently-labelled ferritin nanocages in solution. Single FRB-ferritins were labelled by dimerizing FKBP-mCherry to the nanocage in presence of Rapamycin (Methods, Figure 1a). The same strategy was used to label ferritin clusters: FRB-ferritin, FKBP-ferritin, and FKBP-mCherry were mixed together with Rapamycin (Methods, Figure 2f, right). In order to facilitate the manipulation and observation, we encapsulated the ferritin constructs within water droplets dispersed in mineral oil (Figure 2f, right). Upon clustering in presence of Rapamycin, we observed fluorescent bright dots that freely diffuse in solution (Figure 2f, right). A very low fluorescent background noise was detected within the water droplet, suggesting that the majority of ferritin nanocages formed micrometric clusters. To the contrary, in absence of Rapamycin the fluorescent signal was homogeneous (Figure 2f, left), thus confirming that the clustering is mediated by Rapamycin addition.

Our experiments revealed that engineered FRB- and FKBP-ferritins form monodispersed nanocages, with the capacity to be functionalized with proteins of interest at their surface, and to generate micrometric clusters in a chemically inducible manner.

Spatiotemporal Magnetic Manipulation of Biomineralised Ferritins

In order to provide magnetic properties to our engineered ferritins, the biomineralisation of iron oxide nanoparticles into ferritin cavities was performed by loading iron into FRB- and FKBP-ferritins within a controlled chemical environment (see Methods). TEM images of the mineralized FRB- and FKBP-ferritins revealed the presence of monodispersed iron oxide nanoparticles with an average size of 5 ± 1 nm (Figure 3a). We also performed TEM on clusters assembled from interacting FRB- and FKBP-ferritins in presence of Rapamycin (Figures 3b and S1b), which

permitted the confirmation of the presence of iron oxides within the clusters using scanning transmission electron microscopy (STEM) coupled energy dispersive X-ray analysis (EDX, Figure S1c, d).

To experimentally test the possibility to spatiotemporally manipulate biomineralised ferritins, magnetophoretic experiments were conducted on both single and clustered ferritin nanocages (Figure 3c,d). The FRB-nanocages were fluorescently labelled with FKBP-mCherry by adding Rapamycin and observed within droplets of water dispersed in mineral oil to facilitate their magnetic manipulation (Figure 3c). To estimate the effect of magnetic forces on ferritins, a gradient of magnetic field was produced by a permanent magnet (NdFeB magnet, 0.8 T, $10^2 \text{ T}\cdot\text{m}^{-1}$) positioned at a distance ranging from 50 to 500 μm from the droplets; or by using a micromanipulated magnetic tip to locally enhance the gradient of magnetic field up to $10^4 \text{ T}\cdot\text{m}^{-1}$. Upon the application of a magnetic field gradient of $10^2 \text{ T}\cdot\text{m}^{-1}$, we observed a homogenous concentration of mCherry-labelled and mineralized ferritins within the droplets, indicating that the magnetic forces had no effect on single ferritin cages. The magnetic forces acting on single ferritins were plausibly not strong enough to overpass thermal forces, which is consistent with the weak value of the magnetic moment of the condensed phase forming the ferritin core. However, increasing the gradient up to $10^4 \text{ T}\cdot\text{m}^{-1}$ with a magnetic tip allowed the local recruitment of individual mCherry-labelled ferritins (Method, Figure 3c). The accumulation of mineralized ferritins occurs within 3 minutes and leads to an increase of ferritin concentration at the droplet boundary (Figure 3c). On the other hand, the magnetic manipulation of clusters of mineralized ferritins was possible at a magnetic field gradient of $10^2 \text{ T}\cdot\text{m}^{-1}$ (Figure 3d). Indeed upon magnetic field actuation, we detected a strong accumulation of the bright fluorescent clusters along the magnetic field gradient. It shows that the overall resulting magnetic forces

experienced by each ferritin forming the clusters can overcome the thermal forces and the viscous drag force opposing the cluster mobility.

Overall, our data demonstrate that the magnetic manipulation of biomineralised ferritins is possible. Scaling up the hierarchical organization of the mineralized ferritins permits the demonstration of different behaviours under magnetic field actuation: while the local recruitment of single ferritins implies working in the range of few micrometres from the magnet, the complete asymmetry of clusters of ferritins within the droplets is obtained over distances of the range of 100 μm .

Ferritin Clusters as Biochemical and Magnetic Scaffolds to Nucleate and Manipulate Microtubules

We next investigated how to trigger a specific biological activity using ferritin nanocages as biochemical scaffolds. As proof-of-concept, we focused on the protein TPX2, which nucleates microtubule polymers⁵⁵. The activity of TPX2-ferritin bioconjugates was assessed by monitoring their capacity to nucleate microtubules. We used *Xenopus* egg extracts, a cell-free system well-suited to examine cytoskeleton processes, encapsulated within droplets dispersed in mineral oil to mimic the cell boundary and facilitate observations⁵⁶. In this assay, the incubation of TPX2 (0.5 μM) and fluorescently labelled tubulin (200 nM) within the egg extracts leads to the formation of fluorescent microtubules that assembled into characteristic asters (Figure 4a, left).

As a first step, we tested the capacity of single functionalized ferritins to nucleate microtubules. Chimeric mCherry/TPX2/ferritin nanocages were produced by dimerizing both FKBP-TPX2 and FKBP-mCherry with FRB-ferritin in presence of Rapamycin (Methods). When added to the cell extract at a final concentration of 0.5 μM , the chimeric ferritins nucleate microtubules, demonstrating that TPX2 activity is

maintained when dimerized with ferritin nanocages (Figure 4a, centre). The homogeneous mCherry signal observed within the droplets indicates no permanent colocalization between TPX2 and microtubules, and suggests that the nucleation of the fibres is probably induced by transient interactions between TPX2 and tubulin.

Then, to assess the activity of the micrometric ferritin scaffolds, we assembled clusters of mCherry/TPX2-ferritins by dimerizing FRB-ferritin with FKBP-ferritin, FKBP-mCherry, and FKBP-TPX2 in presence of Rapamycin. When confined within the egg extracts, TPX2-ferritin clusters were also biochemically active and nucleate microtubule asters (Figure 4a, right). Interestingly, the morphologies of the asters triggered by single ferritin nanocages and those triggered by ferritin clusters were different. When microtubules nucleated from TPX2-ferritin clusters, the centre of asters colocalised with a micrometric spherical meshwork of microtubules which entrapped the clusters of ferritins (Figure 4a, right). To examine more closely microtubule organization and polarity, we performed confocal microscopy observations using the protein EB1-GFP, which interacts with microtubule plus-end extremities (Figure 4b). At the vicinity of the centre of the asters, the growth of the microtubules was directed outward with a mean velocity of $15 \pm 5 \mu\text{m}\cdot\text{min}^{-1}$ (N=7), indicating that the growing fibres have their plus-ends pointing towards the droplet boundary. Therefore the scaffold-based ferritin asters have the same polarity as acentrosomal or centrosomal asters found in living systems²⁷.

Finally, we assessed the possibility to spatially manipulate the clusters of mineralized ferritins integrated to the microtubule asters with magnetic forces. In order to localize and direct the forces acting on the clusters, we used a magnetic tip that generates a focalized magnetic field gradient (Method, diameter 80-100 μm , Figure 4c). Remarkably, when the micrometric ferritin scaffolds were entrapped in the centre of the aster, the whole microtubule based-structure was attracted along the gradient of

magnetic field with an average velocity of $33 \pm 23 \text{ nm.s}^{-1}$ (Figure 4e, f). The average velocity of the moving aster increased to around $380 \pm 186 \text{ nm.s}^{-1}$ if a microtubule-depolymerizing drug is added to the extract (nocodazole, Method, and Figure 4f). The large increase in velocity in absence of microtubules can be explained by the reduced friction forces experienced by the ferritin clusters in motion in comparison to the friction of the whole aster-like structures. Additionally, microtubules contribute as rigid and elastic elements that can counterbalance the applied magnetic forces.

Altogether these data demonstrate that engineered ferritin nanocages can be used as biochemical and magnetic scaffolds to trigger and localize cellular processes. In our case, micrometric magnetic scaffolds of ferritins coupled to TPX2 enable the nucleation and the manipulation mesoscopic microtubule assemblies within a confined environment.

Ferritin Scaffolding mimics the Microtubule Organizing Centres of cells

The functional properties of TPX2-ferritin clusters share some similarities with the Microtubule Organizing Centres (MTOCs) of eukaryotic cells, structures that nucleate microtubules and participate in intracellular spatial organization. For instance, the geometrical positioning of MTOCs is important for defining the polarity of cells and depends on the interplay between internal and external cues together with the physical properties of their constituents^{57,58}. To gain insights into the self-organizing properties of our artificial MTOCs, we quantitatively characterized the geometrical positioning of asters nucleated by single TPX2-ferritins and TPX2-ferritin clusters to compare their centring properties (Figure 5). The asters triggered by single TPX2-ferritins have their centre distributed throughout the entire droplet space (Figure 5a, b, TPX2-ferritins). In this case, the normalized standard deviation (SD) and average off centring (OC) of the aster positions were respectively 41% and

53%; where 0% and 100% indicate the centre and the droplet boundary, respectively (Figure 5b). These observations were similar to those obtained for asters triggered by free TPX2 proteins (SD=40% and OC=54%) (Figure 5a,b, TPX2). Remarkably, the asters triggered from micrometric scaffolds of TPX2-ferritin clusters have their centre restricted to a smaller area around to the geometrical centre of the droplet (SD=25% and OC=29%) (Figure 5a, b, TPX2-ferritin clusters). This suggests that the mode of spatial organization of TPX2-ferritins, at the single nanocage level or assembled into micrometric scaffolds, directly influences the geometrical positioning of the asters during microtubule self-organization. To quantify the centring properties of asters nucleated from natural MTOCs, we next examined the positioning of asters nucleated by centrosomes purified from Jurkat cells. Interestingly, the position of the asters nucleated from a centrosome was also restricted to the vicinity of the droplet centre (SD=32% and OC=42%, Figure 5a,b, Centrosome). This observation highlights that natural MTOCs have centring properties intermediate between single TPX2-ferritins and scaffold-based ferritin clusters.

It has been established that the pulling and pushing forces generated by microtubules and motor-dependent microtubules, as well as the mechanical properties of the cell boundary, participate in the overall MTOC centering⁵⁷. We used this framework to interpret our observations and assume that the centring properties of the asters is due to pushing forces exerted by microtubules on the droplet boundary or on the extract cytoplasm. In this picture, the larger off-centre behaviour observed for the asters triggered by single TPX2-ferritins can be induced by pushing forces produced by asymmetrically oriented microtubules. It has been previously proposed that this situation arises from the pivoting of microtubule fibres around the aster pole and favour asymmetrically oriented microtubule asters⁵⁶. On the other hand, the restricted off-centring of asters triggered by micrometric ferritin clusters could arise from

microtubules that do not pivot around the aster pole^{56,58}. As the aster centre is composed of a matrix of ferritin clusters embedded within a microtubule meshwork, it may anchor microtubules. The resulting anchorage introduces a rotational stiffness resisting to the torque produced by microtubules, and maintains the fibre orientation that balances the forces positioning the aster centre.

Altogether our data demonstrates the emergence of different biophysical properties in the centring of microtubule asters, depending on the scale of ferritin organization, from single cages (nanometre) to clusters (micrometre). Furthermore, the incorporation of TPX2-ferritin scaffolds at the aster pole modifies the overall centring properties, which highlights the importance of the local organization of the aster pole for its biological function. These results illustrate how TPX2-ferritin scaffolds can mimic Microtubule Organizing Centres of eukaryotic cells with specific self-organizing properties.

Conclusion

Overall, we have demonstrated that engineered ferritin nanocages can be designed as biochemical and magnetic scaffolds to nucleate and manipulate mesoscopic bioassemblies *in vitro*.

As magnetic interactions can be contactless, remote controlled, and can deeply penetrate into thick materials; there is a strong interest in using tailored and functionalized magnetic nanoparticles to actuate biological processes upon magnetic actuation⁵⁹⁻⁶¹. Integrating such magnetic properties to bio-based scaffolds could open numerous perspectives in nanomedicine, biotechnology, or material chemistry. Our study demonstrates that protein-based magnetic scaffolds can be used to spatiotemporally manipulate biomolecules with magnetic actuation. Our scaffold combines the advantages of being genetically encoded with a synthetic approach,

ensuring their modular biofunctionalisation, biocompatibility, inducible self-assembly properties, which overall provides novel opportunities alternative to the use of synthetic magnetic nanoparticles.

Our study, aiming to assemble an artificial and magnetic centrosome, raises interesting questions about the impact of multiscale assemblies on functional properties. For instance, we show that the mode of spatial organization of TPX2-ferritins, at the single nanocage level or assembled into micrometric scaffolds, influences the centring properties during microtubule self-organization, which eventually can impact the polarity of the overall cytoskeletal organization. This suggests that the fundamental property of the centring of microtubule asters may also depend on the local organization of the aster pole centre. Furthermore, our modular approach is generic and shows how artificial protein-based organelles can be engineered with emergent functional properties, suggesting its extension to mimic other protein-based organelles or to artificially trigger signalling pathways.

Finally, the transposition of our strategy into living cells will be powerful to target and manipulate specific proteins and cellular organelles by combining chemically induced dimerization and magnetic manipulation^{23,60,62}. A fully-genetically encoded strategy, avoiding *in vitro* biomineralisation and injection into cells, will require novel approaches to catalyse enhanced magnetic phases within cells. This will be necessary to overcome the limited magnetic properties of *in vivo* expressed ferritins that is a bottleneck for efficient magnetic manipulation⁶³. Beyond the development of new methods for spatiotemporal control, our strategy could also benefit other applications including biomedical imaging, biosensing, drug delivery, or the design of stimuli-responsive materials.

METHODS

Reagents

Buffers powders, ATP, creatine phosphate, creatine phosphokinase, Nocodazole, H₂O₂, FeSO₄, Sodium citrate, DTT and mineral oil (M5904) were purchased from Sigma-Aldrich (St Louis, MO). Poly(12-hydroxystearic acid) (PHS) and poly(ethylene oxide) (PEO-30) are commercially available (Arlacel P135) and were purchased from UNIQEMA. Tubulins, labelled with Rhodamin or with FITC, were ordered from Cytoskeleton Inc. (Denver, CO). Rapamycin was purchased from Calbiochem. Jurkat centrosomes were kindly provided by M.Thery and J.Sillibourne. Cytostatic-factor-arrested (CSF) *Xenopus laevis* extracts were prepared as previously described⁶⁴. All reagents for buffer preparation were purchased from Sigma-Aldrich.

Expression and purification of recombinant proteins

The plasmid for Escherichia coli expression of the wild type ferritin (*Pyrococcus furiosus*) is a gift from W.R Hagen⁶⁵. FKBP- and FRB-ferritin, mCherry, eGFP and xITPX2dNLS fusion proteins were cloned in a pET28 plasmid. xITPX2dNLS is the *Xenopus laevis* TPX2 with a mutation at residue K284 that disrupt importin- α binding and efficiently induced aster formation⁶⁶. EB1 protein (*Xenopus laevis*) fused to GFP was expressed from a pET21a plasmid. FKBP- and FRB-ferritin, mCherry, eGFP and TPX2 recombinant proteins were produced in Rosetta(DE3)pLysS cells (Merck Millipore) by addition of IPTG (Sigma) and overnight expression. Purification of recombinant proteins was realized using standard his-tagged protein purification protocols.

Native gel retardation assay

After centrifugation (10^4 rpm, 5 minutes, 4°C), different concentrations of FRB-eGFP recombinant protein (15; 10; 5; 2,5; 1 μM) were incubated during 5 minutes at room temperature in presence of 10 μM of recombinant FKBP-ferritin (monomer concentration) and 20 μM of Rapamycin (Calbiochem), in PBS pH 7.4. In each condition, 100 ng of BSA (Bio-Rad) were added as loading control. The electrophoretic mobility of the complexes formed was assed using non-denaturing 7,5 % acrylamide gels (Bio-Rad) in CHES buffer pH 9.3. Protein mobility was first analysed by detecting the fluorescence of the eGFP fusion protein (Gel Doc XR+ System, Bio-Rad), followed by a coomassie staining for the visualization of the total protein pattern in the gel.

Bio-mineralisation of ferritins

The iron oxides nanoparticles were prepared as previously described⁶⁷. Briefly, purified FRB/FKBP-ferritins (24 μM) were mineralized at 65°C in 5 mM HEPES solution. Solution of Ammonium Iron (II) Sulfate hexahydrate was used as iron source. All solutions were degassed with argon and the pH was maintained dynamically at 8.5 using an automatic titrator (718, Titrator, Metrohm). Fe(II) was added to attain a loading factor of 3000 Fe per protein cage. The Fe(II) and H_2O_2 (3:1) were added simultaneously at constant rate of $15 \mu\text{L}\cdot\text{min}^{-1}$ using a syringe pump (Kd scientific). The reaction was considered complete 3 hours after addition of all iron and oxidant solutions. The mineralized sample was dialyzed overnight against 5 mM HEPES solutions.

Chimeric ferritin assembly and cluster formation

Proteins were first sonicated (5 minutes) and centrifuged (10^4 rpm, 5 minutes, 4°C) to remove aggregates. Proteins and Rapamycin were then mixed in HEPES buffer with

an incubation time of 5 minutes at room temperature. Single FRB-ferritins were labelled by dimerizing FKBP-mCherry to the nanocage in presence of Rapamycin with a ratio of 12:1 between monomers and mCherry. The ferritin clusters were formed by mixing FRB-ferritin, FKBP-ferritin, and FKBP-mCherry together with Rapamycin at a ratio of 24:5:2 between monomers and mCherry. Ferritin monomers and TPX2 were mixed at a ratio of 1:0.1 to 1:0.25.

Transmission electron microscopy

Transmission electron microscopy (TEM) was performed at 200 kV using a Jeol 2100 equipped with a LaB6 gun and a Jeol 2100 F with a field emission gun (FEG). Both microscopes had energy dispersive x-ray (EDX) detectors for analyzing chemical compositions. Samples were prepared on carbon-coated copper grids by placing 4 μ L drop solution containing the ferritin solution. On the LaB6-TEM, we studied samples deposited on carbon-coated copper grids negatively stained using an aqueous solution of uranyl acetate at 2% in mass. On the FEG-TEM, we studied samples deposited on carbon-coated copper grids without staining. Iron mineralization was studied by EDX spectra and maps acquired in scanning transmission electron microscopy (STEM).

Microtubule assembly

Microtubule structures were assembled using metaphase *Xenopus laevis* egg extracts, containing an ATP regenerating system (1 mM ATP, 10 mM creatine phosphate, 100 μ g/ μ L creatine phosphokinase, final concentrations), incubated in the presence of 500 nM of FKBP-TPX2 for 30 min at 19°C. Microtubules were labelled either with Rhodamin-labelled tubulin at 100 nM final (Cytoskeleton Inc.), fluorescein-labelled

tubulin at 100 nM final (Cytoskeleton Inc.), or EB1-GFP at 150 nM final. Microtubules were disrupted using nocodazole at a final concentration of 10 μ M.

Extract-in-Oil Droplet Formation

Cellular extract was encapsulated in droplets via water-in-oil emulsion process. Mineral oil contains a biocompatible block copolymer in order to stabilize emulsion and facilitate observations. This method has been previously described and allows the formation of microtubule asters in droplets⁵⁶. Preformed protein clusters mixed to the *Xenopus laevis* egg extracts containing fluorescently labelled tubulin were added to the block copolymer solution (1% (v CSF/v Oil)) at room temperature. The mixture was then gently sheared, by pipetting up and down the solution during few seconds, to generate extract-in-oil droplets. The mechanical dispersion of the biphasic solution formed micrometre-sized extract-in-oil droplets within few seconds. The emulsion was incubated for 20-30 minutes at 19°C.

Imaging and Data Analysis

Fluorescence imaging of microtubule asters was performed using an IX81 (Olympus) and X60 (PlanApo, NA 1,42) oil objective, equipped with an EM-CCD camera (electron multiplying CCD, C9100-02, Hamamatsu, Corporation), and a LED system of illumination (Spectra X, Lumencor). Microscope settings and functions were controlled using Simple PCI software (Hamamatsu). Image analysis was performed using Simple PCI and ImageJ. Confocal microscopy was performed with a Zeiss LSM 710 META laser scanning confocal microscope using X63 (PlanApochromatic, NA 1,4) objective. Image analysis was performed using LSM Software Zen 2009 and ImageJ. Student's t-tests and the interpretation of the p-values: NS means there is no

significant difference between the two distributions. One star means $p\text{value} < 0,05$, two stars means $p\text{value} < 0,01$, three stars means $p\text{value} < 0,001$.

Magnetic manipulation of structures

Two types of magnetic manipulations were done. First, a permanent NdFeB magnet (3 mm length, W-03-N Supermagnete, 0.8 T, $10^2 \text{ T}\cdot\text{m}^{-1}$) was placed next to oil droplets. Second, a magnetic tip was elongated from a guitar string leading to a radius of curvature of 25 μm . The tip was then adapted on the N-S axis of a NdFeB permanent magnet (3 mm length) and placed next to oil droplets using a manual micromanipulator (Narishige). With this system the gradient of magnetic field can reach $10^4 \text{ T}\cdot\text{m}^{-1}$ at the vicinity of the tip.

REFERENCES

1. Kirschner, M., Gerhart, J. & Mitchison, T. Molecular 'Vitalism'. *Cell* **100**, 79–88 (2000).
2. Karsenti, E. Self-organization in cell biology: a brief history. *Nat. Rev. Mol. Cell Biol.* **9**, 255–262 (2008).
3. Good, M. C., Zalatan, J. G. & Lim, W. A. Scaffold Proteins: Hubs for Controlling the Flow of Cellular Information. *Science (80-.)*. **332**, 680–686 (2011).
4. Wheeldon, I. *et al.* Substrate channelling as an approach to cascade reactions. *Nat. Chem.* **8**, 299–309 (2016).
5. Mammen, M., Choi, S.-K. & Whitesides, G. M. Polyvalent Interactions in Biological Systems: Implications for Design and Use of Multivalent Ligands and Inhibitors. *Angew. Chemie Int. Ed.* **37**, 2754–2794 (1998).
6. Whitesides, G. M. Self-Assembly at All Scales. *Science (80-.)*. **295**, 2418–2421 (2002).
7. Delebecque, C. J., Lindner, A. B., Silver, P. A. & Aldaye, F. A. Organization of Intracellular Reactions with Rationally Designed RNA Assemblies. *Science (80-.)*. **333**, 470–474 (2011).
8. Jordan, P. C. *et al.* Self-assembling biomolecular catalysts for hydrogen production. *Nat. Chem.* 1–7 (2015). doi:10.1038/nchem.2416
9. Derr, N. D. *et al.* Tug-of-War in Motor Protein Ensembles Revealed with a Programmable DNA Origami Scaffold. *Science (80-.)*. **338**, 662–665 (2012).
10. Hariadi, R. F. *et al.* Mechanical coordination in motor ensembles revealed using engineered artificial myosin filaments. *Nat. Nanotechnol.* **10**, 696–700 (2015).
11. Iwaki, M., Wickham, S. F., Ikezaki, K., Yanagida, T. & Shih, W. M. A programmable DNA origami nanospring that reveals force-induced adjacent binding of myosin VI heads. *Nat. Commun.* **7**, 13715 (2016).
12. Krishnan, Y. & Bathe, M. Designer nucleic acids to probe and program the cell. *Trends in Cell Biology* **22**, 624–633 (2012).
13. Bhatia, D. *et al.* Quantum dot-loaded monofunctionalized DNA icosahedra for single-particle tracking of endocytic pathways. *Nat. Nanotechnol.* **11**, 1112–1119 (2016).
14. Diehl, M. R. Engineering Cooperativity in Biomotor-Protein Assemblies. *Science (80-.)*. **311**, 1468–1471 (2006).
15. Dueber, J. E. *et al.* Synthetic protein scaffolds provide modular control over metabolic flux. *Nat. Biotechnol.* **27**, 753–759 (2009).
16. Dueber, J. E., Mirsky, E. a & Lim, W. a. Engineering synthetic signaling proteins with ultrasensitive input/output control. *Nat. Biotechnol.* **25**, 660–662 (2007).
17. Grünberg, R. & Serrano, L. Strategies for protein synthetic biology. *Nucleic Acids Res.* **38**, 2663–2675 (2010).
18. Colin, A., Bonnemay, L., Gayraud, C., Gautier, J. & Gueroui, Z. Triggering signaling pathways using F-actin self-organization. *Sci. Rep.* **6**, 34657 (2016).
19. Zhang, J., Li, X. & Li, X. Stimuli-triggered structural engineering of synthetic and biological polymeric assemblies. *Prog. Polym. Sci.* **37**, 1130–1176 (2012).

20. Dobson, J. Remote control of cellular behaviour with magnetic nanoparticles. *Nat. Nanotechnol.* **3**, 139–143 (2008).
21. Hoffmann, C. *et al.* Spatiotemporal control of microtubule nucleation and assembly using magnetic nanoparticles. *Nat. Nanotechnol.* **8**, 199–205 (2013).
22. Bonnemay, L., Hoffmann, C. & Gueroui, Z. Remote control of signaling pathways using magnetic nanoparticles. *Wiley Interdiscip. Rev. Nanomedicine Nanobiotechnology* **7**, 342–354 (2015).
23. Liu, A. P. Biophysical Tools for Cellular and Subcellular Mechanical Actuation of Cell Signaling. *Biophysical Journal* **111**, 1112–1118 (2016).
24. Etoc, F. *et al.* Subcellular control of Rac-GTPase signalling by magnetogenetic manipulation inside living cells. *Nat. Nanotechnol.* **8**, 193–198 (2013).
25. Cho, M. H. *et al.* A magnetic switch for the control of cell death signalling in in vitro and in vivo systems. *Nat. Mater.* **11**, 1038–1043 (2012).
26. Seo, D. *et al.* A mechanogenetic toolkit for interrogating cell signaling in space and time. *Cell* **165**, 1507–1518 (2016).
27. Bornens, M. Organelle positioning and cell polarity. *Nat. Rev. Mol. Cell Biol.* **9**, 874–886 (2008).
28. Fu, J., Hagan, I. M. & Glover, D. M. The Centrosome and Its Duplication Cycle. *Cold Spring Harb. Perspect. Biol.* **7**, a015800 (2015).
29. Harrison, P. M. & Arosio, P. The ferritins: Molecular properties, iron storage function and cellular regulation. *Biochimica et Biophysica Acta - Bioenergetics* **1275**, 161–203 (1996).
30. Kostianen, M. A., Kasyutich, O., Cornelissen, J. J. L. M. & Nolte, R. J. M. Self-assembly and optically triggered disassembly of hierarchical dendron-virus complexes. *Nat. Chem.* **2**, 394–399 (2010).
31. Kostianen, M. A. *et al.* Electrostatic assembly of binary nanoparticle superlattices using protein cages. *Nat Nanotechnol* **8**, 52–56 (2013).
32. Huard, D. J. E., Kane, K. M. & Tezcan, F. A. Re-engineering protein interfaces yields copper-inducible ferritin cage assembly. *Nat. Chem. Biol.* **9**, 169–176 (2013).
33. Kostianen, M. A. *et al.* Hierarchical self-assembly and optical disassembly for controlled switching of magnetoferritin nanoparticle magnetism. *ACS Nano* **5**, 6394–6402 (2011).
34. Men, D. *et al.* Self-Assembly of Ferritin Nanoparticles into an Enzyme Nanocomposite with Tunable Size for Ultrasensitive Immunoassay. *ACS Nano* **9**, 10852–10860 (2015).
35. Bellapadrona, G. & Elbaum, M. Supramolecular protein assemblies in the nucleus of human cells. *Angew. Chemie - Int. Ed.* **53**, 1534–1537 (2014).
36. Cormode, D. P., Jarzyna, P. A., Mulder, W. J. M. & Fayad, Z. A. Modified natural nanoparticles as contrast agents for medical imaging. *Advanced Drug Delivery Reviews* **62**, 329–338 (2010).
37. Wang, Q., Mercogliano, C. P. & Löwe, J. A ferritin-based label for cellular electron cryotomography. *Structure* **19**, 147–154 (2011).
38. Fan, K. *et al.* Magnetoferritin nanoparticles for targeting and visualizing tumour tissues. *Nat. Nanotechnol.* **7**, 459–464 (2012).
39. Fantechi, E. *et al.* A smart platform for hyperthermia application in cancer treatment: Cobalt-doped ferrite nanoparticles mineralized in human ferritin cages. *ACS Nano* **8**, 4705–4719 (2014).
40. Hwang, M. P., Lee, J. W., Lee, K. E. & Lee, K. H. Think modular: A simple

- apoferritin-based platform for the multifaceted detection of pancreatic cancer. *ACS Nano* **7**, 8167–8174 (2013).
41. Vande Velde, G. *et al.* Evaluation of the specificity and sensitivity of ferritin as an MRI reporter gene in the mouse brain using lentiviral and adeno-associated viral vectors. *Gene Ther.* **18**, 594–605 (2011).
 42. He, D. & Marles-Wright, J. Ferritin family proteins and their use in bionanotechnology. *New Biotechnology* **32**, 651–657 (2015).
 43. Stanley, S. A. *et al.* Radio-Wave Heating of Iron Oxide Nanoparticles Can Regulate Plasma Glucose in Mice. *Science (80-.)*. **336**, 604–608 (2012).
 44. Derose, R., Miyamoto, T. & Inoue, T. Manipulating signaling at will: Chemically-inducible dimerization (CID) techniques resolve problems in cell biology. *Pflugers Archiv European Journal of Physiology* **465**, 409–417 (2013).
 45. Fegan, A., White, B., Carlson, J. C. T. & Wagner, C. R. Chemically Controlled Protein Assembly: Techniques and Applications. *Chem. Rev.* **110**, 3315–3336 (2010).
 46. Ross, B., Mehta, S. & Zhang, J. Molecular tools for acute spatiotemporal manipulation of signal transduction. *Current Opinion in Chemical Biology* **34**, 135–142 (2016).
 47. Meldrum, F., Heywood, B. & Mann, S. Magnetoferritin: in vitro synthesis of a novel magnetic protein. *Science (80-.)*. **257**, 522–523 (1992).
 48. Wong, K. K. W., Douglas, T., Gider, S., Awschalom, D. D. & Mann, S. Biomimetic synthesis and characterization of magnetic proteins (magnetoferritin). *Chem. Mater.* **10**, 279–285 (1998).
 49. Uchida, M., Kang, S., Reichhardt, C., Harlen, K. & Douglas, T. The ferritin superfamily: Supramolecular templates for materials synthesis. *Biochimica et Biophysica Acta - General Subjects* **1800**, 834–845 (2010).
 50. Desai, A., Murray, A., Mitchison, T. & Walczak, C. E. in *Methods in cell biology* **61**, 385–412 (1998).
 51. Nguyen, P. a. *et al.* Spatial organization of cytokinesis signaling reconstituted in a cell-free system. *Science (80-.)*. **346**, 244–247 (2014).
 52. Gaetz, J., Gueroui, Z., Libchaber, A. & Kapoor, T. M. Examining how the spatial organization of chromatin signals influences metaphase spindle assembly. *Nat. Cell Biol.* **8**, 924–932 (2006).
 53. Athale, C. A. *et al.* Regulation of Microtubule Dynamics by Reaction Cascades Around Chromosomes. *Science (80-.)*. **322**, 1243–1247 (2008).
 54. Banaszynski, L. A., Liu, C. W. & Wandless, T. J. Characterization of the FKBP-rapamycin-FRB ternary complex. *J. Am. Chem. Soc.* **127**, 4715–4721 (2005).
 55. Wittmann, T., Wilm, M., Karsenti, E. & Vernos, I. TPX2, a novel *Xenopus* MAP involved in spindle pole organization. *J. Cell Biol.* **149**, 1405–1418 (2000).
 56. Pinot, M. *et al.* Effects of Confinement on the Self-Organization of Microtubules and Motors. *Curr. Biol.* **19**, 954–960 (2009).
 57. Vignaud, T., Blanchoin, L. & Théry, M. Directed cytoskeleton self-organization. *Trends Cell Biol.* **22**, 671–682 (2012).
 58. Letort, G., Nedelec, F., Blanchoin, L. & Théry, M. Centrosome centering and decentering by microtubule network rearrangement. *Mol. Biol. Cell* **27**, 2833–2843 (2016).
 59. Gao, J., Gu, H. & Xu, B. Multifunctional Magnetic Nanoparticles: Design, Synthesis, and Biomedical Applications. *Acc. Chem. Res.* **42**, 1097–1107

- (2009).
60. Hughes, J. H. & Kumar, S. Synthetic mechanobiology: Engineering cellular force generation and signaling. *Current Opinion in Biotechnology* **40**, 82–89 (2016).
 61. Fayol, D. *et al.* Use of Magnetic Forces to Promote Stem Cell Aggregation During Differentiation, and Cartilage Tissue Modeling. *Adv. Mater.* **25**, 2611–2616 (2013).
 62. van Bergeijk, P., Hoogenraad, C. C. & Kapitein, L. C. Right Time, Right Place: Probing the Functions of Organelle Positioning. *Trends in Cell Biology* **26**, 121–134 (2016).
 63. Meister, M. Physical limits to magnetogenetics. *Elife* **5**, 589–599 (2016).
 64. Hannak, E. & Heald, R. Investigating mitotic spindle assembly and function in vitro using *Xenopus laevis* egg extracts. *Nat. Protoc.* **1**, 2305–2314 (2006).
 65. Matias, P. M., Tatur, J., Carrondo, M. A. & Hagen, W. R. Crystallization and preliminary X-ray characterization of a ferritin from the hyperthermophilic archaeon and anaerobe *Pyrococcus furiosus*. *Acta Crystallogr. Sect. F Struct. Biol. Cryst. Commun.* **61**, 503–506 (2005).
 66. Schatz, C. A. Importin alpha-regulated nucleation of microtubules by TPX2. *EMBO J.* **22**, 2060–2070 (2003).
 67. Uchida, M. *et al.* Targeting of cancer cells with ferrimagnetic ferritin cage nanoparticles. *J. Am. Chem. Soc.* **128**, 16626–16633 (2006).

Authors' contributions

R.D, WA.W, and M.GJ.N contributed equally to this work. R.D, WA.W, M.GJ.N, F.G and Z.G conceived and designed the experiments. R.D, WA.W, M.GJ.N, A.C, and N.D performed and analysed the experiments. F.G and JM.G contributed materials/analysis tools and performed TEM experiments. J.G. contributed materials/analysis tools. M.GJ.N, R.D, A.C, WA.W, and Z.G wrote the manuscript and all authors commented on it.

Acknowledgements

We acknowledge L.Jullien, C.Chaneac, D.Portehault, A.Gautier, C.Tribet, and the members of the Biophysical Chemistry group of ENS for fruitful discussions. We thank A.G. Tebo for reading carefully the manuscript. The authors also thank M.Thery and J.Sillibourne for kindly providing purified centrosomes, and S. Rudiuk for initial experiments using AFM. WA.W and A.C were supported by a “Ministère de la Recherche” predoctoral fellowship. This work was supported by the CNRS, the ANR (Nanoheater), ARC (PDF20130606991) for R.D, FRM (ING20150532742) for M.GJ.N, and Ecole Normale Supérieure.

Competing financial interests: The authors declare no competing financial interests.

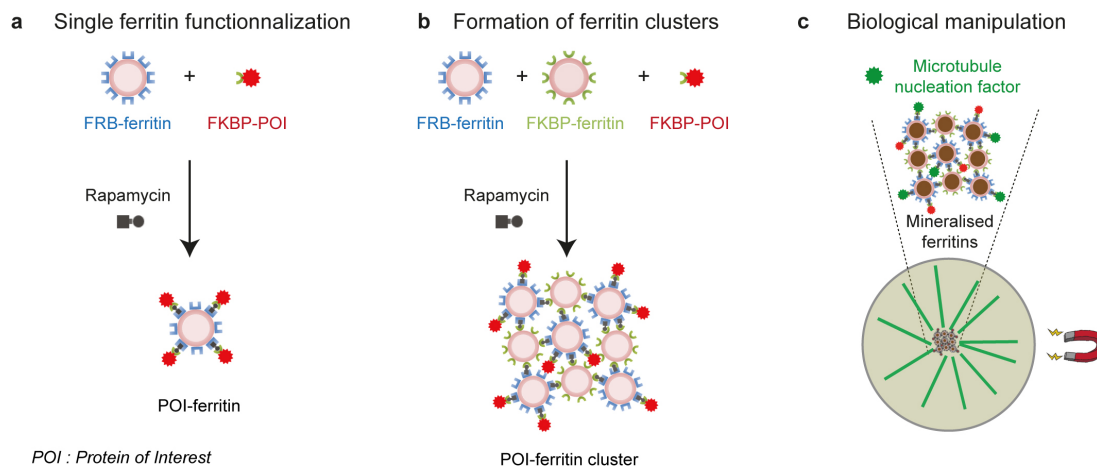


Figure 1 Genetically encoded protein scaffolds with modular biochemical and magnetic functions

a, b, Schematic of the modular approach to functionalize and organize ferritin nanocages. **a,** Chemically inducible dimerization strategy based on the heterodimerization of FKBP and FRB is used to target a protein of interest (POI) at the surface of the ferritin nanocages by addition of Rapamycin. **b,** The formation of ferritin clusters is triggered by multimeric interactions between FKBP- and FRB-ferritins in presence of Rapamycin. **c,** Illustration of the functionalization and magnetic manipulation of biomineralised ferritin clusters to control a microtubule assembly in space and time.

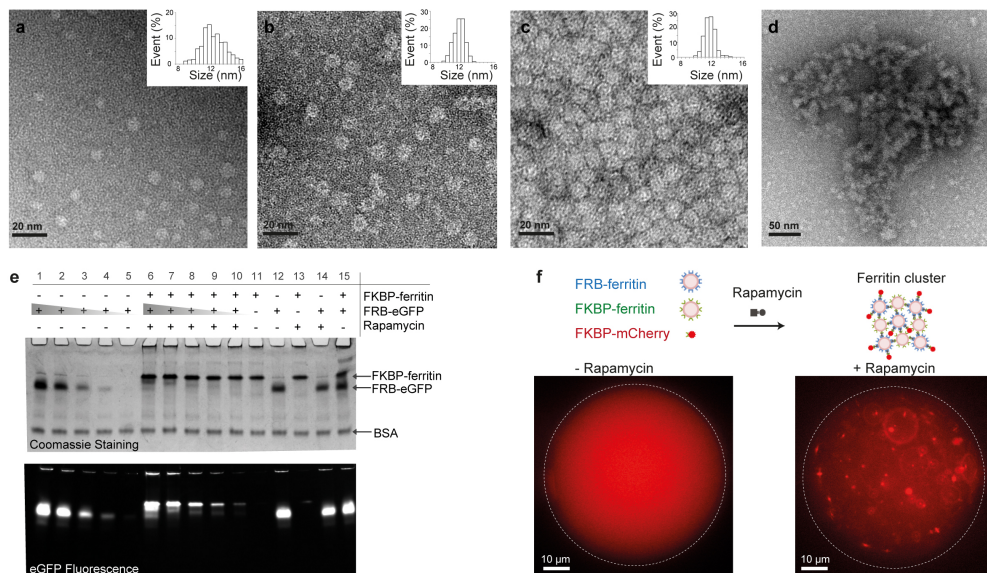


Figure 2 Characterisation of ferritin assemblies and biofunctionalisation

a-d, Transmission electron microscopy of negatively stained (a) FRB-ferritins, (b) FKBP-ferritins, (c) native ferritins, and (d) ferritin clusters (inserts: size distribution histograms). **e**, Acrylamide gel electrophoresis of FKBP-ferritins, FRB-eGFP proteins, and eGFP-ferritin complexes. From lane 11 to 15, 10 μM of FRB-eGFP and 10 μM of FKBP-ferritin migrate freely, in absence (lanes 11, 12 and 15) or presence (lanes 13 and 14) of 20 μM of Rapamycin. On lanes 1 to 5, the monomeric profile of 15 - 10 - 5 - 2.5 - 1 μM of FRB-eGFP is assessed in presence of Rapamycin. On lanes 6 to 10, according to the initial stoichiometry, the migration FRB-eGFP is retarded in presence of Rapamycin and 10 μM of FKBP-ferritin. In each well, BSA was added as loading control. **f**, Schematic of ferritin cluster formation (top). Fluorescence images of a water droplet containing FRB-ferritins, FKBP-ferritins, and FKBP-mCherry (left). The ferritin clusters are formed in presence of Rapamycin (right).

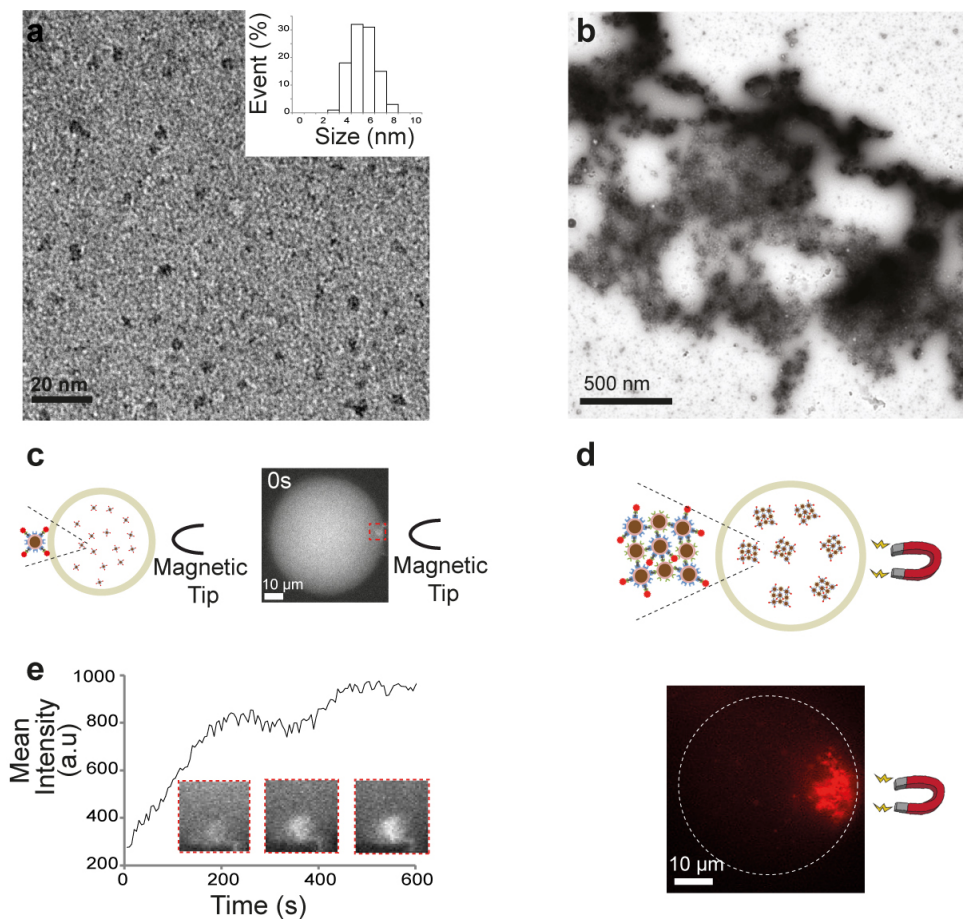


Figure 3 Characterisation and magnetic manipulation of biom mineralised ferritins

a, b, TEM images of mineralized FRB-ferritins and ferritin clusters (negative staining). Monodisperse iron oxide nanoparticles are shown in (a). The addition of Rapamycin and FKBP-ferritins into the FRB-ferritin solution causes the assembly of proteins nanocages to form micrometer-sized structures (b). **c, d,** Fluorescence images of mineralized FRB-ferritins and ferritin clusters. The nanocages were labelled with FKBP-mCherry for fluorescence visualization within droplets of water dispersed within mineral oil (see schematic). Magnetic forces were induced by (c) a magnetic tip for focusing the gradient of forces, or (d) a permanent magnet for a long-range attraction of the clusters. **e,** Mean fluorescence intensity as a function of time at the vicinity of the magnetic tip showing the local recruitment of single ferritins.

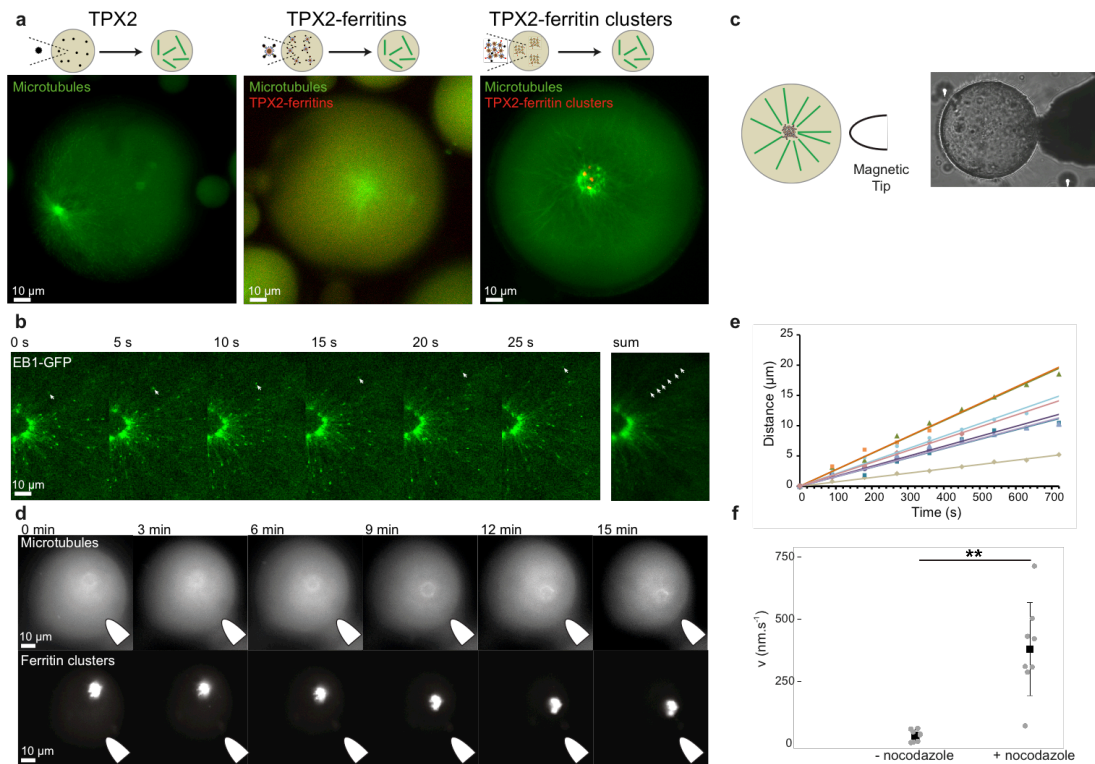


Figure 4 Nucleation and spatiotemporal manipulation of microtubule assemblies upon magnetic actuation.

a, Confocal observation of microtubule polymerization induced by FKBP-TPX2 in a droplet of *Xenopus* egg extract. Microtubules and ferritins are labelled with fluorescein-labelled tubulin and mCherry, respectively. From the left to right, microtubule structures triggered with FKBP-TPX2, mCherry/TPX2-ferritins, and ferritin-TPX2 clusters. **b**, Time-lapse of microtubule growth polymerizing from an aster triggered by ferritin-clusters. EB1-GFP is used as fluorescent reporter of the plus-end microtubule growing extremity. **c**, Schematic of the magnetic control experiment (left). Bright-field observation of the magnetic tip positioned next to an egg extract droplet (right). **d**, Representative time-points of the dynamic of an aster centre upon magnetic field actuation. **e**, Example of the spatiotemporal dynamics of aster centres toward the gradient of magnetic field. **f**, Mean velocity of the asters attracted toward the magnet in absence and in presence of a microtubule-depolymerizing drug (nocodazole).

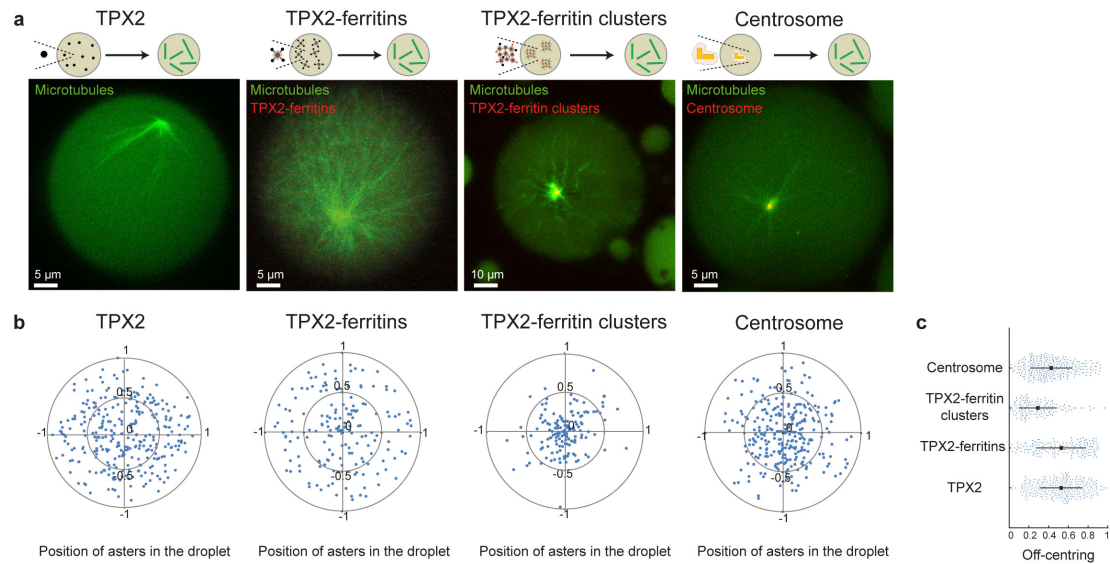


Figure 5 Ferritin Scaffolding mimics the Microtubule Organizing Centres of cells

a, Representative observations of microtubule aster organization triggered by FKBP-TPX2, TPX2-ferritin, TPX2 ferritin-clusters, and centrosomes. Microtubules and ferritins are labelled with fluorescein-labelled tubulin and mCherry, respectively. **b**, Geometrical positioning of asters nucleated by FKBP-TPX2, TPX2-ferritin, TPX2 ferritin-clusters, and centrosomes. 0 and ± 1 indicate the centre and the droplet boundary, respectively. **c**, Mean and standard deviation of the off-centring of the aster positions triggered by FKBP-TPX2, TPX2-ferritin, TPX2 ferritin-clusters, and centrosomes.

Appendix B

Protocol for RanQ69L and Utrophin-Ran purification

Day 0. Pre-culture

Do a pre-culture in 5 mL of LB with the plasmid and the corresponding antibiotics. Incubation overnight at 37°C.

Day 1. Culture and Induction

Dilute the pre-culture in 500 mL of LB with antibiotics and incubate at 37°C. Follow the Optical Density (O.D) regularly.

When O.D is between 0.6 and 0.8, induction of the protein production with 0.5 mM IPTG. Incubation overnight at 18°C.

Day 2. Protein purification

Centrifugation of the bacteria at 4500 rpm for 20 minutes at 4°C.

Washing in cold PBS.

Centrifugation of the bacteria at 4500 rpm for 20 minutes at 4°C.

Re-suspension of the pellet in 10 mL of washing buffer (PBS pH = 7.4, 35 mM Imidazole, 150 mM NaCl, 2 mM MgCl₂, 10% glycerol) + 1 mg lysozyme + 1 mM AEBSF + protease inhibitors

Incubation 30 minutes at 4°C.

Sonication: 10 cycles of 2 seconds with 10 seconds interval with 20 % amplitude.

Make the solution go through a 23G needle to do a mechanical breaking.

Centrifugation at 10000 rpm for 30 minutes at 4°C.

The next steps should be done in a cold room.

Washing of the beads 3 times: centrifugation of 2 minutes at 2000 rpm, rinse with 1 mL of washing buffer, incubation 3 minutes with agitation.

Incubation of the supernatant of the bacteria with the beads during 2 hours on the wheel at 4°C.

Centrifugation at 2000 rpm for 2 minutes.

Washing of the beads associated with the proteins 3 times: 10 mL of washing buffer, 3 minutes incubation on the wheel, centrifugation 2 minutes at 2000 rpm.

Addition of the elution buffer (washing buffer complemented with 500 mM of Imidazole).

Incubation for 15 minutes on the wheel at 4°C.

Put the beads associated with the protein in an elution column.

Elution by fractions of 500 μ L.

Estimation of the protein concentration with a BCA quantitative analysis.

Conservation of the most concentrated fractions.

Addition of 5 mM EDTA, 1 mM DTT, and 100 times of the protein concentration in GTP. Incubation for 40 minutes on ice.

Addition of 50 mM MgCl₂

Dialysis against 1 L of XB1 buffer (140 mM NaCl, 1.5 mM Na₂HPO₄, 50 mM HEPES) for 1 hour and then overnight at 4°C.

Day 3. Concentration and aliquots

Dialysis against 1 L of XB1 buffer for 1 hour at 4°C.

Gels: one verification gel with the supernatants kept at the various steps of the purification. One quantification gel with a BSA ladder.

If needed concentration on columns with centrifugation.

Addition of 10% glycerol and GTP at 100 times of the protein concentration.

Flash-freezing of the aliquots in liquid nitrogen and conservation at -80°C.

Bibliography

- [1] Eric Karsenti. Self-organization in cell biology: a brief history. *Nature reviews. Molecular cell biology*, 9(March):255–262, 2008.
- [2] Laurent Blanchoin, Rajaa Boujemaa-Paterski, Cécile Sykes, and Julie Plastino. Actin dynamics, architecture, and mechanics in cell motility. *Physiological reviews*, 94(1):235–63, 2014.
- [3] Thomas D Pollard and John a Cooper. Actin, a central player in cell shape and movement. *Science (New York, N.Y.)*, 326(5957):1208–1212, nov 2009.
- [4] Alphée Michelot, Julien Berro, Christophe Guérin, Rajaa Boujemaa-Paterski, Christopher J. Staiger, Jean Louis Martiel, and Laurent Blanchoin. Actin-Filament Stochastic Dynamics Mediated by ADF/Cofilin. *Current Biology*, 17(10):825–833, 2007.
- [5] Aditya S. Paul and Thomas D. Pollard. Review of the mechanism of processive actin filament elongation by formins. *Cell Motility and the Cytoskeleton*, 66(8):606–617, 2009.
- [6] Antoine Jegou, Marie-France Carlier, and Guillaume Romet-Lemonne. Formin mDia1 senses and generates mechanical forces on actin filaments. *Nature Communications*, 4(May):1883, 2013.
- [7] R D Mullins, J a Heuser, and T D Pollard. The interaction of Arp2/3 complex with actin: nucleation, high affinity pointed end capping, and formation of branching networks of filaments. *Proceedings of the National Academy of Sciences of the United States of America*, 95(11):6181–6, may 1998.
- [8] Thomas D. Pollard and Gary G. Borisy. Cellular motility driven by assembly and disassembly of actin filaments. *Cell*, 112(4):453–465, 2003.
- [9] Timothy J. Mitchison and Marc Kirschner. Dynamic instability of microtubule growth. *Nature*, 312(15):237–242, 1984.
- [10] Cecilia Conde and Alfredo Cáceres. Microtubule assembly, organization and dynamics in axons and dendrites. *Nature reviews. Neuroscience*, 10(5):319–332, 2009.
- [11] Timothy J. Mitchison and Marc Kirschner. Microtubule assembly nucleated by isolated centrosomes. *Nature*, 312(15):232–237, 1984.
- [12] F J Nédélec, T Surrey, a C Maggs, and S Leibler. Self-organization of microtubules and motors. *Nature*, 389(6648):305–308, 1997.

- [13] Harold A. Fisk, Christopher P. Mattison, and Mark Winey. Centrosomes and tumour suppressors. *Current Opinion in Cell Biology*, 14(6):700–705, 2002.
- [14] Yixian Zheng, Wong Lie Wong, Bruce Alberts, and Timothy J Mitchison. Nucleation of microtubule assembly by a gamma-tubulin-containing ring complex. *Nature*, 378:578–583, 1995.
- [15] A. Ott, M. Magnasco, A. Simon, and A. Libchaber. Measurement of the persistence length of polymerized actin using fluorescence microscopy. *Physical Review E*, 48(3), 1993.
- [16] F. Gittes, B. Mickey, J. Nettleton, and J. Howard. Flexural rigidity of microtubules and actin filaments measured from thermal fluctuations in shape. *Journal of Cell Biology*, 120(4):923–934, 1993.
- [17] Charles S Peskin, Garrett M Odell, and George F Oster. Cellular Motions and Thermal Fluctuations: The Brownian Ratchet. *Biophysical journal*, 65(July):316–324, 1993.
- [18] Marileen Dogterom and Bernard Yurke. Measurement of the Force-Velocity Relation for Growing Microtubules. *Science*, 278(5339):856–860, 1997.
- [19] Alexander Mogilner and George Oster. The polymerization ratchet model explains the force-velocity relation for growing microtubules. *European Biophysics Journal*, 28(3):235–242, 1999.
- [20] Marcel E. Janson, Mathilde E. De Dood, and Marileen Dogterom. Dynamic instability of microtubules is regulated by force. *Journal of Cell Biology*, 161(6):1029–1034, 2003.
- [21] Liedewij Laan, Nenad Pavin, Julien Husson, Guillaume Romet-Lemonne, Martijn Van Duijn, Magdalena Preciado López, Ronald D. Vale, Frank Jülicher, Samara L. Reck-Peterson, and Marileen Dogterom. Cortical dynein controls microtubule dynamics to generate pulling forces that position microtubule asters. *Cell*, 148(3):502–514, 2012.
- [22] AJ Hudspeth. Integrating the active process of hair cells with cochlear function. *Nature reviews. Neuroscience*, 15(9):600–614, 2014.
- [23] Claudia Veigel and Christoph F. Schmidt. Moving into the cell: single-molecule studies of molecular motors in complex environments. *Nature Reviews Molecular Cell Biology*, 12(3):163–176, 2011.
- [24] F Verde, J-M Berrez, C Antony, and E Karsenti. Taxol-induced Microtubule Asters in Mitotic Extracts of Xenopus Eggs: Requirement for Phosphorylated Factors and Cytoplasmic Dynein. *The Journal of cell biology*, 112(6):1177–1187, 1991.
- [25] Poul M Bendix, Gijsje H Koenderink, Damien Cuvelier, Zvonimir Dogic, Bernard N Koeleman, William M Briehar, Christine M Field, L Mahadevan, and David a Weitz. A quantitative analysis of contractility in active cytoskeletal protein networks. *Biophysical journal*, 94(8):3126–3136, 2008.

- [26] A D Mehta, R S Rock, M Rief, J A Spudich, M S Mooseker, and R E Cheney. Myosin-V is a processive actin-based motor. *Nature*, 400(6744):590–593, 1999.
- [27] Melina Schuh. An actin-dependent mechanism for long-range vesicle transport. *Nature Cell Biology*, 13(12):1431–1436, 2011.
- [28] Noriyuki Kodera, Daisuke Yamamoto, Ryoki Ishikawa, and Toshio Ando. Video imaging of walking myosin V by high-speed atomic force microscopy. *Nature*, 468(7320):72–6, 2010.
- [29] J D Huang, S T Brady, B W Richards, D Stenolen, J H Resau, N G Copeland, and N a Jenkins. Direct interaction of microtubule- and actin-based transport motors. *Nature*, 397(6716):267–270, 1999.
- [30] Stephen L Rogers and Vladimir I Gelfand. Myosin cooperates with microtubule motors during organelle transport in melanophores. *Current Biology*, 8(3):161–164, 1998.
- [31] Valeria Levi, Anna S Serpinskaya, Enrico Gratton, and Vladimir Gelfand. Organelle transport along microtubules in *Xenopus* melanophores: evidence for cooperation between multiple motors. *Biophysical journal*, 90(1):318–27, 2006.
- [32] Kari L. Weber, Anna M. Sokac, Jonathan S. Berg, Richard E. Cheney, and William M. Bement. A microtubule-binding myosin required for nuclear anchoring and spindle assembly. *Nature*, 431(7006):325–329, 2004.
- [33] Sarah Woolner, Lori L. O’Brien, Christiane Wiese, and William M. Bement. Myosin-10 and actin filaments are essential for mitotic spindle function. *Journal of Cell Biology*, 182(1):77–88, 2008.
- [34] Mijung Kwon, Maria Bagonis, Gaudenz Danuser, and David Pellman. Direct Microtubule-Binding by Myosin-10 Orients Centrosomes toward Retraction Fibers and Subcortical Actin Clouds. *Developmental Cell*, 34(3):323–337, 2015.
- [35] Péter Lénárt, Christian P Bacher, Nathalie Daigle, Arthur R Hand, Roland Eils, Mark Terasaki, and Jan Ellenberg. A contractile nuclear actin network drives chromosome congression in oocytes. *Nature*, 436(7052):812–818, 2005.
- [36] Masashi Mori, Nilah Monnier, Nathalie Daigle, Mark Bathe, Jan Ellenberg, and Péter Lénárt. Intracellular transport by an anchored homogeneously contracting F-actin meshwork. *Current biology*, 21(7):606–11, apr 2011.
- [37] Masashi Mori, Kálmán Somogyi, Hiroshi Kondo, Nilah Monnier, Henning J. Falk, Pedro MacHado, Mark Bathe, François Nédélec, and Péter Lénárt. An Arp2/3 nucleated F-actin shell fragments nuclear membranes at nuclear envelope breakdown in starfish oocytes. *Current Biology*, 24:1421–1428, 2014.
- [38] Marileen Dogterom and Thomas Surrey. Microtubule organization in vitro. *Current Opinion in Cell Biology*, (25):23–29, 2013.
- [39] Peter J. Foster, Sebastian Furthauer, Michael J. Shelley, and Daniel J. Needleman. Active contraction of microtubule networks. *eLife*, 4(DECEMBER2015):1–21, 2015.

- [40] Clare M. Waterman-Storer, Arshad Desai, J. Chloe Bulinski, and E.D. Salmon. Fluorescent speckle microscopy, a method to visualize the dynamics of protein assemblies in living cells. *Current Biology*, 8(22):1227–S1, 1998.
- [41] Frank PL Lai, Malgorzata Szczodrak, Jennifer Block, Jan Faix, Dennis Breitsprecher, Hans G Mannherz, Theresia EB Stradal, Graham A Dunn, J Victor Small, and Klemens Rottner. Arp2/3 complex interactions and actin network turnover in lamellipodia. *The EMBO Journal*, 27(7):982–992, 2008.
- [42] T J Mitchison and E D Salmon. Mitosis: a history of division. *Nature cell biology*, 3(1):E17–21, 2001.
- [43] Martin Chalfie, Yuan Tu, Ghia Euskirchen, William W Ward, and Douglas C Prasher. Green Fluorescent Protein as a Marker for Gene Expression. *Science (New York, N.Y.)*, 263(5148):802–805, 1994.
- [44] Benjamin Leader, Hyunjung Lim, Mary Jo Carabatsos, Anne Harrington, Jeffrey Ecsedy, David Pellman, Richard Maas, and Philip Leder. Formin-2, polyploidy, hypofertility and positioning of the meiotic spindle in mouse oocytes. *Nature Cell Biology*, 4(12):921–928, 2002.
- [45] Julien Dumont, Karine Million, Kelsey Sunderland, Pascale Rassinier, Hyunjung Lim, Benjamin Leader, and Marie-Hélène Verlhac. Formin-2 is required for spindle migration and for the late steps of cytokinesis in mouse oocytes. *Developmental biology*, 301(1):254–65, jan 2007.
- [46] Manuel Théry, Victor Racine, Anne Pépin, Matthieu Piel, Yong Chen, Jean-Baptiste Sibarita, and Michel Bornens. The extracellular matrix guides the orientation of the cell division axis. *Nature cell biology*, 7(10):947–953, 2005.
- [47] Nicolas Minc, David Burgess, and Fred Chang. Influence of cell geometry on division-plane positioning. *Cell*, 144(3):414–426, 2011.
- [48] T P Loisel, R Boujemaa, D Pantaloni, and M F Carlier. Reconstitution of actin-based motility of *Listeria* and *Shigella* using pure proteins. *Nature*, 401(6753):613–616, 1999.
- [49] Lisa A. Cameron, Matthew J. Footer, Alexander van Oudenaarden, and Julie A. Theriot. Motility of ActA protein-coated microspheres driven by actin polymerization. *Proceedings of the National Academy of Sciences USA*, 96(9):4908–13, 1999.
- [50] Hakim Boukellal, Otger Campàs, Jean François Joanny, Jacques Prost, and Cécile Sykes. Soft *Listeria*: Actin-based propulsion of liquid drops. *Physical Review E - Statistical, Nonlinear, and Soft Matter Physics*, 69(6 1):3–6, 2004.
- [51] Vincent Delatour, Emmanuèle Helfer, Dominique Didry, Kim Hô Diêp Lê, Jean-François Gaucher, Marie-France Carlier, and Guillaume Romet-Lemonne. Arp2/3 Controls the Motile Behavior of N-WASP-Functionalized GUVs and Modulates N-WASP Surface Distribution by Mediating Transient Links with Actin Filaments. *Biophysical Journal*, 94(12):4890–4905, 2008.

- [52] T Surrey, F Nedelec, S Leibler, and E Karsenti. Physical properties determining self-organization of motors and microtubules. *Science (New York, N.Y.)*, 292(5519):1167–71, may 2001.
- [53] Francois Nedelec and Dietrich Foethke. Collective Langevin dynamics of flexible cytoskeletal fibers. *New Journal of Physics*, 9(427), 2007.
- [54] Guillaume Romet-Lemonne, Martijn VanDuijn, and Marileen Dogterom. Three-dimensional control of protein patterning in microfabricated devices. *Nano Letters*, 5(12):2350–2354, 2005.
- [55] Tsutomu Hamada and Kenichi Yoshikawa. Cell-Sized Liposomes and Droplets: Real-World Modeling of Living Cells. *Materials*, 5(11):2292–2305, 2012.
- [56] Shia-Yen Teh, Robert Lin, Lung-Hsin Hung, and Abraham P. Lee. Droplet microfluidics. *Lab on a Chip*, 8(2):198, 2008.
- [57] Sophie Pautot, Barbara J Frisken, and David a Weitz. Production of Unilamellar Vesicles Using an Inverted Emulsion. *Langmuir : the ACS journal of surfaces and colloids*, 19(10):2870–2879, 2003.
- [58] Martin Loose, Elisabeth Fischer-Friedrich, Jonas Ries, Karsten Kruse, and Petra Schwille. Spatial Regulators for Bacterial Cell Division Self-Organize into Surface Waves in Vitro. *Science*, 320(May):789–792, 2008.
- [59] J. Schweizer, M. Loose, M. Bonny, K. Kruse, I. Monch, and P. Schwille. Geometry sensing by self-organized protein patterns. *Proceedings of the National Academy of Sciences*, 109(38):15283–15288, 2012.
- [60] Anne-Cécile Reymann, Jean-Louis Martiel, Théo Cambier, Laurent Blanchoin, Rajaa Boujemaa-Paterski, and Manuel Théry. Nucleation geometry governs ordered actin networks structures. *Nature Materials*, 9(10):827–832, 2010.
- [61] Andrew D. Griffiths and Dan S. Tawfik. Miniaturising the laboratory in emulsion droplets. *Trends in Biotechnology*, 24(9):395–402, 2006.
- [62] V. Noireaux and A. Libchaber. A vesicle bioreactor as a step toward an artificial cell assembly. *Proceedings of the National Academy of Sciences*, 101(51):17669–17674, 2004.
- [63] Léa Laetitia Pontani, Jasper Van Der Gucht, Guillaume Salbreux, Julien Heuvingh, Jean François Joanny, and Cecile Sykes. Reconstitution of an actin cortex inside a liposome. *Biophysical Journal*, 96(1):192–198, 2009.
- [64] K Carvalho, F-C Tsai, E Lees, R Voituriez, Gijsje H. Koenderink, and C Sykes. Cell-sized liposomes reveal how actomyosin cortical tension drives shape change. *Proceedings of the National Academy of Sciences*, 110(41):16456–16461, 2013.
- [65] Laurent Limozin and Erich Sackmann. Polymorphism of cross-linked actin networks in giant vesicles. *Physical review letters*, 89(16):168103, 2002.

- [66] Makito Miyazaki, Masataka Chiba, Hiroki Eguchi, Takashi Ohki, and Shin'ichi Ishiwata. Cell-sized spherical confinement induces the spontaneous formation of contractile actomyosin rings in vitro. *Nature Cell Biology*, 17(4):480–489, 2015.
- [67] Michael Elbaum, Deborah Kuchnir Fygenson, and Albert Libchaber. Buckling Microtubules in Vesicles. *Physical Review Letters*, 76(21):4078–4081, 1996.
- [68] D. Kuchnir Fygenson, M. Elbaum, B. Shraiman, and A. Libchaber. Microtubules and vesicles under controlled tension. *Physical Review E*, 55(1):850–859, 1997.
- [69] T. E. Holy, M Dogterom, B Yurke, and S Leibler. Assembly and positioning of microtubule asters in microfabricated chambers. *Proceedings of the National Academy of Sciences of the United States of America*, 94(12):6228–6231, 1997.
- [70] Kwonmoo Lee, Jennifer L Gallop, Komal Rambani, and Marc Kirschner. Self-Assembly of Filopodia-Like Structures on Supported Lipid Bilayers. *Science*, 329:1341–1346, 2010.
- [71] Phuong A Nguyen, Aaron C Groen, Martin Loose, Keisuke Ishihara, Martin Wuhr, Christine M. Field, and Timothy J. Mitchison. Spatial organization of cytokinesis signaling reconstituted in a cell-free system. *Science*, 50(2012):244–247, 2014.
- [72] Jeremy B. Chang and James E. Ferrell Jr. Mitotic trigger waves and the spatial coordination of the *Xenopus* cell cycle. *Nature*, 500(7464):603–607, 2013.
- [73] Céline Hoffmann, Elsa Mazari, Charlie Gosse, Louise Bonnemay, Sarah Hostachy, Jérémie Gautier, and Zoher Gueroui. Magnetic control of protein spatial patterning to direct microtubule self-assembly. *ACS nano*, 7(11):9647–54, nov 2013.
- [74] M Pinot, F Chesnel, J Z Kubiak, I Arnal, F J Nedelec, and Z Gueroui. Effects of confinement on the self-organization of microtubules and motors. *Current biology*, 19(11):954–60, jun 2009.
- [75] Céline Hoffmann, Elsa Mazari, Sylvie Lallet, Roland Le Borgne, Valérie Marchi, Charlie Gosse, and Zoher Gueroui. Spatiotemporal control of microtubule nucleation and assembly using magnetic nanoparticles. *Nature nanotechnology*, 8(3):199–205, mar 2013.
- [76] L Bonnemay, S Hostachy, C Hoffmann, J Gautier, and Z Gueroui. Engineering spatial gradients of signaling proteins using magnetic nanoparticles. *Nano letters*, 13(11):5147–5152, nov 2013.
- [77] M. C. Good, M. D. Vahey, a. Skandarajah, D. a. Fletcher, and R. Heald. Cytoplasmic Volume Modulates Spindle Size During Embryogenesis. *Science*, 342:856–860, 2013.
- [78] J Hazel, K Krutkramelis, P Mooney, M Tomschik, K Gerow, J Oakey, and JC Gatlin. Changes in Cytoplasmic Volume Are sufficient to drive spindle scaling. *Science*, (November):853–856, 2013.
- [79] Martin Wühr, Yao Chen, Sophie Dumont, Aaron C. Groen, Daniel J. Needleman, Adrian Salic, and Timothy J. Mitchison. Evidence for an Upper Limit to Mitotic Spindle Length. *Current Biology*, 18:1256–1261, 2008.

- [80] Mathieu Pinot, Villier Steiner, Benoit Dehapiot, Byung-Kuk Yoo, Franck Chesnel, Laurent Blanchoin, Charles Kervrann, and Zoher Gueroui. Confinement induces actin flow in a meiotic cytoplasm. *Proceedings of the National Academy of Sciences of the United States of America*, 109(29):11705–10, jul 2012.
- [81] Enas Abu Shah and Kinneret Keren. Symmetry breaking in reconstituted actin cortices. *eLife*, 2014:1–15, 2014.
- [82] R Heald, R Tournebize, T Blank, R Sandaltzopoulos, P Becker, a Hyman, and E Karsenti. Self-organization of microtubules into bipolar spindles around artificial chromosomes in *Xenopus* egg extracts., 1996.
- [83] Andrew W. Grenfel, Magdalena Strzelecka, Marina E. Crowder, Kara J. Helmke, Anne Lore Schlaitz, and Rebecca Heald. A versatile multivariate image analysis pipeline reveals features of *Xenopus* extract spindles. *Journal of Cell Biology*, 213(1):127–136, 2016.
- [84] Eva Hannak and Rebecca Heald. Investigating mitotic spindle assembly and function in vitro using *Xenopus laevis* egg extracts. *Nature protocols*, 1(5):2305–2314, 2006.
- [85] Arshad Desai, Andrew Murray, T. Mitchison, and Claire E Walczak. The Use of *Xenopus* Egg Extracts to Study Mitotic Spindle Assembly and Function in Vitro. In *Methods in cell biology*, volume 61, chapter 20, pages 385–412. 1998.
- [86] Christine M Field, Martin Wühr, Graham a Anderson, Hao Yuan Kueh, Devin Strickland, and Timothy J Mitchison. Actin behavior in bulk cytoplasm is cell cycle regulated in early vertebrate embryos. *Journal of cell science*, 124(Pt 12):2086–2095, 2011.
- [87] C.M. Field, J.F. Pelletier, and T.J. Mitchison. *Xenopus* extract approaches to studying microtubule organization and signaling in cytokinesis. *Methods in Cell Biology*, 137:395–435, 2017.
- [88] Basarab G Hosu, Steven F Mullen, John K Critser, and Gabor Forgacs. Reversible disassembly of the actin cytoskeleton improves the survival rate and developmental competence of cryopreserved mouse oocytes. *PloS one*, 3(7):e2787, jan 2008.
- [89] T. Ebner, M. Moser, M Sommergruber, M. Puchner, R. Wiesinger, and G. Tews. Developmental competence of oocytes showing increased cytoplasmic viscosity. *Human Reproduction*, 18(6):1294–1298, jun 2003.
- [90] Livia Z. Yanez, Jinnuo Han, Barry B. Behr, Renee A. Reijo Pera, and David B. Camarillo. Human oocyte developmental potential is predicted by mechanical properties within hours after fertilization. *Nature Communications*, 7:10809, 2016.
- [91] Jessica Azoury, Karen W Lee, Virginie Georget, Pascale Rassinier, Benjamin Leader, and Marie-Hélène Verlhac. Spindle positioning in mouse oocytes relies on a dynamic meshwork of actin filaments. *Current Biology*, 18(19):1514–9, oct 2008.
- [92] Melina Schuh and Jan Ellenberg. A new model for asymmetric spindle positioning in mouse oocytes. *Current biology*, 18(24):1986–92, dec 2008.

- [93] Jessica Azoury, Karen Wingman Lee, Virginie Georget, Pascale Hikal, and Marie-Hélène Verlhac. Symmetry breaking in mouse oocytes requires transient F-actin meshwork destabilization. *Development (Cambridge, England)*, 138(14):2903–8, jul 2011.
- [94] Maria Almonacid, Wylie W. Ahmed, Matthias Bussonnier, Philippe Mailly, Timo Betz, Raphaël Voituriez, Nir S. Gov, and Marie-Hélène Verlhac. Active diffusion positions the nucleus in mouse oocytes. *Nature Cell Biology*, (August 2014), 2015.
- [95] Agathe Chaigne, Clément Campillo, Nir S Gov, Raphaël Voituriez, Jessica Azoury, Claudia Umaña-Diaz, Maria Almonacid, Isabelle Queguiner, Pierre Nassoy, Cécile Sykes, Marie-Hélène Verlhac, and Marie-Emilie Terret. A soft cortex is essential for asymmetric spindle positioning in mouse oocytes. *Nature cell biology*, 15(8):958–66, aug 2013.
- [96] Christine M. Field, Phuong a. Nguyen, Keisuke Ishihara, Aaron C. Groen, and Timothy J. Mitchison. Xenopus egg cytoplasm with intact actin. *Methods in Enzymology*, 540:399–415, 2014.
- [97] a M Jimenez, M Roché, M Pinot, P Panizza, L Courbin, and Z Gueroui. Towards high throughput production of artificial egg oocytes using microfluidics. *Lab on a chip*, 11:429–434, 2011.
- [98] Tharwat Tadros. Polymeric surfactants in disperse systems. *Advances in Colloid and Interface Science*, 147-148:281–299, 2009.
- [99] Tommaso Cavazza, Isabel Peset, and Isabelle Vernos. From meiosis to mitosis : the sperm centrosome defines the kinetics of spindle assembly after fertilization in Xenopus. *Journal of Cell Science*, 129(May):2538–2547, 2016.
- [100] Hellen C. Ishikawa-Ankerhold, Richard Ankerhold, and Gregor P C Drummen. Advanced fluorescence microscopy techniques-FRAP, FLIP, FLAP, FRET and FLIM. *Molecules*, 17(4):4047–4132, 2012.
- [101] Andrew Wilde and Yixian Zheng. Stimulation of microtubule aster formation and spindle assembly by the small GTPase Ran. *Science*, 284:1359–1362, 1999.
- [102] K E Sawin and T Mitchison. Mitotic spindle assembly by two different pathways in vitro. *J. Cell Biol.*, 112(5):925–940, 1991.
- [103] Peter J. Gillespie, Agnieszka Gambus, and J. Julian Blow. Preparation and use of Xenopus egg extracts to study DNA replication and chromatin associated proteins. *Methods*, 57(2):203–213, 2012.
- [104] Francesca Farina, Jérémie Gaillard, Christophe Guérin, Yohann Couté, James Silibourne, Laurent Blanchoin, and Manuel Théry. The centrosome is an actin-organizing centre. *Nature Cell Biology*, 18(1):65–75, 2016.
- [105] Christine M. Field and Péter Lénárt. Bulk cytoplasmic actin and its functions in meiosis and mitosis. *Current Biology*, 21:825–830, 2011.

- [106] Brian M. Burkel, George Von Dassow, and William M. Bement. Versatile fluorescent probes for actin filaments based on the actin-binding domain of utrophin. *Cell Motility and the Cytoskeleton*, 64(August):822–832, 2007.
- [107] A Hyman, D Drechsel, D Kellogg, S Salser, K Sawin, P Steffen, L Wordeman, and T Mitchison. Preparation of modified tubulins. *Methods in enzymology*, 196(1984):478–485, 1991.
- [108] C Manzo and M F Garcia-Parajo. A review of progress in single particle tracking: from methods to biophysical insights. *Rep Prog Phys*, 78(12):124601, 2015.
- [109] F Amblard, A.C Maggs, B Yurke, A.N Pargellis, and S Leibler. Subdiffusion and Anomalous Local Viscoelasticity in Actin Networks. *Physical Review Letters*, 77(21):4470–4473, 1996.
- [110] I. Y. Wong, M. L. Gardel, D. R. Reichman, Eric R. Weeks, M. T. Valentine, a. R. Bausch, and D. a. Weitz. Anomalous diffusion probes microstructure dynamics of entangled F-actin networks. *Physical Review Letters*, 92(17):178101–1, 2004.
- [111] a Caspi, R Granek, and M Elbaum. Enhanced diffusion in active intracellular transport. *Physical review letters*, 85:5655–5658, 2000.
- [112] Marina Feric and Clifford P Brangwynne. A nuclear F-actin scaffold stabilizes ribonucleoprotein droplets against gravity in large cells. *Nature cell biology*, 15(10):1253–9, 2013.
- [113] Nikta Fakhri, Alok D Wessel, Charlotte Willms, Matteo Pasquali, Dieter R Klopfenstein, Frederick C Mackintosh, and Christoph F Schmidt. High-resolution mapping of intracellular fluctuations using carbon nanotubes. *Science (New York, N.Y.)*, 344(6187):1031–1035, 2014.
- [114] M.T. Valentine, Z.E. Perlman, M.L. Gardel, J.H. Shin, P. Matsudaira, T.J. Mitchison, and D.A. Weitz. Colloid Surface Chemistry Critically Affects Multiple Particle Tracking Measurements of Biomaterials. *Biophysical Journal*, 86(6):4004–4014, 2004.
- [115] Fred Etoc. *Vers un contrôle magnétique de la polarité cellulaire*. PhD thesis, UPMC, 2013.
- [116] Jeremy Malinge, Fanny Mousseau, Drazen Zanchi, Geoffrey Brun, Christophe Tribet, and Emmanuelle Marie. Tailored stimuli-responsive interaction between particles adjusted by straightforward adsorption of mixed layers of Poly(lysine)-g-PEG and Poly(lysine)-g-PNIPAM on anionic beads. *Journal of Colloid and Interface Science*, 461:50–55, 2016.
- [117] P Greenspan, E P Mayer, and S D Fowler. Nile Red: a selective fluorescent stain for intracellular lipid droplets. *The Journal of Cell Biology*, 100(10):965–973, 1985.
- [118] Fabrice de Chaumont, Stéphane Dallongeville, Nicolas Chenouard, Nicolas Hervé, Sorin Pop, Thomas Provoost, Vannary Meas-Yedid, Praveen Pankajakshan, Timothée Lecomte, Yoann Le Montagner, Thibault Lagache, Alexandre Dufour, and Jean-Christophe Olivo-Marin. Icy: an open bioimage informatics platform for extended reproducible research. *Nature Methods*, 9(7):690–696, 2012.

- [119] Bruce Alberts, Alexander Johnson, Julian Lewis, David Morgan, Martin Raff, Keith Roberts, and Peter Walter. *Molecular Biology of the Cell, Sixth Edition*. Garland Science, 2015.
- [120] Guy C. Brown and Boris N. Kholodenko. Spatial gradients of cellular phosphoproteins. *FEBS Letters*, 457(3):452–454, 1999.
- [121] Clifford P Brangwynne, Christian R Eckmann, David S Courson, Agatha Rybarska, Carsten Hoege, Jöbin Gharakhani, Frank Jülicher, and Anthony A Hyman. Germline P granules are liquid droplets that localize by controlled dissolution/condensation. *Science*, 324(JUNE):1729–1732, 2009.
- [122] Jeffrey B Woodruff, Beatriz Ferreira Gomes, Per O Widlund, Julia Mahamid, and Anthony A Hyman. The centrosome is a selective phase that nucleates microtubules by concentrating tubulin. *Cell*, 169(6):1066–1077, 2017.
- [123] Piong Li, Sudeep Banjade, Hui-Chun Cheng, Soyeon Kim, Baoyu Chen, Liang Guo, Marc Llaguno, Javoris V. Hollingsworth, David S. King, Salman F. Banani, Paul S. Russo, Qiu-Xing Jiang, B. Tracy Nixon, and Michael K. Rosen. Phase transitions in the assembly of multivalent signalling proteins. *Nature*, 483:336–340, 2012.
- [124] Sudeep Banjade and Michael K. Rosen. Phase transitions of multivalent proteins can promote clustering of membrane receptors. *eLife*, 3:1–24, 2014.
- [125] C. Loverdo, O. Benichou, M. Moreau, and R. Voituriez. Enhanced reaction kinetics in biological cells. *Nature Physics*, 4(February):134–137, 2008.
- [126] John E Dueber, Ethan a Mirsky, and Wendell a Lim. Engineering synthetic signaling proteins with ultrasensitive input/output control. *Nature biotechnology*, 25(6):660–662, 2007.
- [127] Gabor Forgacs, Soon Hyung Yook, Paul a Janmey, Hawoong Jeong, and Christopher G Burd. Role of the cytoskeleton in signaling networks. *Journal of cell science*, 117:2769–2775, 2004.
- [128] Silvia Valensin, Silvia Rossi Paccani, Cristina Ulivieri, David Mercati, Sonia Pacini, Laura Patrussi, Tim Hirst, Pietro Lupetti, and Cosima T. Baldari. F-actin dynamics control segregation of the TCR signaling cascade to clustered lipid rafts. *European Journal of Immunology*, 32(2):435–446, 2002.
- [129] Y. Yu, A. A. Smoligovets, and J. T. Groves. Modulation of T cell signaling by the actin cytoskeleton. *Journal of Cell Science*, 126(5):1049–1058, 2013.
- [130] A. Chaudhuri, B. Bhattacharya, K. Gowrishankar, S. Mayor, and M. Rao. Spatiotemporal regulation of chemical reactions by active cytoskeletal remodeling. *Proceedings of the National Academy of Sciences*, 108(36):14825–14830, 2011.
- [131] Kripa Gowrishankar, Subhasri Ghosh, Suvrajit Saha, C. Rumamol, Satyajit Mayor, and Madan Rao. Active remodeling of cortical actin regulates spatiotemporal organization of cell surface molecules. *Cell*, 149(6):1353–1367, 2012.

- [132] James E Ferrell Jr and Sang Hoon Ha. Ultrasensitivity part I : Michaelian responses and zero-order ultrasensitivity. *Trends in Biochemical Sciences*, 39(10):496–503, 2014.
- [133] Boris N Kholodenko. Cell-signalling dynamics in time and space. *Nature reviews. Molecular cell biology*, 7(3):165–176, 2006.
- [134] Maïwen Caudron, Gertrude Bunt, Philippe Bastiaens, and Eric Karsenti. Spatial coordination of spindle assembly by chromosome-mediated signaling gradients. *Science (New York, N.Y.)*, 309(5739):1373–1376, aug 2005.
- [135] Petr Kalab and Rebecca Heald. The RanGTP gradient - a GPS for the mitotic spindle. *Journal of cell science*, 121:1577–1586, 2008.
- [136] David T. Miyamoto, Zachary E. Perlman, Kendra S. Burbank, Aaron C. Groen, and Timothy J. Mitchison. The kinesin Eg5 drives poleward microtubule flux in *Xenopus laevis* egg extract spindles. *Journal of Cell Biology*, 167(5):813–818, 2004.
- [137] Jesse C. Gatlin, Alexandre Matov, Aaron C. Groen, Daniel J. Needleman, Thomas J. Maresca, Gaudenz Danuser, Timothy J. Mitchison, and E. D. Salmon. Spindle Fusion Requires Dynein-Mediated Sliding of Oppositely Oriented Microtubules. *Current Biology*, 19:287–296, 2009.
- [138] Shang Cai, Lesley N Weaver, Stephanie C Ems-McClung, and Claire E Walczak. Kinesin-14 Family Proteins HSET/XCTK2 Control Spindle Length by Cross-Linking and Sliding Microtubules. *Molecular Biology of the Cell*, 20:1348–1359, 2009.
- [139] Chaitanya A Athale, Ana Dinarina, Maria Mora-Coral, Céline Pugieux, Francois Nedelec, and Eric Karsenti. Regulation of microtubule dynamics by reaction cascades around chromosomes. *Science (New York, N.Y.)*, 322(5905):1243–7, dec 2008.
- [140] Jan Brugués, Valeria Nuzzo, Eric Mazur, and Daniel J. Needleman. Nucleation and transport organize microtubules in metaphase spindles. *Cell*, 149(3):554–564, 2012.
- [141] Jun Takagi, Takeshi Itabashi, Kazuya Suzuki, Tarun M Kapoor, Yuta Shimamoto, and Shin’ichi Ishiwata. Using micromanipulation to analyze control of vertebrate meiotic spindle size. *Cell reports*, 5(1):44–50, 2013.
- [142] Oliver J. Gruss, Rafael E. Carazo-Salas, Christoph A. Schatz, Giulia Guarguaglini, Jürgen Kast, Matthias Wilm, Nathalie Le Bot, Isabelle Vernos, Eric Karsenti, and Iain W. Mattaj. Ran induces spindle assembly by reversing the inhibitory effect of importin α on TPX2 activity. *Cell*, 104(1):83–93, 2001.
- [143] Simone B Reber, Johannes Baumgart, Per O Widlund, Andrei Pozniakovsky, Jonathon Howard, Anthony a Hyman, and Frank Jülicher. XMAP215 activity sets spindle length by controlling the total mass of spindle microtubules. *Nat. Cell Biol.*, 15(9):1116–22, 2013.
- [144] Kara J. Helmke and Rebecca Heald. TPX2 levels modulate meiotic spindle size and architecture in *Xenopus* egg extracts. *Journal of Cell Biology*, 206(3):385–393, 2014.

- [145] Jedidiah Gaetz, Zoher Gueroui, Albert Libchaber, and Tarun M. Kapoor. Examining how the spatial organization of chromatin signals influences metaphase spindle assembly. *Nature Cell Biology*, 8(9):924–932, 2006.
- [146] Ana Dinarina, Céline Pugieux, Maria Mora Corral, Martin Loose, Joachim Spatz, Eric Karsenti, and François Nédélec. Chromatin Shapes the Mitotic Spindle. *Cell*, 138(3):502–513, 2009.
- [147] Manuel Théry and Michel Bornens. Cell shape and cell division. *Current Opinion in Cell Biology*, 18(6):648–657, 2006.
- [148] OscarM Lancaster, Maël LeBerre, Andrea Dimitracopoulos, Daria Bonazzi, Ewa Zlotek-Zlotkiewicz, Remigio Picone, Thomas Duke, Matthieu Piel, and Buzz Baum. Mitotic Rounding Alters Cell Geometry to Ensure Efficient Bipolar Spindle Formation. *Developmental Cell*, 25(3):270–283, 2013.
- [149] Jessica G. Bermudez, Hui Chen, Lily C. Einstein, and Matthew C. Good. Probing the biology of cell boundary conditions through confinement of *Xenopus* cell-free cytoplasmic extracts. *Genesis*, 55(1-2):e23013, 2017.
- [150] Pablo Fernandez, Matthias Maier, Martina Lindauer, Christian Kuffer, Zuzana Storchova, and Andreas R. Bausch. Mitotic spindle orients perpendicular to the forces imposed by dynamic shear. *PLoS ONE*, 6(12), 2011.
- [151] Jenny Fink, Nicolas Carpi, Timo Betz, Angelique Bétard, Meriem Chebah, Ammar Azioune, Michel Bornens, Cecile Sykes, Luc Fetler, Damien Cuvelier, and Matthieu Piel. External forces control mitotic spindle positioning. *Nature cell biology*, 13(7):771–8, jul 2011.
- [152] Sophie Dumont and Timothy J. Mitchison. Compression Regulates Mitotic Spindle Length by a Mechanochemical Switch at the Poles. *Current Biology*, 19(13):1086–1095, 2009.
- [153] Takeshi Itabashi, Jun Takagi, Yuta Shimamoto, Hiroaki Onoe, Kenta Kuwana, Isao Shimoyama, Jedidiah Gaetz, Tarun M Kapoor, and Shin’ichi Ishiwata. Probing the mechanical architecture of the vertebrate meiotic spindle. *Nature methods*, 6(2):167–72, 2009.
- [154] Carlos Garzon-Coral, Horatiu A. Fantana, and Jonathon Howard. A force-generating machinery maintains the spindle at the cell center during mitosis. *Science (New York, N.Y.)*, 352(6289):1124–7, 2016.
- [155] Clare M Waterman-Storer and E Salmon. Positive feedback interactions between microtubule and actin dynamics during cell motility. *Current Opinion in Cell Biology*, 11(1):61–67, 1999.
- [156] Erik W Dent, Stephanie L Gupton, and Frank B Gertler. The Growth Cone Cytoskeleton in Axon outgrowth and guidance. *Cold Spring Harbor perspectives in biology*, pages 1–40, 2011.
- [157] A Rump, T Scholz, C Thiel, F K Hartmann, P Uta, M H Hinrichs, M H Taft, and G Tsiavaliaris. Myosin-1C associates with microtubules and stabilizes the mitotic spindle during cell division. *Journal of Cell Science*, 124(15):2521–2528, 2011.

- [158] Shu Zon Wu and Magdalena Bezanilla. Myosin VIII associates with microtubule ends and together with actin plays a role in guiding plant cell division. *eLife*, 3:1–20, 2014.
- [159] Matthias Samwer, Heinz-Jürgen Dehne, Felix Spira, Martin Kollmar, Daniel W Gerlich, Henning Urlaub, and Dirk Görlich. The nuclear F-actin interactome of *Xenopus* oocytes reveals an actin-bundling kinesin that is essential for meiotic cytokinesis. *The EMBO journal*, 32(13):1886–1902, 2013.
- [160] L. M. Griffith and T. D. Pollard. The interaction of actin filaments with microtubules and microtubule-associated proteins. *Journal of Biological Chemistry*, 257(15):9143–9151, 1982.
- [161] Auréliane Elie, Elea Prezel, Christophe Guérin, Eric Denarier, Sacniete Ramirez-Rios, Laurence Serre, Annie Andrieux, Anne Fourest-Lieuvin, Laurent Blanchoin, and Isabelle Arnal. Tau Co-Organizes Dynamic Microtubule and Actin Networks. *Scientific Reports*, 5:9964, 2015.
- [162] Jessica L Henty-Ridilla, Aneliya Rankova, Julian A Eskin, Katelyn Kenny, and Bruce L Goode. Accelerated actin filament polymerization from microtubule plus ends. *Science*, 352(6288):1004–1009, 2016.
- [163] Magdalena Preciado Lopez, Florian Huber, Ilya Grigoriev, Michel O Steinmetz, Anna Akhmanova, Gijse H Koenderink, and Marileen Dogterom. Actin-microtubule coordination at growing microtubule ends. *Nature communications*, pages 1–9, 2014.
- [164] J R Sider, C a Mandato, K L Weber, a J Zandy, D Beach, R J Finst, J Skoble, and W M Bement. Direct observation of microtubule-f-actin interaction in cell free lysates. *Journal of cell science*, 112 (Pt 1:1947–1956, 1999.
- [165] Clare Waterman-Storer, Devin Y. Duey, Kari L. Weber, John Keech, Richard E. Cheney, E. D. Salmon, and William M. Bement. Microtubules remodel actomyosin networks in *Xenopus* egg extracts via two mechanisms of F-actin transport. *Journal of Cell Biology*, 150(2):361–376, 2000.
- [166] L S Minamide, A M Striegl, J A Boyle, P J Meberg, and J R Bamberg. Neurodegenerative stimuli induce persistent ADF/cofilin-actin rods that disrupt distal neurite function. *Nature cell biology*, 2(9):628–636, 2000.
- [167] James R Bamberg and O’Neil P Wiggan. ADF / cofilin and actin dynamics in disease. *Trends in biotechnology*, 12(12):598–605, 2002.
- [168] Atsuko Miyazaki, Koichi H. Kato, and Shin Ichi Nemoto. Role of microtubules and centrosomes in the eccentric relocation of the germinal vesicle upon meiosis reinitiation in sea-cucumber oocytes. *Developmental Biology*, 280(1):237–247, 2005.
- [169] D L Gard. Ectopic spindle assembly during maturation of *Xenopus* oocytes: evidence for functional polarization of the oocyte cortex., 1993.
- [170] Amy S. Fabritius, Marina L. Ellefson, and Francis J. McNally. Nuclear and spindle positioning during oocyte meiosis. *Current Opinion in Cell Biology*, 23(1):78–84, 2011.

- [171] Stéphane Brunet and Bernard Maro. Germinal vesicle position and meiotic maturation in mouse oocyte. *Reproduction*, 133(6):1069–1072, 2007.
- [172] Michael B. Elowitz, Michael G. Surette, Pierre Etienne Wolf, Jeffry B. Stock, and Stanislas Leibler. Protein mobility in the cytoplasm of *Escherichia coli*. *Journal of Bacteriology*, 181(1):197–203, 1999.
- [173] S. Soh, Marta Byrska, Kristiana Kandere-Grzybowska, and Bartosz A. Grzybowski. Reaction-diffusion systems in intracellular molecular transport and control. *Angewandte Chemie - International Edition*, 49(25):4170–4198, 2010.
- [174] G. Laloux and C. Jacobs-Wagner. How do bacteria localize proteins to the cell pole? *Journal of Cell Science*, 127(1):11–19, 2014.
- [175] P. T. Tran, L. Marsh, V. Doye, S. Inoué, and F. Chang. A mechanism for nuclear positioning in fission yeast based on microtubule pushing. *Journal of Cell Biology*, 153(2):397–411, 2001.
- [176] Iva M Tolic, Leonardo Sacconi, Geneviève Thon, and Francesco S Pavone. Positioning and Elongation of the Fission Yeast Spindle by Microtubule-Based Pushing. *Current Biology*, 14:1181–1186, 2004.
- [177] Marileen Dogterom, Jacob W J Kerssemakers, Guillaume Romet-Lemonne, and Marcel E Janson. Force generation by dynamic microtubules. *Current opinion in cell biology*, 17(1):67–74, 2005.
- [178] Martin Wuhr, Sophie Dumont, Aaron C. Groen, Daniel J. Needleman, and Timothy J. Mitchison. How does a millimeter-sized cell find its center? *Cell Cycle*, 8(8):1115–1121, 2009.
- [179] S W Grill, P Gönczy, E H Stelzer, and A a Hyman. Polarity controls forces governing asymmetric spindle positioning in the *Caenorhabditis elegans* embryo. *Nature*, 409(February):630–633, 2001.
- [180] Tomomi Kiyomitsu and Iain M. Cheeseman. Chromosome- and spindle-pole-derived signals generate an intrinsic code for spindle position and orientation. *Nature Cell Biology*, 14(3):311–317, 2012.
- [181] Kenji Kimura and Akatsuki Kimura. A novel mechanism of microtubule length-dependent force to pull centrosomes toward the cell center. *BioArchitecture*, 1(2):74–79, 2011.
- [182] K. Kimura and A. Kimura. Intracellular organelles mediate cytoplasmic pulling force for centrosome centration in the *Caenorhabditis elegans* early embryo. *Proceedings of the National Academy of Sciences*, 108(1):137–142, 2011.
- [183] Martin Wüühr, Edwin S. Tan, Sandra K. Parker, H. William Detrich, and Timothy J. Mitchison. A model for cleavage plane determination in early amphibian and fish embryos. *Current Biology*, 20(22):2040–2045, 2010.
- [184] Hirokazu Tanimoto, Akatsuki Kimura, and Nicolas Minc. Shape-motion relationships of centering microtubule asters. *Journal of Cell Biology*, 212(7):777–787, 2016.

- [185] Zuzana Holubcová, Gillian Howard, and Melina Schuh. Vesicles modulate an actin network for asymmetric spindle positioning. *Nature cell biology*, 15(8):937–47, 2013.
- [186] A Chaigne, C Campillo, N S Gov, R Voituriez, C Sykes, M H Verlhac, and M E Terret. A narrow window of cortical tension guides asymmetric spindle positioning in the mouse oocyte. *Nature Communications*, 6:1–10, 2015.
- [187] Agathe Chaigne, Clément Campillo, Raphaël Voituriez, Nir S. Gov, Cécile Sykes, Marie-Hélène Verlhac, and Marie-Emilie Terret. F-actin mechanics control spindle centring in the mouse zygote. *Nature Communications*, 7:10253, 2016.
- [188] Vincent Delatour, Shashank Shekhar, Anne Cécile Reymann, Dominique Didry, Kim Hô Diêp Lê, Guillaume Romet-Lemonne, Emmanuele Helfer, and Marie France Carlier. Actin-based propulsion of functionalized hard versus fluid spherical objects. *New Journal of Physics*, 10, 2008.
- [189] Otger Campàs, Tadanori Mammoto, Sean Hasso, Ralph A Sperling, Daniel O Connell, Ashley G Bischof, Richard Maas, David A Weitz, L Mahadevan, and Donald E Ingber. Quantifying cell-generated mechanical forces within living embryonic tissues. *Nature methods*, 11(2), 2014.
- [190] Friedhelm Serwane, Alessandro Mongera, Payam Rowghanian, David A Kealhofer, Adam A Lucio, Zachary M Hockenbery, and Otger Campàs. In vivo quantification of spatially varying mechanical properties in developing tissues. *Nature Methods*, 14(2), 2016.
- [191] Adam A. Lucio, Donald E. Ingber, and Otger Campàs. Generation of biocompatible droplets for in vivo and in vitro measurement of cell-generated mechanical stresses. *Methods in Cell Biology*, 125:373–390, 2015.
- [192] Thomas A. Burke, Jenna R. Christensen, Elisabeth Barone, Cristian Suarez, Vladimir Sirotkin, and David R. Kovar. Homeostatic actin cytoskeleton networks are regulated by assembly factor competition for monomers. *Current Biology*, 24(5):579–585, 2014.
- [193] Alexis J Lomakin, Kun-Chun Lee, Sangyoon J Han, Duyen A Bui, Michael Davidson, Alex Mogilner, and Gaudenz Danuser. Competition for actin between two distinct F-actin networks defines a bistable switch for cell polarization. *Nature cell biology*, 17(11), 2015.
- [194] Alphée Michelot and David G. Drubin. Building distinct actin filament networks in a common cytoplasm. *Current Biology*, 21(14):560–569, 2011.

Résumé

La division cellulaire est un élément clé du développement. Pendant ce processus, le matériel génétique (chromosomes) est distribué entre les deux cellules filles. Cette distribution est effectuée par le fuseau mitotique ou méiotique ; une mauvaise formation de cette structure peut être critique. Le cytosquelette joue un rôle prédominant dans la division cellulaire. Malgré des progrès importants dans la compréhension de son rôle dans le processus de division cellulaire, de nombreuses questions restent encore sans réponse et des progrès techniques pour étudier ces phénomènes sont nécessaires. Dans cette thèse, nous avons étudié le rôle de l'auto-organisation de l'actine cytoplasmique dans deux systèmes modèles : les extraits cellulaires de Xénope et les ovocytes de souris. En utilisant une approche interdisciplinaire, nous avons développé de nouveaux outils expérimentaux et analytiques pour étudier le rôle de l'actine cytoplasmique pendant la division cellulaire.

En encapsulant les extraits cellulaires de Xénope dans des gouttes, nous pouvons mimer le volume cellulaire. Nous utilisons ce système pour étudier les interactions entre l'actine et les microtubules. Dans un premier projet, nous avons montré que l'auto-organisation de l'actine peut déclencher des cascades de signalisation. Grâce à l'ingénierie de deux propriétés de l'actine, nous avons démontré que l'auto-organisation de ce polymère peut permettre l'assemblage de microtubules. Dans un deuxième projet, nous avons montré que la dynamique de l'actine cytoplasmique peut induire des contraintes sur l'organisation et la dynamique des microtubules. Nos résultats suggèrent que les propriétés dynamiques du réseau d'actine sont un facteur important pour l'assemblage des microtubules.

Dans l'ovocyte de souris, nous avons développé une méthode pour suivre de manière automatique le mouvement d'objets passifs avec des tailles variables. Nous avons utilisé ce système pour étudier l'effet de l'actine cytoplasmique sur le transport à longue portée. Nous avons ainsi validé l'existence d'un mécanisme de centrage non spécifique de gros objets pendant la prophase. Nous avons aussi démontré que ce mécanisme de centrage reste présent pendant le reste de la méiose, en même temps que la migration du fuseau vers le cortex de l'ovocyte.

Mots Clés

Actine, Microtubules, Auto-organisation, Extraits cellulaires de Xénope, Ovocytes de souris, Système biomimétique

Abstract

Cell division is a key element of the development of an embryo throughout all his life. During cell division, the genetic material (chromosomes) is distributed between the two daughter cells. This distribution is achieved by the spindle and a misbehavior in the formation of this structure can be critical. The cytoskeleton polymers are playing a predominant role in cell division. Despite important progresses in the understanding of their role in cell division process, numerous questions still have to be answered and technical progresses to study these phenomena are still needed. In this PhD work, we studied the role of cytoplasmic F-actin self-organization in two model systems: Xenopus egg extracts and mouse oocytes. Using an interdisciplinary approach, we developed new experimental and analytical tools to study the role of cytoplasmic F-actin during cell division.

By encapsulating Xenopus actin-intact egg extracts in droplets, we are able to mimic cellular environment. We use this system to study interactions between F-actin and microtubules. In a first project, we showed that F-actin self-organization can trigger signaling pathways. By engineering two properties of the microfilament self-organization and using Ran dependent microtubule nucleation, we found that F-actin dynamics promotes the robust assembly of microtubules. In a second project, we showed that the dynamics of cytoplasmic F-actin can induce constraints on the microtubule organization and dynamics in aster and spindle structures. Our results suggest that the dynamic properties of cytoplasmic F-actin meshwork are of a primary importance for the proper assembly of microtubule structures.

In the mouse oocyte, we set-up a method to automatically track the movement of passive objects with tunable size. We used this system to examine the effect of cytoplasmic F-actin on long-range transport. We thus validated the existence of a non-specific mechanism for large objects centering during Prophase. We also demonstrated that this centering mechanism is still present during the rest of meiosis, coexisting with the spindle migration toward the cortex.

Keywords

Actin, Microtubule, Self-organization, Xenopus egg extracts, Mouse oocytes, Biomimetic system

